

**Developing a novel 3D alginate platform
for investigating the patterned differentiation
of mouse embryonic stem cells**

Orla M. Fannon

October 2018



Biomedical Engineering Division
School of Biological Sciences
University of Reading

To $MH(TB)^2$

.....

Declaration of original authorship

I confirm that this is my own work and that the use of all material from other sources has been properly and fully acknowledged.

Orla M. Fannon

.....

Table of Contents

Dedication	ii
Declaration of original authorship	iii
Acknowledgements	ix
List of Figures	xi
List of Tables	xiii
List of Abbreviations	xiv
Abstract	1
1 Literature Review	2
1.1 Background	2
1.2 Overview of embryonic stem cell differentiation <i>in vitro</i>	2
1.2.1 Introduction to embryonic stem cells	2
1.2.2 Embryoid body suspension culture	3
1.2.3 Limitations of embryoid body models of differentiation	4
1.3 Patterned differentiation determines cell fate	5
1.3.1 Retinoic acid is essential for nervous system development	5
1.3.2 Mechanism of retinoic acid-induced gene transcription	7
1.3.3 Metabolism of retinoic acid	7
1.3.4 Retinoic acid signalling is tightly regulated <i>in vivo</i>	8
1.3.5 Retinoic acid-induced embryonic stem cell differentiation <i>in vitro</i>	9
1.4 Specification of the dorso-ventral neuraxis	10
1.4.1 Retinoic acid in the ventral spinal cord	10
1.4.2 Sonic hedgehog in the ventral spinal cord	11
1.4.3 Establishing the progenitor domain boundaries during development	11
1.4.4 Subtypes of motor neurons in the central nervous system	11
1.4.5 Motor neuron subtype specification <i>in vitro</i>	13
1.4.6 Lateral motor column motor neurons produce retinoic acid <i>in vivo</i>	14

1.4.7	3D cell culture - a paradigm shift	14
1.5	3D cell culture for investigating cell development	16
1.5.1	Biomaterials as a platform for recreating the extracellular matrix	16
1.5.2	Using 3D biomaterials for stem cell culture	17
1.5.3	Naturally-derived biomaterials	17
1.5.4	Synthetic biomaterials	19
1.5.5	Hybrid biomaterial platforms	20
1.5.6	3D platforms are valuable tools for <i>in vitro</i> research	21
1.6	Alginate hydrogels for stem cell differentiation	23
1.6.1	Properties of alginate	23
1.6.2	Influence of alginate composition on hydrogel characteristics	24
1.6.3	Importance of controlling alginate hydrogel porosity	26
1.6.4	ESC differentiation in 3D alginate platforms	27
1.7	Focus of the current research	28
1.7.1	Objectives of the experimental chapters	30
1.7.2	Hypotheses	31
2	Methods	32
2.1	Cell Culture	32
2.1.1	Aseptic cell culture	32
2.1.2	Preparation of tissue culture plates	32
2.1.3	Culture of feeder-free mouse embryonic stem cells	32
2.1.4	Passaging cell populations by trypsinisation	32
2.1.5	Culture of mouse embryonic fibroblast feeder layers	33
2.1.6	Culture of feeder-dependent mouse embryonic stem cells	33
2.1.7	Separation of embryonic stem cells from feeder layers	33
2.1.8	Embryonic stem cell neuronal differentiation by suspension culture	34
2.1.9	Preparation of laminin-coated coverslips	34
2.1.10	EB dissociation and monolayer culture for immunostaining	34
2.2	Characterisation of HGF11-derived lateral motor column motor neurons	35
2.2.1	Differentiation of motor neurons from HGF11 embryonic stem cells	35
2.2.2	Quantification of endogenous retinoid concentrations	35

Table of Contents

2.3	Viability Assays	36
2.3.1	Live/dead assay for alginate beads	36
2.3.2	Validation of live/dead assay by flow cytometry	36
2.4	Immunofluorescence methods	36
2.4.1	Cryosectioning embryoid bodies and alginate beads	36
2.4.2	Immunocytochemistry	37
2.5	Alginate hydrogels for cell culture	39
2.5.1	Formation of cell-encapsulating alginate hydrogels	39
2.5.2	Depolymerisation of alginate beads	39
2.5.3	Live/dead viability counts by flow cytometry	39
2.6	Alginate co-culture	41
2.6.1	Boyden chamber co-culture	41
2.6.2	Formation of alginate tubes for co-culture	42
2.7	Quantitative polymerase chain reaction	42
2.7.1	RNA extraction and DNA synthesis	42
2.7.2	Primer validation and efficiency	45
3	Characterisation of alginate hydrogels	47
3.1	Introduction	47
3.2	Optimising alginate beads	48
3.2.1	Identifying a suitable base for alginate hydrogel solutions	48
3.2.2	Optimising the seeding cell density and differentiation duration	52
3.3	Cell viability in alginate beads	55
3.4	LMW vs HMW beads	56
3.5	Discussion	61
3.5.1	Understanding alginate composition	63
3.5.2	Alginate porosity affects stem cell behaviour	64
3.5.3	Alginate composition influences cell-matrix interactions	65
3.6	Chapter summary	68
4	Neural differentiation in alginate beads	69
4.1	Introduction	69
4.2	Methods	70

.....	
4.2.1	Differentiating embryonic stem cells 70
4.2.2	Pixel quantification of immunofluorescent images 70
4.2.3	Depolymerisation and viability of harvested cells 71
4.2.4	Gene expression analysis 71
4.3	Results 73
4.3.1	Encapsulated aggregates were embryoid bodies 73
4.3.2	Germ layer presence may vary spatially between culture conditions . . 73
4.3.3	Spatial variability in the presence of cells from the three germ layers . 79
4.3.4	Alginate hydrogel depolymerisation reduces cell viability 80
4.3.5	Gene expression in beads and embryoid bodies 83
4.4	Discussion 86
4.4.1	Alginate beads present a suitable platform for investigating embryogenesis 86
4.4.2	The influence of alginate G:M composition on differentiation 87
4.4.3	Germ layer differentiation was not influenced by aggregate spatial location 89
4.4.4	Alginate hydrogels do not support cell harvesting after experiments . 91
4.4.5	Future research based on the current experiments 93
4.5	Conclusion 93
5	A novel source of retinoic acid for <i>in vitro</i> cell culture 95
5.1	Introduction 95
5.2	Methods 96
5.2.1	Culture of feeder-dependent mouse embryonic stem cells 96
5.2.2	Embryoid body suspension culture 97
5.2.3	Characterisation of the HGF11-derived motor neurons 97
5.2.4	Quantification of retinoic acid and Raldh2 98
5.2.5	Embryonic stem cell differentiation using endogenous retinoic acid . . 98
5.3	Results 99
5.3.1	Validating the presence of the Foxp1 transgene 99
5.3.2	HGF11-derived motor neurons have a lateral motor column identity . 100
5.3.3	HGF11-derived motor neurons produced Raldh2 and retinoic acid . . 101
5.4	Discussion 104
5.4.1	HGF11-derived motor neurons produced a stable source of retinoic acid 104

.....	
5.4.2 Applications of a cell-derived source of retinoic acid	106
5.4.3 HGF11-derived motor neurons are a novel tool for differentiation . . .	108
5.5 Conclusion	110
6 Creating a novel 3D alginate platform	112
6.1 Introduction	112
6.2 Methods	114
6.2.1 Testing the activity of cell-produced retinoic acid	114
6.2.2 Generation of retinoic acid gradients in alginate hydrogel tubes	115
6.3 Results	115
6.3.1 Retinoic acid in the medium did not induce differentiation	115
6.3.2 A localised retinoic acid gradient induced embryoid body differentiation	117
6.4 Discussion	124
6.4.1 A cell-produced source of retinoic acid can be used for differentiation .	124
6.4.2 Alginate tubes are a novel platform for studying differentiation <i>in vitro</i>	126
6.4.3 A novel alginate platform for investigating signalling gradients <i>in vitro</i>	126
6.5 Conclusion	128
8 Summary discussion	130
8.1 Summary of results	130
8.2 Importance of the current results for 3D cell culture applications	130
8.2.1 Applications of embryoid body culture within alginate hydrogels . . .	130
8.2.2 Co-culture experiments are important for 3D culture	131
8.2.3 Advantages of the novel 3D platform	132
8.2.4 <i>In vivo</i> applications of the 3D platform for patterned differentiation .	133
8.2.5 A novel platform for investigating 9-cis-RA activation of RAR/RXRs	134
8.2.6 Concluding remarks	136
Appendix	138
References	140

Acknowledgements

I would first like to thank and acknowledge my supervisors Dr Evangelos Delivopoulos, Dr Angela Bithell and Professor Ben Whalley. I was lucky to have supervisors who always had time to help me brainstorm, listen to my problems and support me both personally and with the research. You all made yourself available for me when I needed help, and I would not have succeeded without your wisdom, dedication, time and knowledge, so I am truly grateful to have had you on my team. An extra shout out to Ben for being an eternal optimist and a running enthusiast who encouraged everyone to be optimistic runners - both of which kept me going more than once! Thank you all so much for helping me to get here and being there for the last four years.

I would also like to acknowledge Professor Slawomir Nasuto and Dr Yoshi Hayashi who have contributed their time and resources to my research, and been a sounding board for my ideas. Thank you both for your help with my presentations, your support in my science outreach activities, and for bringing awareness of our lab and our research to the world. You were both a great inspiration and I have had so many opportunities to share my research with the public because of your work. Those opportunities were some of the most exciting and rewarding parts of my PhD so thank you for efforts in keeping the lab in the public eye and for helping me to share science with others.

To the Hopkins gang, thanks for being such fun, kind, smart and incredible friends. I am so lucky to have been able to do my research alongside such amazing people. You have all helped me with the science and been there for me no matter what happened. Tino, thanks for all your dedication to my experimental brainstorming, you are a star, and I know you'll do great things for science. Yuhan and Ines, you are so dedicated, motivated, talented and hard working, I can't tell you enough how you inspired me. I'm really lucky to have you as friends and I'm happy that we got to do this together, because I can't think of anyone else I'd rather work with during a PhD. To Benemesis and Danielle, you guys are so great thanks for being super fun and always so happy and cheery, it has been so great.

Acknowledgements

.....

To Tina Farrelly, you are a fantastic teacher, who expected big things from me and trusted me when I said I could do it, but on my own terms. I know I drove you up the walls sometimes but I hope this makes up it. Thank you believing in me and for all of your teaching, effort and support - without you, I wouldn't have stuck with science and I'm so grateful to you.

To my Neuronions, you're all the best craic ever and I'm so lucky to have you. Ines and Saloni, you're the best friends I could ever ask for and I can never thank you both enough for all the support and encouragement and advice you've given me over the last four years.

To the Cooking Crowd, Margaret and Niall, Jane, Brid and Paddy, Angela and Eamon and the O'Kanes, you genuinely never once stopped believing in me and you have always had my back. You have all been part of this and in some way or another, you've helped me on the path to where I am today. Thank you all.

For my family, there are no words to thank you for the sacrifices you've made so that I can be here. I love you all and I owe you big time, forever. Granny Maisie, thanks for lighting all of those candles. To my new family, thanks for feeding me, taking care of me, making coffees and being a part of this, I love you too. To my Grandad Connolly, Grandad Fannon and Dimitris, I'm sad you won't be here to see this but I hope I make you proud.

To Ioannis, you've are my rock. I would say I owe you but instead I'll say we're even, let's never do it again, we make an incredible team and I love you the most.

.....

List of Figures

1	Shh gradient in progenitor domains	12
2	Chemical structure of alginate	24
3	Images of alginate beads containing encapsulated ESCs	40
4	Diagram of the Boyden chamber setup for alginate co-culture experiments . .	41
5	Diagram of a gradient maker and the equipment required to make alginate tubes	43
6	Simplified gradient maker setup outlining the proposed gradients in tube . . .	44
7	Aggregate formation in alginate:DMEM and alginate:H ₂ O beads	49
8	EBs and escaping aggregates from alginate beads	51
9	EBs and escaping aggregates from alginate beads	53
10	Effect of gelatin concentration on aggregate formation	54
11	Viability of encapsulated cells in alginate beads	57
12	Effect of molecular weight on aggregation	59
13	Aggregates vary across the bead depth	60
14	Cell viability of encapsulated ESCs in LMW and HMW beads	62
15	Quantification of cell viability in LMW and HMW beads	63
16	Cryosection plan for samples	72
17	Beads and EBs are suitable conditions for ESC differentiation to each germ layer	74
18	Spatial location of β -III-tubulin and Nestin	75
19	Spatial location of AFP and SMA	76
20	Pixel counting data for ratios of germ layer marker to nuclear stain	77
21	Within-experiment variability in cell viability	83
22	Neural gene expression was comparable in beads and embryoid bodies	84
23	HGF11-derived MNs were HB9 ⁺ , GFP ⁺ and Foxp1 ⁺	100
24	Magnified images of HGF11-derived MNs	101
25	CGR8-derived MNs were negative for GFP	102
26	MN differentiation from HGF11-ESCs	102
27	HGF11-derived MNs produce a stable concentration of RA, but not Raldh2 .	105
28	Brightfield images of alginate beads from co-culture experiments	116
29	Endogenous RA did not induce EB formation from encapsulated ESCs	117
30	Encapsulated cells were not differentiated by the HGF11-MN source of RA .	118

List of Figures

.....

31	Brightfield images of alginate tubes formed using a gradient maker	120
32	Alginate tubes contained markers for endoderm and mesoderm	121
33	Alginate tubes contained ectoderm marker β -III-tubulin	122

.....

List of Tables

1	Details of antibodies used for immunocytochemistry experiments	38
2	Primer efficiencies for real time PCR	46
3	Alginate conditions tested for optimisation of ESC encapsulation	48
4	Product details for LMW and HMW alginate solutions	58
5	Details of primers used for quantitative PCR	72
6	Significance values for pixel counts	78
7	Average percentage viability of harvested cells	81
8	Individual replicates for cell viability after depolymerisation	82
9	Endogenous Raldh2 concentration	103
10	Retinoic acid concentration produced by lateral motor column motor neurons	104

List of Abbreviations

2D	Two-dimensional
3D	Three-dimensional
β -ME	β -mercaptoethanol
ADFNK	Advanced DMEM-F12:NBM (1:1) with 10% knockout serum replacement
AFP	α -fetoprotein
ANOVA	Analysis of variance
bHLH	basic-helix-loop-helix
BMP(s)	Bone morphogenetic protein(s)
CaCl ₂	Calcium chloride
cDNA	complementary DNA
cm	Centimetre
CNS	Central Nervous System
Cyp26	Cytochrome P450 26
DEAB	4-(diethylamino)benzaldehyde
ddH ₂ O	double distilled water
DMEM	Dulbecco's modified eagle medium
DNA	Deoxyribonucleic acid
dPBS	Dulbecco's phosphate buffered saline
EB(s)	Embryoid Body(ies)
ECM	Extracellular Matrix
EDTA	Ethylenediaminetetraacetic acid
ELISA	Enzyme-linked immunosorbent assay
ESC(s)	Embryonic stem cell(s)
FBS	Fetal bovine serum
FDA	Fluorescein diacetate
FGF	Fibroblast growth factor
Foxp1	Forkhead box protein 1
G	Gauge (needle gauge)
GABA	γ -aminobutyric acid
gDNA	genomic DNA

.....

GFP	Green fluorescent protein
GDNF	Glial derived neurotrophic factor
GFAP	Glial fibrillary acidic protein
G-residues	Homopolymer α -L-guluronic acid residues
h	Hour(s)
HB9	Homeobox protein B9
HD	Homeobox domain
Hepes	4-(2-hydroxyethyl)-1-piperazineethanesulfonic acid
HMC	Hypaxial motor column
HMW	High molecular weight alginate
ICC	Immunocytochemistry
IGF	Insulin-like growth factor
IKVAV	isoleucine-lysine-valine-alanine-valine
kPa	Kilopascals
LIF	Leukaemia inhibitory factor
LMC	Lateral motor column
LMCl	Lateral lateral motor column
LMCm	Medial lateral motor column
LMW	Low molecular weight alginate
MEF(s)	Mouse embryonic fibroblast(s)
MgCl ₂	Magnesium chloride
min	Minute(s)
mL	Millilitre
mM	Millimolar
MMC	Median motor column
MN(s)	Motor neuron(s)
M-residues	Homopolymer β -D-mannuronic acid residues
MSCs	Mesenchymal stem cells
NaCl	Sodium Chloride
ng	nanograms
NGF	Nerve growth factor
nM	nanomolar

List of Abbreviations

.....

NT3	Neurotrophin 3
OCT	Optimal cutting temperature
Pax6	Paired box protein Pax 6
PCR	Polymerase chain reaction
PDMS	Polydimethyl-siloxane
PEG	Polyethylene glycol
PFA	Paraformaldehyde
PGA	Polyglycolic acid
PGC	Preganglionic motor column
PI	Propidium iodide
PLGA	Poly(lactic-co-glycolic acid)
PLL	Poly-L-lysine
PMC	Phrenic motor column
Pou5f1	POU class 5 homeobox 1
RA	Retinoic Acid
Raldh	Retinaldehyde dehydrogenases
RAR(s)	Retinoic acid receptor
rcf	Relative centrifugal force
RNA	Ribonucleic acid
RNase	Ribonuclease
ROUT	Robust regression and outlier removal
RXR(s)	Rexinoic X receptor
s	Second(s)
Shh	Sonic Hedgehog
SMA	α -smooth muscle actin
TO	Thiazole orange
μ g	Microgram
μ L	Microlitre
μ m	Micrometer
μ M	Micromolar
w/v	Weight per volume
v/v	Volume per volume

Abstract

Standard 2D cell culture does not recreate the complex features of the *in vivo* environment, such as soluble factor gradients, cell migration into multiple planes, or cell-cell and cell-matrix interactions.¹⁻³ 3D cell culture addresses these limitations by using 3D biomaterial scaffolds, such as alginate hydrogels, to recreate the *in vivo* cell microenvironment *in vitro*.^{4,5} 3D platforms can be used to create gradients of soluble factors, vary the biomaterial substrate stiffness, permit cell-matrix interactions or promote cell migration.^{6,7} Currently available 3D platforms are prone to the burst release of soluble factors from the biomaterials, making it difficult to tightly control the soluble factor concentration.⁷ This limits the use of 3D platforms for investigating processes such as patterned neuronal differentiation, or cell fate specification in response to small changes in soluble factor concentration.

This project proposes a novel 3D alginate platform for patterned differentiation. The first part of this thesis describes experiments to optimise alginate hydrogels for the encapsulation, aggregation and differentiation of embryonic stem cells (ESCs), and demonstrates that encapsulated ESCs form embryoid bodies containing cells from the three germ layers. Exogenous retinoic acid (RA) is used for *in vitro* neuronal differentiation protocols, but exogenous RA is not stable in cell culture and is easily degraded by light. The second part of the thesis outlines experiments to validate a cell-derived source of RA, which produces a stable concentration of RA *in vitro* and addresses the limitations of exogenous RA. The final section describes the novel 3D platform that combines the results from the previous sections using an adapted gradient maker protocol, to create 3D co-culture alginate tubes. The tubes support patterned differentiation of ESCs in response to the concentration gradient of cell-derived RA incorporated into the platform.

The novel 3D platform produced in this project contributes a novel tool to the field of 3D cell culture. The 3D platform is a tool for investigating ESC differentiation in response to a 3D concentration gradient of a cell-derived source of retinoic acid. For experiments that require a gradient of RA, the ability to maintain a stable source of RA over several days is an advantage of using this 3D platform over the currently available alternatives. In addition, alginate hydrogels are highly tunable. Thus, the ability to tune the scaffold properties, change the cell types encapsulated, or introduce gradients of alternative soluble factors makes this a versatile tool for 3D culture.

Chapter 1. Literature Review

1.1 Background

For over a century, scientists have been investigating the development of the nervous system in an attempt to understand the mechanisms of cell development. Ramon y Cajal's demonstration that neuronal morphology differs for each type of neuron was a major driving force in nervous system research.⁸ Tissue regeneration, the complex development of neural networks and the restoration of function after trauma to the nervous system are of particular interest. Disease or injury to the central nervous system (CNS) activates an inflammatory response and disrupts homeostasis. If homeostasis is not restored, the cellular microenvironment continues to damage cell populations and leads to loss of function.⁹ Neurodegeneration, spinal cord injury and traumatic brain injury have a devastating and debilitating effect on quality of life and all three are underpinned by irreparable, irreversible damage to the CNS.¹⁰⁻¹² Neural plasticity and neurite outgrowth are widespread within the developing nervous system, but mature axons have a limited capacity for growth and repair, and injured neurons are incapable of self-regeneration thus leading to a long-term impairment after damage to the adult nervous system.^{13,14} The limited regenerative capacity of the CNS, in combination with the current lack of effective therapies to restore function after CNS injury, highlights an unmet need for methods to enhance our understanding of tissue regeneration and cell development.

1.2 Overview of embryonic stem cell differentiation *in vitro*

1.2.1 Introduction to embryonic stem cells

The first mouse embryonic stem cell (ESC) line was isolated from the inner cell mass of an 3.5 day blastocyst in 1981.¹⁵ This breakthrough contributed to methods for generating human ESCs and in 1998, the first human ESCs were isolated from *in vitro* fertilized embryos.¹⁶ ESCs are defined by their ability to differentiate into any cell in the body, and their ability to indefinitely self-renew.^{1,17,18} Mouse ESCs are maintained in a pluripotent, undifferentiated state *in vitro* by supplementing the culture medium with leukaemia inhibitory factor (LIF), or factors acting on the LIF receptor pathway, to suppress differentiation of the stem cells.¹⁹ LIF is insufficient to maintain pluripotency in human ESCs and instead, human ESCs are cultured on fibroblast feeder layers, which release differentiation inhibiting factors

to maintain an undifferentiated state.^{20,21} In the absence of any differentiation suppressing factors, ESCs undergo spontaneous differentiation into cell types from the three embryonic germ layers: endoderm, mesoderm and ectoderm.^{1,18,22} Cell fate specification can be controlled by supplementing the culture medium with exogenous morphogens such as retinoic acid (RA), bone morphogenetic proteins (BMPs), Wnt, Noggin or sonic hedgehog (Shh), to induce differentiation toward a specific cell fate.^{4,23,24}

Since ESCs were first isolated, they have been differentiated into a range of cell types *in vitro*, including but not limited to hepatocytes, pancreatic cells, cardiomyocytes, neurons, and glia.^{15,25–29} Their ability to generate cells from all three embryonic germ layers makes ESCs a valuable tool for *in vitro* research. For example, mouse ESC lines have been used to generate *in vitro* models of neuronal differentiation,^{24,30} embryogenesis,^{31,32} and neuronal functional activity.^{33,34} Likewise, human ESCs have been used to generate an *in vitro* model of spinal muscular atrophy for examining the mechanisms of the disease,³⁵ and to generate functional islet-cells for an *in vitro* model of diabetes.³⁶ The value of ESC models as a research tool depends on the ability to consistently and efficiently differentiate ESCs toward a desired cell fates, using well-defined and reproducible protocols. One commonly used method is embryoid body (EB) suspension culture, which offers an easy, reproducible, and scalable method for differentiating ESCs toward a range of cell types *in vitro*.

1.2.2 Embryoid body suspension culture for embryonic stem cell differentiation

EB suspension culture is a well characterised method for inducing ESC differentiation.^{22,31} In brief, ESCs are reseeded in suspension onto a non-coated tissue culture dish and cultured for several days (for mouse ESCs) or weeks (for human ESCs) in the absence of differentiation inhibiting factors.³⁷ During the initial days in suspension the ESCs form spheroid, multicellular aggregates called EBs, via cell-cell interactions.^{9,19,38} By adding signalling morphogens to the medium, EBs can be directed to differentiate into specific cell types:²² RA induces differentiation to neurons and astrocytes,^{15,39} ascorbic acid induces differentiation to cardiomyocytes,³⁰ and Activin A and Wnt3A promote hepatocyte differentiation.⁴⁰ EB suspension protocols offer limited control over the size of the EBs and consequently over the diffusion of nutrients and/or morphogens into the EBs. In addition, the agglomeration of EBs can lead to a necrotic core, limiting their utility in long-term culture and reducing the control over ESC differentiation.^{22,41–43} These size and agglomeration factors can be con-

.....

trolled using hanging-drop or microwell methods of EB formation, where an exact number of cells is aggregated in a small volume of liquid, or by using bioreactors to control the rate of formation of EBs. These methods provide control the EB conditions, but are more labour intensive and expensive compared to the suspension method.^{22,44}

EBs mimic many aspects of embryogenesis including proliferation, morphogenesis, differentiation, and region-specific differentiation into the three germ layers.^{19,38,43,45} As observed in the developing embryo, EBs are highly organised structures with inherent and complex signalling interactions that influence ESC differentiation.⁴⁴ Once ESCs have aggregated to form a multicellular EB, the outer layer differentiates into primitive endoderm and creates a laminin- and collagen-rich basement membrane. Then apical-basal polarity is established, followed by ESC differentiation into cell fates from the three germ layers.^{22,42,46} EB suspension culture produces heterogenous cell populations and the differentiation efficiency of EB protocols varies.¹⁹ The Wichterle and Peljto protocol typically generates 30-50% motor neurons (MNs),⁴⁷ a γ -aminobutyric acid (GABA) differentiation protocol generates approximately 86% GABAergic neurons,⁴⁸ and another protocol only achieved 10% differentiation to functional contracting cardiomyocyte.¹⁹ Some studies have reported protocols for increasing the purity of the desired populations through mechanical dissociation,⁴⁹ antibiotic selection,⁵⁰ or cell sorting techniques.^{19,51} McCreedy et al., (2012) reported that enrichment of the MN cultures by puromycin selection could increase purity to $58 \pm 1.5\%$ MNs.²⁸ However, as yet, there are no protocols that increase the efficiency of EB differentiation to 100% purity.¹⁹ If the EB-derived cell populations are generated for transplantation, any carry-over of non-target cells will have undesired effects within the host tissue and carry over of pluripotent stem cells can lead to teratoma formation.⁵⁰ Adverse or uncontrolled paracrine signalling effects by the transplanted cells may also occur, and may counteract the clinical efficacy of the transplant procedure.^{41,52}

1.2.3 Limitations of embryoid body models of differentiation

EB models of ESC differentiation have provided valuable insight to the mechanisms of patterned cell differentiation, but they cannot fully capture the process of embryogenesis.¹ EBs do not produce trophoblast, which is required for the formation of the extraembryonic tissues.⁵³ To recreate the extraembryonic tissues and examine the effects of the cell microenvironment on ESC differentiation, some studies have combined EB culture with three-

dimensional (3D) biomaterials scaffolds. In one study, mouse ESCs were differentiated into EBs and then encapsulated into hydrogel scaffolds to induce patterned vasculogenic and cardiogenic differentiation of individual EBs.⁵⁴ Another study created an *in vitro* model of gastrulation using mouse EBs, which were transferred to gelatin after differentiation. Their results showed that to undergo self-organisation and axis formation, EBs require implantation into an extracellular matrix (ECM)-like structure.⁵⁵ A breakthrough study showed that mouse EBs permitted to undergo prolonged differentiation in suspension culture spontaneously formed an organoid. The EB-derived organoid generated patterned differentiation that recapitulated self-organisation in the neural tube, displayed apical-basal polarity and expressed gene markers for diencephalon, spinal cord, and floor plate tissues.^{32,56} The study showed that after extended culture, the organoids formed neuroepithelial cysts, induced floor plate patterning and generated correct dorsoventral organisation.³² These 3D biomaterial or organoid cultures have provided novel methods to investigate and control ESC differentiation within EB cultures. Incorporating 3D cell culture with EB protocols may allow us to gain a greater understanding of the mechanisms of cell fate specification.

1.3 Patterned differentiation during development determines stem cell fate

The nervous system is the result of temporo-spatially controlled cell differentiation, axonal migration, and synapse formation.⁸ During neurogenesis, the neural tube differentiates and undergoes specification of the rostro-caudal and dorso-ventral axes, through the actions of morphogens including Noggin, fibroblast growth factors (FGFs), Wnts, β -catenins, BMPs, Shh and RA.^{26,57,58} This specification is dependent on localised cross-activating and cross-repressive gradients of signalling morphogens that induce intracellular signalling cascades and activate transcription factors that determine cell fate specification.⁵⁷⁻⁵⁹ These localised signalling gradients, and the temporo-spatial activation and inactivation of signalling cascades are responsible for generating the diversity of cell types in the adult CNS.^{31,60,61}

1.3.1 Retinoic acid is essential for nervous system development

RA is the most biologically active member of the retinoid family, a group of small lipophilic molecules derived from vitamin A.^{62,63} RA plays a major role in patterning the rostro-caudal and dorso-ventral axes, and is involved in neural differentiation, patterning the neural plate, and axonal extension.^{63,64} Maternal vitamin A deficiency, and subsequently RA deficiency in

.....

the embryo, results in CNS abnormalities and structural malformations in the dorsal spinal cord.^{63,65} Contrastingly, excess RA is teratogenic and results in severe malformation of hindlimb regions and abnormalities in hindbrain development.⁶⁶

Retinoids are not produced endogenously in mammals and must be absorbed from vitamin A in food. Once absorbed, they are stored as retinyl esters in the liver, lungs, and kidneys.^{64,67} Retinoids are transported from these storage sites to cells by retinol, which circulates in the blood bound to RA-binding protein 4. At the site of action, retinol is uptaken via RA-binding protein 4 receptors, enters the cytoplasm and binds retinol-binding protein 1. Within the cytoplasm, a two-step process metabolises retinol into RA: (1) retinol is oxidised by retinol dehydrogenase and converted to retinaldehyde, and (2) retinaldehyde is oxidised by retinaldehyde dehydrogenase to produce RA.^{64,68} During development, the first stage of RA synthesis is primarily controlled by retinol dehydrogenase 10, expressed in the floor plate and in somites near the developing spinal cord.⁶⁹ The second stage is controlled by three retinaldehyde dehydrogenases (Raldh1, Raldh2, Raldh3) which have distinct spatio-temporal domains in the embryo.⁶⁹ Raldh2 is the most well-defined of the retinaldehyde dehydrogenases: it is expressed within the mesenchyme just after gastrulation, and is later expressed in MNs, the meninges and the roof plate of the spinal cord.^{64,69} Raldh2 is the only retinaldehyde dehydrogenase known to play a role in spinal cord development and all RA synthesis before E8.5 is regulated by Raldh2. After this stage, Raldh1 and Raldh3 contribute to RA synthesis in the eyes and olfactory system.^{67,69}

In animal models of development, null mutants for retinaldehyde dehydrogenases have a range of developmental defects: *Raldh1*^{-/-} mutants show defects in dorsal retina formation, *Raldh3*^{-/-} mutants develop nasal and ocular deficits, and *Raldh2*^{-/-} mouse mutants exhibit abnormal MN specification and forebrain development.^{67,69} In loss-of-function *Raldh2* chick mutants there is a loss of posterior rhombomeres (5-7) and an expansion of anterior rhombomeres (2-4). Experiments in a loss-of-function *Raldh2* mouse model determined that Raldh2 is almost solely responsible for RA production during embryogenesis.^{63,70} Applying exogenous RA to mutant embryos can rescue the animal from some of the above defects and allow normal development from the day of rescue onwards: for example, *Raldh2*^{-/-} mouse mutants can be rescued from lethality by supplementation with exogenous RA at E7.5.⁶⁵

1.3.2 Mechanism of retinoic acid-induced gene transcription

RA influences cell fate specification by regulating gene expression through its actions on retinoic acid receptors (RARs). RA binds cellular RA binding proteins in the cytoplasm and enters the cell nucleus, where it acts by binding to transcription factor nuclear RARs (subtypes: α , β , γ).⁶⁴ In their unbound form, RARs form heterodimers with retinoid X receptors (RXRs; subtypes α , β , γ) and bind to RA-response elements, deoxyribonucleic acid (DNA) sequences that repress gene transcription. Upon RA binding to the RAR/RXR receptor complex, a conformational change in the receptor recruits co-activators in place of the RA-response element repressors, and the co-activators bind the RAR region of the receptor complex that contains the RA ligand site.⁷¹ Once co-activators are recruited, they initiate signalling cascades to modulate RA-RAR downstream targets involved in neuronal differentiation and cell patterning.^{64,68,71}

RARs form heterodimers with RXRs and there is wide heterogeneity in RAR/RXR dimers due to the combinations of their α , β , and γ subunits.⁷² RXRs were orphan receptors until a metabolite of RA, 9-cis-RA, was identified as their physiological ligand.⁷³ 9-cis-RA can bind to both RARs and RXRs and activates downstream signalling cascades of both receptors, whereas RA can only bind to RARs.^{74,75} The *in vivo* concentration of 9-cis-RA in the spinal cord is 30-fold lower than the concentration of RA, and is only detectable when embryos are exposed to teratogenic concentrations of RA. In *Raldh2*^{-/-} embryos, RA deficiency could be rescued using 9-cis-RA at concentrations 4-fold higher than the concentration of RA required to rescue the embryos.⁷⁵ These studies showed that extremely high levels of RA are required to reach a sufficient concentration of 9-cis-RA for RXR activation *in vivo*, and it is believed that RXR activation by 9-cis-RA is a protective measure against RA-induced teratogenicity.⁷⁶

1.3.3 Metabolism of retinoic acid

After RA binds and activates RARs, it returns from the nucleus to the cytoplasm, where it is inactivated by members of the cytochrome P450 26 (Cyp26) family: Cyp26a1, Cyp26b1, and Cyp26c1. Cyp26s oxidise RA into polar metabolites, which can then be conjugated and excreted.^{63,67,70} Cyp26a1 is the primary degrading enzyme for inactivation of RA during gastrulation.⁶³ Exogenous RA induces Cyp26a1 activity in the hindbrain regions, however depleting RA signalling does not eliminate Cyp26a1 expression, suggesting that Cyp26a1

is expressed to prevent RA-induced teratogenicity after RA surpasses a certain threshold. Once activated, Cyp26a1 does not require RA-RAR binding for ongoing expression.^{63,70} Shimozone et al., (2013) demonstrated in mice treated with 4-(diethylamino)benzaldehyde (DEAB) that RA is not required for the onset of Cyp26 enzymes *in vivo*, and Hernandez et al., (2007) reported that Cyp26a1 can be upregulated by exogenous RA whereas Cyp26b1 and Cyp26c1 are not upregulated by exogenous RA.^{77,78} Another study demonstrated using CD336, an RAR α -selective agonist, that RAR α activation upregulates Cyp26a1 and Cyp26b1, but downregulates Cyp26c1.⁶² The above studies show that the effects of RA on Cyp26 are not global, and that there are distinct effects of each Cyp26 enzyme on RA metabolism. The resulting localised patterns of RA activation and inactivation may contribute to the patterned differentiation of the neural tube.⁶² It is unclear whether a gradient of RA, or the combined actions of Cyp26s and Raldh2, are responsible for patterned differentiation along the neural tube. The effects of Cyp26 and Raldh activity on RA can be exploited *in vitro* to investigate and identify the mechanisms of cell fate specification by RA. Global activation, or inactivation, of both offers a novel strategy for controlling stem cell fate *in vitro*, and identifying Cyp/Raldh activation and inactivation effects on cell fate.

1.3.4 Retinoic acid signalling is tightly regulated *in vivo*

Cyp26s and retinaldehyde dehydrogenases are expressed in complementary, non-overlapping regions during gastrulation, and their interactions determine the availability of RA *in vivo*.^{64,66,79} RA upregulates Cyp26a1, and downregulates Raldh2, thus inducing its own metabolism and inactivation in a negative feedback loop. The combined expression patterns of retinaldehyde dehydrogenases and Cyp26 enzymes along the neural tube results in patterned inactivation of RA signalling, and regulates RA-induced gene transcription.^{63,67,70} Depleting the expression of all Cyp26 enzymes induces hindbrain posteriorisation in zebrafish embryos.⁷⁸ Sakai et al., (2001)⁷⁹ found that *Cyp26*^{-/-} mutant mouse embryos exhibited abnormal hindbrain and hindlimb development. They further estimated that *Cyp26*^{-/-} mutation is fatal in two thirds of embryos, and proposed that Cyp26 enzymes are crucial for preventing RA-induced teratogenesis by metabolising RA. Another study showed consistent findings: *Cyp26a1*^{-/-} embryos without exogenous RA exhibited a greater level of abnormal development compared to *Cyp26a1*^{-/-} embryos treated with exogenous RA.⁷⁸

1.3.5 Retinoic acid-induced embryonic stem cell differentiation *in vitro*

RA can be used to induce mouse ESC differentiation to a neural fate *in vitro*. The first protocol for RA-induced ESC differentiation was reported in 1995, when mouse ESCs were induced toward a neural fate using an EB suspension culture and exogenous RA.³⁹ The resulting cell population had greater numbers of β -III-tubulin positive cells and increased neurite extension compared to EBs cultured without RA. In 2003, RA-induced EB differentiation was used to promote radial-glia-like cell fates from mouse ESCs.⁸⁰ In 2014, EB culture was used to differentiate mouse ESCs into functional, beating cardiomyocytes,⁵⁵ and in the same year, another study used RA to induce single mouse ESCs to differentiate to cell fates from the three germ layers, and subsequently undergo self-organisation.⁸¹

RA-induced differentiation protocols have been used to generate *in vitro* analogues for many *in vivo* cell types, however, there are limitations to *in vitro* RA differentiation methods. The main limitation of these protocols is that exogenous RA is unstable in cell culture.^{82,83} RA is light-sensitive and isomerises rapidly when exposed to light, which can result in inconsistent concentrations of RA or its metabolites in the culture medium.⁸³ One study showed that 24h after RA was added to cell-free culture medium, only 69% and 27% of the RA was recovered in serum-supplemented and serum-free medium, respectively⁸² - the experiments were carried out under yellow light to minimise any light-induced degradation of RA, and the results suggested that in less tightly controlled environments, and with cells present in the culture conditions, the concentrations of RA at 24h would be substantially lower.⁸² The instability of RA is a limiting step for fully understanding the effects of RA on cell development using an *in vitro* system. To investigate the interactions between Raldh2, Cyp26a1 and RA *in vitro*, a durable, stable concentration of RA is required to ensure that any results observed are not due to uncontrolled degradation and isomerisation of the RA.

Exogenous RA is used to induce neural differentiation *in vitro*, but some protocols use supraphysiological concentrations of exogenous RA, which creates conditions *in vitro* that do not normally occur *in vivo*.⁸⁴ First, the metabolism of supraphysiological concentrations of RA generates *in vitro* concentrations of 9-cis-RA that are not observed in the developing embryo.⁷⁵ It is proposed that dual ligand binding of RA and 9-cis-RA to RARs and RXRs simultaneously, may activate downstream signalling pathways *in vitro* that are only activated *in vivo* in response to teratogenic concentrations of RA.⁷⁵ Experiments on RXR antagonism in

mouse embryos demonstrated that 9-cis-RA is not required for embryogenesis, therefore, the high concentrations of 9-cis-RA *in vitro* are likely activating off-target signalling pathways that are not involved in cell development.^{75,76} Second, supplementing supraphysiological concentrations of RA to the culture medium exposes all of the ESCs to high concentrations of RA, whereas *in vivo*, the concentrations of RA are tightly regulated to prevent teratogenicity and for the correct cell fate specification.⁸⁴ One study compared mouse ESCs treated with 25 nanomolar (nM) or 1 micromolar (μ M) RA *in vitro*, and showed that compared to a concentration of 25nM of RA, supplementing 1 μ M of RA downregulated Fgf8, upregulated Cdx1, and upregulated Wnt8a agonists. These genes are involved in neural plate patterning and their altered expression in response to high concentrations of RA points to a mechanism of forced neural differentiation *in vitro*, that may rely on off-target pathways not normally activated during development.⁸⁴

1.4 Specification of the dorso-ventral neuraxis

1.4.1 Retinoic acid in the ventral spinal cord

RA is essential for the specification of the dorso-ventral neuraxis.³¹ Hox genes are a direct downstream target of RA signalling, and cross-repressive actions between Hox genes are responsible for defining rhombomere boundaries, specifying progenitor domains and determining cell fate specification.^{63,64,66,79} Within the ventral neural tube, there are five progenitor domains (p0, p1, p2, pMN, p3) that generate the MNs and interneurons of the ventral domains of the spinal cord (v0, v1, v2, sMN, v3). The identities of these progenitor zones are defined by their expression of homeobox domain (HD) and basic-helix-loop-helix (bHLH) proteins.^{31,85} Okada et al., (2004) reported that EBs treated with low levels of RA express a midbrain-hindbrain HD protein profile, whereas EBs treated with high levels of RA express a rostral spinal cord Hox profile.³¹ RA induces the expression of paired box protein Pax 6 (Pax6), which subsequently interacts with homeobox protein Nkx6.1 to upregulate expression of Olig2, a marker of MN progenitor cells. The cross-repressive interactions between HD proteins Pax6 (class I) and Nkx6.1 (class II) are required to establish the MN progenitor domain, and subsequently for the generation of the diverse population of mature MNs.⁸⁶

1.4.2 Sonic hedgehog in the ventral spinal cord

Shh is a ventralising morphogen expressed from the notochord and floor plate, and is necessary for the specification of dorso-ventral identity in the ventral spinal cord.⁸⁷ Shh actions are transduced via Smoothed, the signal transducing subunit of the Shh receptor. Shh pathways regulate the expression of bHLH and HD proteins in ventral progenitor domains, which in turn regulate patterned differentiation of the dorso-ventral axis.^{87,88} The differentiation and specification of MNs during embryogenesis is induced by the interaction of the neuralising effects of RA and the ventralising effects of Shh.^{12,47} RA works in combination with the Shh to regulate expression of HD and bHLH proteins that define ventral progenitor domain identity and the subsequent differentiation of spinal MNs.^{31,60}

1.4.3 Establishing the progenitor domain boundaries during development

HD proteins can be divided into class I and class II transcription factors. The cross-repressive interactions of these transcription factors establishes progenitor domain boundaries.^{60,89} The combined actions of RA and Shh regulate ventralisation of the neural tube through their actions on class I and II genes: RA signalling activates expression of class I genes and inactivates expression of class II genes, Shh signalling activates expression of class II genes and Shh is repressed by the actions of class I genes.^{31,87} As class I genes are repressed by Shh signalling, this permits increased signalling of class II genes, which are further activated by Shh signalling.^{31,87,90} This feedforward induction of HD proteins drives a gradient of Shh signalling throughout the ventral spinal cord, such that the actions of Shh on class I and II proteins defines the ventral and dorsal limits of progenitor domains (see Figure 1).

1.4.4 Subtypes of motor neurons in the central nervous system

The CNS is host to a diverse range of MNs with distinct identities that correspond to their position along the spinal cord. MNs are a well characterised class of neurons, both molecularly and functionally, thus are commonly studied *in vitro* as a paradigm for investigating nervous system development and disease.⁷² The differentiation pathways for MNs are well-defined, and *in vitro* protocols for MN differentiation are robust and reproducible. MNs are unique in that their cell bodies remain with the CNS, but their axons project to targets in the peripheral nervous system.⁹¹ All MNs arise from the pMN progenitor domain and become

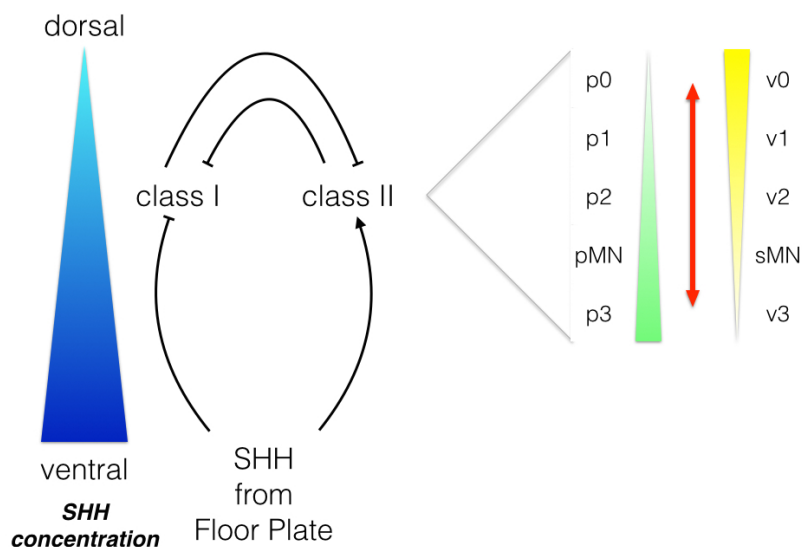


Figure 1: Formation of the Shh gradient in progenitor domains. Shh signalling from the floor plate represses class I HD proteins, and activates class II HD proteins. Class I and class II HD proteins repress each other, and this cross-repressive inhibition establishes the progenitor domain boundaries in the ventral neural tube. Red arrow: cross repressive interactions between class I and class II HD proteins; yellow gradient: class I transcription factors; green gradient: class II transcription factors)

refined into subclasses according to the location of their cell body within the spinal column.⁸⁷ The subclasses of MNs correspond to their columnar, divisional and motor pool identities, which in turn are dependent on the target muscle of their axonal projections.^{60,72} Groups of MNs sharing axonal projection targets cluster together to form five columnar identities, spread along the rostro-caudal axis:

- Phrenic motor column (PMC)
- Preganglionic motor column (PGC)
- Hypaxial motor column (HMC)
- Medial motor column (MMC)
- Lateral motor column (LMC)

PMC MNs are located at the cervical level of the spinal cord and are required for innervation of the diaphragm. PGC and HMC MNs are located at the thoracic spinal cord level and innervate the sympathetic ganglia and the abdominal musculature, respectively.^{87,92} MMC neurons are generated along the length of the spinal column and innervate dorsal axial musculature.⁸⁵ LMC MNs, generated at brachial and lumbar levels, are responsible for limb innervation and can be subdivided into divisional and pool identities, lateral LMC (LMC1)

and medial LMC (LMCm), which innervate the dorsal and ventral muscles of the limb, respectively. LMCl and LMCm are further divided into motor pool identities, according to their specific target muscle within the limb, and a vertebrate LMC MN can belong to 1 of ~50 distinct MN subgroups.⁹³

1.4.5 Motor neuron subtype specification *in vitro*

ESCs have been successfully differentiated into MNs *in vitro* by supplementing combinations of RA and Shh to the culture medium.^{24,50,94} Shh is commonly used to ventralise differentiating ESCs into spinal motor neurons *in vitro*. Purmorphamine, HhAg1.3 (a Shh agonist) and SAG (a Smoothed agonist) are cheaper substitutes for full Shh protein in MN differentiation protocols.^{24,58,95,96} The standard *in vitro* MN differentiation protocol, defined by Wichterle et al., (2002), adds exogenous RA and Shh (or Shh substitute) to the culture medium to generate MNs of an MMC identity.⁴⁷ The Wichterle and Peljto (2002) protocol generates 30-50% homeobox protein B9 (HB9)⁺ post-mitotic MNs by EB suspension culture.²⁴ LMC neurons can be generated *in vitro* using RA and Shh (or Shh substitute) and the Hox accessory factor forkhead box protein p1 (Foxp1).^{97,98} Foxp1 is expressed in LMC and PGC neurons, but not in MMC and HMC neurons, thus the expression Foxp1 distinguishes between these MNs populations. High expression of Foxp1 is a marker of LMC neurons, whereas low expression is a marker for PGC, thus allowing distinction between the two Foxp1⁺ MN populations.¹²

Ectopic expression of Hox genes *in vivo* can induce MNs to an alternate motor pool identity, and alter the axonal projections of the newly programmed MNs.⁹³ Depleting *Raldh2* from the paraxial mesoderm induces a 50% decrease of RA in the spinal cord, leading to a reduced number of LMCl neurons but only a small decrease in the total number of MNs.⁶⁹ This indicates that in the absence of RA, LMCl MNs differentiate toward another MN subclass, either due to the lack of RA-induced transcription factor activity or the de-repression of transcription factors usually inhibited by RA. *Raldh2*^{-/-} mutants treated with exogenous RA display disorganised brachial LMCs.⁶⁵ Ricard et al., (2013) reported that MNs derived from *Cyp26a1*^{-/-} ESCs using the standard RA and Shh protocol were induced toward a PGC/LMC columnar identity, rather than an MMC identity.⁸⁵ These findings indicated that an increased level of RA signalling induces a shift in Hox gene expression, which in turn affects the columnar, divisional or pool identity of the cell. This offers a potential avenue for patterning ESC

.....
 differentiation to generate a mixed population of LMC and MMC MNs *in vitro*.

These studies indicate a changing role for RA in cell fate specification during sequential stages of development. In the early stages, RA is responsible for patterning the rostro-caudal axis and in combination with Shh, establishing ventral progenitor domain boundaries.^{31,72} Later in development, RA is involved in the specification of the dorso-ventral axis - RA is required for Pax6 activation, and indirectly for Olig2 expression in MN progenitors, and subsequently influences the identities of the mature MNs generated by these Olig2⁺ progenitors.^{50,90,99} By exploiting the effects of RA and Shh *in vitro*, the controlled exposure of ESCs to both morphogens can pattern their differentiation towards a desired MN fate.

1.4.6 Lateral motor column motor neurons produce retinoic acid *in vivo*

LMCm MNs are identified by their expression of Raldh2, the major RA synthesising enzyme.¹⁰⁰ During limb innervation, the Raldh2 in LMCm synthesises RA and this source of retinoids determines cell fate specification of the later differentiating LMCl MNs.⁷² Early in differentiation, all LMCs express Isl1 (a marker for LMCm MNs) and as LMCl MNs differentiate, they are exposed to RA produced by LMCm MNs, at which point Isl1 is downregulated and Lim1 is upregulated to specify an LMCl fate. RA also serves as an axonal guidance signal for the LMCl MNs, which follow the axonal trajectories of the earlier differentiated LMCm to innervate their target muscles.^{12,90,97} RA signalling in LMCl MNs activates a cross-repressive interaction between Isl1 and Lim1 in both LMCl and LMCm MNs, which subsequently determines the medial position of LMCm and lateral position of LMCl MNs in the spinal cord.⁷² The LMC MN-derived RA signal is independent of the earlier RA produced by the paraxial mesoderm: Raldh2 is first expressed at E7.5 and is maintained up to E10.5, at which point, Raldh2 is downregulated until it reappears at E12.5, during differentiation of limb-innervating LMC MNs.¹⁰⁰⁻¹⁰²

1.4.7 3D cell culture - a paradigm shift

Since mouse ESCs were first isolated, they have provided researchers with a rapid method to investigate cell development *in vitro*.¹⁶ ESCs and ESC-derived cell lines are useful tools for probing new areas of research or testing theories of development.^{15,16} Despite the advances that have been made using ESC lines and available differentiation protocols, there is still a limited understanding of the mechanisms and processes involved in cell development

and differentiation.^{103,104} A major barrier to our understanding of nervous system development is the reduction of the intricate *in vivo* process of development into the simplified two-dimensional (2D) paradigms used *in vitro*. 2D cell culture removes many physiological components of the cell niche, including the cell-matrix interaction, ability to migrate into multiple planes, and formation of long-range signalling gradients.^{1,2} This over-simplification inhibits the potential to recreate cell processes *in vitro* that precisely mimic their *in vivo* counterparts, including migration into multiple planes, responding to gradients of soluble factors and cell-matrix interaction.^{3,105} Our lack of knowledge drives the need for novel, adaptable and more complex *in vitro* platforms that we can use to investigate cell differentiation, the pathophysiology of disease and the mechanisms of tissue regeneration.^{106,107}

In 2006, a landmark study by Engler et al., demonstrated that human mesenchymal stem cells (MSCs) responded to the substrate stiffness of the biomaterials that they were cultured on. In their experiment, they cultured human MSCs on inert polyacrylamide scaffolds with a substrate stiffness of 0.1-1 kilopascals (kPa), or a substrate stiffness of 34kPa. Their results showed that the MSC/cytoskeletal interaction was important for determining cell fate.⁶ The mechanosensitivity demonstrated by the Engler study represented a turning point for investigating the processes of cell development *in vitro* and posed some important questions for tissue culture research. If tissue culture plastics have a substrate stiffness in the gigapascal range,^{2,35} this raises the question of how suitable the cell microenvironment provided by tissue culture plastics is for recreating the *in vivo* microenvironment?¹⁰⁸

3D cell culture aims to address these questions, and the limitations associated with traditional 2D cell culture, by combining *in vitro* cell culture protocols with 3D biomaterial scaffolds.¹⁰⁹ In doing so, 3D cell cultures can generate novel platforms for investigating cell behaviours *in vitro* that more closely resemble and recapitulate the conditions cells experience *in vivo*. These approaches hold the potential to improve our understanding of the temporal and spatial processes involved in creating the vast diversity of cell types in the body.¹¹⁰ The cell microenvironment or cell niche is comprised of ECM, a complex structural architecture of fibrous proteins, proteoglycans, glycosaminoglycans and soluble factors.^{44,105,111,112} In their physiological microenvironment, all cells are surrounded by ECM, which informs the cell about its environment.¹¹³ Cell-ECM interactions are involved in a range of cell processes including gene transcription, cell migration, patterned differentiation, and cellular regeneration.⁶ 3D cell culture platforms aim to recreate some, if not all, of the complexities of the cell

niche by providing culture conditions that recapitulate the substrate stiffness, binding sites, and signalling cues present in cells physiological microenvironment.^{86,105,106} For each of the cell types in the body, the cell niche and available signalling factors vary both temporally and spatially, thus creating these environments in the dish is difficult to achieve.^{3,114} The challenge for 3D cell cultures is to tightly control the *in vitro* environment, by providing culture conditions that mimic the *in vivo* cell niche, whilst also limiting the number of uncontrolled factors present in the experimental paradigm, so that we can gain high quality information from the results.

1.5 3D cell culture for investigating cell development

1.5.1 Biomaterials as a platform for recreating the extracellular matrix

Each cell type has a specific ECM and the interaction between the cell and the cell-specific ECM is responsible for directing cell fate specification.¹¹¹ The chemical, structural and mechanical composition of an ECM interact to provide the essential cell microenvironment to induce the desired cell fate, at the correct temporal and spatial point in development.¹¹⁵ The three components are interlinked, with the chemical and structural composition influencing the specific substrate stiffness (i.e. mechanical strength), and the chemical composition defining the porosity and topography of the ECM. ECM provides a structure for cell anchorage, supports cell-cell interaction and cell migration, and provides guidance cues to stem cells through the precise release of sequestered signalling morphogens.^{3,44,105}

The ECM influences cell fate specification by temporally or spatially controlling the activation and inactivation of signalling pathways.⁴⁴ Tight regulation over the morphogenic cues, cell adhesion factors, signalling gradients, and cross-repressive interactions between soluble factors that are available to cells within a given cell niche, are ultimately responsible for generating the diverse cell populations in the body.^{44,103,112} Understanding the integration of chemical, structural, and mechanical signals provided by the ECM, and their influence on cell fate specification can inform researchers about the processes involved in cell development.^{17,116} 2D and EB suspension protocols have provided valuable insight into the mechanisms of cell development, but a dynamic and complex 3D platform that can recapitulate the ECM will generate more physiologically relevant information.^{29,117} These 3D systems should be capable of providing cell-cell and cell-matrix interactions, and of supporting long-term cell culture such that the influence of the cell niche over long periods can be

investigated *in vitro*.¹¹⁸

1.5.2 Using 3D biomaterials for stem cell culture

A biomaterial's chemical and mechanical composition are important characteristics to consider when developing a 3D platform.¹¹⁵ The substrate stiffness is strongly linked with cell fate specification, therefore to provide an *in vitro* system for examining physiological cell behaviours, the culture conditions must first provide a substrate stiffness to mimic the ECM. Tissue culture plastic is the most frequently used material for *in vitro* culture, but is a suboptimal material for recreating the native ECM.¹⁰³ As mentioned earlier, tissue culture plastic has an elastic modulus in the gigapascal range, which is similar to the *in vivo* stiffness of bone but much higher than the stiffness of the ECM and basement membrane.^{2,35} The Engler study demonstrated substrate stiffness is a critical factor in cell development, thus recreating the complex *in vivo* mechanisms of cell development in a dish requires a new approach.

A biomaterials approach concentrates on building 3D platforms from natural, synthetic or ECM biomaterials to mimic the *in vivo* microenvironment and promote cell behaviours typical of the physiological environment.^{9,14,110,117} A secondary aim of these platforms is that the 3D scaffolds provide the optimal microenvironment for the mature cell population, thus as the ESCs differentiate, the mature populations experience a microenvironment similar to their *in vivo* counterparts.¹¹ Each biomaterial has advantages and limitations, and the specific application for which a biomaterial can be used for depends on the biomaterial composition and the aims of the experiment.³ Naturally derived biomaterials are inherently biocompatible, whereas synthetic biomaterials allow greater control of the batch-to-batch consistency and over the composition of the scaffold.^{2,3,119} More recently, hybrid biomaterials have been formed from combinations of natural and synthetic biomaterials to exploit the advantages of both and create highly-tuned 3D microenvironments for *in vitro* research.

1.5.3 Naturally-derived biomaterials

Many studies have used naturally-derived or ECM-based proteins as biomaterial scaffolds, including laminin, fibronectin, collagen, fibrin, and hyaluronic acid.^{4,117,120} ECM-based proteins are used in 2D cultures to support cell attachment to glass coverslips or tissue culture plastics, however they can also be layered to form 3D scaffolds or used to functionalise biomaterials that do not contain inherent cell binding sites, to support cell-matrix interac-

.....

tions in those scaffolds.^{4,105} These materials are derived from animal or plant tissues and are inherently biocompatible, making them an ideal substrate for cell encapsulation and 3D cell culture.^{3,111} Naturally-derived scaffolds are inherently biocompatible and easy to produce but they often have batch-to-batch variability, in animal-derived materials due to the gender, age or health status of the originating animal-, or in plant-derived materials due to the species and methods of processing or isolation.^{3,121} These variations can be problematic for reproducing experimental protocols, and have implications for controlling the outcomes between experiments and between research labs.

Animal-derived biomaterials

Animal-derived scaffolds including collagen, fibronectin, fibrin, and hyaluronic acid can be used to create 3D cell culture platforms *in vitro*^{105,122} or used to functionalise non-adhesive scaffolds to allow cell attachment.^{4,111} Kothapalli and Kamm (2013) investigated the effects of different naturally-derived biomaterials on the differentiation of mouse ESCs into neuronal and glial lineages in 3D culture compared to 2D culture. Their results showed that collagen-I, laminin, Matrigel and gelatin promoted significantly higher neural differentiation and significantly higher neurite outgrowth of mouse ESC-derived EBs relative to EBs differentiated by suspension culture.⁹ Another study showed that collagen/Matrigel scaffolds were suitable for ESC-derived EB differentiation to cardiac cells, and showed that the 3D culture of EBs was capable of inducing cell migration out of the EBs and into the surrounding scaffold.³⁰ Matrigel is composed of laminin, collagen and growth factors, and is commonly used for cell culture however it is a poorly defined biomaterial that suffers from batch-to-batch variability, that contributes to variations in the concentrations of growth factors within the biomaterial, and this in turn limits the ability to determine which signals are involved in the cellular responses observed and reduces the ability to replicate those effects across experiments.^{2,4} Of interest, decellularised EBs have been used to investigate 3D cell behaviours and the results showed that the EB-derived scaffolds supported mouse ESC proliferation and earlier differentiation of the seeded ESCs relative to standard EBs.¹²³

Plant-derived biomaterials

Plant-based biomaterials such as alginate, agarose, cellulose and silk are used for 3D cell culture, and can be combined with ECM-based proteins to promote cell attachment and

cell-matrix interactions.^{3,105,124,125} The advantages of plant-based materials over animal-derived materials are that plant-based materials are more well defined. Some animal-derived materials, such as Matrigel, are not fully defined and can have uncontrolled or unknown effects on the behaviour of the encapsulated cells.¹¹⁶ Given that 3D cultures will induce novel cell behaviours due to cell-matrix interactions, the ability to limit uncontrolled effects by using plant-based materials offers a distinct advantage over animal-derived counterparts. Cellulose is the most abundant naturally occurring glucose-based polymer and can be derived from natural fibers. As it is plant-based, cellulose is naturally cytocompatible, and an added advantage of cellulose scaffolds is their capacity to be enzymatically degraded *in vitro* or naturally biodegraded *in vivo* without damaging the encapsulated cells.¹²⁶ Muller et al. (2006) demonstrated that cellulose hydrogels provided a suitable scaffold for cartilage tissue engineering using chondrocytes.¹²⁴ Stenberg et al., (2011) demonstrated that an agarose scaffold could increase EB formation efficiency by 10% and promote a 3-fold increase in the size of EBs formed from human ESCs.¹²⁷ Bozza et al., (2014) demonstrated that 1% weight per volume (w/v) alginate hydrogels conjugated with fibronectin or hyaluronic acid had significantly fewer cells positive for markers of pluripotency, and significantly more cells positive for β -III-tubulin⁺ compared to their EB counterparts.¹¹⁷ These studies provide evidence that plant-derived biomaterials can support 3D cell culture and can be adapted to promote enhanced cell differentiation efficiency compared to the standard EB suspension protocol.

1.5.4 Synthetic biomaterials

Synthetic polymer biomaterials

As an alternative to both animal- and plant-derived scaffolds, synthetic biomaterials provide 3D ECM biomimetics that offer increased control over the composition, internal structure and cell-binding sites available within a synthetic scaffold.^{4,105,128} Synthetic biomaterials are commonly formed from poly-ethylene-glycol (PEG), poly-lactic-glycolic-acid (PLGA), poly-dimethyl-siloxane (PDMS), or combinations of polymers.^{3,4,129} Synthetic biomaterials do not contain any inherent cell binding sites, and this absence of binding sites is both an advantage and a limitation. Although they require addition of cell binding sites to support 3D cell culture, synthetic scaffolds are a ‘blank slate’ on which the complex cell niche required for a given paradigm can be created. As with plant-based scaffolds, the synthetic scaffolds can

be functionalised with animal-derived proteins including collagen and laminin, to provide integrin binding sites and support cell-matrix interactions.⁹⁴ A layered hybrid silk:ECM scaffold functionalised with poly-L-lysine (PLL) was used to produce a model for investigating cell migration across the boundaries between scaffolds.¹³⁰ The study also showed that hybrid scaffolds were superior to hydrogel-only scaffolds, as the hydrogel-only scaffolds collapsed over the course of cell culture and reduced the transport of nutrients, oxygen and waste products through the scaffold compared to the hybrid scaffolds.

Biosynthetic self-assembling peptide biomaterials

Self-assembling peptides are a new form of biomaterial scaffold that are used for *in vitro* cell culture.¹³¹ Self-assembling peptides are formed from chains of hydrophilic and hydrophobic natural amino acids, that spontaneously self-assemble to create nano-fibrous scaffolds for cell culture.^{2,131} Self-assembling peptides are typically high purity, which limits the variability in composition that exists in animal- and plant-derived scaffolds.¹³¹ They are functionalised with ECM-derived attachment factors to increase cell-matrix interactions, and can be designed to provide cell-matrix interaction sites at precise locations along the chains thus allowing enhanced control over cell-matrix interactions that cannot be achieved using either animal- or plant-derived scaffolds.^{2,116,132} Cheng et al., (2013) created an injectable self-assembling peptide that was capable of supporting neural stem cell differentiation, and after injecting the scaffolds into the host spinal cord, they observed migration of the neural stem cells into the host spinal cord and the reduced formation of the glial scar at the location of the injection site.¹⁰ In another study, a self-assembling scaffold increased the formation of EBs from mouse ESCs, and enhanced the subsequent differentiation of the EBs to a neuronal fate.¹³³ When the scaffold was functionalised with the laminin-derived epitope isoleucine-lysine-valine-alanine-valine (IKVAV), the functionalised scaffold further enhanced neuronal differentiation of the EBs, compared to unfunctionalised scaffold.

1.5.5 Hybrid biomaterial platforms

The ability to combine the robust reproducibility of synthetic biomaterials with the inherent integrin binding sites and mechanical properties of a naturally-derived biomaterial are attractive characteristics of a hybrid scaffold.¹²¹ For example, ceramic and alginate hybrid platforms have been created to induce bone and cartilage regeneration.¹³⁴ The synthetic

ceramic provides the substrate stiffness and mechanical composition to support bone development, whereas the alginate top layer provides the softer substrate required for cartilage development. The platforms tested that did not contain the combined hybrid ceramic-alginate environment did not generate cartilage, demonstrating that the cell-scaffold interaction was essential for generating cartilage.¹³⁴ A hybrid alginate:carbon nanotube scaffold was created to control the uneven crosslinking structure observed in alginate scaffolds used to culture.¹³⁵ The results showed that HeLa cells cultured on the hybrid scaffold had significantly higher cell proliferation compared to on alginate alone. Guillaume et al., (2015) reported similar results, with alginate:collagen hybrid scaffolds having enhanced proliferation and ECM deposition by encapsulated MSCs compared to cells cultured on alginate alone.

1.5.6 3D platforms are valuable tools for *in vitro* research

Many studies have used 3D culture methods to investigate the interaction between 3D biomaterials and cell behaviours. For example, one study generated a nanocomposite synthetic scaffold that recreated the native microenvironment and substrate stiffness of mature cartilage, and showed that encapsulated human chondrocytes cultured on the scaffold produced cartilage that mimicked *in vivo* cartilage.¹³⁶ Another study created synthetic RGD-functionalised PEG hydrogels with substrate density gradients on the hydrogel surface, and demonstrated that cell infiltration into the scaffold was dependent on the underlying surface gradients.¹³⁷ Yang et al., (2015) introduced an IKVAV gradient into a PEG hydrogel, and reported that neural differentiation efficiency significantly increased with increasing IKVAV concentration.¹³⁸ Of interest, they observed that mouse ESCs had a temporary decrease in proliferation when switched from tissue culture plastic to the PEG hydrogels, but recovered after 3 days. Similar results were reported by Ali et al., (2015) who showed that mouse ESC behaviour in response to changing substrate stiffness was stage dependent: pluripotent stem cells were capable of recovering and adapting to the new environment but non-pluripotent cells were unable to adapt to 3D culture.¹³⁹ These two studies suggest that the stage of differentiation at the time of encapsulation is important for predicting cell fate specification, and this may be an important factor to consider when designing 3D cell culture experiments and interpreting the results.

A limitation of 2D cell culture is the inability to introduce concentration gradients of soluble factors. 3D platforms address this issue by providing gradients to cells *in vitro* using

biomaterials platforms: biomaterials with incorporated soluble factors, such as growth factors and morphogens, can be used to create concentrations gradients of signalling factors in the scaffold and examine the effects on cell fate.¹⁴⁰⁻¹⁴² Wang et al., (2009) used silk-based scaffolds loaded with concentration gradients of BMP and/or insulin-like growth factor (IGF) to promote differentiation of encapsulated MSCs. They showed that the MSCs had preferential differentiation to osteogenic cell fates in response to high concentration BMPs, and chondrogenic differentiation in response to low concentration BMPs. They also showed that joint IGF:BMP gradients promoted even higher osteogenic differentiation compared to BMP gradients alone.¹⁴³ Wang and Irvine (2011) generated chemokine-loaded alginate microspheres and incorporated these microspheres into cell-containing collagen scaffolds. They investigated the chemoattractive effects on the encapsulated cells and demonstrated that cells migrate towards and made physical contact with the chemokine-loaded microspheres from distances of up to 200 micrometre (μm).¹⁴⁴ These results highlight the benefits of using biomaterial scaffolds for investigating cellular responses to localised signalling factor gradients.

Unfortunately, the current techniques to incorporate growth factors and morphogens into biomaterial platforms either create a homogenous distribution of soluble factors within the scaffold, without any control over the spatial or temporal pattern of releases, or cannot maintain constant concentrations of soluble factors within the biomaterial for extended periods of time. Despite the positive results by Wang et al., (2009) discussed above, microsphere loading efficiency was only 41% and 14% for BMP and IGF, respectively. In addition, they reported a burst release of 40% of the IGF over the first 48 hours (h) of cell culture (there was no burst release of BMP).¹⁴³ Wang and Irvine (2011) reported that 15-20% of the loaded chemokines were burst-released from the microspheres within 4-5h in cell culture.¹⁴⁴ Another study loaded RA into PCL microspheres and then introduced the RA-loaded microspheres into human EB suspension cultures to investigate the effect of localised RA release on the EB differentiation.¹⁴⁵ They reported a burst release of RA at approximately 15% over the first 48h of cell culture, and a cumulative release of 50% of the RA over 28 days in culture, although the remaining RA was sufficient to induce EB differentiation.

Improved systems for incorporating soluble factors within biomaterial platforms are being developed to create stable concentrations and/or gradients of signalling factors. Novel heparin-based delivery systems can incorporate growth factors directly into the biomaterial and maintain stable concentrations over long periods of time. One research group has devel-

oped a heparin-based delivery system to incorporate neurotrophin 3 (NT3), platelet-derived growth factor (PDGF) and glial-derived neurotrophic factor (GDNF) into fibrin based scaffolds, maintaining stable concentrations over long periods of time.^{41,50} An alternative method uses either photoimmobilisation, or click chemistry, to incorporate growth factors into biomaterials.¹⁴⁶ McKinnon et al., (2013) created a PEG hydrogel functionalised with ECM-derived peptides using click chemistry, and showed that their scaffold promoted neurite outgrowth of the encapsulated ESC-derived MNs.⁹⁴ Click chemistry can use covalent binding techniques to incorporate the growth factors or integrin binding sites into a biomaterial, and synthetic and natural biomaterials can both be modified using click chemistry, making this an easy to adopt protocol regardless of the biomaterial used for cell encapsulation.^{147,148}

1.6 Alginate hydrogels for stem cell differentiation

Alginate is a plant-derived biomaterial isolated from the ECM of brown algae.¹⁴⁹ Alginate hydrogels are cytocompatible, tunable and degradable biomaterials that are commonly used as *in vitro* 3D platforms.^{43,117,150} To create an alginate hydrogel, alginic acid is dissolved at the desired weight per volume (w/v) to produce an alginate solution, which is then immersed into a polymerisation buffer containing divalent ions, allowing the solution to crosslink and form an alginate hydrogel.¹⁴⁹ Alginates have a wide range of compositions and structures depending on the plant species from which the alginic acid is isolated, and the properties of a specific alginate affect the type of biomaterial scaffold produced.¹⁵¹

1.6.1 Properties of alginate

Alginate is a linear polysaccharide composed of (1→4) linked chains of β -D-mannuronic acid (M-residues) and α -L-guluronic acid (G-residues). Each chain contains a combination of homopolymer G- and M-residues, and copolymer G-M residues (see Figure 2).^{149,152} The proportion of G-, M- and G-M residues and the G:M ratio determine the characteristics of the resulting hydrogel.¹⁵¹ The factors affected include the viscosity and molecular weight of the alginate solution, the internal porosity, mechanical strength, substrate stiffness, and rate of degradation of an alginate hydrogel.^{5,153,154}

Unmodified alginate hydrogels do not support cell attachment or proliferation, and must be functionalised with ECM proteins such as collagen, gelatin, fibronectin, or laminin.^{149,155} Functionalisation of alginate hydrogels allows cell attachment to the scaffold, promoting cell-

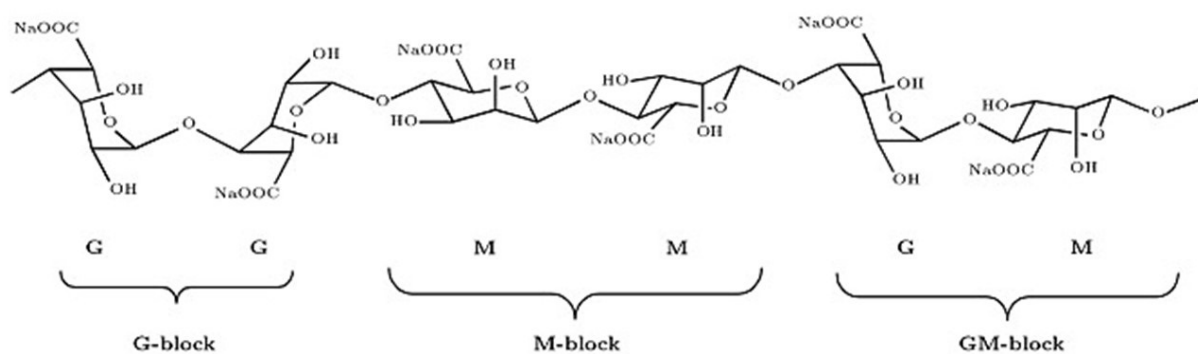


Figure 2: Chemical structure of alginate.¹⁵² Diagram shows the structure of a homopolymer G-residue, homopolymer M-residue, and a copolymer G-M residue of an alginic acid.

matrix interactions, and allowing cell migration, proliferation and/or differentiation of cells either encapsulated inside, or cultured on the alginate hydrogels.^{109,117} Alginate can also be functionalised by adding integrin receptor binding sites within the hydrogels, using ‘click’ chemistry, to guide cytoskeletal organisation and influence gene transcription downstream of integrin receptors, and thus influence cell fate specification.^{4,117,150}

Although alginate hydrogels are versatile and easy to use, their limitations include batch-to-batch variability of the alginic acid powders, instability in cell culture medium over time, and variations in the internal consistency of the resulting alginate hydrogels according to the type of gelation used, the concentration of calcium chloride and the G:M ratio of the alginic acid.^{149,156,157} The gelation process itself requires submerging the alginate/cell solution in a bath of high concentration calcium chloride (1-1.%) for several minutes.¹⁵³ The pore size of the alginate hydrogels can limit the diffusion of larger molecules through the hydrogel, and reduce their interaction with the encapsulated cells. In addition, the negatively charged alginate may prevent positively charged molecules from diffusing through the scaffold.¹²⁰ This is of particular importance for experimental paradigms using an alginate hydrogel for drug delivery/growth factor delivery after scaffold implantation.¹⁵⁸ The following sections outline the interaction of the G:M ratio of an alginic acid on alginate hydrogel characteristics.

1.6.2 Influence of alginate composition on hydrogel characteristics

The molecular weight of an alginate depends on the length and number of the G- and M-residues in the alginic acid, and the viscosity of the alginate solution increases as a function of the molecular weight.^{122,158} The greater the proportion of homopolymer G-residues, the

.....

greater the viscosity of the alginate solution, and the higher the elastic modulus of the resulting hydrogel.^{5,151} The G-residues in the alginate contain the binding sites for ionic crosslinking and contribute to the stiffness and porosity of the hydrogel, whereas the M-residues do not form crosslinks, thus the elastic modulus of an alginate hydrogel increases as a function of the fraction of G-residues.^{5,149,156} Alginate hydrogels are formed by polymerising the alginate solution in a crosslinking buffer containing divalent ions, such as calcium chloride (CaCl_2), magnesium chloride (MgCl_2) or barium chloride.¹⁵⁶ During polymerisation the divalent ions crosslink adjacent G-residues between homopolymer G-G residues and/or copolymer G-M residues. This leads to the formation of a gel network and alginate hydrogels with a higher proportion of G-residues will have a higher elastic modulus and smaller pores, due to the increased number of crosslinks forming between G-residues in the solution.^{5,151,156} The increased number of crosslinks results in a higher substrate stiffness in high-G alginates relative to high-M alginates which can affect cell behaviour. For example, Kandam et al., (2012) showed that umbilical cord derived MSCs encapsulated in G-rich alginate hydrogels had significantly lower viability compared to M-rich alginate hydrogels.¹⁵⁷

The concentration of the crosslinking solution also influences the stiffness of the resulting hydrogel, and even when holding the alginate concentration constant, increasing or decreasing the crosslinking concentration can affect the cell viability of encapsulated cells.^{149,151,157} The greater the proportion of divalent ions available to crosslink, the more G-residues form crosslinks and become saturated, thus increasing the elastic modulus of the resulting alginate hydrogel.^{149,153} The elastic modulus of alginate hydrogels is also increased by increasing the concentration (w/v) of an alginate solution, as there are more G-residues present for crosslinking. Li et al., (2011) reported the elastic modulus of 0.5%, 1.1% and 2.2% alginate as 3.7kPa, 7.35kPa and 13.13kPa respectively.¹⁵⁹ Increasing the concentration of the alginate w/v also increases the viscosity of the solution and affects cell viability.¹⁴⁹ At higher viscosities, alginate hydrogels reduce the viability of encapsulated cells due to the shear forces exerted on the cells during mixing with the viscous alginate solution. This can be overcome by combining low and high molecular weight solutions to form alginate solutions with good structural stability but at a lower viscosity that does not affect cell viability during mixing.¹⁴⁹ The influence of the G:M ratio, molecular weight and viscosity of the alginate solution are thus important factors to consider when choosing an alginic acid, and producing alginate hydrogels for cell encapsulation applications.^{149,151}

.....

Alginate's molecular weight can be reduced by γ -irradiation to break down the G-, M- and G-M residues: this creates shorter alginate chains that have reduced interactions in solution but can still form crosslinks during polymerisation to support the hydrogel structure. The γ -irradiation reduces the molecular weight of the alginic acid and the viscosity of the alginate solution, without affecting the mechanical stability of the resulting hydrogel.^{149,158} The less viscous alginate solution reduces the shear forces on the cells and is therefore more suitable for cell encapsulation. The ability to control the mechanical properties of an alginate hydrogel independently of viscosity is thus an important characteristic of this biomaterial and represents an advantage of using alginate hydrogels for producing 3D platforms.^{154,158} Given the importance of tuning the ECM composition and stiffness to promote differentiation to a desired cell fate, the ability to control many factors of alginate hydrogels makes them an attractive biomaterial for 3D cell culture applications.

1.6.3 Importance of controlling alginate hydrogel porosity

The porosity of a biomaterial scaffold must be sufficient to allow diffusion of oxygen, nutrients and waste throughout the scaffold, whilst simultaneously surrounding the encapsulated cells to provide support and cell-matrix interactions.¹⁶⁰ A study in collagen-glycoaminoglycan scaffolds demonstrated that the porosity of the scaffold influenced osteoblast behaviour, with osteoblasts showing higher infiltration into a scaffold with larger porosity.¹⁶¹ A study in polycaprolactone scaffolds showed that larger pore sizes support chondrocyte and osteoblast growth, but smaller pore sizes supported fibroblast growth.¹⁶²

The porous nature of alginate allows both the diffusion of medium throughout the scaffold and the release of waste products back into the medium. Wang et al., (2009) and Horiguchi et al., (2014) investigated the penetration of soluble factors into alginate hydrogel beads of varying compositions, and both reported that penetration of a soluble factor into the alginate beads decreased as a function of molecular weight.^{150,163} Wang et al., (2009) demonstrated that alginate porosity decreases with increasing w/v of the alginate solution, with pore sizes of 10.9 μ m, 5 μ m and 3.4 μ m in alginate beads of 0.5%, 1% and 2%, respectively.¹⁵⁰ Horiguchi et al., (2014) investigated the diffusion of molecules of increasing molecular weight into alginate capsules of different composition (uncoated, hollow-liquid core, and PLL coated alginate beads). Their results showed that regardless of the alginate composition, the rate of penetration of molecules into the beads decreased with the increasing molecular weight of the

.....

molecule, and that at a molecular weight of 40kDa or more, only 50% of the molecules would diffuse through the alginate beads after 24h.¹⁶³

This property of alginate hydrogel beads represents both a limitation and a technical advantage for cell encapsulation. The inability to use soluble factors of high molecular weight can limit the use of alginate for some differentiation protocols. For example, full length Shh typically used for MN differentiation protocols is approximately 19.8kDa, and based on the results from Horiguchi et al., (2014), less than 75% of this would penetrate alginate beads of 1% w/v at 24h.¹⁶³ On the other hand, given that a major limitation of 2D cell cultures is that cells are exposed to a homogenous concentration of soluble factors in the culture medium, using alginate hydrogels represents an opportunity to introduce gradients of soluble factors by controlling the hydrogel porosity and manipulating the size of the soluble factors.

In knowing that the size of a soluble factor will affect the time taken to penetrate the alginate hydrogel, and that the porosity of the scaffold further influences this diffusion rate, we can manipulate the composition of alginate hydrogels to create gradients of soluble factors. Exploiting these properties may permit spatial and/or temporal exposure of the encapsulated cells to developmental cues, which more closely recreates the *in vivo* environment. For 3D cell culture, the ability to alter many variables of alginate hydrogels means that platforms can be adapted for many cell types and applications. By creating growth factor gradients in 3D, we can closely examine the cell-matrix-gradient, or cell-cell-gradient interactions to identify any effects that the gradient has on cell fate at different points along the gradient or different stages of differentiation.

1.6.4 ESC differentiation in 3D alginate platforms

Alginate hydrogels have been used to promote ESC differentiation into a range of cell types. Studies have differentiated encapsulated ESCs in alginate hydrogels into neurons,^{117, 159} hepatocytes,⁷ motor neurons,¹⁶⁴ and pancreatic Islet-like cells.³⁶ Alginate platforms have been used to develop ESC aggregates *in vitro*, and the results showed that alginate hydrogels prevent the agglomeration of encapsulated aggregates, thus preventing the formation of a necrotic core.^{165, 166} EB agglomeration is a limiting factor for EB suspension cultures as the increased size of agglomerated EBs creates a necrotic core and also reduces the differentiation efficiency of the protocol.^{22, 41-43}

Some studies have developed cell-laden alginate platforms for *in vivo* applications. When

alginate hydrogels are implanted, they protect encapsulated cells from antibodies and antigens within the host tissue.^{150,159,167} Qian et al., (2014) used an alginate hydrogel loaded with gelatin microspheres to demonstrate that the platform could be used as a soluble factor delivery system *in vivo*.¹⁶⁸ Their alginate:gelatin hybrid platform reduced the burst release of growth factors observed in previous platforms. Burst release at 2h was reduced from 30% to 5%, and cumulative release at 1 week was reduced from 95% to 50% in the hybrid alginate:gelatin platform versus the alginate only platform.¹⁶⁸ Another study differentiated encapsulated mouse ESCs into insulin-producing cells that efficiently responded to glucose challenge, demonstrating that the cells behaved in a similar way compared to their *in vivo* counterparts.¹⁵⁰ The cell-laden scaffold could be implanted to provide a source of insulin for diabetic patients that behaves similarly to endogenous insulin. Alginate typically degrades slowly *in vivo* however one study developed an alginate model with incorporated alginate lyase-loaded PLGA microspheres in the scaffold, which provided a controlled method for degrading the scaffold after implantation to the host tissue.¹⁵⁵ The above studies demonstrated that cell-laden alginate scaffolds can be adapted for *in vivo* applications.

1.7 Focus of the current research

The evidence from the literature points to a need for further development of 3D culture platforms to generate more complex systems for investigating the mechanisms of ESC differentiation *in vitro*. For example, the *in vivo* process of development relies on 3D gradients of RA to correctly specify cell fates and progenitor boundary domains, to promote axonal migration and to prevent RA-induced teratogenicity. 2D cell culture protocols cannot recreate these 3D gradients, and cells in monolayer are exposed to uniform concentrations of soluble factors in the medium. The previously described 3D platforms have generate 3D signalling gradients, but their limited control over the concentration of soluble factors, or the use of exogenous RA to induce ESC differentiation, represent limitations of the existing 3D systems.

The primary goal of this PhD project was to develop a novel 3D platform for investigating the patterned differentiation of mouse ESCs to cell fates from the three germ layers using alginate hydrogels. The platform aimed to address the limitations of previous 3D systems by introducing a cell-derived source of RA into the novel 3D platform, thereby providing encapsulated ESCs with a stable concentration of RA that was not prone to degradation or burst release. In the current project, a cell density gradient plus a consequent gradient of

.....

cell-derived RA were incorporated into the 3D platform. The ability to introduce gradients into the scaffold was an important feature of the system as it created a more versatile 3D platform could be adapted for future experiments.

3D cell cultures are important platforms for recapitulating the *in vivo* environment when investigating the mechanisms of cell development *in vitro*.^{4,106} Altering the concentration of an alginate solution, or the concentration of the crosslinking buffer changes the properties of alginate hydrogels, thus these factors can be easily manipulated to design finely-tuned scaffolds for 3D cell culture. However, the G:M ratio of a specific alginate will impact how changes to the alginate or crosslinking concentrations affect the viscosity, internal porosity, elastic modulus and mechanical stability of an alginate hydrogel.¹⁶⁹ Despite the influence of the G:M ratio on the scaffold architecture, no study has conducted a side-by-side comparison of the effects of using alginates of different G:M ratios on the differentiation efficiency of the alginate hydrogels. As a direct consequence of this, there is currently no evidence to support using one type of alginate over another for ESC differentiation.

The present thesis aimed to address this question by investigating the impact of two types of alginate (high G-residue versus high M-residue) on ESC encapsulation and differentiation in 3D hydrogels. The ability to select an optimal alginate subtype for ESC differentiation will contribute to developing more efficient, finely-tuned 3D platforms for investigating cell development. An ongoing challenge in using alginate for 3D cell cultures is that some studies using alginate hydrogels do not report the G:M ratio of the alginate used. Without knowing what type of alginate was used in a given experiment, the ability to reproduce experiments between labs is limited but there are no published studies that demonstrate the importance of reporting the G:M ratio. The experiments described in this thesis aimed to generate strong evidence to support the use of either high-G or high-M alginates when recreating 3D platforms for ESC differentiation. By demonstrating that ESCs encapsulated in alginate hydrogels of different G:M ratio, molecular weight and viscosity are viable, capable of forming aggregates, and by showing that both types of alginate hydrogel remain intact over the course of cell culture, the experiments demonstrate that the G:M composition may not exert significant effects on ESCs. Alternatively, if one (or both) compositions of alginate has a negative impact on viability, does not support aggregation, or does not maintain hydrogel structure during cell culture, this shows that the choice of alginate must be carefully considered before designing a 3D platform for ESC encapsulation.

Previous studies in alginate demonstrated that ESCs can be encapsulated and differentiated in 3D platforms, however, no study to date has investigated if the ESC aggregates formed within alginate hydrogels are EBs containing cells from each of the three primary germ layers. Two studies using alginate hydrogels have investigated ESC differentiation towards the germ layers where the cells were cultured on layers of alginate after the hydrogels were polymerised, but no study has examined the effects of pre-encapsulation of the ESCs on germ layer differentiation within the aggregates.^{165,166} As the foundation for 3D cell culture is the knowledge that cell-matrix interaction significantly affects cell fate, it was possible that the encapsulated ESCs did not differentiate in the same way as ESCs seeded onto pre-polymerised alginate scaffolds. Thus it was important to demonstrate that germ layer differentiation occurred when ESCs were encapsulated, and then differentiated within alginate hydrogels.

This thesis describes experiments to investigate whether the encapsulated ESC-derived aggregates were canonical EBs. The aim of these experiments was to bridge the gap in the available literature by demonstrating that alginate beads are capable of supporting differentiation of canonical EBs, containing cells from the three germ layers. Providing evidence of germ layer differentiation within the alginate hydrogels would increase the utility of the platform to include studies of embryogenesis, germ layer self organisation, ESC differentiation to cell derivatives from each germ layer, or the outcomes of long-term EB culture within alginate beads. In demonstrating the ability to generate cell types from all three germ layers, the experiments show that alginate hydrogels are suitable for experiments differentiating any cell type derived from any germ layer, but conversely, by demonstrating that the encapsulated ESCs will only differentiate one or two of the germ layers, the results provide evidence that this 3D culture method is not suitable for investigating ESC differentiation towards cell fates from the unsupported germ layers. In that instance, the previously described methods of seeding the ESCs onto pre-polymerised scaffolds are optimum for generating cell fates from germ layers not present within aggregates encapsulated within alginate.

1.7.1 Objectives of the experimental chapters

- Chapter 3 aimed to demonstrate that alginate hydrogels are suitable biomaterials for ESC encapsulation and 3D cell culture, and build the foundation for experiments investigating ESC differentiation within the alginate hydrogels.
- Chapter 4 outlines experiments to demonstrate that alginate hydrogels support ESC differ-

.....

entiation to cell fates from the three primary germ layers, and experiments to determine whether high-G or high-M residue alginate hydrogels are optimum for ESC neuronal differentiation, relative to standard EBs.

- Chapter 5 describes experiments to validate a cell-derived source of endogenous RA from HGF11-derived LMC MNs, which can provide a stable concentration of RA *in vitro* over several days.
- Chapter 6 describes the development of a novel 3D alginate platform, for investigating patterned ESC differentiation *in vitro*, generated by incorporating the platform components outlined in Chapters 3-5 using an adapted gradient maker protocol.

1.7.2 Hypotheses

- Hypothesis 1: Alginate hydrogels are a suitable biomaterial scaffold for culturing and differentiating encapsulated ESCs, as demonstrated by the presence of viable cells and markers of embryoid body germ layers within the scaffolds.
- Hypothesis 2: There will be an influence of alginate molecular weight/G:M content on the relative differentiation of encapsulated ESCs towards the ectodermal germ layer as examined using relative gene expression by quantitative PCR.
- Hypothesis 3: Lateral motor column, motor neurons differentiated from the HGF11 ESC line will produce a source of endogenously produced retinoic acid.
- Hypothesis 4: An alginate hydrogel tube containing a gradient of retinoic acid producing cells will induce varying levels of ESC differentiation along the retinoic acid gradient.

Chapter 2. Methods

2.1 Cell Culture

2.1.1 Aseptic cell culture

All cell culture work was carried out using aseptic techniques. Alginate, CaCl₂, forceps, and spatulas were autoclaved. The gradient maker and tubing were decontaminated with 70% ethanol. Cells were cultured in a humidified incubator at 37°C, 5% CO₂. A full list of reagents used is listed in Appendix 1, p.138.

2.1.2 Preparation of tissue culture plates

Mouse embryonic fibroblasts (MEFs) and ESCs were cultured on gelatin-coated tissue culture flasks: 0.1% gelatin solution in Dulbecco's phosphate buffered saline (dPBS) was added to each flask at a sufficient volume to coat the base of the flask. The flasks were incubated for 2h at 37°C, or overnight at 4°C, and washed once in dPBS before seeding cells.

2.1.3 Culture of feeder-free mouse embryonic stem cells

CGR8 mouse ESCs from passage 10-20 were used for alginate characterisation and co-culture experiments. CGR8 are feeder-free mouse ESCs derived from the inner cell mass of a pre-implantation, 3.5 day male mouse (*Mus musculus*, strain 129).¹⁷⁰ CGR8 maintain their pluripotency in the absence of feeder layers with the addition of a high concentration of LIF to the culture medium. CGR8 were cultured in ESC medium composed of Dulbecco's modified eagle medium (DMEM)-high glucose, 10% ES-qualified fetal bovine serum (FBS; Lot No. FB-1001H), 100 units/millilitre (mL) penicillin, 100 microgram (µg)/mL streptomycin, 2 millimolar (mM) L-glutamine, 100µM beta-mercaptoethanol (β-ME), and 1000 units of LIF/mL. Medium was changed daily to maintain pluripotency and ESCs were passaged at a ratio of 1:8 at 80% confluence (~every 2 days).

2.1.4 Passaging cell populations by trypsinisation

To passage the cells, the culture medium was aspirated, the cells were washed once in dPBS, and 3mL or 6mL of 0.25% trypsin:ethylene-diamine-tetraacetic-acid (EDTA; 1X) was added to the T25 or T75, respectively, for 2-5 minutes (min) until the cells detached from the flask.

Trypsin was quenched using an equal volume of culture medium (3mL or 6mL) and the cell suspension was pelleted by centrifugation (5min, 200 relative centrifugal force (rcf)). The supernatant was aspirated, the cell pellet was resuspended in fresh medium, and the cells were seeded at the required ratio into a new gelatin-coated flask.

2.1.5 Culture of mouse embryonic fibroblast feeder layers

MEFs (*Mus musculus*, strain CF1) were cultured as feeder layers for the HGF11 ESC. MEF medium was composed of DMEM-high glucose, 10% FBS, 100 units/mL penicillin, 100µg/mL streptomycin, and 2mM L-glutamine. Cells were passaged at a ratio of 1:2 at 80% confluence (~every 3 days). At passage 6, confluent flasks of MEFs were inactivated with 10µg/mL Mitomycin-C treatment for 2h. After inactivation, the cells were washed 3 times with dPBS, and cultured in MEF medium for up to 10 days, with medium changes every 2 days. MEF medium was replaced with ESC medium 30min before seeding with HGF11 ESCs.

2.1.6 Culture of feeder-dependent mouse embryonic stem cells

The HGF11 feeder-dependent mouse ESC line was a gift from Professor Bennett Novitch, University of California, Los Angeles. HGF11 are a transgenic cell line derived from HB9::Foxp1 transgenic mice. When HGF11 are differentiated to MN fate, the ESCs express green fluorescent protein (GFP) and Foxp1 under control of the HB9 promoter and can be induced toward GFP⁺/Foxp1⁺ LMC MN fate.¹² HGF11 were cultured on MEF feeder layers in DMEM-high glucose, 10% FBS, 100 units/mL penicillin, 100µg/mL streptomycin, 2mM L-glutamine, 1X non-essential amino acids, 100µM β-ME, and 1000 units of LIF/mL. Medium was changed daily to maintain pluripotency and HGF11 ESCs were passaged at a ratio of 1:8 at 80% confluence (~every 2 days).

2.1.7 Separation of embryonic stem cells from feeder layers

The presence of feeder cells in EB suspension cultures reduces differentiation efficiency,¹⁰⁴ so MEFs were separated from HGF11 ESCs before seeding the ESCs for EB culture. After trypsinisation, the MEF-HGF11 cell suspension was pelleted by centrifugation (5min, 200rcf), and resuspended in 5mL ADFNK medium: **A**dvanced **D**MEM-**F**12:**N**eurobasal medium (1:1), 10% **K**nockout serum replacement, 100 units/mL penicillin, 100µg/mL streptomycin, 2mM L-glutamine and 100µM β-ME. This cell suspension was plated onto a gelatin-coated

100mm dish (0.1% gelatin). After 45min, MEFS had adhered to the dish and ESCs remained in suspension. The ESC suspension was aspirated, cells were counted using trypan blue exclusion and used for differentiation experiments.

2.1.8 Embryonic stem cell neuronal differentiation by suspension culture

ESCs differentiated using the EB suspension culture method served as control conditions for alginate bead experiments. ESCs were reseeded at 5×10^4 cells/mL in ADFNK, and the cell suspension was plated onto 100mm suspension dishes and cultured for 6 days, with $1 \mu\text{M}$ RA added on days 2 and 4. To change the medium, the dishes were swirled gently to gather the EBs in the centre of the dish, and the EBs and medium were aspirated into a 15mL falcon tube. The EBs were centrifuged to pellet (3min, 200rcf) and resuspended in 10mL ADFNK supplemented with $1 \mu\text{M}$ RA.

2.1.9 Preparation of laminin-coated coverslips

To prepare laminin-coated coverslips for immunocytochemistry (ICC) and enzyme-linked immunosorbent assay (ELISA) experiments, glass coverslips were added to each well of 12-well plates, and sterilised by ultraviolet irradiation for 2h. Laminin at $2 \mu\text{g}/\text{centimetre (cm)}^2$ in dPBS was added to each well, the plates were placed on a rocker for 15min at room temperature, then incubated at 37°C overnight. Prepared plates were used immediately, or sealed with Parafilm and stored at 4°C for up to 2 weeks. The wells were washed twice with dPBS before seeding cells.

2.1.10 EB dissociation and monolayer culture for immunostaining

On day 6 of differentiation, EBs were collected and dissociated to form a single cell suspension. The EB suspension was centrifuged (3min, 200rcf) to form a pellet, resuspended in dPBS, re-centrifuged (3min, 200rcf) and the pellet was resuspended in 5mL of 0.25% trypsin-EDTA (1X). The EBs were placed on a rocker for 5-10min at room temperature, then 5mL of ADFNK was added to the suspension to dilute and reduce the activity of the trypsin-EDTA. The cell suspension was recentrifuged (5min, 200rcf) to form a pellet, resuspended in 5mL of ADFNK, and passed through a $70 \mu\text{m}$ cell strainer. Cells were counted using trypan blue exclusion, replated at the required cell density onto laminin-coated coverslips and cultured for 2 days in ADFNK supplemented with 5 nanograms (ng)/mL GDNF. After 24h, the cells

adhered to the coverslip and extended neurite processes. On day 8 (48h after replating), cells were fixed for 20min in 3.7% paraformaldehyde (PFA), washed once in dPBS, and the plates were sealed with Parafilm and stored at 4°C until immunostaining.

2.2 Characterisation of HGF11-derived lateral motor column motor neurons

2.2.1 Differentiation of motor neurons from HGF11 embryonic stem cells

HGF11 ESCs were differentiated using the Wichterle and Peljto EB differentiation protocol:²⁴ mouse ESCs were differentiated toward a MN lineage by EB suspension culture, adding 1µM RA and 1.5µM purmorphamine on days 2 and 4; this protocol generates 30-50% MN populations by day 6 of differentiation. On day 6, the EBs were collected, dissociated by trypsinisation, counted via trypan blue exclusion and replated onto laminin-coated coverslips at 1×10^5 cells/cm² for ICC, or at 17.5×10^5 cells/cm² for ELISA experiments (see subsection 2.2.2, p.35). For ICC, cells were cultured for 2 additional days in ADFNK supplemented with 10ng/mL GDNF, then fixed and stored for immunostaining. Control conditions were HGF11 ESCs differentiated with 1µM RA only or CGR8 wildtype ESCs differentiated to MNs using the Wichterle and Peljto protocol.

2.2.2 Quantification of endogenous retinoid concentrations

Competitive ELISAs were used to confirm that HGF11-derived MNs can produce endogenous RA and Raldh2, and to quantify the concentration of RA and Raldh2 released by these MNs into the culture medium. HGF11 ESCs were differentiated as above, and replated at 1×10^5 cells/cm² onto laminin-coated coverslips. The cells were cultured for 6 days after replating (12 days of differentiation) in ADFNK supplemented with 5ng/mL GDNF to enhance the maturation and survival of MNs.²⁴ Half of the medium was changed every 2 days, allowing 48h build up of RA and Raldh2 in the medium before samples were collected for ELISA. Cells were tested on days 8 through 12 to confirm the presence of RA and Raldh2 in the medium at each timepoint.

2.3 Viability Assays

2.3.1 Live/dead assay for alginate beads

Cell viability inside alginate beads was tested using fluorescein diacetate (FDA)/propidium iodide (PI) or thiazole orange (TO)/PI. ESCs were encapsulated in alginate beads and cultured for 6 days. On day 6, the beads were incubated in live/dead buffer for 5-10min in the dark. Live/dead buffer was either 30 μ M FDA and 20 μ M PI (in early optimisation experiments) or 100nM TO and 10 μ M PI (in all subsequent experiments). After incubating for 5-10min, the live/dead buffer was aspirated and the beads were washed once in dPBS. Beads were imaged using a Zeiss Axiovert A1 inverted microscope and Axiovision software (v4.0).

2.3.2 Validation of live/dead assay by flow cytometry

ESCs were used to set up a live/dead assay template for flow cytometry analysis. To validate the assay, 100nM TO and 10 μ M PI were tested on single population of (i) live cells (positive control for TO, negative control for PI) and (ii) dead cells (negative control for TO, positive control for PI). CGR8 were passaged, counted using trypan blue exclusion, and aliquoted at 1x10⁶ cells/mL in dPBS. For dead cell populations, the cells were pelleted and resuspended in 100% ethanol for 15min at room temperature. Live and dead cell aliquots were single labelled with either 100nM TO or 10 μ M PI, and the samples were incubated for 10-20min at room temperature. Cells were analysed using a BD Accuri C6 flow cytometer and C-Flow Sampler software (v1.0). Cell populations were thresholded at 200,000, flow rate was 14 microlitre (μ L)/min, and 10,000 events were collected per condition. Populations were gated for debris using forward and side scatter (FSC vs SSC), and single stained controls were used to gate live/dead populations on FL1 vs FL3.

2.4 Immunofluorescence methods

2.4.1 Cryosectioning embryoid bodies and alginate beads

Alginate beads and EBs were fixed at day 6 of differentiation for 1h in 3.7% PFA, cryoprotected for 4-6h in 30% sucrose solution, embedded in optimum cutting temperature compound (OCT) and stored at -80°C. Samples were sectioned at 15-30 μ M, collected on gelatin-coated microscope slides, dried overnight at 37°C and stored at 4°C. Microscope slides were coated to prevent the negatively charged alginate sections from washing off the slides during im-

munostaining. To apply the coating, standard microscope slides were washed in a 0.2% gelatin:0.02% chromium potassium sulfate dodecahydrate solution; slides were dipped into the solution 5 times for 5s, then air-dried for 1min; this was repeated 5 times. The slides were dried overnight at room temperature. All sections were outlined with an ImmEdge wax pen for immunostaining.

2.4.2 Immunocytochemistry

To prepare cells for ICC all samples were blocked and permeabilised in 20% normal goat serum (NGS) in 0.05% Triton-X-100 for 1.5h at room temperature. Primary antibodies were applied for 1.5h at room temperature or overnight at 4°C. Samples were washed in dPBS (2x10min). Secondary antibodies were applied for 2h at room temperature, and then washed once in dPBS. Nuclei were counterstained with Hoechst 1:25,000 for 10min at room temperature. A full list of antibodies and concentrations used is listed in Table 1. Samples were washed in dPBS (2x10min), double distilled water (ddH₂O) (1x5min), and mounted using Vectashield mounting medium. Samples were imaged using a Zeiss Axioimager A1 fluorescent microscope and Axiovisionsoftware (v4.0). Immunofluorescence negative controls were fixed and stained under the same conditions as experimental samples. Negative control tissues used for immunofluorescent analysis were as follows:

- Negative controls for alginate beads: CGR8 were encapsulated in alginate beads and cultured for 6 days in ESC medium with LIF to prevent differentiation.
- HGF11-derived MN characterisation: HGF11 ESCs were cultured on gelatin-coated coverslips in ESC medium until confluent.
- HGF11-derived MN GFP/FoxP1 validation: HGF11 ESCs were differentiated using 1µM RA only. CGR8 ESCs were differentiated with 1µM RA and 1.5µM purmorphamine toward a MN lineage.

.....

Table 1: Details of antibodies used for immunocytochemistry experiments

Primary Antibody	Supplier	Code	Host	Conc.
α -fetoprotein	Thermo Fisher	PA5-21004	Rabbit IgG	1:200
α -smooth muscle actin	Abcam	ab7817	Mouse IgG2a	1:300
α -smooth muscle actin	Abcam	ab5694	Rabbit IgG	1:300
β -III-tubulin	Abcam	ab41489	Chicken IgY	1:300
β -III-tubulin	Abcam	ab18207	Rabbit IgG	1:300
Foxp1	Thermo Fisher	PA5-52006	Rabbit IgG	1:100
HB9	Santa Cruz	sc515769	Mouse IgG2a	1:200
HB9	Thermo Fisher	PA5-23407	Rabbit IgG	1:150
Nestin	Santa Cruz	sc101541	Rat IgG	1:250
Secondary Antibody	Supplier	Code	Host	Conc.
anti-chicken Alexa Fluor 647	Abcam	ab150171	Goat IgY	1:500
anti-chicken IgY fluorescein	Aves Labs	F1005	Goat IgY	1:500
anti-mouse Alexa Fluor 488	Life Tech	A11001	Goat IgG	1:500
anti-mouse Alexa Fluor 568	Life Tech	A11004	Goat IgG	1:500
anti-rabbit Alexa Fluor 488	Life Tech	A27034	Goat IgG	1:500
anti-rabbit Alexa Fluor 568	Life Tech	A11011	Goat IgG	1:500
anti-rabbit Alexa Fluor 647	Life Tech	A21245	Goat IgG	1:500
anti-rat Alexa Fluor 594	Life Tech	A11007	Goat IgG	1:500
Hoechst 33342, 10mg/ml	Life Tech	H3570	n/a	1:25,000

Abbreviations: Conc, concentration; HB9, homeobox protein B9

2.5 Alginate hydrogels for cell culture

2.5.1 Formation of cell-encapsulating alginate hydrogels

CGR8 were resuspended in 1% w/v alginate:0.1% gelatin at a cell density of 3×10^6 cells/mL alginate. Two molecular weights of alginate were tested: low molecular weight, low viscosity alginate with a high G:M ratio (hereafter referred to as LMW) and high molecular weight, high viscosity alginate with a low G:M ratio (hereafter referred to as HMW). Alginate beads were formed by manually extruding the alginate-cell suspension from a syringe with a 21 gauge (G) needle, into a bath of 100mM CaCl_2 /10mM 4-(2-hydroxyethyl)-1-piperazineethanesulfonic acid (Hepes) (see Figure 3, p.40). The alginate beads were polymerised for 5min at room temperature, washed once with ADFNK, and cultured for 6 days in ADFNK with $1 \mu\text{M}$ RA added on days 2 and 4. Cell density per bead was calculated by dividing the volume of alginate by the number of beads: LMW beads, $\sim 6 \times 10^4$ cells/bead; HMW beads, $\sim 5 \times 10^4$ cells/bead. On day 6, beads and EBs (used as control conditions) were collected and used for depolymerisation experiments, or prepared for cryosectioning (see subsection 2.4.1, p.36).

2.5.2 Depolymerisation of alginate beads

On day 6 of differentiation, alginate beads were collected for depolymerisation to harvest the encapsulated cells. To harvest the cells, scaffolds were depolymerised using a depolymerisation buffer to chelate the CaCl_2 crosslinks inside the beads, allowing the alginate to return to a liquid state. To determine the optimum conditions for depolymerising and harvesting cells, the number of cells and the cell viability for each condition were recorded. Cell viability was tested using trypan blue exclusion or live/dead assay via flow cytometry.

2.5.3 Live/dead viability counts by flow cytometry

The viability of cells harvested from alginate beads was assessed by live/dead assay and flow cytometry. To harvest the cells, the beads were collected using a spatula, washed once in dPBS, and the depolymerisation buffer was added for the required length of time. Once the encapsulated aggregates were released, the depolymerisation buffer was diluted using dPBS, the cell suspension was centrifuged (5min, 200rcf) and resuspended in 1mL dPBS. Cells were double stained using TO and PI, incubated for 10-20min at room temperature and analysed via flow cytometry using a BD Accuri flow cytometer and C Flow Sampler software (v1.0).

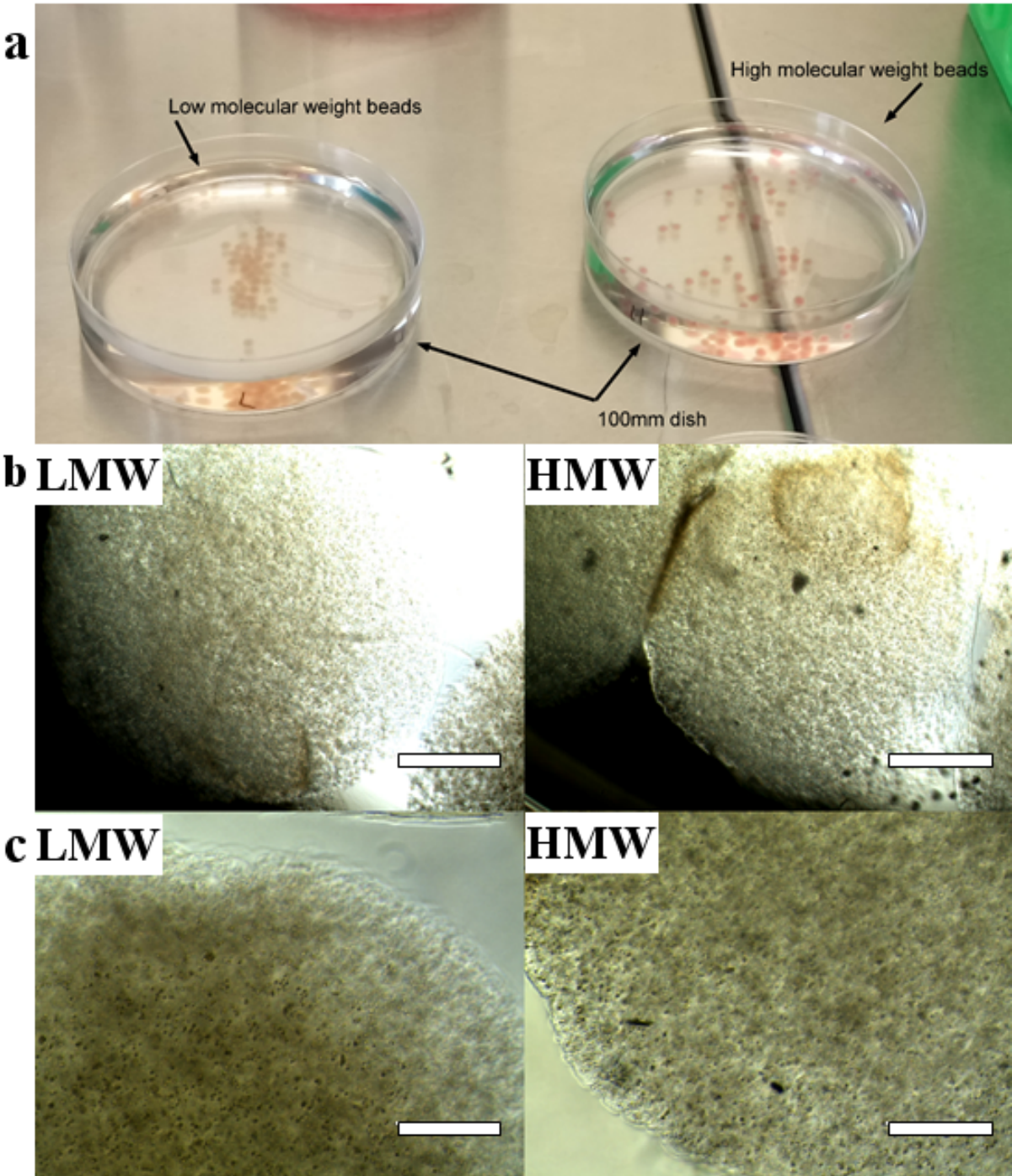


Figure 3: Images of alginate beads with encapsulated ESCs on day 0. The images show alginate beads containing encapsulated ESCs immediately after polymerisation: (a) beads formed from 1mL of alginate:cell suspension by manual extrusion from a 21G needle; (b) low magnification brightfield images of beads after polymerisation; (c) high magnification brightfield images of beads after polymerisation. Scale Bar: (b) 1mm; (c) 400µm

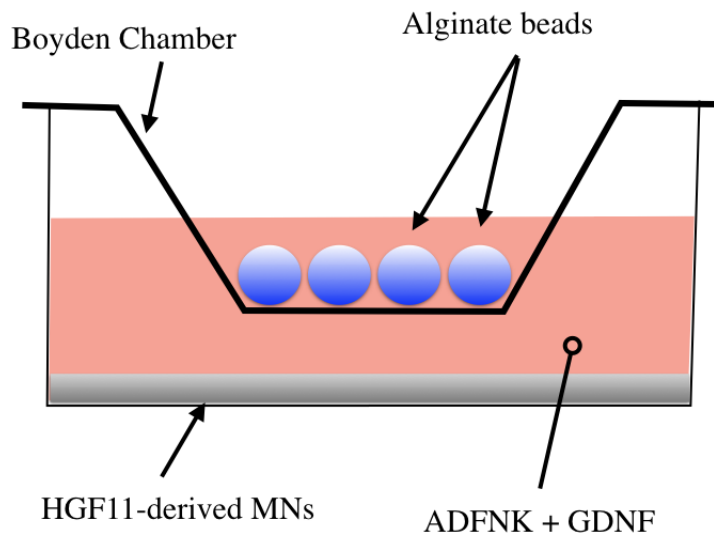


Figure 4: Diagram of the Boyden chamber setup for alginate co-culture experiments. To test the activity of endogenously produced RA, alginate beads were co-cultured with differentiated, RA producing, HGF11-derived MNs. This setup allowed the alginate beads to be cultured in the same medium as the RA without having the beads in close proximity to the mature MNs. The Boyden chamber also allowed easy medium changes every 2 days and easy collection of the beads at the end of the culture period.

2.6 Alginate co-culture

2.6.1 Boyden chamber co-culture

To test the ability of the endogenously produced RA from HGF11-derived MNs to differentiate ESCs toward a neuronal lineage, alginate beads containing CGR8 were co-cultured with HGF11-derived MNs (see Figure 4, p.41). To prepare the co-culture, HGF11 ESCs were differentiated to day 6 as above (see subsection 2.2.1, p.35), and replated onto laminin-coated coverslips in 12-well plates. On the day that the HGF11-derived MNs were replated, alginate beads were prepared (day 0 of alginate differentiation) and transferred into Boyden chambers (8-10 beads per chamber). After 48h (day 2 of alginate differentiation), half of the medium on the HGF11-derived MNs was replaced and each Boyden chamber containing alginate beads was transferred into a well containing HGF11-derived MNs. After 2 days (day 4 of alginate differentiation), half of the medium was changed, and on day 6 (day 6 of alginate differentiation), the beads were fixed, cryopreserved and immunostained for markers of the three germ layers (see subsection 2.4, p.36).

2.6.2 Formation of alginate tubes for co-culture

To investigate the potential for endogenous RA to induce patterned differentiation of ESCs at increasing concentrations, mature HGF11-derived MNs were co-cultured with CGR8 ESCs inside an alginate tube. The tube was created with a standard gradient maker using the setup shown in Figure 5. A simplified colour-coded diagram of the system and a description of the process involved in creating alginate tubes is presented in Figure 6. To create the alginate tubes containing gradients of two cell types, the alginate cell suspensions are loaded into each chamber of the gradient maker (A & B). When the pump was switched on, a volume of alginate from chamber B was drawn into the tubing to form the Leading Edge (L). This simultaneously draws an equal volume of cell suspension from chamber A into chamber B, which was then mixed with the cell suspension in chamber B. In this manner, the cell suspension from chamber A was continuously drawn into and mixed with the suspension in chamber B.

Whilst the tube was formed through the action of the peristaltic pump, the cell suspension in chamber B was diluted with a the cell suspension drawn in from chamber A, such that the Trailing Edge (T) contains a low concentration of cell suspension B and a high concentration of cell suspension A. For this experiment, both chambers had cell suspensions containing equal cell densities of CGR8, and chamber B also contained HGF11-derived MNs. This results in an alginate tube with a consistent cell density of CGR8, and an decreasing cell density of RA-producing MNs along the length of the tube (see Figure 6, p. 44).

2.7 Quantitative polymerase chain reaction

2.7.1 RNA extraction and DNA synthesis

Quantitative polymerase chain reaction (PCR) was used to assess the gene expression of markers for the three germ layers in EBs and in cells encapsulated in alginate beads. Alginate beads were cultured for 6 days (see subsection 2.5.1, p.39), and on day 6, the cells were harvested using 50mM EDTA, 120mM sodium chloride (NaCl) and 10mM HEPES (pH 7.4) for 5min at room temperature. The aggregate suspension and EBs were centrifuged (3min, 200rcf) to pellet, and ribonucleic acid (RNA) was extracted using a Qiagen RNeasy kit, according to the manufacturers instructions. In brief, the cell pellet was resuspended in 200µl RLT buffer and vortexed for 30s to lyse the cells and eliminate ribonucleases (RNase).

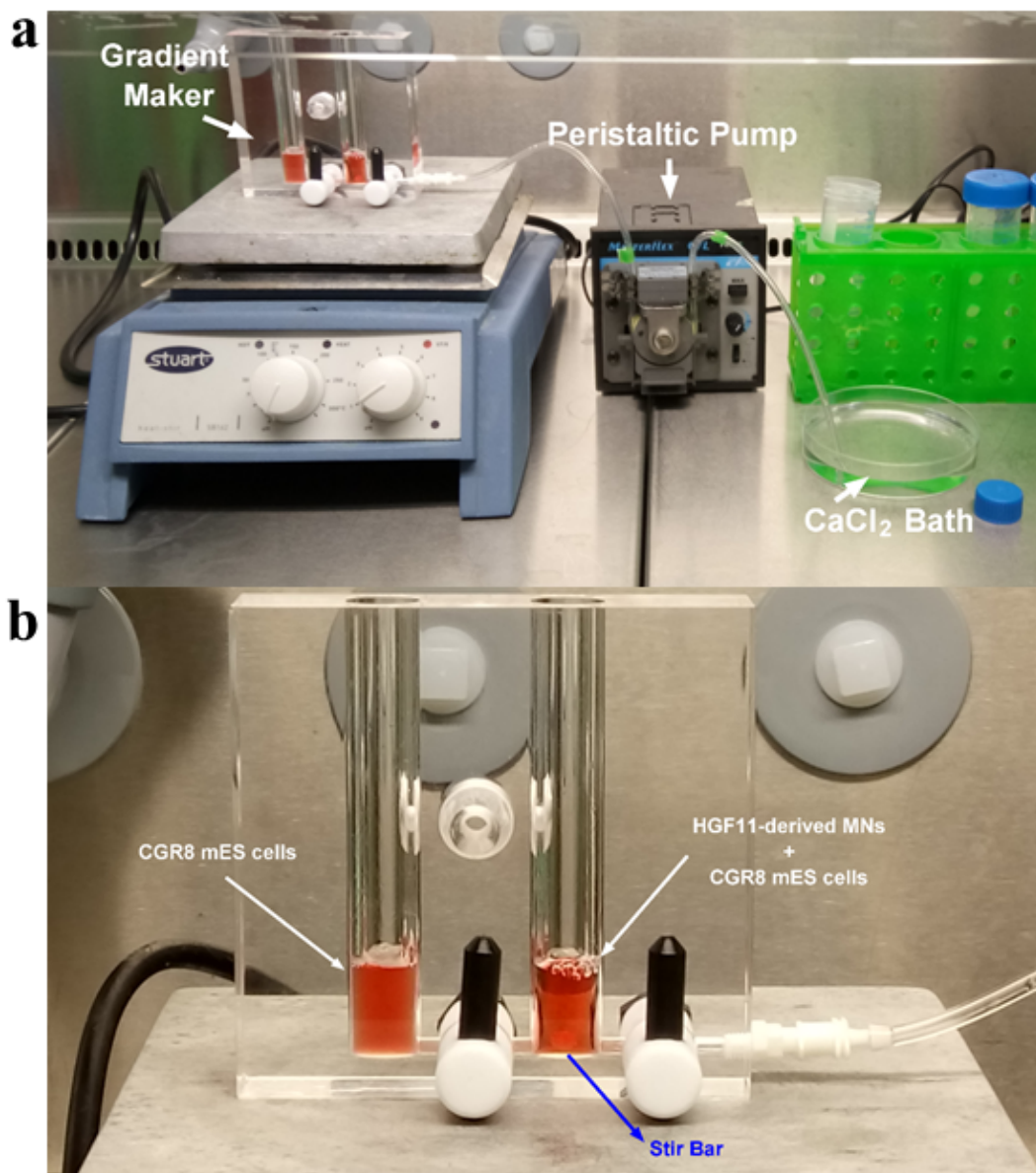


Figure 5: Diagram of a gradient maker and the equipment required to make alginate tubes. The gradient maker was used to form alginate tubes, to test the effect of localised RA concentrations on ESC differentiation: (a) the gradient maker setup and equipment for making the alginate tubes, (b) a close-up image of the gradient maker showing the two chambers containing alginate-cell suspension solutions for forming alginate tubes.

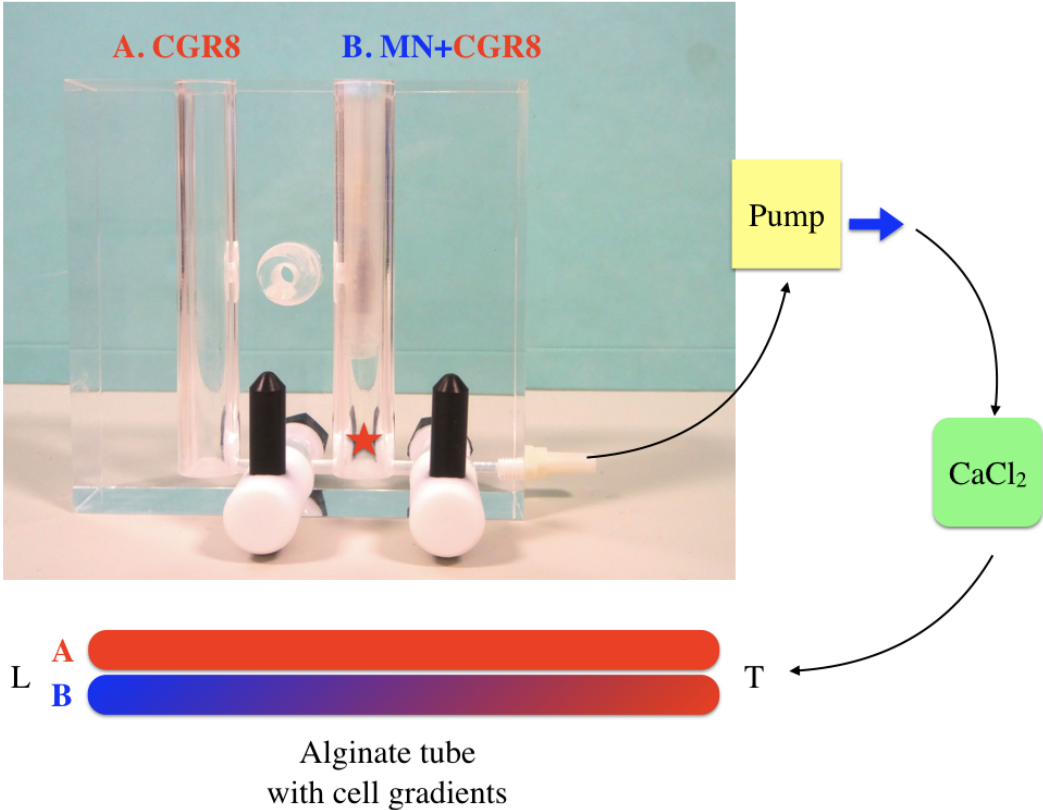


Figure 6: Diagram of gradient formation in the tubes. The gradient was formed from two alginate:cell solutions: (A) alginate containing CGR8 only, and (B) alginate containing CGR8+HGF11-derived MNs. An equal volume of alginate solutions A and B are added to chamber A and B, respectively. The peristaltic pump is switched on and draws a volume of alginate B from chamber B into the tubing forming the Leading Edge (L) of the hydrogel, which has a high concentration of alginate B, and low concentration of alginate A. This simultaneously draws an equal volume of alginate A from chamber A into chamber B, which is then mixed with the alginate B in chamber B by the stir bar (red star). As this process continues, alginate A from chamber A is continuously drawn into and mixed with alginate B in chamber B, and the alginate in chamber B is drawn into the tubing and towards the CaCl₂ where it crosslinks to form a hydrogel tube. The alginate solution in chamber B is continuously diluted with the solution from chamber A such that the Trailing Edge (T) contains a low concentration of alginate B and a high concentration of alginate A. This results in a hydrogel tube containing a cell density gradient similar to that depicted by the blue and red coloured gradients in the diagram. MN: HGF11-derived MNs, CGR8: wildtype ESCs, Red star: location of stir bar.

200µl of 70% ethanol was added to the sample, and mixed gently. This suspension was transferred to an RNeasy mini spin column, and centrifuged (15s, 8000g) to bind the RNA to the column membrane. The supernatant was discarded, and the column was washed once with 700µl, and then twice with 500µl of RPE buffer. The mini spin column was transferred to a fresh 1.5mL eppendorf and 30µl of nuclease free water was added to the column. The column was centrifuged for 1min at full speed to elute the RNA into the collection tube. RNA concentration was measured using a Thermo Scientific Nanodrop 2000 spectrophotometer. RNA samples were stored at -80°C.

Some RNA samples harvested from LMW beads were concentrated using the Qiagen RNeasy MinElute Cleanup kit. In brief, the sample was adjusted to a starting volume of 100µl with nuclease free water. 350µl RLT buffer was added to the sample, and then 250µl of 100% ethanol was added and mixed gently. The suspension was transferred to an RNeasy MinElute spin column, centrifuged (15s, 8000g) to bind the RNA to the column membrane, and the supernatant was discarded. The membrane was washed once with RPE buffer, once with 80% ethanol, and then the column was dried by centrifugation (5min, full speed). The column was transferred to a fresh 1.5mL eppendorf, 12µl of nuclease free water was added to the centre of the membrane, and the column was centrifuged for 1min at full speed to elute the RNA into the collection tube.

The Qiagen Quantinova Reverse Transcription kit was used for complementary DNA (cDNA) synthesis and genomic DNA (gDNA) elimination. For gDNA elimination, 500ng of template RNA and 2µl of gDNA removal mix (containing RNase inhibitors) were added to a 200µl eppendorf. The sample was mixed and incubated for 2min at 45°C. For cDNA synthesis, 1µl of Quantinova reverse transcription enzyme and 4µl of Quantinova reverse transcription mix (containing deoxyribonucleotide triphosphates and Mg²⁺) were added to the template/gDNA reaction. The samples were incubated in a PCR thermal cycler for 3min at 25°C, 10min at 45°C, and 5min at 85°C to inactivate the reverse transcriptase enzyme. To prepare the no reverse transcription controls, the reactions were set up as above but the reverse transcription enzyme was omitted.

2.7.2 Primer validation and efficiency

The primers for POU class 5 homeobox 1 (Pou5f1), Nestin (Nes), Pax6 and β-actin (Actb) were tested in-house using a five point standard curve (see Table 2). The positive control

.....

sample was combined cDNA from EBs and cells harvested from alginate beads (4 EB, 4 HMW, and 3 LMW samples). ESC cDNA was used as the negative control. The quantitative PCR was run using the Qiagen Quantinova SYBR green kit, according to the manufacturer instructions. In brief, 0.75 μ l of cDNA template, 10 μ l of SYBR Green PCR master mix, 2 μ l of QN ROX reference dye, and 1 μ l each of forward and reverse primer (final concentration 0.7 μ M) were added to each reaction, and the volume was adjusted to 20 μ l with nuclease free water. The plates were sealed with a PCR plate seal, mixed for 5min on a plate mixer, and spun with a plate spinner for 30 seconds (s). The thermal cycler conditions were: 2min at 95°C, followed by 40 cycles of 5s at 95°C and 10s at 60°C. Data were collected using an Applied Biosystems StepOnePlus Real-Time PCR system and StepOne Software (v2.3).

Table 2: Primer efficiencies for real time PCR. Primer efficiencies were measured using a 5pt standard curve, on combined cDNA from EBs and Beads. The slopes and efficiencies were calculated using the StepOne Software.

Primer	Slope	r²	Efficiency
Pou5f1	-3.168	0.98	106%
Nestin	-3.126	0.99	108%
Pax6	-3.30	0.99	100%
β -actin	-3.11	0.99	109%

Chapter 3. Characterisation of alginate hydrogels as a suitable scaffold for encapsulating mouse embryonic stem cells

3.1 Introduction

Alginate hydrogels are a commonly used biomaterial for 3D cell culture,^{43,105,117} and have previously been used to encapsulate ESCs and induce cell differentiation to GABAergic neurons,⁴³ insulin-producing cells,¹⁵⁰ and hepatocytes.⁷ Alginate is inherently biocompatible, scalable for high-throughput applications, and allows easy modulation of characteristics such as porosity, elastic modulus, cell adhesion factors and the size/shape of the scaffold.^{43,105,171,172} EBs are used for *in vitro* cell culture experiments to mimic early embryogenesis as they can induce ESC differentiation toward cell fates from the three embryonic germ layers (endoderm, mesoderm and ectoderm).^{19,38,173} EB suspension culture generates high numbers of differentiated cells, however there is limited control over the size of the EBs, the diffusion of signalling morphogens into the EBs, and the efficiency of cell differentiation.

Biomaterials such as alginate offer increased control over the size of EBs and can promote increased differentiation efficiency of encapsulated ESCs.^{43,174,175} Alginate beads have been used to differentiate encapsulated mouse ESCs using RA and studies using these protocols reported that ESCs encapsulated in alginate beads formed cell aggregates, had high viability at the end of the culture period and produced a higher proportion of neurons relative to EB controls.^{43,150,159} To date, no study has demonstrated that the aggregates within alginate beads are canonical EBs comprised of cells from the three germ layers; this topic will be addressed in chapter 4 and to avoid confusion, this chapter refers to the cell aggregates in alginate beads as aggregates, and to cell aggregates formed by suspension culture as EBs.

This chapter outlines experiments to validate and characterise alginate beads of 1% w/v, crosslinked in 100mM CaCl₂ as a suitable biomaterial for mouse ESC culture. These alginate/CaCl₂ concentrations were selected based on the results from previous studies that demonstrated successful ESC encapsulation in alginate hydrogels formed using these conditions.^{43,117,142} Alginate hydrogel beads of different composition and size, and a range of cell densities were tested to identify the optimum conditions for ESC encapsulation and subsequent aggregate formation. The conditions tested in these experiments are listed in Table 3.

Table 3: Alginate conditions tested for optimisation of ESC encapsulation

Variation	Conditions Tested		
Alginate Base Solution	DMEM	ddH ₂ O	
Alginate Molecular Weight	Low	High	
Needle Gauge	21G	30G	
Gelatin Concentration	0%	0.1%	0.5%
Cell Density (cells/mL alginate)	2x10 ⁶	3x10 ⁶	5x10 ⁶

These experiments optimised the conditions for cell encapsulation, assessed whether ESCs within the alginate beads formed cell aggregates, and determined if those aggregates were comparable in size and shape to EBs differentiated by suspension culture.^{17,176} The formation of aggregates inside the beads was assessed by brightfield microscopy, and cell viability was investigated using a live/dead assay. Initial experiments used HMW alginate for cell encapsulation, however following high variations in cell viability in early experiments, a literature review on cell viability in alginate hydrogels was conducted. The review found that alginate molecular weight and viscosity significantly affected cell viability and cell-matrix interactions. Alginates of higher molecular weight produce alginate solutions with higher viscosity and expose cells to shear forces during encapsulation which reduces cell viability.^{154,171,177} All subsequent experiments compared the effects of LMW and HMW alginate for cell encapsulation to assess differences in viability or cell fate between the two compositions.

3.2 Optimising alginate beads for embryonic stem cell encapsulation

3.2.1 Identifying a suitable base for alginate hydrogel solutions

Methods

HMW alginate was dissolved at 1% w/v in (i) DMEM-high glucose, or (ii) ddH₂O, and gelatin was added to each solution at a final concentration of 0.1% v/v. CGR8 were passaged by trypsinisation, pelleted by centrifugation (5min, 200g) and resuspended at a cell density of 5x10⁶ cells/mL in (i) alginate:DMEM or (ii) alginate:ddH₂O. The solution was extruded from a syringe with a (i) 21G or (ii) 30G needle into a bath of 100mM CaCl₂, and polymerised for 5min at room temperature. Beads were washed once in dPBS and cultured for 8 days in ADFNK. 1 μ M RA was added to the medium on days 4 and 6 to induce neural differentiation.

Results

Alginate:DMEM was optimum for embryonic stem cell encapsulation

The formation of cell aggregates inside the alginate beads was compared on day 8 of differentiation. Brightfield images showed that ESCs encapsulated using an alginate:DMEM solution produced large numbers of aggregates in beads formed using both a 21G needle (see Figure 7a) and a 30G needle (see Figure 7b). Cells encapsulated in an alginate:ddH₂O solution formed a small number of aggregates in beads formed using a 21G needle (see Figure 7c) and zero aggregates in beads formed using a 30G needle (see Figure 7d). These results showed that an alginate:DMEM solution was optimum for ESC encapsulation and that an alginate:ddH₂O solution was not a suitable composition.

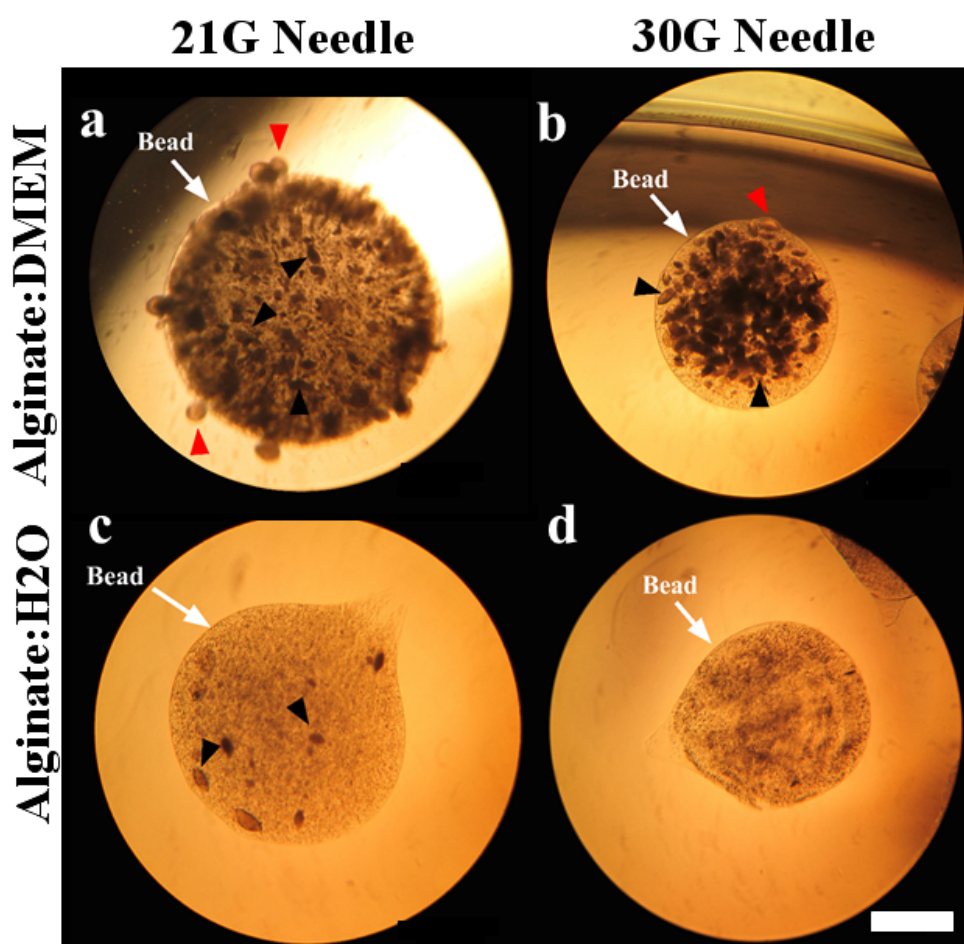


Figure 7: Representative images of aggregate formation by encapsulated ESCs in four alginate bead conditions. Alginate:DMEM beads contain high numbers of aggregates in 21G beads (a) and 30G beads (b). Alginate:H₂O beads contain small numbers of aggregates in 21G beads (c), and no aggregates in 30G beads (d). n=1, 3 beads per condition. Arrowheads: black - encapsulated aggregates; red - escaping aggregates. Scale Bar: 1mm

Encapsulated aggregates migrate out of alginate beads

At day 8 of differentiation, there were cell aggregates floating in the cell culture medium of the 21G and 30G alginate:DMEM conditions, that had migrated out of the alginate beads (see Figure 8a and b). These aggregates were similar in size and shape to EBs formed by suspension culture (see Figure 8c versus d), and were visually indistinguishable from the EBs (8b versus d). The encapsulated aggregates were visible at the edges of the beads and there were striation marks in the direction that the aggregate had migrated from the interior of the beads into the medium. This indicated that the encapsulated aggregates were interacting with the alginate matrix and was evidence that the cell aggregates observed floating in the cell culture medium had migrated out of the beads as whole aggregates, and were not formed from single ESCs that had aggregated within the medium (see Figure 8e).

Conclusion

The aggregate formation observed in this experiment was consistent with previously reported results for ESCs encapsulated in alginate beads.^{43,117} The results indicated that alginate:ddH₂O hydrogels were suboptimal for supporting aggregate formation, compared with alginate:DMEM beads. Previous research reported that alginate solutions formed from H₂O had a 2-fold higher elastic modulus compared to alginate solutions formed in α -minimum essential medium.¹⁷¹ If this was true for alginate:DMEM versus alginate:ddH₂O, the increased elastic modulus may have inhibited ESC aggregation by restricting cell-matrix interactions. The 21G-DMEM condition had a smaller number of escaped aggregates versus 30G-DMEM beads, indicating that they were more suitable for maintaining cell encapsulation during cell culture. The following experiment builds on these results to further optimise the alginate encapsulation conditions by examining the effect of reduced cell density and increased gelatin concentration on aggregate migration from the beads.

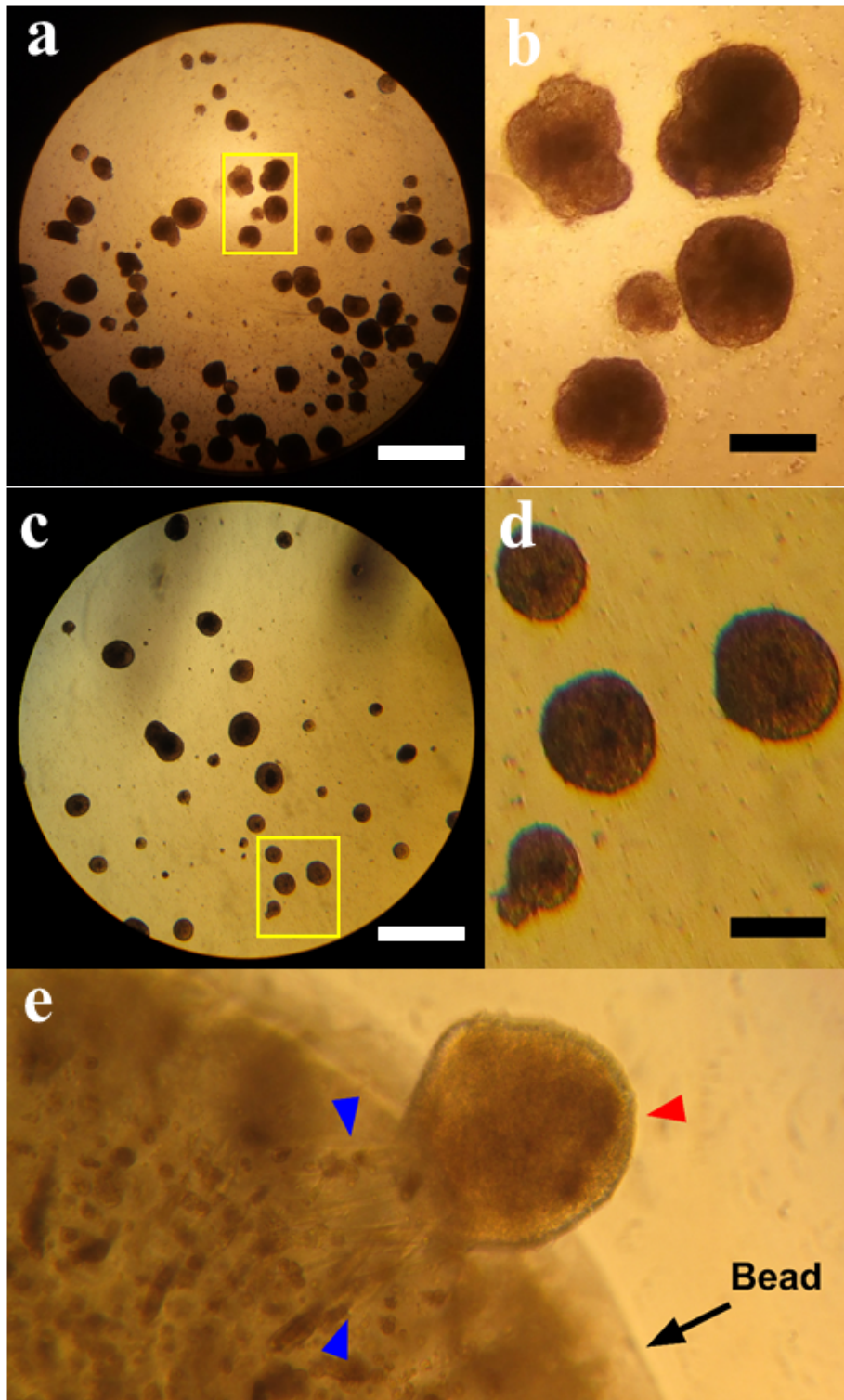


Figure 8: Brightfield images of escaped cell aggregates, EBs and an aggregate migrating from a bead. Canonical EBs (a) were similar in size and shape to cell aggregates that escaped from alginate:DMEM beads (c). Magnified images showed that EBs formed by suspension culture (b) were visually indistinguishable from the free floating aggregates (d). The escaped aggregates migrated out of the beads as whole aggregates, and appear to interact with the alginate matrix, forming striations in the bead (e, blue arrowheads). Arrowheads: red - escaping aggregate; blue - striation marks. Scale Bars: white - 500 μ m; black - 200 μ m

3.2.2 Optimising the seeding cell density and differentiation duration

This experiment aimed to reduce the number of aggregates escaping from the 21G-DMEM beads by manipulating the seeding cell density and gelatin concentrations of the alginate beads. The cell density was reduced from 5×10^6 cells/mL to 2×10^6 cells/mL alginate, based on results from a previous study that reported a cell density of 2×10^6 cells/mL is optimum for maintaining high viability of cells encapsulated in alginate.¹⁵⁰ Alginate does not contain cell adhesion sites and must be functionalised to allow cell attachment and to provide a suitable environment for anchorage-dependent cells.^{105,178} The previous experiment used 0.1% v/v gelatin to support cell adhesion to the alginate. This experiment tested low gelatin (0.1%) and high gelatin (0.5%) concentrations to examine whether increased gelatin concentration could enhance aggregate formation or limit migration of the aggregates into the medium. The previous experiment used an 8 day neural differentiation protocol¹⁷⁶ however Montgomery et al., (2015) reported that a 6 day protocol adding 1 μ M RA at days 2 and 4 was as efficient as the 8 day protocol for neural differentiation.¹⁷ This experiment tested whether this 6 day protocol was sufficient for aggregate formation by ESCs encapsulated in alginate beads.

Methods

HMW alginate was dissolved at 1% w/v in DMEM-high glucose and gelatin was added at a final concentration of 0.1% v/v or 0.5% v/v. CGR8 were passaged by trypsinisation, pelleted by centrifugation (5min, 200g) and resuspended at a cell density of 2×10^6 cells/mL. The solution was extruded from a syringe with a (i) 21G or (ii) 30G needle into a bath of 100mM CaCl₂, and polymerised for 5min at room temperature. Beads were washed once in dPBS and cultured for 6 days in ADFNK. 1 μ M RA was added to the medium on days 2 and 4 to induce neural differentiation. The formation of aggregates was assessed by brightfield microscopy. Data were collected for n=1-2 experiments with 2-3 beads imaged per condition.

Results

Embryonic stem cells formed aggregates at a reduced cell density

ESCs encapsulated in alginate at a reduced cell density of 2×10^6 cells/mL successfully formed aggregates by day 6 of differentiation (see Figure 9). The aggregates were a mixture of circular and tubular shapes, but no aggregates were observed migrating across the edges of

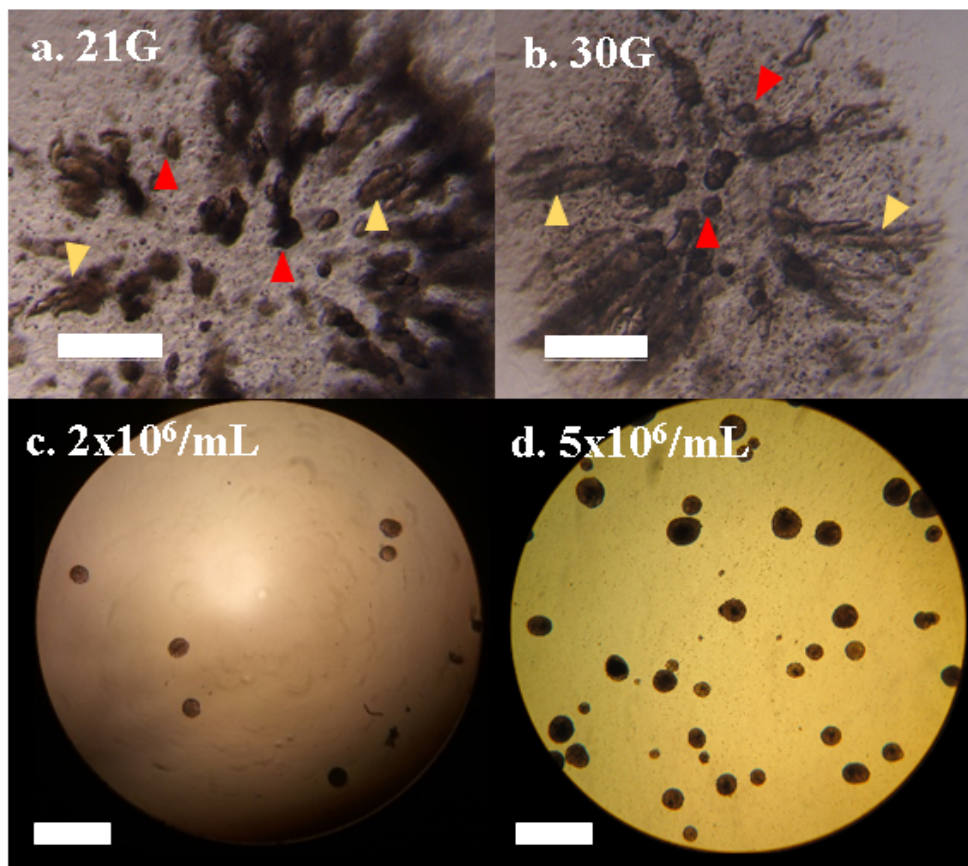


Figure 9: Brightfield images of encapsulated and escaped aggregates at a reduced cell density. ESCs encapsulated at a cell density of 2×10^6 cells/mL formed aggregates by day 6 in 21G (a) and 30G (b) beads. The encapsulated aggregates were circular (red arrowheads), or elongated in shape (yellow arrowheads). There were fewer escaped aggregates at this cell density (c) relative to the higher cell density of 5×10^6 cells/mL (d). Scale Bar $500 \mu\text{m}$

the beads. The number of aggregates migrating from the beads was reduced and very few aggregates were observed in the medium at day 6 (compare Figure 9c and d). This indicated that a lower cell density was optimal for maintaining the cells inside the scaffold compared with the higher cell density of 5×10^6 cells/mL.

Gelatin concentration did not affect aggregate formation

Brightfield images of alginate beads (HMW plus 0.1% or 0.5% gelatin) across 6 days of differentiation showed that aggregate formation was visually comparable between low-gelatin and high-gelatin conditions (see Figure 10). Some beads with low-gelatin conditions appeared to have more aggregates in the scaffold (see Figure 10, D4, 0.1% versus 0.5%), but this was not observed for all beads per gelatin condition. The low-gelatin condition generated beads with rounder aggregates whereas the high-gelatin condition generated more elongated/tube

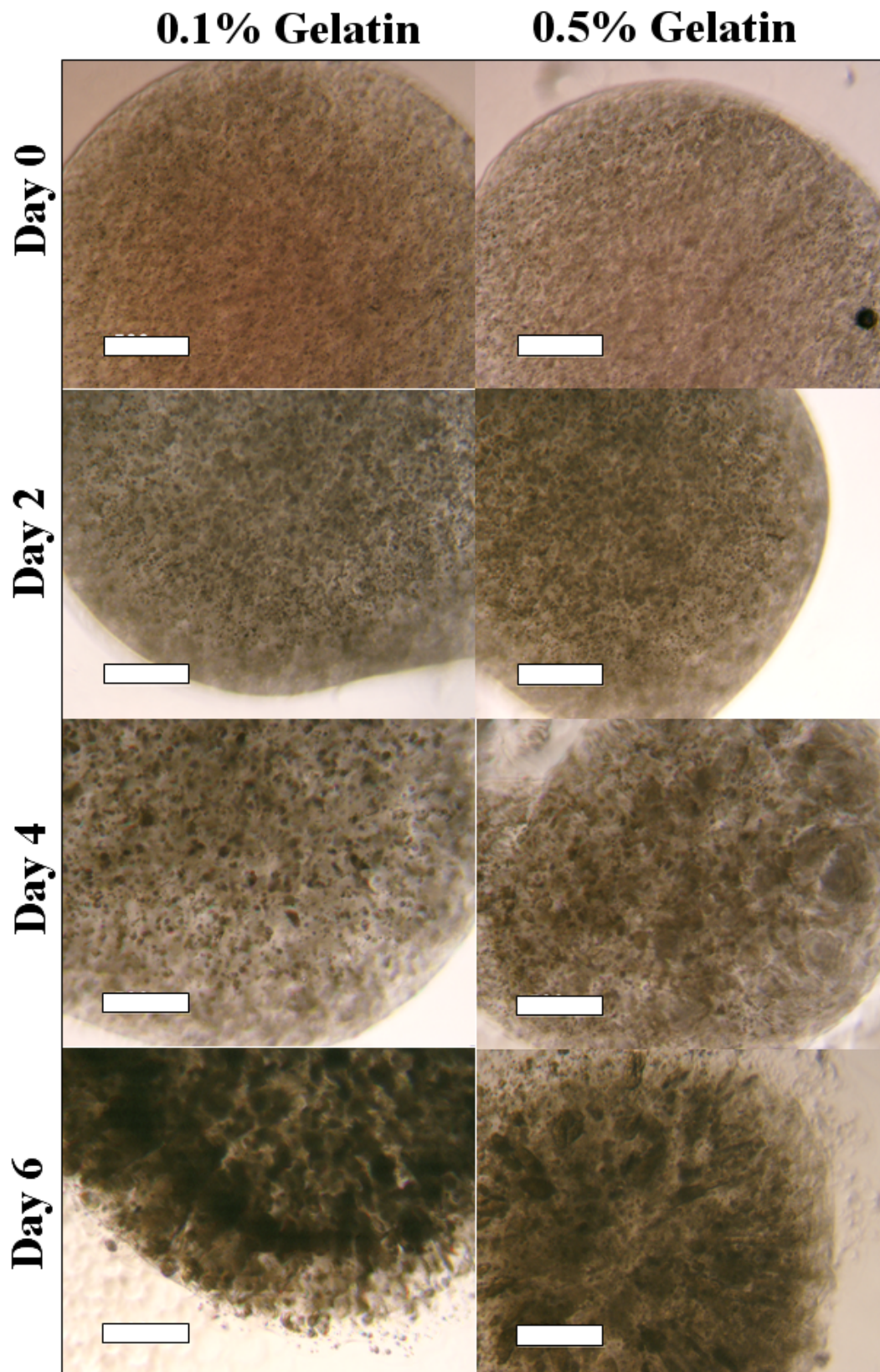


Figure 10: Brightfield images of aggregate formation from ESCs for high and low gelatin concentrations. Aggregate formation was similar across both conditions, with aggregates visible from day 4 of differentiation. Some low-gelatin beads produced higher numbers of round aggregates compared to high-gelatin beads, but this was not consistent across all beads. $n=2$, 2-3 beads per condition. Scale Bar: 500 μ m

shaped aggregates. This difference could be due a change in the porosity of the alginate at the higher gelatin concentration or may represent a different ability of the encapsulated cells to interact with the alginate matrix and form rounded aggregates.

Conclusion

These results showed that a cell density of 2×10^6 cells/mL and a 6 day differentiation protocol were suitable for ESC differentiation within alginate beads. There were no differences in the formation of aggregates between the low- and high-gelatin conditions, thus subsequent experiments used 0.1% v/v gelatin. The encapsulated ESCs successfully formed aggregates by day 6 of culture in all conditions tested, and there were very few aggregates free floating in the medium, indicating that these conditions were more suitable for maintaining the encapsulated cells within the scaffold compared to the conditions in the previous experiments.

3.3 Assessing the viability of encapsulated embryonic stem cells

In the previous experiments, there were some alginate beads that did not contain any aggregates after 6 days of cell culture. This result indicated that there was variability within the beads which affected ESC aggregation. It was possible that an inconsistent cell-alginate suspension resulted in some beads having a cell density below the minimum threshold for cell viability (2×10^6 cells/mL alginate), thus the encapsulated cells did not form aggregates in some beads. Increased mixing of the cell-solution would improve homogeneity, however extended mixing would expose the cells to high shear forces and also reduce viability.^{169,171} As an alternative, in the present experiments the cell density was increased from 2×10^6 cells/mL to 3×10^6 cells/mL alginate. This cell density was chosen to increase the individual bead cell density to maintain cell viability, whilst keeping the cell density low enough to limit aggregate migration out of the beads.

Methods

CGR8 were encapsulated in HMW alginate of 1% w/v in DMEM:0.1% v/v gelatin at a cell density of 2×10^6 cells/mL alginate. Beads were cultured for 6 days in ADFNK and $1 \mu\text{M}$ RA was added on days 2 and 4 to induce neural differentiation. Viability was tested on days 2, 4, and 6. At each timepoint, beads were incubated in 2mL of live/dead buffer ($20 \mu\text{M}$ FDA; $30 \mu\text{M}$ PI). The assay was also carried out using 100nM TO and $10 \mu\text{M}$ PI with similar results.

.....

Data were collected for n=2 experiments, 2-3 beads per experiment. Beads were imaged using a Zeiss A1 Inverted Epifluorescent Microscope using Axiovision software (v4.0).

Results

Cell viability was high in alginate beads

Live/dead assay showed that encapsulated cells contained viable cells over 6 days of culture (see Figure 11). On day 6, larger aggregates contained live cells (green labelled cells) but smaller aggregates contained dead cells (red labelled cells). The cell death in single cells was expected as aggregation is required for cell survival in alginate hydrogels.¹⁷² There was variable aggregation and some beads did not form any aggregates by day 6. The encapsulated aggregates varied in shape from circular to elongated/tubular (see Figure 9). Round aggregates contained dead cells clustered in the center, and elongated aggregates contained dead cells at the tips of the aggregates. These findings were consistent with Wilson et al., (2014), who observed dead cells at the tips of elongated aggregates within alginate beads.¹⁷⁹

Conclusion

ESCs encapsulated in alginate remain viable over 6 days in culture. The viability of aggregates within the beads may be influenced by internal porosity, elastic modulus or alginate molecular weight, thus to examine the effects of alginate molecular weight on cell viability, the following experiments compared aggregate formation by encapsulated ESCs in alginate hydrogels formed from two different types of alginate.

3.4 Embryonic stem cell aggregate formation and viability in LMW versus HMW beads

This experiment examined the effects of two types of alginate on the viability and extent of aggregate formation. The two alginates tested were low molecular weight, low viscosity alginate with a high G:M ratio (60:40), and high molecular weight, high viscosity alginate with a low G:M ratio (40:60). The alginate G-residues contain ionic binding sites, thus a higher G-residue content alginate has a stiffer elastic modulus relative to a low G-residue content alginate due to the increased number of crosslinks present within the structure. The higher number of crosslinks creates alginate hydrogels with a smaller pore size relative to low G-residue content hydrogels.^{149, 156, 177}

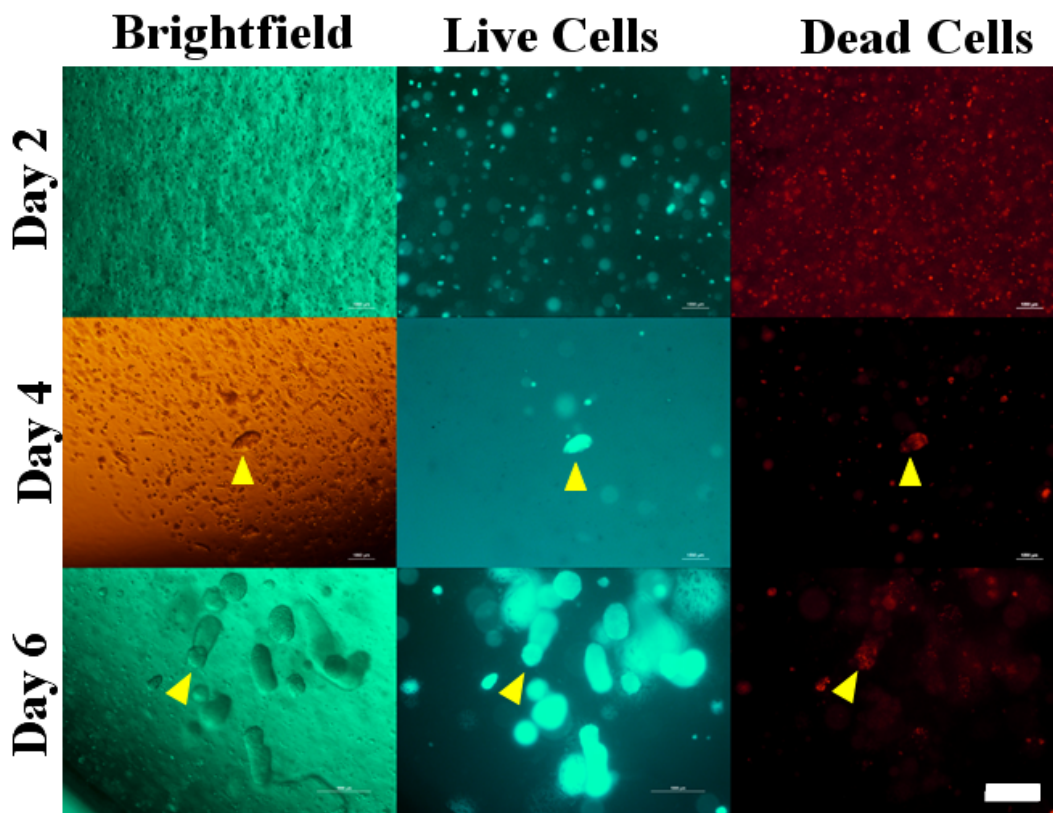


Figure 11: Live/dead assay showed that alginate beads contained viable cells across 6 days of culture. By day 2, there were live and dead single cells within the beads; by day 4, the cells formed aggregates inside the beads; by day 6, there were large numbers of aggregates, containing both live and dead cells (yellow arrowheads). $n=2$ with 2-3 beads per condition. Scale Bar: 1mm

Methods

To investigate the effect of alginate molecular weight on ESC aggregation, LMW and HMW alginate solutions were prepared at 1% w/v in DMEM-high glucose, 0.1% v/v gelatin. Details for the alginates used are listed in Table 4. CGR8 were resuspended in each alginate solution at a cell density of 3×10^6 cells/mL alginate, polymerised and cultured in ADFNK. 1 μ M RA was added on days 2 and 4 to induce neural differentiation. The formation of aggregates was assessed by brightfield microscopy on day 0, 2, 4 and 6 of differentiation. Live/dead assay was used to examine differences in viability between aggregates in the LMW and HMW beads, and to assess the cell viability at the increased cell density of 3×10^6 /mL. On day 6 of differentiation, beads were transferred to a 12-well plate, and incubated in live/dead buffer (100nM TO; 20 μ M PI) for 5-10min at room temperature. Beads were imaged on a Zeiss A1 Inverted Epifluorescent Microscope using Axiovision software (v4.0).

Live/dead images were quantified in ImageJ. Live and dead images were analysed simultaneously: for each live/dead image pair, the background was subtracted, images were thresholded and particle analysis was carried out to count the number of aggregates per condition containing live and dead cells. The number of aggregates containing live and dead cells was converted to a percentage of total aggregates counted in Image J and the results were analysed using a t-test in GraphPad Prism (v7.0).

Table 4: Product details for LMW and HMW alginate solutions

Product Details	LMW	HMW
Supplier	Sigma #71238	Acros Organics #17777
Viscosity (at 1% w/v)	100-200 mPas	350-550 mPas
Molecular weight	100,000-200,000g/mol	450,000-550,000g/mol
G:M content	65-75%:35-25%	40%:60%

Results

Alginate composition affects aggregate formation within beads

The formation of aggregates by the encapsulated cells was assessed by brightfield microscopy at day 6 of differentiation (see Figure 12). Both the LMW and HMW beads had aggregate formation within the scaffold, and aggregates were observed within the beads by day 4 of differentiation. As was observed in the previous experiments (at cell densities of 2×10^6 /mL and 5×10^6 /mL), when ESCs were encapsulated at 3×10^6 cells/mL alginate, the encapsulated cells form aggregates of both a rounded/circular and elongated/tubular shape. This effect was observed in alginate beads formed from low and high molecular weight alginate.

Aggregate shape varies across the depth of the beads

LMW and HMW alginate beads contained both circular and elongated aggregates (see Figure 13). Brightfield images across different planes of the beads showed that circular aggregates were confined to the centre of the bead (see Figure 13a and b), and elongated aggregates formed near the edges (see Figure 13c and d). These results further support the theory that the internal topography and porosity of the alginate beads influences aggregate formation. The porosity of the scaffold affects the diffusion of oxygen, waste and nutrients;¹⁸⁰ as the

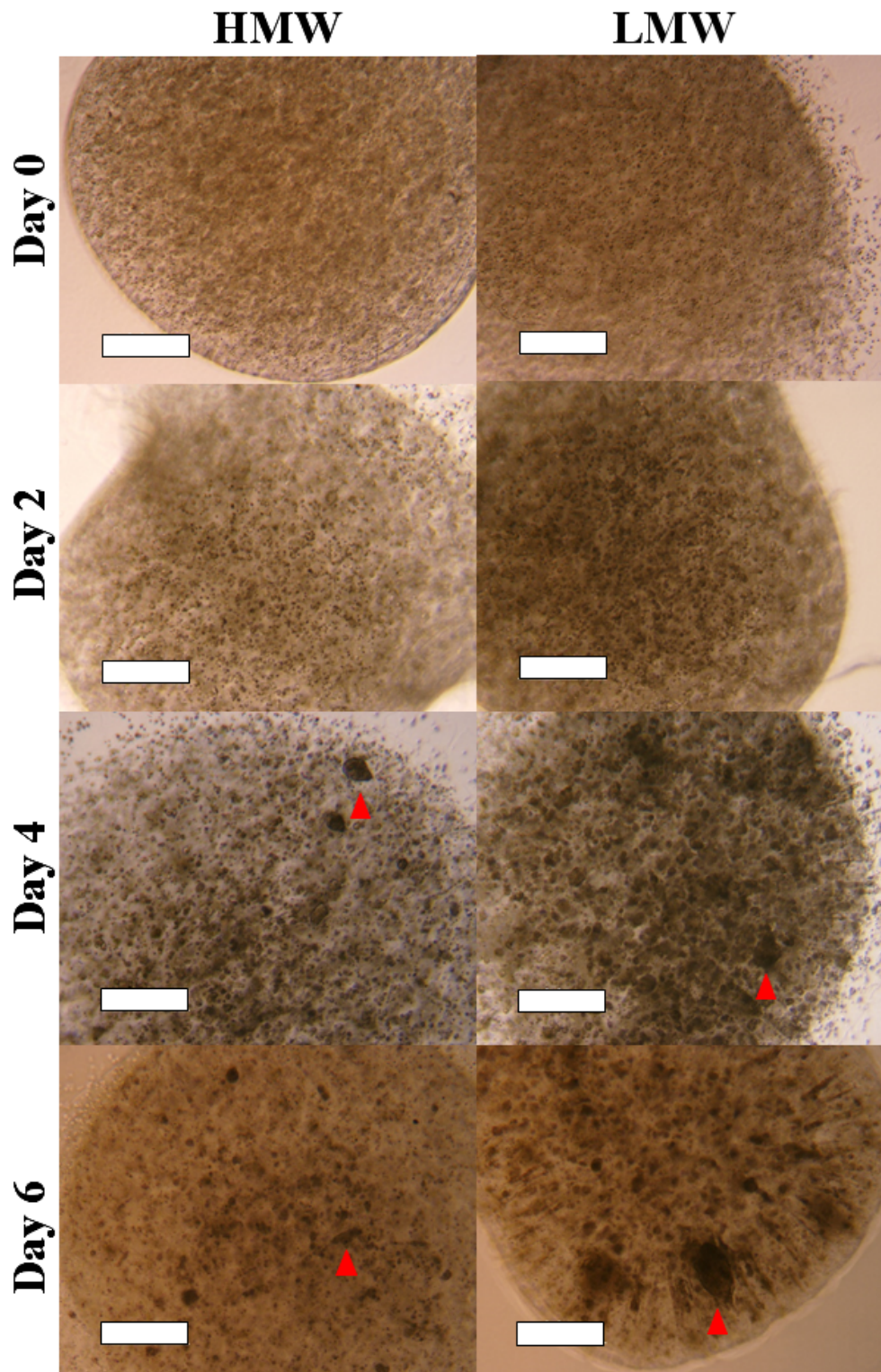


Figure 12: Brightfield images of aggregate formation in beads of two alginate molecular weights. There was aggregate formation in both LMW and HMW alginate beads, with rounded aggregates visible from day 4 (red arrowheads). Although some aggregates in LMW were very large ($\sim 300\mu\text{M}$), these were infrequent, and the majority of beads contained smaller circular and tubular aggregates. Scale Bar: $500\mu\text{m}$

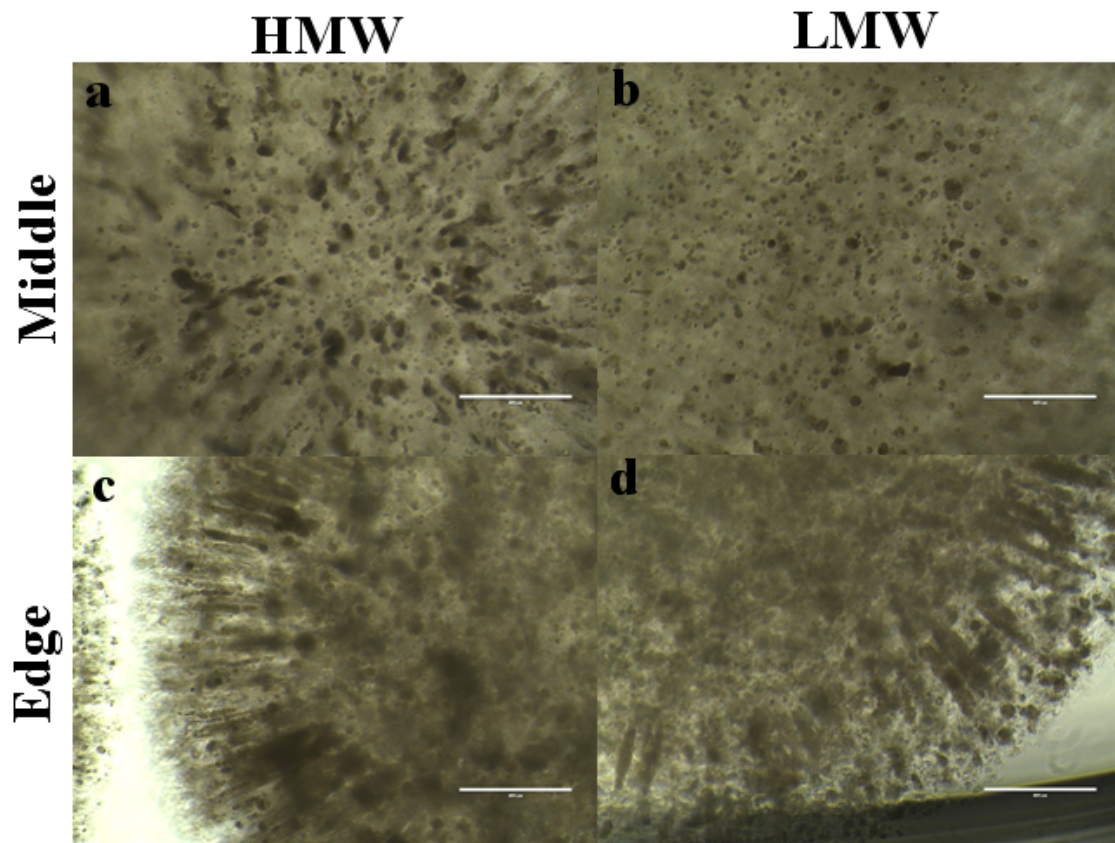


Figure 13: Brightfield images of aggregate formation at day 6, showing aggregates at the the centre and exterior of alginate beads. There were changes in aggregate shape according to their location within the beads. Aggregates near the edges/exterior of the beads were elongated in shape, and those in the central mass of the beads were more circular and compact. Scale Bar: 400 μ m

cells proliferate/aggregate within the beads, competition for nutrients or space may result in the aggregates migrating toward the culture medium. Alternatively, it was possible that the elongated aggregates were migrating out of the bead; matrix-dependent cell behaviour has been observed in mouse ESCs encapsulated in gelatin-glutaraldehyde scaffolds, with cells displaying varied affinities for the matrix at different stages of differentiation.¹³⁹ In the present experiments, aggregate migration could indicate that as differentiation progresses the differentiated aggregates migrate towards the culture medium, or away from the alginate scaffold due to a change in preference/compatibility with the alginate scaffold.

Molecular weight of alginate did not affect viability

The live/dead assay showed that both HMW and LMW alginate beads contained viable encapsulated cells at day 6 of differentiation (see Figure 14, p. 62). These results were

.....

similar to those from the 2×10^6 cells/mL cell density experiment (see Figure 11, p. 57). The majority of live cells (green) were observed within cell aggregates, dead cells (red) were observed as single cells or within smaller aggregates, and the elongated aggregates contained dead cells at the tips of the aggregates (see Figure 11, p. 57, white arrowheads).

The proportion of aggregates containing live/dead cells was counted for each alginate condition (see Figure 15). The results of a two-tailed t-test showed that there was no significant difference between LMW and HMW beads in the number of aggregates containing live or dead cells ($t(1)=5$, $p=0.1257$).

Conclusion

Both LMW and HMW beads showed aggregate formation by the encapsulated ESCs, and there were no observable differences in the cell viability or the shape and size of the encapsulated aggregates. There were aggregates of different shape and size at the exterior and the interior of the beads but this was true for both LMW and HMW beads. Based on the literature the G:M ratio and molecular weight of the alginates was LMW and HMW beads were expected to have a significant effect on cell behaviours, thus these results were unexpected. As these experiments could not definitively identify which alginate type was more suitable for ESC encapsulation, all subsequent experiments used alginate hydrogels of both subtypes. The following chapters will encapsulate ESCs in alginate hydrogels of LMW and HMW to determine whether the encapsulated aggregates are differentiating to a neuronal fate, and investigate if the G:M ratio of the alginate significantly affects the cell types generated by differentiating the encapsulated ESCs.

3.5 Discussion

This chapter outlined the experiments carried out to identify the optimum alginate hydrogel conditions for the encapsulation on mouse ESCs. The experiments aimed to demonstrate that alginate biomaterials could maintain high cell viability of the encapsulated cells during cell culture, and that the alginate beads supported ESC aggregate formation. The alginate composition variables that were examined are listed in Table 3, p.48.

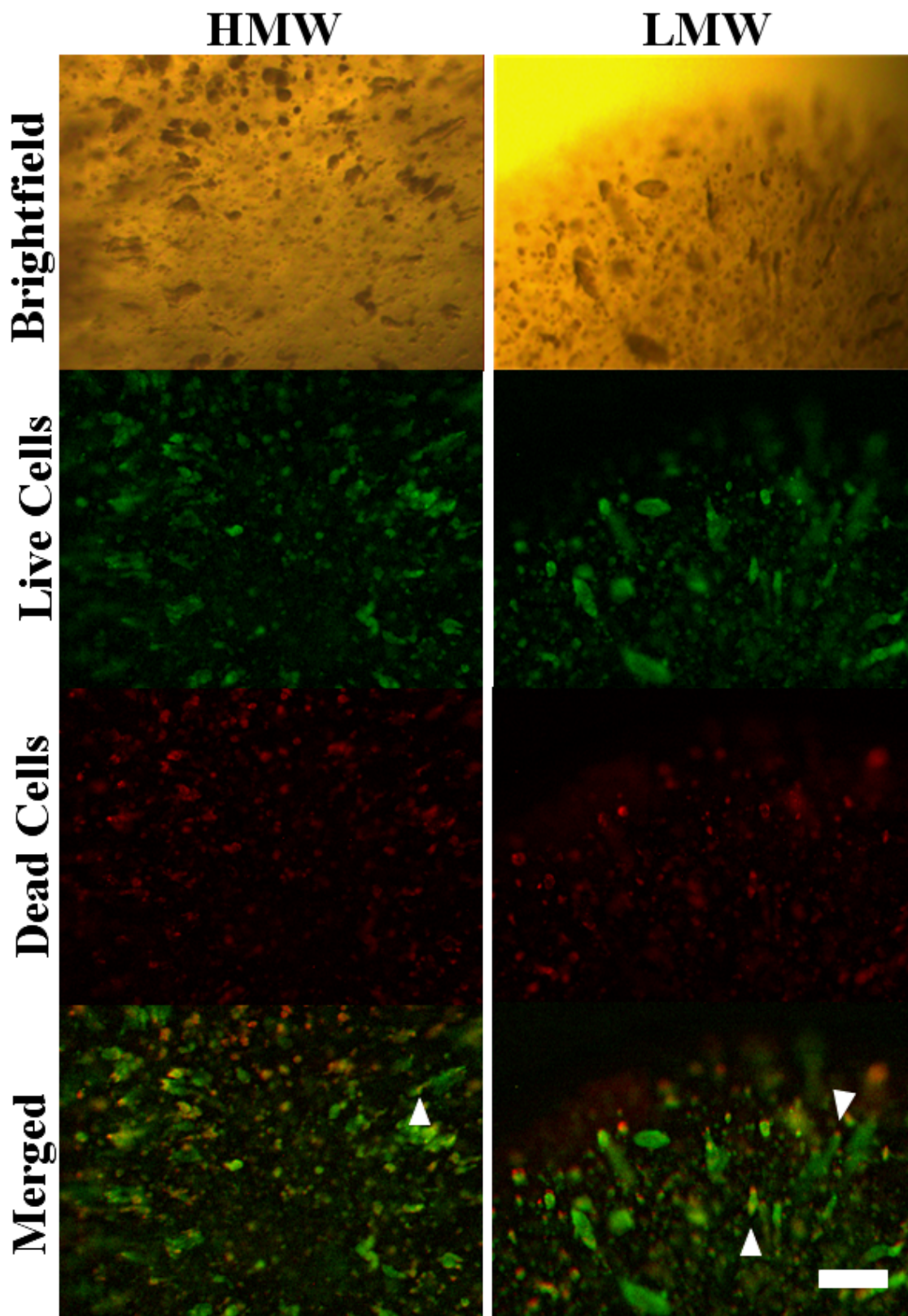


Figure 14: Cell viability of encapsulated ESCs in LMW and HMW beads. Alginate beads of LMW and HMW contained both live cells (green labelled cells) and dead cells (red labelled cells) on day 6 of differentiation. The merged images demonstrated that aggregates contained a mixture of live and dead cells, with the dead cells localised to the tips of tube/lens shaped aggregates (white arrowheads). BF: brightfield; Scale Bar: 500 μ m

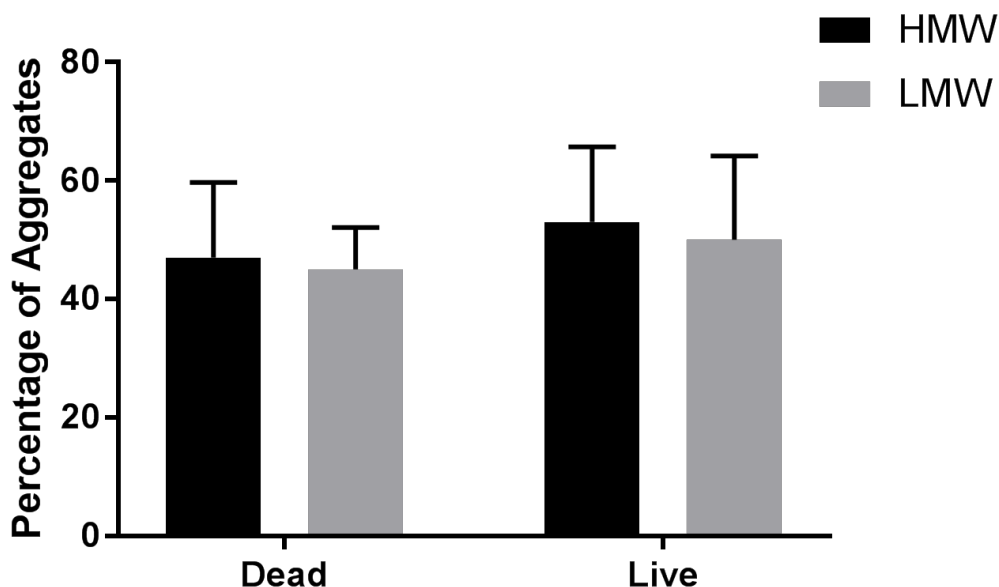


Figure 15: Quantification of cell viability in LMW and HMW beads. The percentage of aggregates containing live and dead cells was quantified using ImageJ, however a two-tailed t-test observed no significant difference between alginate conditions ($p=0.1257$). $n=2$ technical replicates for 2 independent experiments. Data are presented as mean and SEM.

3.5.1 Understanding alginate composition is critical for 3D culture applications

An initial experiment showed that alginate:DMEM hydrogels were superior to alginate:ddH₂O hydrogels for supporting ESC aggregation inside the scaffold. The aggregates inside the alginate:DMEM beads were observed migrating out of the scaffolds, with a high rate of migration in the beads formed using smaller 30G needles. The extent of aggregates escaping from the 30G beads restricts their utility cell encapsulation, as the cell viability in alginate is dependent on cell density.¹⁵⁰ Retaining more cells inside the scaffold is necessary to predict higher cell viability, thus uncontrolled migration from the beads should be minimised. Addae et al., (2012) reported increased neuronal differentiation observed in their study due to the higher number of cells available within the scaffolds to be differentiated, and not due to an increased percentage of cells differentiating.⁴³ Their results support the choice of a 21G needle to create larger beads for subsequent experiments, as the lower number of escaped aggregates can retain a larger number of cells within the scaffold to be differentiated.

Alginate hydrogels require divalent ions to bind the structure together, and the hydrogels lose their mechanical integrity in the presence of monovalent ions, as the monovalent ions in the medium compete with divalent calcium ions for binding sites on the alginate G-

residues.^{120,169,180–182} In cell culture, the negatively charged alginate polymerises with the positively charged salts in the culture medium,^{183,184} and over the course of differentiation, this slow crosslinking contributes to the degradation of the beads. This effect may have contributed to aggregates near the exterior of the beads being released into the medium. One explanation for the larger number of aggregates escaping from the 30G beads was that the beads produced using a 30G needle were smaller in diameter, thus a larger proportion of these beads disintegrated relative to their size during cell culture and permitted a higher number of aggregates to migrate out of the beads. Alternatively, the levels of aggregate migration out of the beads may also have reduced the mechanical strength of the beads as the aggregates burst through the exterior of the beads, which would result in a cumulatively larger number of cell aggregates to migrate out of the beads.^{169,185}

This slow degradation of alginate hydrogels was both an advantage and a limitation of using alginate as a cell culture scaffold. as the alginate degradation results in a change in the elastic modulus of the scaffold over time, the behaviour of the encapsulated cells should be monitored to ensure that the degradation of the scaffold does not have an uncontrolled effect on the cell fate or behaviour.^{174,186} For the purposes of these experiments, this was a limitation of using alginate, as stem cell spreading,¹⁸⁷ and differentiation⁶ are closely inter-linked with the elastic modulus of a biomaterial scaffold. Conversely, for alginate hydrogel *in vivo* applications, as the alginate was unstable in a physiological environment, carefully controlling the rates of degradation offers a technical advantage over other hydrogels, and could provide a method of controlled degradation of an implanted alginate cell scaffold.¹⁸⁴ This controlled disintegration could be used for sequential or time-controlled release of different cell types/growth factors from the scaffold into the implantation site, or to ensure the scaffold remains in place for a sufficient period of time to exert the desired effects on the implantation site, before being degraded and excreted.

3.5.2 Examining the relationship between alginate internal structure and embryonic stem cell behaviours

The viscosity of alginate solutions is dependent on the molecular weight of the alginate, which is in turn dependent on the number, length, and ratio of the G-residues to M-residues in that specific alginate.^{149,156} The G-residues crosslink with the divalent ions in the crosslinking buffer (in this case, CaCl_2), but the M-residues do not contain ionic binding sites, thus a

higher M content within the alginate solution predicts a larger porosity within the scaffolds.⁵ The porosity of the hydrogel is linked to the mechanical stability, and diffusion of nutrients, oxygen and waste through the scaffold.¹⁸⁰ Alginate salts with a high G:M ratio form hydrogels with a smaller pore size but a more mechanically stable hydrogel, whereas a high M:G ratio results in larger pore size and less mechanical stability.^{5,148} These factors were independent of the molecular weight of alginate, as HMW alginate can be irradiated to reduce the molecular weight whilst keeping the G:M ratio constant.¹⁷¹ The alginate used for the above experiments was HMW, high viscosity with a high M:G ratio (60%:40%), and may have resulted in reduced cell viability by shear stress on cells during mixing due to the high viscosity.¹⁶⁹

This internal variability in elastic modulus (reducing cell spreading) and internal porosity (affecting cell proliferation) may have contributed to the failed cell aggregation inside the empty beads observed in these experiments, and in previous studies.^{178,179,187} The specific localisation of viable cells between circular and tubular aggregates may support this theory: the cell-matrix interaction is elastic modulus dependent such that variations in the internal topography/stiffness of the beads produced aggregates of different shapes/sizes. Wilson et al., (2014)¹⁷⁹ proposed that the shape of the aggregates was dependent on localised weaknesses of the bead porous structure. As the alginate used in this experiment had a high M:G ratio, the pores would have been larger but with weak stability, and as the aggregates increased in size, they may have outgrown the pore space and broken down the internal structure of the beads. The prevalence of dead cells within the circular aggregates suggested they reached a restrictive boundary in this localised weakness, where a higher proportion of G-residues were located next to each other, and without room to expand the cells experienced cell death. Contrastingly, the elongated aggregates may have formed along a larger weak fissure within the bead, and the dead cells at the tips of these elongated aggregates might indicate the point at which those aggregates met a high concentration of crosslinked G-residues which created a restrictive boundary in the beads.¹⁷⁹

3.5.3 Alginate composition influences cell-matrix interactions

The results from experiments comparing alginate beads of LMW and HMW beads were unexpected. Based on the literature, it was predicted that there would be observable differences in the level of cell aggregation in the scaffolds due to the differences in G:M ratios and subsequently porosity of the alginate solutions.^{105,120,171} The G-residue content of the LMW

alginate was higher than the G-residue content of the HMW alginate (60 versus 40%, respectively), and as the G-residues are responsible for crosslinking with CaCl_2 , this predicted that LMW beads would have a higher elastic modulus, more stable internal structure and smaller pore size compared to HMW beads.^{120,148,154} These variations were expected to produce changes in the size or shape of the encapsulated aggregates in the LMW and HMW alginate beads but that effect was not observed. The HMW alginate was thus expected to have a negative effect on cell viability due to the higher shear forces on the cells during mixing, but this result was also not observed here - both LMW and HMW beads contained viable aggregates of circular and elongated shape. The similar results between the two alginate subtypes may mean that the differences in G:M ratio and porosity are exerting different effects on the cells, but not affecting viability or aggregation.

One explanation is that cell proliferation rates may have differed between the two alginate types. Previous experiments showed that molecular weight affects the initial cell viability (immediately after encapsulation) but not the proliferation rates,^{163,169} whereas alternative studies have shown that the properties of alginate beads can affect proliferation and migration depending on the ability of the cells to interact with the matrix.¹⁸⁸ The rates of proliferation within the beads was not tested for this thesis, but as the cell viability and proliferation were expected to change according to the internal characteristics of the beads, future experiments to assess the proliferation profiles of in both alginate types might identify whether different proliferation rates resulted in similar sized aggregates between LMW and HMW beads. Poh et al.,(2014)⁸¹ reported that single ESCs plated onto a fibrin scaffold were capable of proliferating to form an aggregate which contained organised germ layers. Single ESCs encapsulated in alginate were expected to undergo cell death,¹⁵⁰ however given the wide variability in cell behaviour depending on the alginate characteristics, it was possible that some single cells proliferated here and formed aggregates which would have affected the number and size of the aggregates observed in brightfield images.

Alternatively, the internal composition may have affected the ability of the cells to interact with the matrix, but not with each other, thus they maintained viability through cell-cell interactions despite the G:M variation between alginates. The images in Figure 13 showed that aggregate shape changed across different planes of the beads, with circular aggregates in the central mass of the bead, and elongated aggregates at the exterior. The cause of this localised variation might depend on substrate stiffness, crosslinking buffer, and the stage of

cell differentiation. Ali et al., (2015) showed that encapsulated ESCs have changing affinities for a scaffold according to the stage of cell differentiation.¹³⁹ Their study showed that prior to the expression of β -tubulin, ESCs were capable of adapting to the elastic modulus of a scaffold, but after β -tubulin expression, the cells lost this ability and were strongly influenced by the scaffold stiffness. In the present study, the elongated aggregates may therefore indicate that the cells were migrating out of the scaffold after they differentiate as the hydrogel properties were no longer suitable for those cells.

The change in aggregate shape between the centre and edge of the beads could indicate there was a non-uniform substrate stiffness within the beads, due to one of two changes in the alginate: (i) inhomogeneous crosslinking, or (ii) uncontrolled degradation in culture. Alginate polymerisation with CaCl_2 is gentle for cells, but is difficult to control due to the fast rate of gelation and typically generates hydrogels with a non-uniform structure.^{154,189} This creates inconsistency between the beads and across experiments, in terms of internal porosity and the stiffness gradient from the exterior to interior of the bead. This represents an uncontrolled factor in these experiments and could explain why some beads failed to form any aggregates, when others had aggregates of varied size/shape, and also provides an explanation for the varied aggregate shape across different planes of the beads.

As mentioned above, alginate beads degrade slowly in medium due to the divalent calcium ions of the structure competing for binding sites with the monovalent ions in the culture medium.¹⁶⁹ The exterior of the beads was in direct contact with the medium, causing degradation of the scaffold and changes the elastic modulus of the beads. Based on the findings of Ali et al., discussed above, if the encapsulated ESCs experienced a change in stiffness as the exterior of the beads degraded, this would have lesser effect on the aggregates at day 4 relative to day 6. This may also explain the change from circular aggregates at day 4 to a mixture of circular/elongated aggregates at day 6, where the differentiated cells have started to change their formation and migrate out of the beads. Future experiments to investigate this effect could quantify the elastic modulus of the beads at different timepoints to assess any significant differences in aggregate behaviour according to elastic modulus. Another set of experiments could incorporate CaCl_2 washes between medium changes to re-polymerise the beads and return the elastic modulus to the original state.

3.6 Chapter summary

The results from chapter 3 showed that ESCs encapsulated at a cell density of 3×10^6 cells/mL, in alginate beads of 1% alginate:DMEM with 0.1% gelatin, and extruded using a 21G needle provide suitable conditions for ESC encapsulation and aggregate formation. Beads formed under these conditions formed aggregates over 6 days of differentiation, contained viable cells after 6 days in culture and had low levels of aggregate migration from the beads. The results did not show any observable differences between beads formed from LMW and HMW alginate, thus both alginate types will be used for subsequent experiments.

Chapter 4 will investigate whether mouse ESCs encapsulated in alginate beads form EBs, as defined by the presence of cells from all three germ layers within the aggregates. EBs recapitulate early embryogenesis *in vitro* and generate cells from all three germ layers, endoderm, mesoderm, and ectoderm. The experiments will assess the neural differentiation of encapsulated ESCs, and to what extent this compares with cells differentiated using an EB suspension protocol. The presence or absence of the three germ layers will be tested by ICC, and the results from LMW and HMW beads will be compared against control EBs. The aim of these experiments was to verify that alginate scaffolds are suitable for inducing neural differentiation of ESCs, and the expression of neural markers Nestin and Pax6 will be tested by quantitative PCR to verify whether LMW or HMW beads are optimum for promoting a neural cell fate.

Chapter 4. Optimising alginate hydrogels for mouse embryonic stem cell neural differentiation

4.1 Introduction

The results from Chapter 3 identified the optimum conditions in LMW and HMW alginate beads for ESC encapsulation and aggregation. An advantage of using alginate hydrogels for 3D culture is the tunability of the biomaterial: small changes to the molecular weight, viscosity, or concentration of crosslinking buffer can generate an alginate hydrogel of the desired porosity and elastic modulus.^{109,140,150,159} ESCs encapsulated in alginate beads have previously been differentiated to neurons, insulin-producing cells, and hepatocytes.^{7,43,150} Several studies have reported the formation of aggregates from murine stem cells encapsulated within alginate beads^{7,150,159,163} but to date, no study has investigated if these aggregates are canonical EBs, as defined by the presence of cells from the three germ layers (endoderm, mesoderm, ectoderm). Gerecht-Nir et al.(2004)¹⁶⁵ reported that human ESCs cultured on alginate hydrogels aggregated to form canonical EBs, expressing cells from the three germ layers, however the ESCs were seeded onto a pre-gelled hydrogel, whereas the present study introduced the cells into the alginate before polymerisation. Using biomaterials to control the ESC/EB microenvironment offers new paradigms for investigating and controlling stem cell fate,⁴⁴ and creates novel avenues for using cell-laden or growth factor-loaded biomaterials to investigate cell differentiation, proliferation and migration.^{143,144,190}

This chapter investigates the ability to generate canonical EBs from mouse ESCs encapsulated in alginate beads. The encapsulated ESC-derived aggregates and EBs were compared by examining the presence of cells positive for markers of the three germ layers by ICC: endoderm (α -fetoprotein, AFP), mesoderm (α -smooth muscle actin, SMA), and ectoderm (Nestin, β -III-tubulin). As the main purpose of this thesis was to develop a novel platform for ESC differentiation, the experiments aimed to determine which alginate composition (LMW or HMW) was optimal for ESC differentiation by comparing cell viability, aggregation and the presence of cells from the three germ layers between the two alginates. The gene expression of neural progenitor marker Nestin and immature neuronal marker β -III-tubulin was compared to determine whether alginate beads supported similar levels of neural differentiation to standard EBs.

4.2 Methods

4.2.1 Differentiation of encapsulated embryonic stem cells to neuronal fate

LMW beads, HMW beads and EBs were cultured for 6 days in ADFNK with 1 μ M RA added on days 2 and 4 to induce neuronal differentiation. On day 6, EBs and beads were collected, fixed and cryosectioned (see subsection 2.4). Samples were immunostained for markers of each germ layer: endoderm (AFP), mesoderm (SMA), and ectoderm (Nestin, β -III-tubulin). To identify any spatial differences in differentiation toward each germ layer, the EBs and beads were serially sectioned at 15 μ m and 20 μ m, respectively, and samples were imaged on 3 planes, each separated from the next by 150 μ m to 200 μ m (see Figure 16). All of the EBs and beads from each experiments were cryopreserved in one embedding mould. Primary antibodies were rabbit anti-AFP, mouse anti-SMA, rabbit anti- β -III-tubulin, and rat anti-Nestin. Alexafluor secondary antibodies were goat anti-rat 594, goat anti-rabbit 488, goat anti-rabbit 568, and goat anti-mouse 488 (see Table 1, p.38). Images were collected for n=3 experiments, 3 technical replicates per sample (EBs and beads), and 2-3 beads/EBs were imaged per technical replicate. Samples were imaged using a Zeiss Axioimager A1 fluorescence microscope and Axiovision software (v4.0).

4.2.2 Pixel quantification of immunofluorescent images

Serially sectioned beads and EBs were imaged and semi-quantitative analysis was carried out by pixel counting using ImageJ. To prepare the images for pixel counting, images for each condition (AFP, SMA, Nestin, β -III-tubulin, Hoechst) were stacked, scaled and thresholded. Particle analysis was set to include object areas of 500 μ m² - infinity and a circularity of 0.00-1.00. Images were analysed and data was exported to Microsoft Excel. For each image, the area of germ layer marker was divided by the area of Hoechst; this ratio was used to control for the higher number of cells in EBs versus alginate beads. Pixel counting was used to measure any difference in the markers of germ layer present across serial sections per sample (A, B and C; see Figure 16). Data were tested for outliers using the robust regression and outlier removal (ROUT) method at 10%, and for normality using Shapiro Wilk. Cleaned data were analysed by two-way analysis of variance (ANOVA) and multiple comparisons were carried out with Tukeys post-hoc analysis in GraphPad Prism (v7.0).

4.2.3 Depolymerisation and viability of harvested cells

Three depolymerisation buffers were used to dissolve the alginate beads and harvest the aggregates. Depolymerisation buffers were prepared in ddH₂O and buffered to pH 7.4:

- 100mM Sodium Citrate
- 50mM EDTA + 95mM NaCl + 20mM Hepes
- 50mM Sodium Citrate + 10mM Hepes

The alginate beads were collected on day 6 of differentiation, washed once in dPBS and incubated in 5mL of buffer until the beads were fully dissolved (3-5min for LMW; 8-10min for HMW). During depolymerisation, alginate crosslinks are disrupted and the solution becomes more viscous; 5mL of dPBS was added after depolymerisation to dilute the buffer and reduce the viscosity before centrifuging to protect the cells from shear stress. The aggregates were pelleted by centrifugation (3min, 200g), and resuspended in trypsin-EDTA 0.25% (5min, room temperature) to dissociate the aggregates into single cells. The cell suspension was recentrifuged (5min, 200g) to pellet, and resuspended in 1mL of live/dead buffer consisting of 100nM TO and 10 μ M PI for 5-10min (see subsection 2.3, p.36). The percentage of live and not viable cells (injured + dead) was counted by flow cytometry; 10,000 events were collected per sample using a BD Accuri Flow Cytometer and C Flow Sampler software. Statistical analysis was carried out in GraphPad Prism (v7.0). Data were tested for outliers using the ROUT method at 10%, the cleaned data were tested for normality by Skapiro-Wilk, and analysed using a two-tailed t-test or two-way ANOVA.

4.2.4 Gene expression analysis

The relative expression of neural genes Nestin and Pax6, and pluripotency gene Pou5f1 were compared between EBs, LMW beads and HMW beads by quantitative PCR. RNA was extracted using a Qiagen RNeasy kit, and cDNA synthesis was carried out using the Qiagen Quantinova kit; quantitative PCR was run using a Qiagen Quantinova SYBR green kit (see subsection 2.7, p.42 for detail). The primers are listed in Table 5. Samples were run in triplicate for 3 independent experiments. Data were tested for outliers using the ROUT method at 10%, tested for normality using the Shapiro-Wilk test. The expression of neural genes was analysed by two-way ANOVA using GraphPad Prism (v7.0).

Table 5: Details of primers used for quantitative PCR

Name	Sequence (5' - 3')	bp	Tm	GC (%)								
Fwd Pou5f1	GAAGCCGACAACAATGAGAA	20	62.8	45								
Rev Pou5f1	TCTCCAGACTCCACCTCACA	20	63.7	55								
Fwd Pax6	CGGAGGGAGTAAGCCAAGAG	20	65.0	60								
Rev Pax6	TCTGTCTCGGATTTCCCAAG	20	64.1	50								
Fwd Nestin	TTGCAGACACCTGGAAGAAG	20	63.1	50								
Rev Nestin	TCAAGGGTATTAGGCAAGGG	20 </tr <tr> <td>Fwd β-actin</td> <td>AGAGGGAAATCGTGCGTGAC</td> <td>20</td> <td>66.5</td> <td>55</td> </tr> <tr> <td>Rev β-actin</td> <td>CAATAGTGATGACCTGGCCGT</td> <td>21</td> <td>66.0</td> <td>52</td> </tr>	Fwd β -actin	AGAGGGAAATCGTGCGTGAC	20	66.5	55	Rev β -actin	CAATAGTGATGACCTGGCCGT	21	66.0	52
Fwd β -actin	AGAGGGAAATCGTGCGTGAC	20	66.5	55								
Rev β -actin	CAATAGTGATGACCTGGCCGT	21	66.0	52								

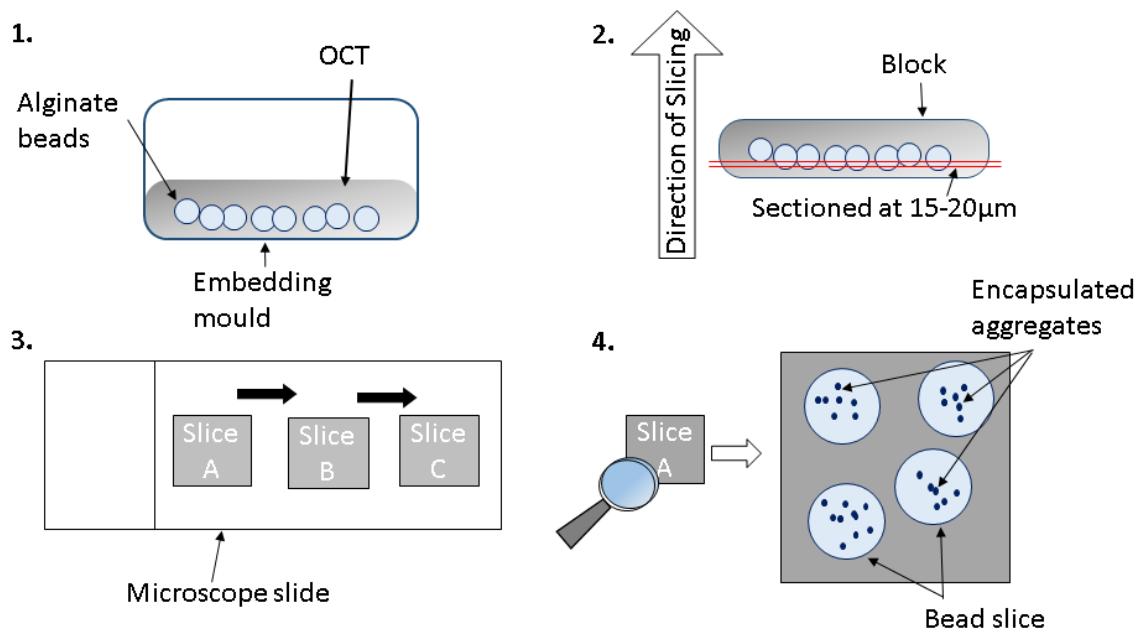


Figure 16: Cryosection slicing plan for alginate beads. ICC was carried out on serial sections of alginate beads to identify spatial effects on cell differentiation. For each condition, all of the beads were embedded in OCT embedding medium and cryopreserved in one brain mould (1), samples were serially sectioned at 20 μm for beads, and 15 μm for EBs (2), serial sections were separated so slice A to B, and slice B to C were 200 μm apart for beads, and 150 μm apart for EBs (3), and multiple beads per slice per condition were imaged (4).

4.3 Results

4.3.1 Encapsulated aggregates in alginate were canonical embryoid bodies

The presence of cells from the three germ layers within EBs and alginate beads was investigated using immunofluorescent staining. The results demonstrated that EBs, LMW and HMW beads contained cells positive for endoderm (AFP), mesoderm (SMA), and ectoderm (nestin, β -III-tubulin) indicating the presence of cells from each of the three germ layers (see Figure 17). The images showed that aggregates contained cells positive for each germ layer, for each differentiation condition. The presence of the cells from all three germ layers within all three conditions indicated that these protocols were suitable for generating cell types from each of the three germ layers. These results also demonstrated that alginate beads of LMW and HMW were suitable hydrogels for neural differentiation, as determined by the presence of neuroectoderm markers nestin and β -III-tubulin. This result was consistent with previous studies using RA to induce neural differentiation in alginate hydrogels.^{117,150,159,191} This novel result provides the first evidence that mouse ESCs encapsulated in LMW and HMW alginate beads form canonical EBs, comparable to control EBs formed by suspension culture.

4.3.2 Germ layer presence may vary spatially between culture conditions

Alginate beads and EBs were serially sectioned and immunostained to investigate if there were spatial variations in germ layer differentiation across sequential sections of the samples (see Figure 16). Immunofluorescent images showed that there were aggregates positive for the three germ layers across all sections imaged in all three culture conditions (LMW, HMW, EBs). Cross-sections of the images indicated that the number of aggregates containing cells positive for each germ layer marker may vary across different planes of the samples. For EBs and aggregates encapsulated in HMW beads there appeared to be higher numbers of aggregates that contained β -III-tubulin⁺ cells (see Figure 18) and AFP⁺ cells (see Figure 19). Contrastingly, LMW beads appeared to contain higher numbers of encapsulated aggregates that contained Nestin⁺ cells (see Figure 18) and SMA⁺ cells (see Figure 19).

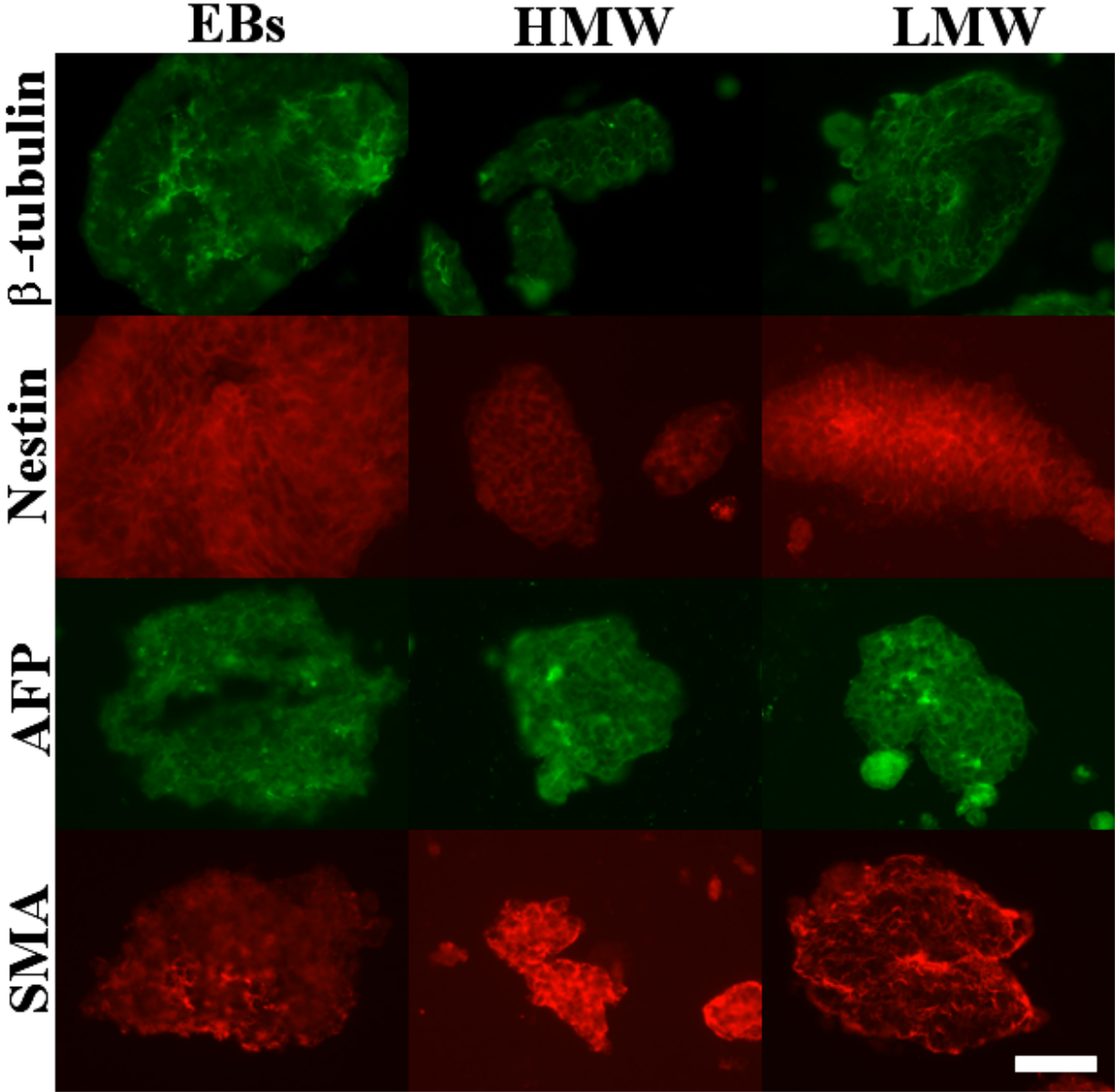


Figure 17: Immunofluorescent staining showed that beads and EBs were suitable for inducing ESC differentiation towards all three germ layers. Encapsulated aggregates in EBs, LMW and HMW beads cultured within the same cell culture population were positive for β -III-tubulin (green; top row), Nestin (red; 2nd row), AFP (green; 3rd row) and SMA (red; bottom row) indicating the presence of the three germ layers. Scale Bar: 50 μ m.

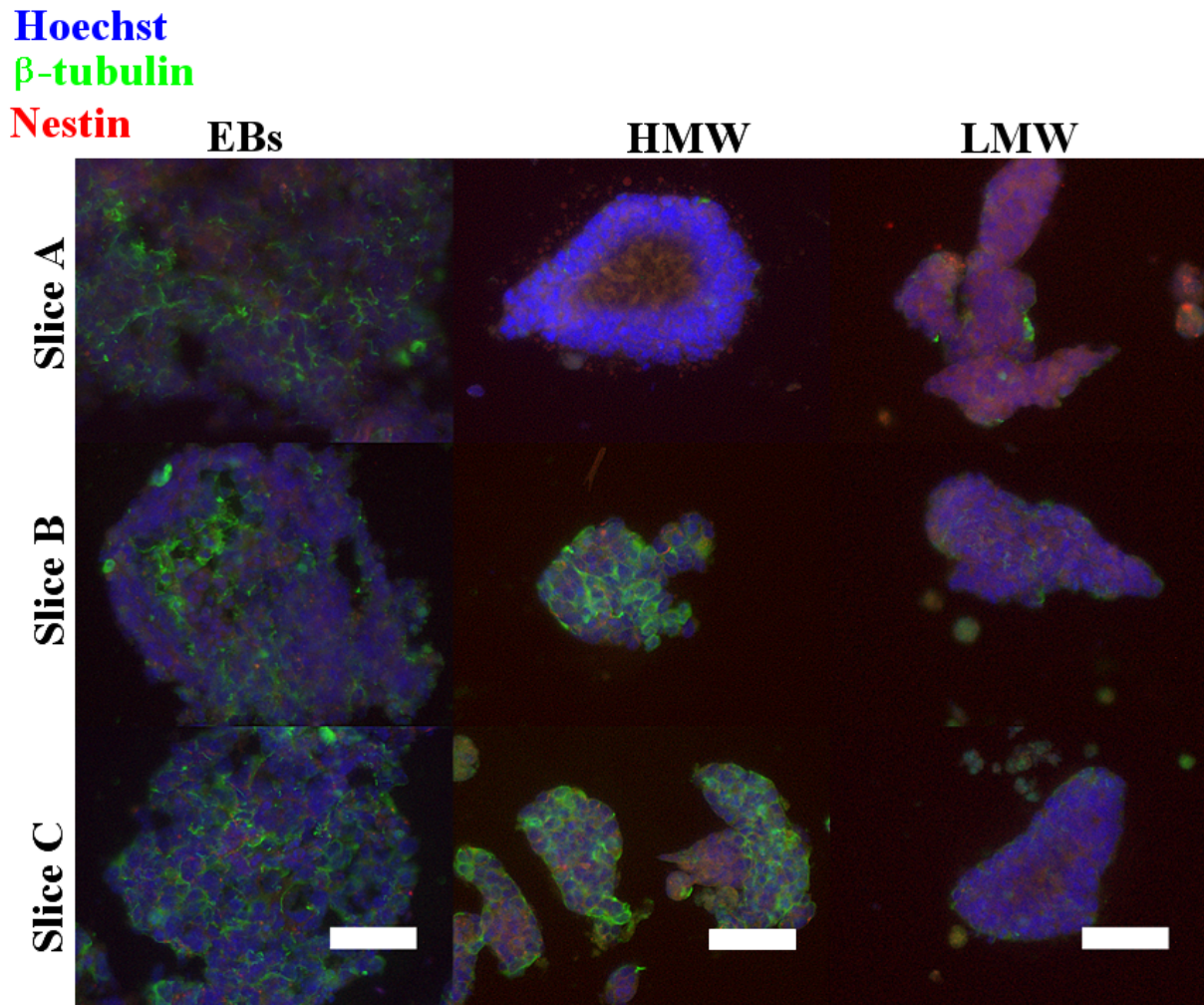


Figure 18: Spatial variations in β -III-tubulin and Nestin. Images showed variations in ectoderm markers in sequential sections of EBs and beads. There appeared to be more Nestin⁺ aggregates in LMW beads, and more β -III-tubulin⁺ aggregates in EBs and HMW beads. Scale Bars: 50 μ m.

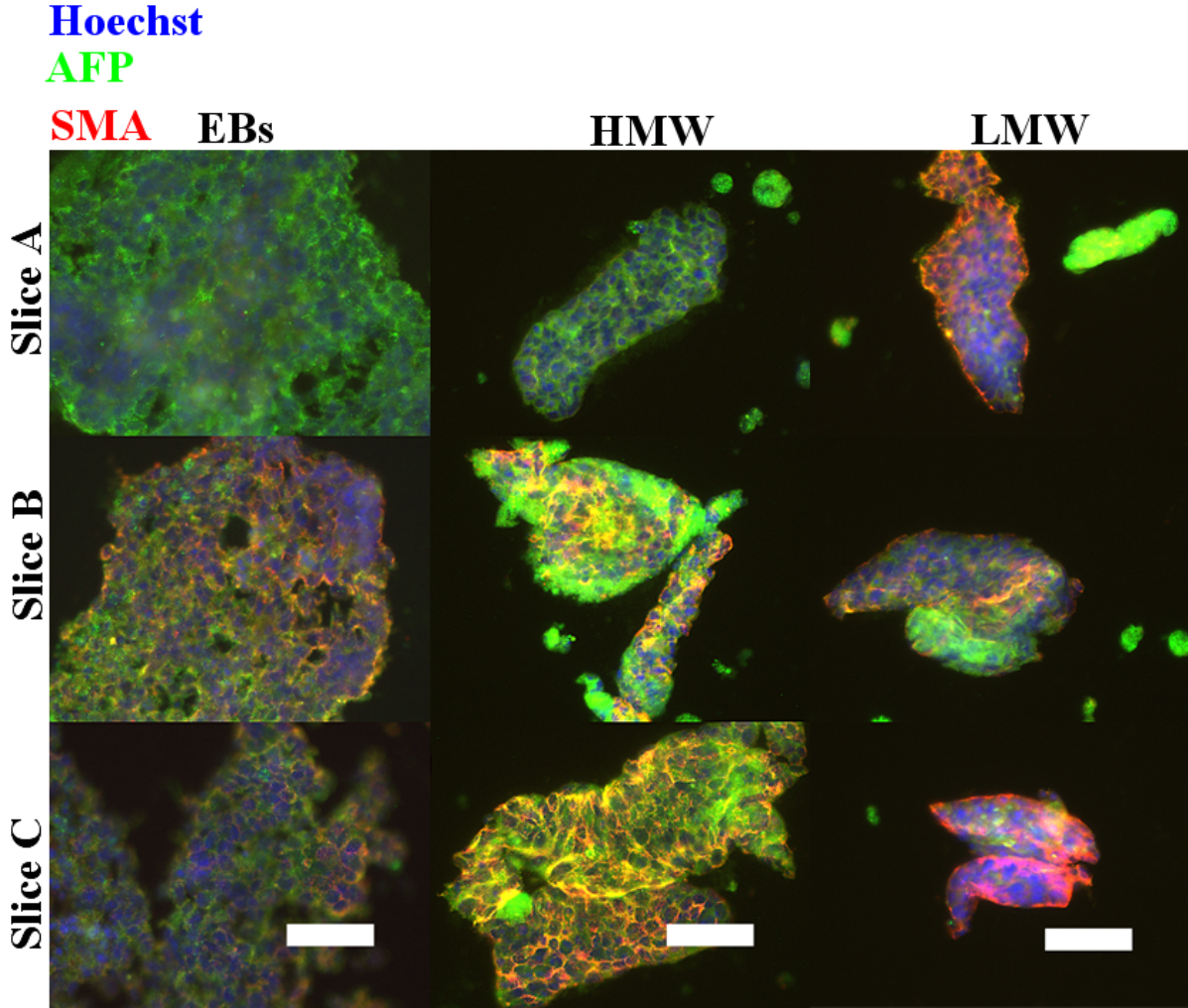


Figure 19: Spatial variation in AFP and SMA. Images showed variations in endo-derm/mesoderm markers at sequential sections of EBs and beads. There appeared to be more AFP⁺ aggregates in EBs and HMW beads, and more SMA⁺ aggregates in LMW beads. Scale Bar: 50µm.

To further investigate whether the spatial variation in germ layer presence observed in immunofluorescent images were significant, pixel counting was used to quantify the area of fluorescence in all images. As there were low levels of proliferation in alginate beads, the HMW and LMW beads were expected to contain fewer aggregates compared with cells cultured as EBs.¹⁵⁰ To control for the lower number of cells in alginate beads relative to EBs, the pixel values for each image was converted to a ratio by dividing the area of the fluorescent signal for each germ layer marker (AFP, SMA, Nestin and β -III-tubulin) by the area of fluorescent signal for the cell nuclei marker (Hoechst). Figure 20 shows a plot of the ratio values for germ layer marker to nuclear staining, for each differentiation condition. For each germ layer marker, the images were analysed by two-way ANOVA to compare the differentiation condition (EBs, HMW beads, LMW beads) with germ layer presence or with slice position (A, B or C).

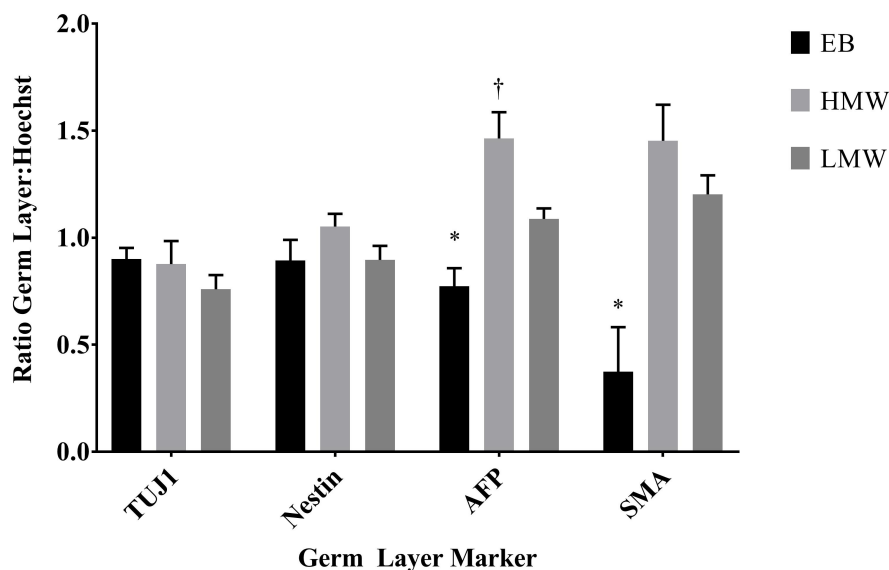


Figure 20: Pixel counting data for ratios of germ layer marker to nuclear stain. Data from the pixel counting quantification of germ layer markers relative to nuclear stain, for each differentiation condition (EB, HMW, LMW). The ratio values indicated that there may be a higher proportion of cells positive for Nestin, AFP and SMA in HMW beads relative to EBs and LMW beads. Data are presented as mean and SEM. * indicates significance versus LMW and HMW beads. † indicates significance versus LMW beads. See Table 6 for p values.

Pixel counting was used to assess the total area of fluorescence for β -III-tubulin, Nestin, AFP and SMA relative to Hoechst between LMW beads, HMW beads and EBs (irrespective of slice position). The ratio data from all images per group (EBs, LMW, HMW) per germ layer marker (β -III-tubulin, Nestin, AFP, SMA) were combined and tested using a two-way

ANOVA to compare the differentiation condition with germ layer presence. The results from pixel counting supported the theory that there were fewer cells in beads relative to EBs: the total area covered by Hoechst across all images for EBs ($124,883\mu\text{m}^2$) was more than 2-fold greater than in HMW beads ($54,157\mu\text{m}^2$) and LMW beads ($41,794\mu\text{m}^2$). The results showed a significant interaction between differentiation condition and germ layer presence ($F(6,308)=4.4$, $p<0.001$, $df=6$), which indicated that manipulating the differentiation condition for ESCs could be a useful tool to control the cell fate. Tukey’s post-hoc analysis determined that there was significantly more AFP and SMA in LMW and HMW beads relative to EBs, and significantly more AFP in HMW beads relative to LMW beads; there were no significant differences between any of the groups for the presence of β -III-tubulin or Nestin (see Table 6). These results showed that the alginate conditions (LMW and HMW) were sufficient to differentiate cells to an ectoderm cell fate at equivalent levels to EBs formed by suspension culture. The results further suggested that for protocols aiming to induce differentiation to an endoderm or mesoderm fate, alginate hydrogels might offer improved culture conditions compared to the standard EB suspension culture: based on the current results, HMW beads were predicted to promote higher levels of AFP differentiation relative to LMW beads. Although the results did not show any significant differences in the presence of neural markers Nestin and β -III-tubulin, there was a 2-fold greater proportion of Hoechst in the EB conditions indicating a greater number of cells in this condition. This result was consistent with previous reports that alginate limits cell proliferation, and therefore the use of an EB suspension protocol is optimal where large scale differentiation to neural cells is required.

Table 6: Significance values for pixel counting experiment. All significance values are adjusted p values for multiple comparisons

	AFP		SMA		β -III-tubulin		Nestin	
	p	MD	p	MD	p	MD	p	MD
EB vs. HMW	<.001	-0.69	.001	-1.1	.978	0.024	.372	-0.16
EB vs. LMW	.033	-0.31	.020	-0.83	.459	0.14	>.99	-0.003
HMW vs. LMW	.004	0.38	.404	0.25	.547	0.12	.366	0.16

MD, mean difference.

4.3.3 Spatial variability in the presence of cells from the three germ layers

To identify any spatial variations in cells from each germ layer across different planes of EBs, HMW or LMW beads, the images from serial sections were analysed by pixel counting to assess any interaction between differentiation condition (EBs, HMW, LMW) and slice position (A, B or C). The results from pixel counting indicated that there was no interaction between differentiation condition and slice position for β -III-tubulin ($F(4,57)=0.31$, $p=0.87$) or Nestin ($F(4,55)=0.54$, $p=0.7$). There was a significant interaction between differentiation condition and slice position for AFP ($F(4,89)=2.7$, $p=0.035$, $df=4$). Tukey's post-hoc analysis found a significantly higher proportion of AFP in Slice B relative to Slice A for EBs ($p=0.036$). Slice B was located 150 μ m from Slice A in the sample, indicating that different cell types might be present on different planes of EBs.

There was a significant interaction between differentiation condition and slice position for SMA ($F(4,86)=3.3$, $p=0.016$, $df=4$). Tukey's post-hoc analysis found a significantly higher level of SMA in Slice B relative to Slice A for aggregates in HMW beads ($p=0.007$). Slice B was located 200 μ m from Slice A in the sample, indicating that different cell types may be present at different planes of the beads. These results were consistent with previous results showing a bi-lateral change in endoderm presence in EBs, with one side of the EB having a greater proportion of AFP.⁵⁵ Although the analysis showed significant differences in germ layer presence across slice position, the results should be interpreted with caution. Each alginate bead contained multiple cell aggregates of different sizes throughout the bead, thus as the beads were serially sectioned from top to bottom, subsequent sections (Slice A, B, or C) may have originated from the same aggregate or from two (or more) aggregates lying close together. Significant differences were only observed in 1/89 comparisons for AFP, and 1/86 comparisons for SMA which suggested that the observed differences perhaps do not represent a spatial variation in germ layer presence in the aggregates, but rather a difference in the proportions of AFP and SMA between two different aggregates within 150-200 μ m of each other during sectioning. Future experiments can identify any spatial distribution of cells from the three germ layers by sectioning an individual EB or bead and immunostaining all of the sections for the germ layer markers. In this way, a 3D reconstruction of the images would provide definitive results on the spatial location of cells from each of the germ layers across the whole EB or bead.

4.3.4 Alginate hydrogel depolymerisation reduces cell viability

Previous research reported that cells cultured in biomaterials were more functionally active (measured by electrophysiology) and displayed markers of mature cells earlier in cell culture (measured using immunocytochemistry) relative to their 2D/monolayer counterparts.^{27, 192, 193} The current experiments attempted to harvest viable aggregates from the LMW and HMW beads so that the differentiated cells could be replated to investigate the stage of differentiation of the cells compared to standard EBs, or to test using electrophysiology if the cells differentiated in 3D were more or less functionally active relative to their EB counterparts. Three depolymerisation buffers were used to harvest the cell aggregates from alginate beads, and the viability of the harvested cells was tested by live/dead assay using flow cytometry. The average cell counts within the gated regions used for flow cytometry were consistent across EBs, LMW beads and HMW beads, and for cell densities of 2×10^6 and 3×10^6 cells/mL alginate (see Table 7). The average results from all depolymerisation experiments (see Table 7) demonstrated that alginate depolymerisation had a negative effect on cell viability. The highest average percentage of viable cells (36%) was harvested from LMW alginate beads, with an initial ESC encapsulation density of 2×10^6 /mL alginate and depolymerised using 100mM sodium citrate (see Table 7, Column 1). The average viability of cells harvested from alginate ranged from 16-36%, with a combined average viability of 25% for all depolymerisation experiments. These viability ranges were between 1.9-fold and 4.3-fold lower than the average viability of 68% for EBs. Given the limitations in retrieving the cells from the beads, these results showed that alginate was less suitable for experimental protocols that require the cells to be harvested from the hydrogel for downstream applications.

The data for viability counts from depolymerisation were highly variable between experiments (see Table 8). No depolymerisation protocol was consistently capable of harvesting live cells from the beads. In initial experiments at the lower cell density of 2×10^6 /mL, the percentage of viable cells only exceeded 50% in one experiment (see Table 8, Exp 1). The depolymerisation/cell harvesting using the EDTA buffer was more variable than with sodium citrate buffers, and in 2 of 5 experiments there was a very small cell pellet with fewer than 10,000 events counted by flow cytometry so these data were excluded from analysis (see Table 8, red font). The variability was thought to be due to an inhomogenous distribution of cells within the beads due to insufficiently mixing the alginate-cell suspension, resulting in the cell

Table 7: Average viable cell counts for depolymerisation experiments. Cell viability for EBs was higher than for cells harvested from alginate: at a lower cell density, cells harvested from LMW alginate have higher viability than HMW but at a higher cell density, this difference was eliminated. ⁺100mM sodium citrate; ⁺⁺50mM sodium citrate+10mM Hepes; [#]50mM EDTA+95mM NaCl+20mM Hepes. n=5 for SC/EBs; n=3 for EDTA

	SC ⁺		SC ⁺⁺		EDTA [#]		EBs
<i>Cell Density</i>	2x10 ⁶ /mL		3x10 ⁶ /mL		3x10 ⁶ /mL		5x10 ⁴ /mL
<i>Alginate mW</i>	LMW	HMW	LMW	HMW	LMW	HMW	n/a
<i>Gated Cells</i>	8818	8780	9668	9625	9656	9600	9064
<i>Live Cells</i>	3138	1402	3017	2574	2376	2165	6200
<i>% Viable</i>	36%	16%	24%	27%	25%	23%	68%

density for some beads falling below the minimum threshold of 2x10⁶/mL alginate required to maintain cell viability.¹⁵⁰ Although increased mixing would homogenise the alginate-cell suspension, this was not a suitable option as the extended mixing would place extensive shear stress on the cells thus reducing viability. To counter this, the cell density was increased but even at the higher cell density there was large variability in the percentage of viable cells, with a maximum viability of 46% achieved in one of five experiments (see Table 8, Exp 5). Although the between-experiment viability was inconsistent, the within-experiment viability was consistent at both the lower and higher cell densities; this result was unexpected and suggested that the effects on cell viability were caused by an uncontrolled factor either during cell encapsulation or cell harvesting (see Figure 21). In experiments using a cell density of 2x10⁶ cells/mL there was a downward trend in percentage viability over five experiments (see Figure 21a); at the higher cell density of 3x10⁶ cells/mL, there was no clear trend, with the percentage of viable cells increasing and decreasing between experiments (see Figure 21b).

A two-tailed t-test found that at the lower cell density there was significantly higher viability in cells harvested from LMW beads compared to HMW beads ($t(18)=4.49$, $p<0.001$). At this cell density, there were many beads that did not contain aggregates after differentiation, consistent with previous results by Wilson et al.(2014).¹⁷⁹ This effect was attributed to an inhomogenous cell-alginate solution resulting in the initial cell density of the beads falling below the minimum threshold of 2x10⁶/mL alginate. To address this issue, the cell density was increased to 3x10⁶ cells/mL alginate for subsequent experiments (see subsection 3.3 for

Table 8: Individual replicates for the percentage of viable cells harvested per experiment. There was high variability in the percentage of live cells harvested for each depolymerisation buffer and at both cell densities. Cell densities are per mL/alginate. Data were collected for n=5 experiments, 2 technical replicates per experiment. Values in red were excluded from statistical analysis as the samples contained fewer than 10,000 events. +100mM sodium citrate; ++50mM sodium citrate+10mM Hepes; #50mM EDTA+95mM NaCl+20mM Hepes.

Buffer:	SC ⁺		SC ⁺⁺		EDTA [#]	
Cell Density:	2x10 ⁶		3x10 ⁶		3x10 ⁶	
Exp,Rep	LMW	HMW	LMW	HMW	LMW	HMW
1,1	60	67	12	20	15	14
1,2	64	43	13	13	11	9
2,1	38	7	43	42	40	41
2,2	32	7	43	44	43	41
3,1	45	8	18	21	19	17
3,2	42	11	13	15	21	14
4,1	37	7	10	13	24	0
4,2	34	16	6	13	0	33
5,1	22	2	45	42	4	2
5,2	13	1	33	46	3	0
Average	35	16	24	27	25	23

full details). At this higher cell density, two alternative depolymerisation buffers were used to try and increase the percentage of viable cells harvested: (i) 50mM sodium citrate+10mM Hepes, and (ii) 50mM EDTA+95mM NaCl+20mM Hepes. A two-way ANOVA found no significant effect of the alginate molecular weight or the depolymerisation buffer on the viability of harvested cells ($F(1,36)=0.16$, $p=0.691$, $df=1$). The result showed that an increase in the seeding cell density eliminated any significant difference in viability due to molecular weight, but in absolute values, the new conditions decreased the percentage of viable cells harvested from LMW beads, and increased the percentage of viable cells harvested from HMW beads. This suggested that alginate hydrogels of different G:M ratio might require a specific depolymerisation buffer to successfully harvest viable cells. The depolymerisation buffer competes with the CaCl_2 for binding sites on the G monomers and disrupts the hydrogel crosslinks, thus the proportion of G residues in the alginic acid influences the rate at which alginate

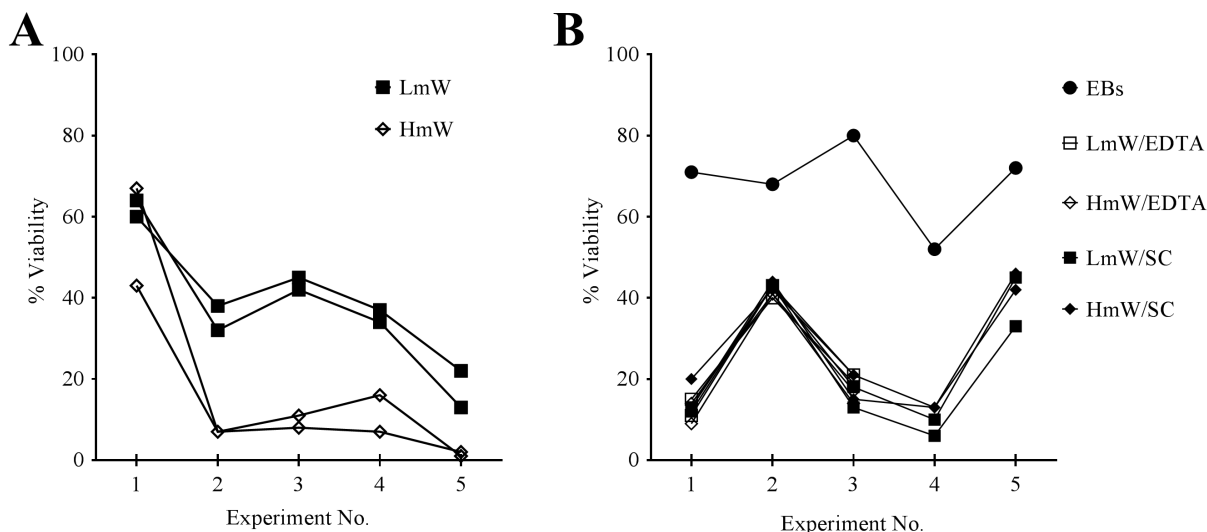


Figure 21: The within-experiment variability across depolymerisation experiments. The percentage of viable cells harvested from alginate beads over each condition followed a similar trend within experiments, but had high variability between experiments. SC: sodium citrate; $n=5$, except EDTA $n=3$.

hydrogels were degraded to release the encapsulated cells.^{169,181} Alginate hydrogels with higher proportions of G residues would take longer to depolymerise relative to hydrogels with a higher proportion of non-crosslinking M residues due to the greater number of crosslinks present in a high-G alginate.

4.3.5 Neural gene expression was comparable in beads and embryoid bodies

The expression of neural (Nestin, Pax6) and pluripotency (Pou5f1) markers was assessed by quantitative PCR to determine which alginate condition (LMW or HMW) was more suitable for differentiation of mouse ESCs to a neural fate, and to examine the differences in gene expression between ESCs differentiated as EBs and ESCs differentiated in alginate beads. A two-way ANOVA did not show an interaction between the differentiation conditions (LMW, HMW, EBs) and the expression of Pou5f1, Nestin or Pax6 ($F(4,21)=1.4$, $p=0.260$, $df=4$). Tukey's post-hoc analysis showed that there was a significantly higher expression of Pou5f1 in both HMW beads ($p=0.047$) and in LMW beads ($p=0.047$) compared to EBs. The presence of Pou5f1 was expected as alginate beads have previously been shown to maintain stem cell pluripotency over long periods of time and EBs are known to maintain some ESCs at their core during differentiation.^{194,195}

There was no significant difference in the expression of Pou5f1 between HMW and LMW beads ($p=0.982$) and there were no significant differences in the expression of Nestin or Pax6

.....

in any differentiation condition ($p > 0.999$ for all comparisons). This result demonstrated that alginate beads of HMW and LMW were capable of supporting neural differentiation, and that there was no significant difference in the expression of Nestin/Pax6 by cells differentiated in alginate beads relative to cells differentiated as EBs (see Figure 22). This was an unexpected finding, as based on the literature, the softer HMW hydrogels were expected to support higher levels of neuronal cell differentiation compared to the stiffer LMW beads. The current experiment did not investigate the presence of astrocytes markers in the differentiated cells, however, astrocytes typically differentiate on stiffer substrates compared to neurons.^{196–198} As astrocytes also express Pax6, the gene expression levels in LMW and HMW beads might represent a mixed neuron and astrocyte population, and additional experiments to quantify the gene expression of astrocyte marker glial fibrillary acidic protein (GFAP) could determine if there is a significant difference in the proportion of neurons and astrocytes (if present) between the beads or EBs. This may help to determine whether one alginate composition was optimal to support neuronal differentiation of the encapsulated ESCs.

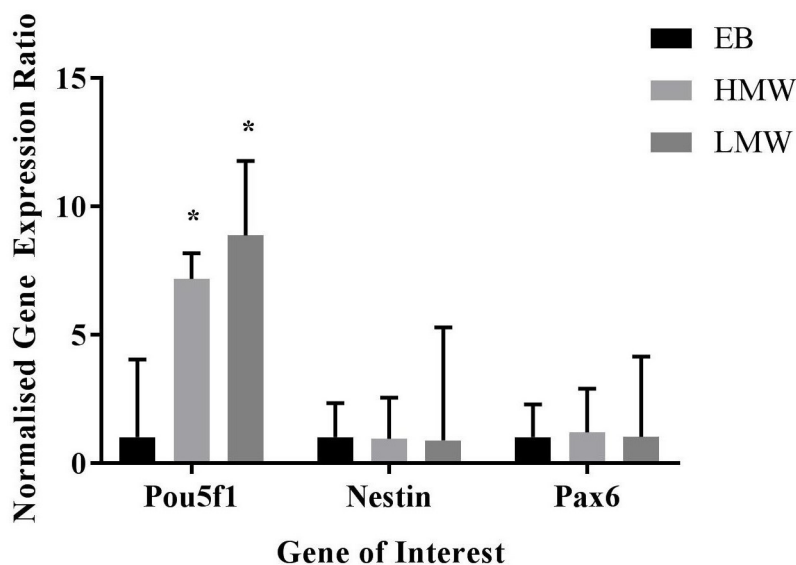


Figure 22: Gene expression for neural and pluripotency markers in beads and EBs. There was no significant difference between the expression of Nestin and Pax6 between beads and EBs (a), however beads had significantly higher expression of pluripotency marker Pou5f1 relative to EBs, but significantly lower expression relative to ESCs (b). * $p < 0.05$ versus EBs, triplicate values for $n = 3-4$. Data are presented as mean and SEM. HMW and LMW data were normalised to EBs = 1.

This finding supports the use of alginate hydrogels as a platform for neural differentiation. There was no significant difference in the levels of gene expression for markers of neural differentiation between the EBs and cells encapsulated in LMW or HMW beads. There was

.....

a high level of expression of the pluripotency marker Pou5f1 in the alginate beads which indicated that there were residual ESCs in the alginate hydrogels that had not been differentiated. Within the present protocol, this was a limitation of the cell culture paradigm however previous research by Addae et al., (2012) used alginate hydrogels for differentiation and the authors reported that the increased differentiation efficiency observed in their experiments was the result of the increased availability of ESCs in the beads for differentiation.⁴³ Their results indicated that under the right conditions, the alginate conditions presented here could produce a higher efficiency of neural differentiation relative to the EB condition resulting in a higher percentage of differentiated cells but a lower total number of cells compared to EB suspension culture. Further investigation into the mechanisms of ESC differentiation in alginate might provide avenues for expanding the neuronal differentiation efficiency in alginate hydrogels. Given the large proportion of cells that did not differentiate, this indicated that there may be insufficient RA supplemented to the culture medium to induce differentiation of all ESCs, or there may be microenvironmental factors at play which inhibit the change from a pluripotent to a differentiating state. For the purpose of the experiments in this thesis, the comparable levels of neuronal gene expression in beads and EBs indicated that these hydrogels were suitable for the development of the novel 3D differentiation platform outlined in Chapter 6.

4.4 Discussion

4.4.1 Alginate beads present a suitable platform for investigating embryogenesis

The results from this chapter demonstrated that alginate beads were capable of supporting differentiation of ESCs into cells from the three germ layers, and that the relative gene expression of neural markers by the encapsulated EBs was comparable with EBs formed by suspension culture. The results from depolymerisation were inconsistent and cell harvesting produced variable percentages of live cells, suggesting that alginate is more suitable for experiments where cell harvest is not required. The results found no difference between LMW and HMW alginate beads in neural gene expression or the germ layer presence; this was an unexpected result as the previously published results indicated that molecular weight would affect cell differentiation. These novel results expand the range of protocols for which alginate hydrogels can be adapted to include *in vitro* studies of embryogenesis in biomaterials, and 3D *in vitro* models for investigating the interaction or development of multiple tissues encapsulated within a hydrogel.

Previous studies on EBs in alginate hydrogels have seeded the cells onto the pre-gelled hydrogels to investigate germ layer presence,¹⁶⁵ or examined the effect of altering substrate stiffness during the cell culture period on ESC differentiation toward the three germ layers.¹⁶⁶ However, there was previously no evidence that aggregates formed by ESCs encapsulated in alginate hydrogels before polymerisation were EBs. Given that cell culture in biomaterials exerts significant effects on cell fate,⁶ stem cell spreading,¹⁸⁷ proliferation¹⁵⁰ and cell-matrix interactions,¹⁹⁹ the aggregates formed from ESCs encapsulated in alginate *before* polymerisation might not have been EBs. Alginate beads were previously used to maintain ESC pluripotency over long periods of time,¹⁹⁴ so the formation of aggregates inside the alginate could prevent downstream fate commitment and instead maintain the ESCs in a pluripotent state, resulting in aggregates of ESCs and not EBs. The results from the present experiments indicated that the aggregates formed in the alginate beads were canonical EBs, and by verifying that the three germ layers were present in both LMW and HMW alginate beads, this chapter has contributed to novel avenues for investigating cell differentiation in alginate, specifically for investigating the process of embryogenesis using EB-alginate cultures. The ability to differentiate EBs within alginate hydrogels provides several technical advantages for *in vitro* cell culture. A current limitation of EB suspension culture is the inability to restrict

the size of the EBs and prevent agglomeration of EBs or the attachment of EBs to the culture dish; this limits control over cell differentiation and results in high heterogeneity of the differentiated cell population.^{44,173} Larger EBs and agglomerated EBs have limited soluble factor delivery to cells at the centre of the EB, and this creates a necrotic core.^{44,127,200} These limitations can be successfully countered using the hanging drop method²² or bioreactor systems²⁰¹ to limit the size of the EBs, however these methods are more labour intensive and not easily scalable.⁴⁴ EB-alginate culture can be used as an alternative to these methods, as it is a scalable platform that can limit the size of the EBs and prevent agglomeration.^{150,173,194} EB-alginate culture offers an additional advantage over hanging-drop or bioreactors, as in addition to controlling EB size, the alginate hydrogel properties can be adapted to mimic the microenvironment of the desired cell fate, or investigate the interaction between the microenvironment and cell differentiation.^{44,159,165,200} A limitation of EB-alginate culture is the low quantity of EBs forming inside the hydrogels compared to EB suspension cultures, due to the limited ESC proliferation inside the alginate. A second limitation of the alginate-EB cell cultures is the inability to harvest viable cells from the hydrogels for downstream applications such as electrophysiology, or comparisons between the 3D encapsulated cell culture and 2D counterparts. These were clear disadvantages for protocols that require large quantities of cells for additional assays, however where the experimental aim is to investigate cell behaviour, control cell fate or aid tissue regeneration within a 3D environment, the results from the current experiments demonstrated that alginate hydrogels provide a suitable platform for these applications.

4.4.2 The influence of alginate G:M composition on differentiation

A critical feature of biomaterial cell culture is the ability to investigate how modulating biomaterial properties such as substrate stiffness or porosity can influence cell fate and cell behaviour. In mouse ESCs, the temporo-spatial effects of increasing substrate stiffness on primary germ layer expression has been investigated using alginate hydrogels.¹⁶⁶ Dixon et al., (2014) demonstrated using an alginate-collagen biomaterial that a temporo-spatial change in substrate stiffness could induce cell-state switching from a pluripotent self-renewing state to differentiation,²⁰² and the interaction between stem cell stage of differentiation and cell-matrix attachment has been examined using a gelatin-glutaraldehyde biomaterial.¹³⁹ The two alginate salts used in these experiments varied in molecular weight/viscosity and G:M ratio:

.....

(i) HMW, high viscosity, low G:M ratio, and (ii) LMW, low viscosity, high G:M ratio. The effects of molecular weight, viscosity, and G:M ratios on alginate hydrogel properties are interdependent, and their combined influence affects the behaviours of encapsulated cells.^{149,156} The low G:M ratio of the HMW alginate reduces its crosslinking potential with the divalent CaCl_2 , resulting in a soft hydrogel with a low elastic modulus; contrastingly, the high G:M ratio of the LMW alginate contains a larger proportion of G chains that crosslink with the CaCl_2 , resulting in a stiffer and more stable hydrogel.^{109,148,154}

Based on previous studies that used alginate salts of the same composition as the alginates used for these experiments, the beads in the present study were estimated to have an elastic modulus of approximately 7.3kPa for LMW beads,¹⁵⁹ and 1-5kPa for HMW beads.^{5,177,203} The *in vivo* substrate stiffnesses for neural cell fates are 0.1-1kPa for neurons, >7kPa for oligodendrocytes, and 9-10kPa for astrocytes, and the LMW and HMW hydrogels span these ranges however the LMW modulus is also close to the *in vivo* substrate stiffness for myogenic cell fates (8-10kPa).^{196-198,204} Based on the evidence from the literature, the differences in the composition of the LMW and HMW alginates were predicted to have a significant effect on hydrogel porosity and substrate stiffness, which subsequently were expected to significantly influence cell differentiation toward the primary germ layers.^{6,169,187} In contrast to the literature, the results from these experiments demonstrated that both LMW and HMW alginate hydrogels contained cells from each of the three germ layers (see Figure 17, p.74), and contained cells with comparable levels of gene expression of neural markers Nestin and Pax6 (see Figure ??, p.??). These results indicated that the molecular weight, viscosity or G:M ratio of alginate hydrogels may not have as significant an effect on cell differentiation as previously reported.

The initial substrate stiffness was predicted to be 7.3kPa for LMW and 1-5kPa for HMW beads, which falls into the *in vivo* range of tissue stiffnesses for neural tissues, but a decrease in the substrate stiffness would not inhibit neural differentiation as the *in vivo* elastic modulus for neural tissues is very soft, ranging from 60Pa for notochord,²⁰⁵ 85Pa in the neural tube,²⁰⁵ 200Pa in the human spinal cord^{132,206} up to 3.4kPa in the early blastocyst.²⁰⁷ Ali et al., (2015) showed that neural differentiation was possible on gelatin-glutaraldehyde biomaterial scaffolds up to 30kPa, but that the day of differentiation at the point of cell encapsulation was a greater predictor of the cell differentiation than the substrate stiffness.¹³⁹ In their experiments, the greatest effects of substrate stiffness on cell differentiation occur on

day 4 of differentiation at the onset of β -III-tubulin expression: cells encapsulated up to day 4 of differentiation were capable of cell-matrix interaction and successful generation of neural precursors as prior to this point the encapsulated stem cells could adapt to their microenvironment.^{139,208} Candiello et al., (2013) reported similar results, with alginate hydrogels of stiffnesses from 400-1400Pa showing similar levels of ectoderm expression at day 5 of differentiation.¹⁶⁶ The current experiments encapsulated pluripotent ESCs into the alginate biomaterials, and based on the results from in the above studies, the early stage of encapsulation may mean that the ESC were more amenable to adapting to their specific alginate environment and subsequently differentiated efficiently resulting in comparable levels of gene expression for neural and pluripotency markers between cells in both alginate compositions.

In the current study, the encapsulated stem cells had aggregated into large numbers of EBs by day 4 of differentiation, so it was possible that the substrate stiffness of the alginate beads had reduced to an elastic modulus that was suitable to support EB differentiation at this point in cell culture. Previous research showed that an alginate hydrogel elastic modulus decreased by approximately 40% over the first 9 days of cell culture, which supports this theory.¹⁸³ However, EBs form their own microenvironment in suspension culture which exerts biomechanical and chemical effects on the aggregated stem cells.^{44,209} This microenvironment controls nutrient/waste diffusion, and can form signalling gradients with the EB, and influences cell-cell interaction.^{22,44,200} Once the encapsulated ESCs in alginate have aggregated to form EBs, it was possible that the influence of this localised EB microenvironment may overcome the effect of the alginate hydrogel substrate stiffness. As the EBs provide a localised microenvironment, the predicted differences between LMW and HMW beads based on the previous research would not be observed, and subsequently, the localised EB microenvironment may have supported comparable levels of ESC differentiation, and consequently, the comparable gene expression between the ESCs differentiated in LMW and HMW beads relative to standard EBs.

4.4.3 Germ layer differentiation was not influenced by aggregate spatial location

Alginate beads in cell culture medium slowly degrade over the course of the culture period due to the interaction between the monovalent ions in the medium with the guluronic acid binding points in the alginate.^{169,180,208} Encapsulated aggregates escaped from the alginate beads by day 4 of culture which indicated that they were capable of breaking the alginate

.....

structure, or that the alginate had degraded sufficiently to release aggregates at the exterior of the beads into the medium.^{169,179} In addition, alginate hydrogels crosslinked by extrusion into CaCl_2 have an inconsistent structure, in terms of both porosity and elastic modulus, due to the rapid crosslinking of the divalent CaCl_2 with the G-residues, which creates a stiffness and porosity gradient from the exterior toward the interior of the beads.^{154,177} Cell fate determination is significantly influenced by the porosity and substrate stiffness of alginate hydrogels,^{6,178,179,187} so although the aggregates in LMW and HMW beads contained cells positive for markers of the three germ layers, the beads were serially sectioned to examine if there were any differences in the spatial distribution of cells from each germ layer markers within the beads. A difference in the level of AFP at different levels of the beads and EBs was expected based on previous research that showed EBs were non-uniform at day 6, and had an increased density of endoderm at one end of the EBs versus the other.⁵⁵ Spatial localisation of AFP and β -III-tubulin positive cells was expected, with more AFP⁺ cells at the exterior of the aggregates and more β -III-tubulin⁺ cells at the interior of the aggregates.¹⁹⁵

Semi-quantitative analysis using pixel counting did not find a significant difference in the presence of cells positive for the germ layer markers across sequential sections of the beads. This suggested that the differences in G:M ratio between the two alginate hydrogels did not exert the significant effect on cell differentiation that was expected based on the literature. The G:M composition of the alginate hydrogels is known to create beads of differing porosity and substrate stiffness, and consequently, the aggregation and differentiation of the encapsulated ESCs may be expected to be significantly different between the LMW and HMW beads.^{166,169} Consistent with the results from Fuchs et al., (2012),⁵⁵ there was a significant difference in the presence of AFP at different locations within EBs, however as multiple EBs were embedded per block, serial sections may have originated from two or more EBs lying close together and not from the same structure so further experiments are required to validate these results. The bilateral difference in AFP expression was not observed in any of the encapsulated aggregates, which indicated that either the encapsulated aggregates were at a different stage of development compared to the standard EBs, or perhaps that ESC encapsulation affected the distribution of cell differentiation within the beads. The inability to successfully harvest the aggregates from the alginate beads was a major disadvantage, as harvesting the cells at different timepoints to examine the influence of the cell-matrix interaction on differentiation towards each of the germ layers would be a useful *in vitro*

.....
paradigm.

4.4.4 Alginate hydrogels do not support cell harvesting after experiments

Previous literature has reported that cells encapsulated in alginate can be harvested using sodium citrate or EDTA based buffers that de-crosslink the hydrogels and release the encapsulated cells.^{43,159} This study attempted to harvest cells from alginate hydrogels using three different buffers however the experiments were not successful. One technical replicate from a total of ten experiments achieved the highest viability of 67%, and changes to the cell density and the composition of the depolymerisation buffers did not increase the consistency or percentage of viability achieved. Alginate hydrogels have previously been shown to generate neurons with greater functional maturity compared to their EB-generated counterparts (measured by electrophysiology),⁴³ and to generate mature dopaminergic neurons earlier in cell culture compared to neurons generated using a 2D differentiation system (measured by ICC).¹⁴⁰ The ability to harvest viable cells from the hydrogels would be useful for designing experiments to examine the effects of 3D culture on cell development over time, the differences between ESCs differentiated in biomaterials compared to their 2D counterparts, or for using the harvested cells for downstream applications such as electrophysiology experiments. A previous study showed that mouse embryos embedded into a biomaterial scaffolds *in vitro* had significantly different levels of development when implanted into female mice, compared to the mouse embryos cultured on tissue culture plastics.²¹⁰ In a similar way, encapsulating and harvesting the differentiating aggregates from alginate beads at different timepoints could create platforms for analysing the temporo-spatial changes to differentiation in response to changes in cell-matrix interaction at different stages of development.

Research by Ali et al., (2015)¹³⁹ may hold an explanation for the wide variability in viability of harvested cells between experiments. Their results showed that stem cell-matrix interaction was dependent on the stage of differentiation of stem cells at the time of seeding them on the 3D scaffold: pluripotent cells had the greatest ability to adapt to being cultured on a biomaterial, whereas once cells expressed β -III-tubulin they had the lowest ability to adapt to 3D culture. If the ESC bank had any drift from pluripotency, and underwent spontaneous differentiation between passages (and thus between alginate experiments), each subsequent alginate experiment would have had a lower number of pluripotent stem cells encapsulated, and a higher number of spontaneously differentiated cells. Given that the

.....

ability to adapt to the 3D environment changes with the level of pluripotency, any partially differentiated cells would not have interacted in the same way as the ESCs with the alginate matrix, and this may have had negative effects on cell viability. The pluripotency of the stem cell populations was not verified before encapsulation, thus future experiments could investigate if this variable was responsible for the variability between the experiments.

Although the experiment did not successfully harvest the encapsulated cells, they highlighted a potential benefit of using alginate hydrogels of different composition for 3D cell culture. As mentioned above, alginate beads degrade over the course of the culture period due to monovalent salts in the cell medium competing with CaCl_2 at G monomer binding sites.¹⁶⁹ Alginate hydrogels with a high G:M ratio degrade at a faster rate than those with a high M:G ratio, due to the larger proportion of G residue binding spots being de-crosslinked in the hydrogel^{155,177} and LMW hydrogels degrade faster due to their shorter G and M chains versus HMW alginates.^{155,165,177} This effect was observed during depolymerisation with the LMW beads degrading and releasing their encapsulated aggregates faster than the HMW beads. The G:M ratio and the length of the G or M chains of an alginic acid composition are interlinked with the rate of degradation of the hydrogel and this factor provides the opportunity to tightly control the rate of degradation of an alginate hydrogel. If the alginate hydrogels will be used for *in vivo* implantation for cell transplants or release of growth factors for a paracrine effect, the ability to temporally control the degradation of the hydrogel offers a technical advantage that can be exploited to allow slow release of incorporated growth factors into the medium. Alternatively a controlled degradation of the beads in future experiments could examine the effects of substrate stiffness on cell differentiation by encapsulated ESCs. The stiffness of an alginate hydrogel has been observed to decrease rapidly during the first week in cell culture^{183,186} and the rate of alginate degradation *in vivo* can be estimated based on the concentration of potassium and NaCl in the localised area surrounding the implant site.¹⁸⁴ The ability of alginate to degrade in a physiological environment was therefore both a limitation and a benefit of using these hydrogels, and the ability to use alginate as a bio-material depends on the purpose of the platform, the required time in cell culture or *in vivo*, the cell types encapsulated and the specific composition of the hydrogel being used for cell encapsulation.

4.4.5 Future research based on the current experiments

The current experiment investigated ESC differentiation toward the three germ layers and investigated the spatial distribution of the germ layer markers in beads and EBs. In the experiment, multiple beads and EBs were embedded in one block which limited the ability to fully investigate the spatial location of cells positive for the germ layer markers. Future experiments to serially section an individual bead and examine the germ layer distribution within the beads will be useful for determining which bead composition is optimal for ESC differentiation to a given germ layer. The results from the quantitative PCR indicated that alginate beads might be superior to EBs for endoderm and mesoderm differentiation, and serially sectioning an individual bead could verify if this is the case. Stem cells can be differentiated toward neural fates on substrates with an elastic modulus $<30\text{kPa}$ ¹³⁹ however the specific neural subtype varies with substrate stiffness: neurons on softer substrates, oligodendrocytes on medium substrates, and astrocytes on the stiffest substrates.¹⁹⁶ Quantitative PCR investigated the relative gene expression of neural markers, but not markers for the three germ layers; additionally, Pax6 is expressed by neurons and astrocytes, thus using Pax6 to quantify the expression of neural genes in LMW and HMW beads could not distinguish between the proportion of neurons and astrocytes in each alginate condition. Further investigations of the relative expression of markers of neurons, astrocytes and cells from the germ layers may identify a significant difference according to alginate composition. A future experiment to examine the relative gene expression of all three germ layers, and neuron and astrocyte specific genes, will allow a more in-depth investigation of the specific cell types present in the two alginate hydrogels.

4.5 Conclusion

The results from this chapter showed that HMW and LMW alginate beads were suitable biomaterials for neural differentiation. EBs, HMW and LMW methods using a differentiation protocol with $1\mu\text{M}$ RA were sufficient to derive cells from all three germ layers, expanding the potential for the current work to include studies of embryogenesis. The results from depolymerising were inconclusive and a consistently successful method for harvesting viable cells from the alginate hydrogels is still required. The results from quantitative PCR showed that the relative gene expression for neural markers was similar between EBs and both LMW

.....

and HMW alginate beads, indicating that alginate:EB culture is a suitable platform for neural cell differentiation and can produce aggregates containing equivalent expression levels of Nestin and Pax6 to ESCs differentiated using the EB suspension protocol.

Chapter 5. Developing a novel tool for 3D ESC culture - LMC MNs are a novel source of endogenous RA

5.1 Introduction

RA is a key signalling morphogen in neural differentiation and neuronal patterning *in vivo*^{31,64} and is required for successful vertebrate embryogenesis.²¹¹ RA is synthesised by Raldh2 in the presomitic mesoderm^{65,67,212} and Raldh2 is responsible for all RA synthesis prior to E8.5 in the mouse embryo.²¹³ Loss of mesodermal RA or knockdown of Raldh2 is lethal by E8.75.^{71,214} RA is first detected at E7.5 during the late primitive streak stage, and is required for body axis extension,⁷¹ and patterning the rostrocaudal and dorsoventral axes of the neural tube.^{64,211,213} The ability to stimulate stem cell differentiation *in vitro* using RA is a valuable research tool for investigating embryogenesis and cell-fate specification.^{31,71,215,216} ESC differentiation protocols use RA concentrations from 1nM to 1 μ M to induce ESC differentiation toward a neuronal lineage, which spans the *in vivo* concentration of 1nM to 300nM for endogenous RA in the developing mouse embryo.^{86,217}

Cell-laden biomaterial platforms hold potential for tissue engineering applications for spinal cord injury or neurodegenerative conditions, as they can deliver cells directly to the site of injury and/or initiate cell migration or regeneration of the host cells via a paracrine effect.^{17,145,218} Previous experiments to induce patterned neuronal differentiation combined 3D biomaterials with RA to investigate the effects of RA signalling on ESC differentiation. Binan et al., (2014) showed that a RA- and purmorphamine-loaded PLGA scaffold could direct neural stem-like cells to a MN fate.¹¹ Other experiments have shown that polymer microspheres loaded with RA^{145,159,175} or nanospun fibres loaded with RA or growth factors NT3 and PDGF^{17,219} can successfully control morphogen release and induce neuronal differentiation of encapsulated/seeded stem cells. These platforms demonstrated the potential for using combined biomaterial-cell culture platforms to generate novel paradigms for investigating tissue regeneration.

A limitation of these platforms is the inability to control how much RA is released from the scaffold over time, due to RA leaching or burst release from the scaffolds.^{11,145} Although the decreasing concentration of RA over time is a technical limitation of the scaffolds, the ability of RA to diffuse through the scaffolds/into the medium represents a distinct advantage

.....

of using biomaterial scaffolds over 2D cell culture protocols: in monolayer/2D cell culture, signalling morphogens or growth factors can diffuse freely throughout the medium, whereas 3D biomaterials cell culture allows for concentration gradients of signalling or growth factors to be created, more closely resembling the *in vivo* environment.^{4,44,200} RA signalling acts in a paracrine manner *in vivo* and this paracrine effect can be recapitulated in 3D biomaterial platforms by incorporating RA into the scaffold and allowing the RA to leach from the biomaterial and into the medium or at close proximity to the encapsulated ESCs.^{64,71,201} This offers a useful *in vitro* platform for investigating the effect of RA gradients on ESC differentiation.

The results from chapter 4 showed that encapsulated ESCs in alginate beads could be differentiated toward cell types from the three germ layers using exogenous RA. Exogenous RA is unstable in cell culture and is prone to light-induced degradation during medium changes, which may result in a reduced concentration of RA present in the medium relative to the concentration that was initially supplemented to the medium. Developing a source of RA that can be incorporated into a biomaterial scaffold, without a decreased in RA concentration over time, would present a major breakthrough for investigating embryogenesis or patterned differentiation *in vitro*. This chapter outlines experiments to characterise a cell-derived source of endogenous RA, which could be used as a stable source of RA for *in vitro* research. To generate this source of RA, transgenic HGF11 ESCs (see subsection 2.1.6, p. 33) will be differentiated to Raldh2⁺ LMC MNs. This MN-produced source of Raldh2 is known to be physiologically active and capable of synthesising endogenous RA *in vivo*.^{85,220,221} The aim was to generate a source of RA that can be incorporated into 3D biomaterials platforms, in order to overcome the limitations of the currently available RA-incorporated platforms described above. To do so, this source of RA must be capable of generating a stable concentration of RA in the culture medium for 4 days (a duration sufficient to induce ESC differentiation) and must be physiologically active (i.e. capable of differentiating mouse ESCs).

5.2 Methods

5.2.1 Culture of feeder-dependent mouse embryonic stem cells

HGF11 ESCs were cultured on feeder layers (CF1 mouse embryonic fibroblasts) in mouse ESC medium with LIF until confluent. The cells were passaged by trypsinisation (every 2 days),

and split at a ratio of 1:8. For EB experiments, any carry-over of mouse embryonic fibroblasts into the EB suspension can inhibit differentiation, so the feeder layers were separated before replating the stem cells for EB culture: the flask of HGF11 was passaged as normal, pelleted and resuspended in ADFNK. The cell suspension was plated into a gelatin-coated 100mm petri dish for 30min at 37°C, 5% CO₂. At this point, feeder cells had adhered to the surface of the dish, and HGF11 ESCs remained in suspension. The stem cell suspension was aspirated, cells were counted via trypan blue exclusion, and replated at the required cell density for EB suspension culture.

5.2.2 Motor neuron differentiation via embryoid body suspension culture

HGF11 ESCs were differentiated to MNs using the EB suspension protocol described Wichterle et al., (2002).⁴⁷ After separation from the feeder layers, HGF11 ESCs were replated at 5x10⁴ cells/mL ADFNK in an un-coated 100mm dish, and cultured for 6 days with 1µM RA and 1.5µM purmorphamine added on days 2 and 4 to induce MN differentiation. On day 6, the EBs were collected, pelleted by centrifugation (3min, 200g), washed once in dPBS, and resuspended in 0.25% trypsin-EDTA. The cells were dissociated for 10min on a rocker to form a single cell suspension, then the cell suspension was pelleted, and resuspended in ADFNK supplemented with 5nM GDNF. Cells were plated at the required cell densities onto well plates coated with laminin at 2µg/cm². Half of the medium was changed every 2 days.

5.2.3 Characterisation of the HGF11-derived motor neurons

Immunofluorescent staining

After EB dissociation the HGF11-derived MNs were plated at a cell density of 1x10⁶ cells/cm² onto laminin-coated 12-well plates. The MNs were cultured for 2 additional days and then fixed and immunostained (see subsection 2.4). To verify the presence of the transgene, which drives GFP and Foxp1 under the control of HB9, the MNs were immunostained for GFP, HB9 and Foxp1 co-localisation. Primary antibodies were mouse anti-HB9 and rabbit anti-Foxp1; GFP was expressed at a level that could be visualised without antibody staining so no GFP antibody was required. Secondary antibodies were goat anti-mouse 568, goat anti-rabbit 568 and goat anti-rabbit 647.

Flow cytometry cell counting

To determine the proportion of cells that differentiated into MNs (GFP⁺), the cells were counted by flow cytometry using the GFP reporter. The MN differentiation protocol was expected to generate 30-50% MNs.^{12,24} After EB dissociation, the single cell suspension was counted by flow cytometry to quantify the proportion of MNs differentiated using this cell line. The control condition was HGF11 ESCs differentiated using only 1 μ M RA without purmorphamine. Purmorphamine is the ventralising morphogen required to produce MNs and the control condition was expected to generate lower numbers of MNs compared to the experimental condition (7% compared to 30-50%).^{12,104} For each sample, 10,000 events were counted using a BD Accuri C6 flow cytometer and C-Flow Sampler software (v1.0).

5.2.4 Quantification of retinoic acid and Raldh2 produced by HGF11-derived motor neurons

To determine whether the HGF11-derived MNs were producing Raldh2 and/or RA, the dissociated EBs were replated at a cell density of 1.75x10⁶ cells/cm² and cultured in ADFNK supplemented with 5nM/mL GDNF. The medium was collected and tested using competitive ELISA to quantify the concentration of RA and Raldh2 produced by the MNs. To compare the concentration of RA and Raldh2 present in the medium across several timepoints (day 8 to 12), freshly collected medium for all timepoints was tested simultaneously. In all samples, the medium was changed by 50% 48h before being collected for ELISA to allow the RA/Raldh2 concentration to build up in the culture medium for 2 days. This duration was selected to time match with the standard protocols, which replace the cell culture medium and add fresh RA every 2 days. Statistical analysis was carried out in GraphPad Prism (v7.0). Data were tested for outliers using the ROUT method at 10%, tested for normality using the Skapiro-Wilk method, and analysed using a one-way ANOVA and multiple comparisons were conducted using Tukey's post-hoc analysis.

5.2.5 Investigating mouse embryonic stem cell differentiation using a novel source of retinoic acid

A co-culture experiment was designed to assess whether the endogenous RA produced by the HGF11-derived MNs was sufficient to induce neural differentiation. To set up the co-culture

.....

experiment, the HGF11 ESCs were first differentiated to MNs by EB suspension culture, and then dissociated and replated onto laminin-coated well plates. On the same day, CGR8 ESCs were encapsulated in alginate beads, of both LMW and HMW (see subsection 2.5.1) and the beads were transferred into Boyden chambers (6-8 beads per chamber). This denoted day 0 for alginate beads, and d6 for the HGF11-derived MNs. After 48h, the medium on the MNs was changed by 50% and the Boyden chambers containing the alginate beads were transferred into the wells containing the HGF11-derived MNs (see Figure 4) - this was day 2 of differentiation for cells in the alginate beads and day 8 for the HGF11-derived MNs. After another 48h, there were cells attached to the Boyden chambers in the wells containing alginate beads indicating that some ESCs had escaped from the beads; on this day, the medium was changed again by 50%. After another 48h, which denoted day 6 of differentiation for the alginate beads, the beads were fixed in the Boyden chamber for 1h in 3.7% PFA, then transferred into OCT in brain-embedding moulds and prepared for cryosectioning (see subsection 16). Samples were cryosectioned and immunostained for markers of the three germ layers.

5.3 Results

5.3.1 HGF11-derived motor neurons express the *Foxp1* transgene

The HGF11 ESC line is derived from transgenic HB9::*Foxp1* mice, which drives *Foxp1* and GFP expression under control of HB9. When the HGF11 ESCs are differentiated towards a MN fate, the expression of *Foxp1* in post-mitotic HB9⁺ MNs forces an LMC MN fate.^{12,97} To verify that the differentiation was successful, the HGF11-derived MNs were immunostained to demonstrate co-localisation of GFP, HB9 and *Foxp1*. The control conditions were wild type CGR8-derived MNs differentiated using the same protocol, which do not express *Foxp1*, thus differentiate to a medial motor column, MN fate: these MNs do not express *Raldh2* and do not synthesise RA. The results showed that HGF11-derived MNs were positive for GFP, HB9 and *Foxp1* (see Figure 23), and the wild type CGR8-derived MNs did not contain any GFP⁺ cells, indicating that HB9 promoter for GFP and *Foxp1* was specific to the HGF11 ESCs (see Figure 25). There were some GFP⁻, HB9⁺, *Foxp1*⁺ cells in the CGR8-derived condition; this was expected as spontaneous differentiation to a LMC fate occurs in approximately 0.5% of EB-differentiated cells.^{12,104}

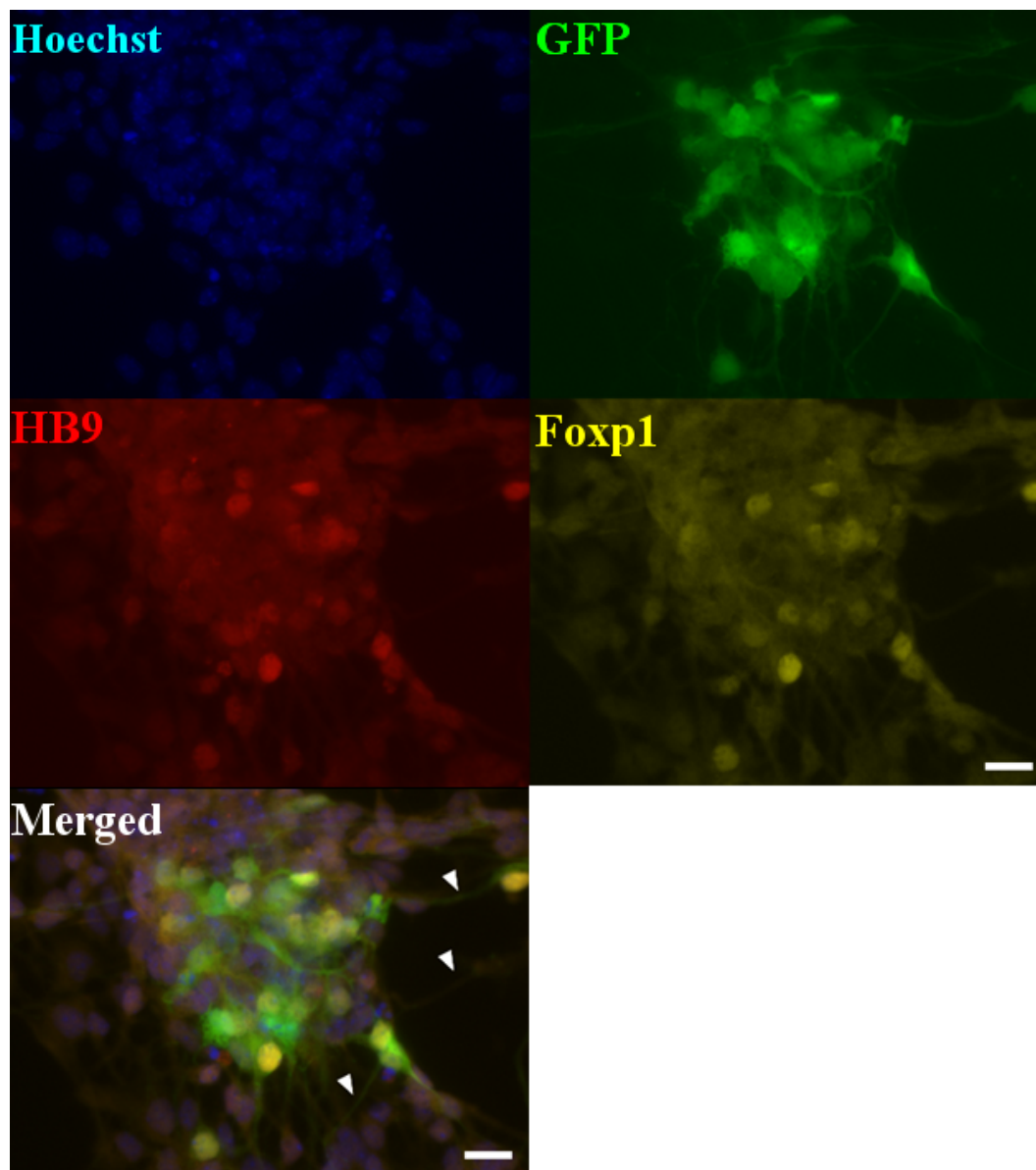


Figure 23: HGF11-derived MNs were GFP⁺, HB9⁺ and Foxp1⁺. (a) HGF11-derived MNs were positive for Hoechst (blue), GFP (green), HB9 (red) and Foxp1 (yellow), with some GFP⁺ neurites present (white arrowheads). n=3 independent experiments, 5 images per condition. Scale Bar: 20 μ m

5.3.2 HGF11-derived motor neurons have a lateral motor column identity

To determine the proportion of cells that were GFP⁺ LMC MNs, the differentiated HGF11-EBs were dissociated and the single cell suspension was counted by flow cytometry. The results showed that approximately 30% of the cells were GFP⁺, which was consistent with the previous reports of 30% by Wichterle et al., (2008)²⁴ and 40% by Adams et al., (2014)⁹⁷ (see Figure 26). The cells in the control condition generated 7% GFP⁺ cells which was consistent with the expected levels of spontaneous differentiation to a MN fate.^{12,104} The control condition was generated by differentiating HGF11 ESCs using 1 μ M RA without pur-

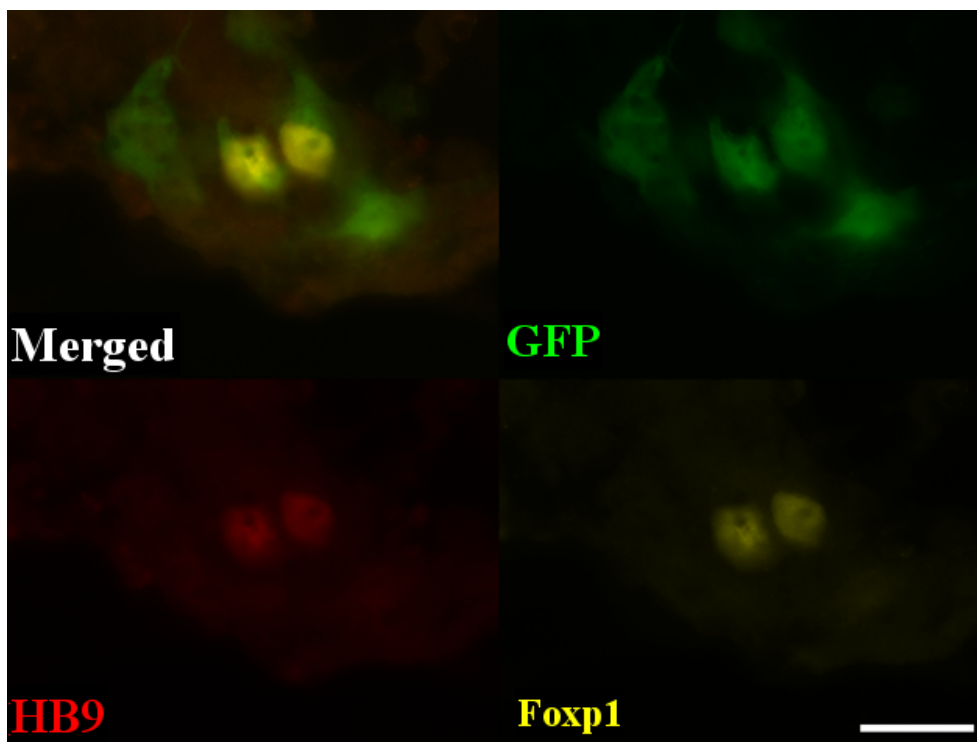


Figure 24: Magnified images (40X) showed that not all of the GFP⁺ (green) cells were HB9⁺ (red) and/or Foxp1⁺ (yellow) indicating a mixed population. Scale Bar: 20 μ m

morphamine. Purmorphamine is the ventralising morphogen required to drive a MN fate, and ESCs differentiated using RA only are expected spontaneously generate low numbers of HB9⁺ MNs - the presence of GFP in the control conditions was due to GFP driven under control of the HB9 promoter in spontaneously differentiating MNs.

5.3.3 HGF11-derived motor neurons produced Raldh2 and retinoic acid

To measure the concentration of Raldh2 and RA produced by HGF11-derived MNs, the culture medium from monolayer HGF11-MN cultures was tested by competitive ELISA. The results from the ELISA analysis of Raldh2 concentrations showed that the MNs produced Raldh2 throughout the day 8 to day 12 period. The average concentration of Raldh2 produced by HGF11-derived MNs ranged from 6.63ng/mL to 7.55ng/mL (see Table 9), but the concentrations were highly variable between experiments and the r^2 value was low. This may be due to the experimental design whereby each technical replicate was taken from a separate well; this method was chosen to capture any variation in the concentration of Raldh2 or RA being produced between wells in an individual experiment. A one-way ANOVA did not detect a statistically significant difference in the concentration of Raldh2 across the five timepoints $F(4,12)=0.19$, $p=0.939$, $df=4$ (see Figure 27a).

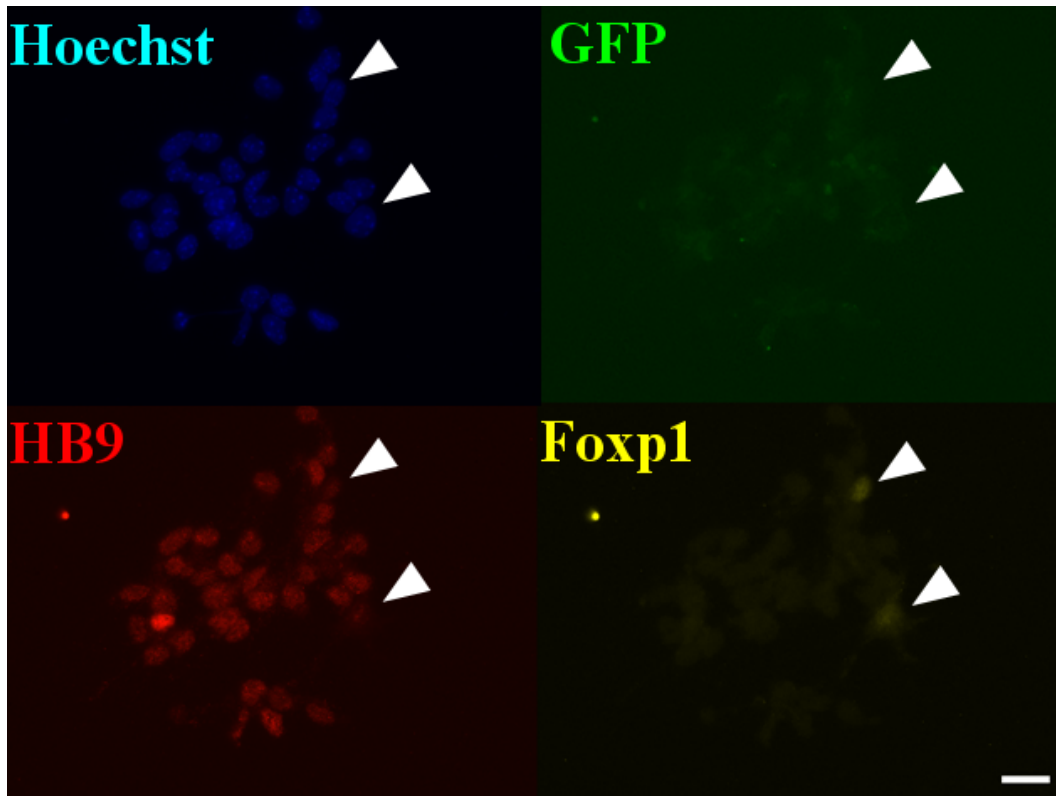


Figure 25: CGR8-derived MNs were HB9⁺ and GFP⁻, demonstrating that the GFP expression under the control of HB9 was specific to the transgenic HGF11 cell line. The control condition contained GFP⁻, HB9⁺, Foxp1⁺ cells (arrowheads) which was expected due to spontaneous differentiation to an LMC lineage. Scale Bar: 20 μ m

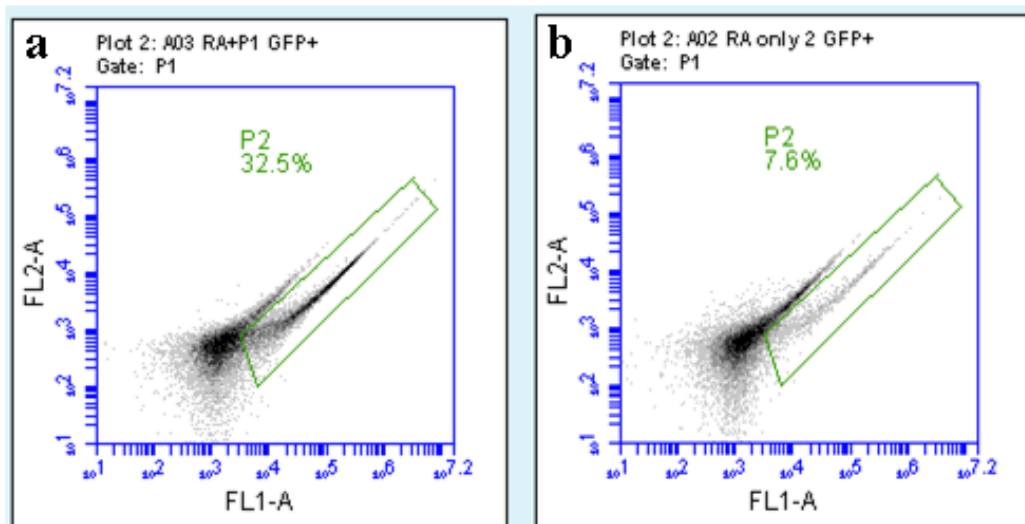


Figure 26: MN differentiation from HGF11-ESCs. (a) HGF11 ESCs differentiated to a MN fate contained approximately 30% GFP⁺ MNs. (b) HGF11 ESCs differentiated with RA and without pumorphamine contain approximately 7% spontaneously differentiating MNs. n=2 experiments, 10,000 events per condition

Table 9: HGF11-derived MNs produced Raldh2. There was between-experiment variability in the Raldh2 concentration produced by the cells throughout day 8 to day 12, but the within-experiment concentrations were consistent. Text in red indicates outliers that were excluded from statistical analysis. n=4 experiments, 2-3 technical replicates per experiment.

	Concentration (ng/mL)				Mean
D8	0.00	5.95	13.05	3.37	7.45
D9	2.41	10.73	16.06	3.94	7.47
D10	2.30	5.50	15.36	3.37	6.63
D11	3.67	5.12	15.62	4.06	7.12
D12	2.45	9.22	15.32	3.20	7.55
r	0.86	0.86	0.88	1	

ELISA analysis of RA concentrations showed that the cells were producing RA throughout the day 8 to day 12 period, with the average concentration range of RA from 65pg/mL to 105pg/mL or 214-291pM (see Table 10). The concentration of RA produced by the HGF11-derived MNs was much lower than the *in vivo* concentration of 122nM RA previously reported for the E9.5 neural tube.²¹⁷ Although the concentration was low, it remained consistent over the five day period tested. As the standard neural differentiation protocol adds RA on days 2 and 4 of differentiation, the five day time period observed here was sufficient to test ESC differentiation using this novel endogenous source of RA. A one-way ANOVA did not detect a statistically significant difference in the concentration of RA in the culture medium across the five timepoints $F(4,9)=1.53$, $p=0.274$, $df=4$. The individual concentrations of RA produced ranged from 49.31ng/mL to 96.09ng/mL across day 8 to day 12; mean concentrations increased from 64.98ng/mL at day 8 to 87.53ng/mL at day 12 but this effect was not significant (see Figure 27b).

Raldh2 is responsible for the RA synthesis by the HGF11-derived MNs and to determine if there was any correlation between the concentration of Raldh2 and RA in the culture medium, data were analysed using a two-tailed Pearsons correlation coefficient. The results showed that there was no correlation between the concentration of Raldh2 and RA across the five timepoints $r(4)=-0.55$, $p=0.337$ (see Figure 27c). This result was difficult to interpret based on the limited data from these experiments. Raldh2 is the sole enzyme responsible for synthesising RA in these cells, however high concentrations of RA downregulate Raldh2

Table 10: HGF11-derived MNs produce RA. The concentrations of RA produced across the five timepoints were not significantly different. The mean concentration ranged from 214-291pM. Text in red indicates outliers which were excluded from statistical analysis. n=3 experiments, 2-3 technical replicates per experiment.

	Concentration (ng/mL)			Mean	pM
D8	53.59	65.90	75.47	64.98	216
D9	49.31	65.85	77.81	64.32	214
D10	59.24	68.69	92.17	73.36	244
D11	68.32	168.88	79.21	73.76	246
D12	96.09	92.10	74.41	87.53	291
r²	0.93	0.9	0.98		

in vivo to protect the cells from RA-induced teratogenicity during embryogenesis.^{212,222} If the cells from these experiments behave in the same way as their *in vivo* counterparts, using these cells as an *in vitro* tool requires a detailed understanding of the timescale of RA-induced Raldh2 inhibition.

5.4 Discussion

5.4.1 HGF11-derived motor neurons produced a stable source of retinoic acid

The HB9::Foxp1 transgenic HGF11 ESC line was differentiated toward a MN lineage. The differentiated cells were positive for GFP, HB9 and Foxp1 indicating that they were LMC MNs. Adams et al., (2014) demonstrated that these HGF11-derived MNs were de facto LMC MNs, capable of innervating muscle explants *in vitro* and migrating to the correct positional location in the neural tube when injected into chick embryos.^{12,97} These LMCs produce a source of RA responsible for limb innervation during embryogenesis: earlier differentiating medial LMC MNs express Raldh2, which synthesises the RA responsible for both differentiating and providing axonal guidance to the later differentiating, lateral LMC MNs.^{12,90,223}

Although these cells were identified by their expression of Raldh2, which is known to produce physiologically active RA *in vivo*, no previous study has investigated the potential for using these MNs to create an *in vitro* source of RA. In the experiments presented here, the concentration of RA produced by these cells was quantified using ELISA, and the results

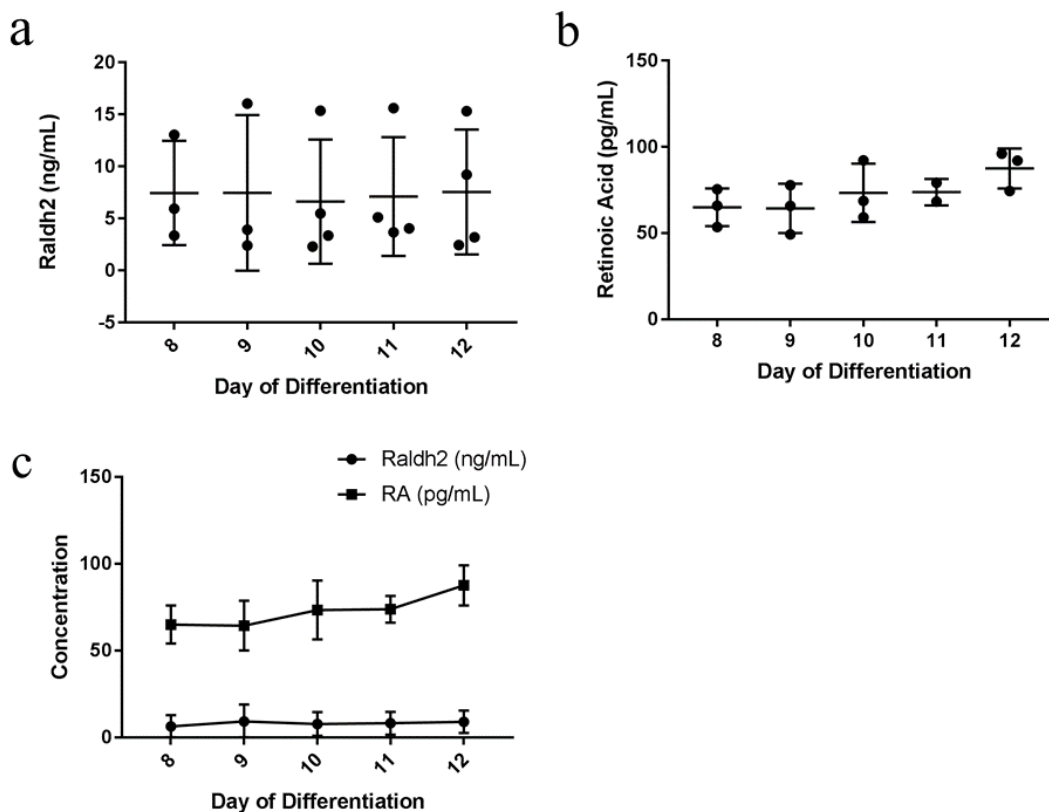


Figure 27: HGF11-derived MNs produce a consistent concentration of RA and Raldh2. Over 5 consecutive days, RA and Raldh2 were present in the medium. (a) the concentrations of Raldh2 varied between wells but did not vary significantly over 5 days of culture $p=0.939$; (b) the concentration of RA did not vary significantly from day 8 to day 12 $p=0.234$, indicating the cells are a stable source of RA for future experiments; (c) there was no correlation between the concentration of Raldh2 and RA $p=0.337$. Error bars: mean and SD. $n=3-4$, 2-3 technical replicates per experiment

showed that the culture medium from HGF11-derived MNs contained both Raldh2 and RA. The concentration of Raldh2 and RA did not vary significantly over the 5 timepoints tested, indicating that these cells can be used as a stable concentration of RA *in vitro* for a 6 day neural differentiation protocol. In demonstrating this, the experimental system described here has produced a novel tool for *in vitro* research. If the feedback loop between Raldh2 and RA concentrations can be characterised, it would provide a novel avenue for investigating cell differentiation. The cell-generated source of endogenous RA is a novel experimental tool and further experiments to determine whether there is an observable or predicatable correlation between Raldh2 and RA concentrations over time would be useful for regulating the concentrations of RA produced by the cells. The HGF11-derived MNs could subsequently be incorporated into biomaterials platforms to investigate the temporal effects of gradients of RA and Raldh2 cross-inhibition on ESC differentiation. This type of experiment is not possible using 2D or monolayer cell culture protocols as morphogen gradients cannot be created

.....

using the standard cell culture methods. The combination of biomaterials platforms with controlled morphogen release holds potential for investigating cell development in response to gradients of signalling factors.

These LMCs hold significant potential for investigating (i) the intricate relationship between Raldh2 concentration, RA synthesis and subsequent Raldh2 downregulation, and (ii) neural differentiation using a stable and endogenous source of RA. Several studies have proposed that endogenous RA may induce differentiation patterns that differ from those generated using exogenous RA, because unlike exogenous RA, the metabolites of endogenous RA are believed to activate both RA receptors and retinoid X receptors.^{71,76,78} This allows propagation of receptor activation after the RA has been metabolised and is believed to activate downstream signalling pathways that are not activated by exogenous RA. There is also evidence that exogenous RA may have *in vitro* effects that are not observed *in vivo* by initiating off-target effects via FGF8⁷¹ or by failing to inhibit Raldh2 and subsequently teratogenicity.²¹² FGF8 contains an RA-response element that is activated by endogenous RA during embryogenesis and is involved in inhibition of caudal FGF8 signalling; when exogenous RA is added to the medium, the supra-physiological concentrations (1-10 μ M⁸⁶) can force FGF8 activation to induce off-target effects.⁷¹ Opposing gradients of RA and FGF8 are involved in midbrain-hindbrain patterning thus the incidence of off-targets effects *in vitro* can have significant effects on cell development.

5.4.2 Applications of a cell-derived source of retinoic acid

Okada et al., (2004) reported that RA concentrations from 1nM to 1 μ M were sufficient to induce ESC differentiation toward the three germ layers, however 1nM concentrations induced more mesodermal differentiation, and higher concentrations induced more neural differentiation.³¹ In the present experiment, the observed concentration range of RA produced by the HGF11-derived MNs (215-290pM) was lower than the reported *in vivo* range (1-300nM)²¹⁷ and the concentration range of 1nM to 1 μ M exogenous RA used *in vitro*.^{24,31,58} The previously reported physiological concentrations were determined using HPLC from whole tissues: Horton et al., (1995) dissected E10.5 embryos and quantified RA per region: spinal cord (250nM), forebrain (8nM), midbrain (10nM), hindbrain, somites and mesenchyme or limb buds (all 30-40nM) and neural tube (122nM).²¹⁷ Ulven et al., (2001) quantified RA in the E12.5 spinal cord: brachial (74nM), thoracic (36nM) and lumbar (200nM).⁷⁶ These concen-

.....

trations are all substantially higher than the concentrations of RA observed in the present experiments, however the present experiment tested the culture medium using ELISA, which can only detect the concentration of free RA in the medium and cannot quantify RA sequestered inside the cells (bound to cellular RA binding proteins or RARs).⁷⁶ Thus it is possible that the concentration of RA produced by the HGF11-derived MNs would closer the physiological range if the RA was quantified from whole cells and not isolated from the medium.⁷⁶ During embryogenesis, the cross-repressive actions of localised RA, FGF8 and Wnt signalling gradients within subregions of the neural tube are responsible for patterning the progenitor domains, and as the physiological concentrations previously reported were collected from whole tissue, they did not capture any localised concentrations of RA within the tissues.^{224, 225}

In the present experiments, each well contained 2mL of culture medium, refreshed by 50% every two days. Despite the volume and medium changes, the concentration of RA quantified by ELISA analysis was not significantly different throughout days 8 to 12. This provided evidence that the HGF11-derived MNs were producing sufficient RA within a 48h period to compensate for the dilution of RA due to medium changes, and maintain a stable concentration over several days. The ability of the cells to replenish the concentration in such a large volume of medium indicated that the concentrations of RA observed in the present experiment may be substantially higher near the source HGF11-derived MNs before they dilute into the medium. This indicated that this endogenously produced source of RA holds the potential to induce ESC differentiation if the RA source (HGF11-derived MNs) is placed in close proximity to the target ESCs. This would mimic the *in vivo* environment where localised concentrations of RA are responsible for patterning cell differentiation.

Commonly used *in vitro* RA-induced differentiation protocols supplement exogenous RA into the culture medium every 2-3 days to induce ESC differentiation using EB suspension culture.^{43, 117} The current RA differentiation protocols are limited by the instability of RA in the culture medium, and RA degradation in response to light, which both result in a decreasing concentration of RA during changes of medium. This unstable concentration of RA introduces an uncontrolled variable and fails to provide stable morphogenic action *in vitro*. The effects of RA *in vivo* are tightly regulated by cross-repressive actions of RA, Raldh2 and Cyp26a, the enzyme responsible for metabolising RA.²¹² The uncontrolled degradation of RA throughout the course of an *in vitro* experiment cannot recapitulate the tight control

that exists during embryogenesis. The novel method presented here has produced an *in vitro* tool that provides a source of RA that remains at a stable concentration over at least 5 days of culture. This source of RA was endogenously produced by HGF11-derived MNs which replenish the RA concentration between medium changes, which offers a distinct advantage over the standard protocols which are prone to light-induced degradation of exogenous RA. This source of RA can therefore be applied to *in vitro* experiments of cell differentiation, and hold the potential to build new protocols for investigating ESC differentiation.

5.4.3 HGF11-derived motor neurons are a novel tool for differentiation

Several studies have loaded morphogens into biomaterials scaffolds to investigate cell differentiation, morphogen release rates, or to create EBs or cell aggregates that incorporate microbeads of RA inside the aggregate. Willerth et al., (2008) created a fibrin scaffold delivery system that incorporated NT3 and Shh, or NT3 and PDGF, into the fibrin fibres, and used the fibrin delivery systems to culture mouse ESC-derived neural precursor cells.²¹⁹ Their results showed that the cells cultured on the fibrin scaffold with an incorporated delivery system had significantly higher numbers of cells positive for Nestin, β -III-tubulin, and O4 but significantly lower numbers of cells positive for GFAP compared to the unmodified fibrin scaffolds.²¹⁹ Of note, the authors aimed to implant the scaffold into the damage spinal cord to aid regeneration, thus specifically engineered their fibrin delivery system to inhibit astrocyte differentiation and prevent astrocyte-induced inhibition of neuronal regeneration. Their results demonstrated that their fibrin delivery system could increase differentiation efficiency if the growth factors and morphogens were released to the encapsulated cells from within the scaffolds, relative to the cells which received the signalling morphogens in the medium. Carpenedo et al., (2010) created RA-loaded PLGA microspheres that were incorporated into EBs by suspension culture. Their results showed that localised RA signalling inside the EBs caused accelerated re-organisation and stratification of the EBs, and development of the primitive streak, compared to the standard EB protocol.¹⁷⁵ Binan et al., (2014) used RA-loaded PLGA fibres to control differentiation of neural stem-like cells: their results showed a significant increase in neurite length for the cells differentiated on RA-loaded fibres versus unloaded fibres. All of the above 3D platforms demonstrated that when ESCs were exposed to localised sources of signalling factors and morphogens, the 3D platforms were capable of increasing the efficiency of the differentiation protocol. They further demonstrated that

growth factor- or morphogen-loaded scaffolds hold potential as *in vitro* tools for manipulating cell differentiation in a manner that is not possible using standard protocols. In the standard protocols, all cells have access to a uniform concentration of the soluble factors present in the medium, and cannot only extend neurites within a single plane. Biomaterial 3D platforms introduce the potential to incorporate localised gradients and support extension of neurites into multiple planes, which supports the formation of more complex cell morphologies and subsequently the formation of complex and long-range neuronal networks that more closely mimic the physiological microenvironment, relative to cells cultured on 2D tissue culture plastics.^{4,226}

The studies discussed above reported positive results, using localised sources of signalling factors in biomaterials, but a major limitation of their experimental designs was the burst release of the loaded growth factor or morphogen over time. Carpenedo et al. (2010), did not report the concentration of RA that was loaded into the microspheres or directly investigate the burst release, however the authors conducted a burst release profile for Cell Tracker Red-loaded microspheres formed using the same method. Their microspheres had a burst release from the microspheres within the first 24h, indicating that the RA-loaded microspheres would have a rapidly decreasing concentration when incorporated into the EBs. Similar to the burst release observed in the Carpenedo study, the RA-loaded PLGA fibres generated by Binan et al., (2014) had significant burst release of RA from the fibres into the culture medium in the first 24h, resulting in a 75% decrease in RA concentration from 200nM to 50nM. This concentration decreased by a further 50% over a subsequent five days resulting in a final concentration of 25nM.¹¹ Willerth et al., (2008) used a heparin-based system to maintain the NT3 within the scaffolds, but their most efficient result only retained 40% of initial concentration of NT3 within the scaffold. The platforms described above exposed the encapsulated cells to an initial peak of high-concentration RA followed by a decreasing concentration of RA throughout the culture period. This is not representative of physiological environment, where RA concentrations are tightly regulated. Although the physiological concentration of RA ranges from 1nM to 300µM, not all cells are exposed to the highest concentration *in vivo* thus for the previously described platforms, it is possible that the initial burst release exposed some cells to teratogenic concentrations of RA. The novel source of RA presented here can address that limitation by providing a stable, consistent source of RA that prevents any uncontrolled, burst release or teratogenic effects.

Despite the burst release of RA from the above scaffolds, the concentration was still substantially higher than the concentration of RA released by the HGF11-derived MNs but there is still potential for the novel source of RA to induce ESC differentiation *in vitro*. ESCs can be differentiated toward fates from the three germ layers *in vitro* using concentrations of exogenous RA as low as 1nM supplemented to the culture medium.³¹ The concentration presented here was five times lower but (i) was an endogenously produced source of RA which makes it inherently cytocompatible, and (ii) remains at a stable concentration over time which more closely recapitulates the *in vivo* environment. This novel source of RA addresses the limitation of the burst release observed for the existing platforms. In addition, as the source of RA was constantly replenishing the RA concentration in the medium, it also reduces the implications of light-induced degradation of exogenous RA for both the efficiency and reproducibility of *in vitro* protocols. Finally, as the RA was produced by LMC MNs, these cells can be incorporated into existing, or novel, 3D platforms to investigate the effects of localised RA gradients on ESC differentiation. Given the number of platforms that have been developed to investigate this effect, and the results showing enhanced differentiation efficiency when localised signalling gradients were provided to encapsulated cells, the novel source of RA outlined in this chapter holds great potential for 3D *in vitro* investigation of cell development in response to gradients of signalling morphogens.

5.5 Conclusion

There is an unmet need for *in vitro* 3D platforms that can deliver concentrations gradients of signalling morphogens to ESCs and mimic the *in vivo* environment during development. Currently used platforms are limited by burst release of the loaded morphogen or signalling factor, which introduces an uncontrolled variable into those protocols. The experiments presented in this chapter have produced a novel *in vitro* tool that addresses the limitation of burst release. The HGF11-derived MN source of RA can be incorporated into a 3D platform to provide sustained, controlled release of a stable concentration of RA over at least 5 days. This tool offers novel avenues for investigating the effects of RA on cell differentiation *in vitro*. Previously described 3D platforms reported that differentiation efficiency was increased when the encapsulated cells were exposed to localised concentrations of growth factors or morphogens. The source of RA presented here can be used to create new 3D platforms that offer localised concentrations of RA, without the limitation of burst release of RA during

the initial stages of cell culture. The previous chapters have demonstrated that alginate is a suitable 3D biomaterial for ESC encapsulation and differentiation. Based on the experiments presented in the current and previous chapters, the next chapter presents experiments to create a novel 3D platform for inducing patterned differentiation.

Chapter 6. Creating a novel 3D platform to promote patterned neuronal differentiation of embryonic stem cells

6.1 Introduction

Tissue engineering has combined biomaterials with cell cultures, growth factors or signalling morphogens for a range of applications. Hydrogels have been used to promote axonal regeneration in peripheral nerves in rats,²²⁷ neurons have been observed to extend their axons from a fibrin scaffold implanted into the spinal cord of rats,²²⁸ growth factor-loaded scaffolds have induced osteogenic regeneration *in vitro*,^{6,150} and implanted 3D scaffolds have been used to promote host cell infiltration and regeneration with the spinal cord.²¹⁹ The ability to engineer personalised, functional tissues has real-world applications, both for investigating tissue regeneration after spinal cord injury or neurodegenerative disorders, and for developing novel platforms for stem cell therapy.^{17,105,115}

3D cell cultures using biomaterial scaffolds can recreate the *in vivo* cell microenvironment allowing us to gain a deeper understanding of the mechanisms of cell differentiation, disease, degeneration and regeneration.³ Smith et al., (2015) investigated gene expression and functional activity of human neural stem cells differentiated in 2D versus 3D cell cultures, and observed significantly greater spontaneous activity, and a significant upregulation of genes related to cytoskeletal activation of the neurons cultured in 3D platforms.²⁷ In a landmark study, Meinhardt et al., (2014) generated a 3D model of neural tube patterning using a Matrigel scaffold. Their neural tube formed a floor plate with dorso-ventral patterning and represents a novel system for investigating morphogen activity in 3D, specifically the process of neuroectoderm differentiation and gastrulation.³² Engler et al., (2006) demonstrated that the elastic modulus of a substrate affects cell development,⁶ and Poh et al., (2014) showed that embryogenesis could be controlled *in vitro* by varying substrate stiffness.⁸¹ Despite these breakthroughs and advances, the influence of the cell microenvironment on cell behaviour and cell fate specification is still poorly understood. To date, no 3D platform has been reported that can control all of variables that exist *in vivo*, including substrate stiffness, localised signalling gradients, cell-matrix interactions and paracrine signalling, making it difficult to capitalise on these protocols and create functional tissue with therapeutic value.^{205,229,230}

The development of the nervous system is the result of finely-tuned, temporo-spatial

control over cell differentiation, axonal migration, and synapse formation.⁸ The large diversity of cell types are the result of region-specific patterned differentiation, resulting from localised changes in morphogen signalling. Cell fate specification is determined by the specific actions of gradients of signalling morphogens within the cell microenvironment.^{57,58} During neural tube differentiation, specification of the rostro-caudal and dorso-ventral axes is dependent on cross-repressive gradients of signalling morphogens, such as RA, which determines cell fate specification by regulating gene expression.^{63,64} These signalling gradients are lost *in vitro*, as signalling factors such as RA or BMPs are supplemented into the culture medium, thus all of the cells are exposed to a uniform concentration of that soluble factor. Without temporospatial gradients of signalling factors, these tissue culture protocols cannot establish a vital component of *in vivo* neural tube development. To combat this, 3D biomaterial platforms have combined signalling morphogens with cells *in vitro* to induce localised effects on cell behaviour or patterned differentiation.^{11,17,219}

Alginate has previously been used for 3D cell culture using growth factor diffusion,¹⁴³ cell delivery,¹⁸⁰ and cell guidance cues;¹⁴⁴ alginate is a suitable material for these applications due to its cytocompatibility^{140,150} and the ease of diffusion of soluble factors throughout the gels.¹²² Kuo and Wang (2013) described controlled acceleration of stem cell differentiation into neurons on 3D alginate-chitosan scaffolds by incorporating nerve growth factor (NGF) into the 3D platform to promote stem cell differentiation.²³¹ Lin et al., (2017) used macroporous alginate scaffolds to control neurite outgrowth indicating that alginate could be a host scaffold for aiding neural regeneration.¹⁷⁸ Zhang et al., (2013) showed increased gene expression for markers of the three germ layers, and greater mesoderm differentiation in soft core alginate-chitosan-alginate microcapsules.¹⁷⁴ These findings, in combination with the results from Chapter 3 and Chapter 4, are strong indicators that alginate is a suitable scaffold for tissue engineering applications, and for protocols investigating embryogenesis, self-organisation of the embryonic germ layers, and patterned differentiation.

The current chapter outlines a set of experiments used to develop a novel alginate platform for 3D cell culture applications by combining the 3D alginate beads and the LMC-derived source of RA developed and validated in the previous chapters. The previous chapters have demonstrated successful survival, aggregation and differentiation of ESCs encapsulated in alginate hydrogels. The encapsulated cells were shown to form EBs which differentiated into cells from all three primary germ layers. The previous experiments characterised a stable

.....

source of RA, produced by HGF11-derived LMC MNs, which has the potential to drive ESC differentiation *in vitro*. As this is a cell-produced source of RA, the LMC MNs can also be incorporated into 3D platforms for investigating the influence of localised RA gradients on ESC differentiation. The present chapter aimed to develop a novel 3D alginate platform for creating localised RA signalling gradients, and subsequently investigating the effects of the localised concentration of RA on ESC differentiation *in vitro*. This chapter outlines experiments to test the physiological activity of the endogenous RA and determine if this cell-derived source of RA can differentiate mouse ESCs to a neural cell fate. The experiments combined these findings with the results from previous chapters to create a novel 3D platform for patterned cell differentiation using a co-culture technique. This novel platform was created using an adapted gradient maker protocol¹⁴² and the resulting alginate tube 3D platforms were tested for patterned ESC neuronal differentiation by investigating the presence/absence of cells from each of the three germ layers at each end of the scaffold.

6.2 Methods

6.2.1 Co-culture experiment to test the physiological activity of HGF11-motor neuron produced retinoic acid

A co-culture experiment was designed to test the ability of an LMC MN produced source of RA, secreted into the medium, to induce differentiation of ESCs encapsulated in alginate beads. Alginate beads of LMW and HMW were produced using the standard method (see subsection 2.5.1), and the alginate beads were transferred into a Boyden chamber well-insert at 8-10 beads per well. The beads were cultured in ADFNK without RA for 2 days. On day 2 of differentiation, the Boyden chambers were transferred into 12-well plates where each well contained HGF11-derived MNs on day 8 of differentiatio. This setup was used so that the encapsulated ESCs in beads were exposed to the RA produced by the MNs but were not in close proximity to the source of the RA. The Boyden chamber setup for the co-culture experiment is shown in Figure 4, p.41. The beads were cultured for 4 days in co-culture with the HGF11-derived MNs, with half of the medium changed every 2 days. This protocol thus mimicked the 2-/4+ RA differentiation protocol, with 2 days in ADFNK only, and 4 days in medium containing the cell produced RA. On day 6, the beads were collected from the Boyden chambers, fixed and cryopreserved for immunostaining. The beads were serial sectioned at 15 μ m, and stained for Nestin and β -III-tubulin.

6.2.2 Generation of retinoic acid gradients in alginate hydrogel tubes

To investigate the effect of a localised concentration gradient of RA on ESC differentiation, a gradient maker was used to create alginate tubes with a graded cell density of HGF11-derived MNs (to produce a graded concentration of RA), and a constant cell density of CGR8 ESCs. Figure 5 (p.43) shows the gradient maker setup used to form the alginate tubes. In brief, HGF11 ESCs were differentiated toward a MN lineage by EB suspension culture (see subsection 2.2.1), the cells were dissociated to form a single cell suspension, and this single-cell suspension was mixed with an equal cell density of CGR8 ESCs. This CGR8:HGF11-MN cell suspension was pelleted by centrifugation (5min, 200g) and resuspended at 6×10^6 /mL in 0.5% LMW alginate. This cell density is equivalent to 3×10^6 /mL for each cell type. A second cell suspension of CGR8 ESCs, without HGF11-derived MNs, was pelleted and resuspended at 3×10^6 /mL in 0.5% LMW alginate.

To create the tubes, 1.5mL of each alginate-cell suspension (CGR8 only or CGR8:HGF11-derived MNs) was loaded into each chamber of the gradient maker (A and B). Chamber A contained the CGR8 only cell suspension, and chamber B contained the CGR8:HGF11-derived MNs cell suspension. The tubes were formed as per the protocol in subsection 5 and resulted in an alginate tube with a consistent cell density of CGR8, and an decreasing cell density of HGF11-derived MNs from the leading edge to the trailing edge of the tube (see Figure 6, p.44). The alginate tube was polymerised in CaCl_2 for 5min at room temperature. The tube was cultured in ADFNK supplemented with GDNF (5ng/mL) for 6 days, with medium changes on days 2 and 4. On day 6, the tube was collected, fixed, cut into sections of approximately 1cm length and cryopreserved in OCT. For immunostaining, the first and last section of each tube was stained for markers of the three germ layers (AFP, SMA, β -III-tubulin), and the cell types present at each end of the tube were compared. The results were collected for n=2 independent experiments where tube 1 = 8cm, tube 2 = 5cm.

6.3 Results

6.3.1 HGF11-motor neuron retinoic acid in the medium did not induce differentiation of encapsulated embryonic stem cells

The results from the co-culture/Boyden chamber experiment showed that the concentration of LMC-produced RA in the culture medium was not sufficient to induce differentiation of

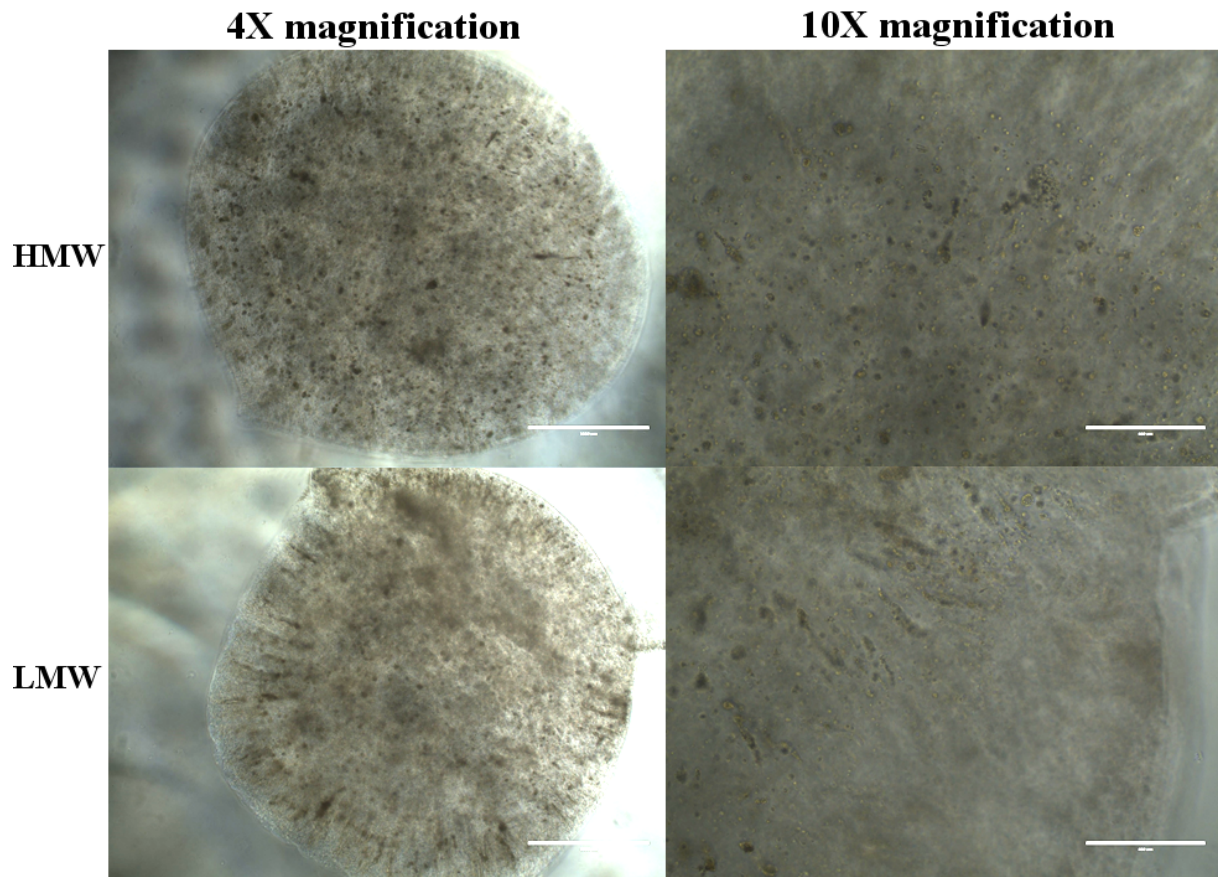


Figure 28: Brightfield images of alginate beads after 6 days of co-culture with HGF11-derived MNs. Low and high magnification images of the alginate beads showed that the encapsulated cells generated very few aggregates by day 6 in both HMW and LMW beads. Scale Bar: 4X magnification, 1mm; 10X magnification, 400 μ m

ESCs encapsulated within alginate beads, when the beads were physically isolated from the source of RA. Brightfield images showed that cells encapsulated in LMW and HMW alginate contained very few aggregates by day 6 of co-culture with HGF11-derived MNs (see Figure 28). These aggregates were visible near the exterior of the beads and were long and tubular shaped, which contrasts to the circular EBs formed in beads differentiated using exogenous RA (see Figure 12, p.59).

As it was difficult to confirm aggregate formation by brightfield images, the beads were fixed and cryosectioned to investigate the extent of aggregate formation inside the beads. Nuclear staining using Hoechst showed that the beads contained single cells or small aggregates with the aggregates clustered near the exterior edges of the bead, consistent with what was observed in brightfield images (see Figure 29). This result demonstrated that the 215-290pM range of endogenous RA produced by the HGF11-derived MNs was not sufficient to induce aggregate formation within the beads, in both LMW and HMW alginate beads. This result

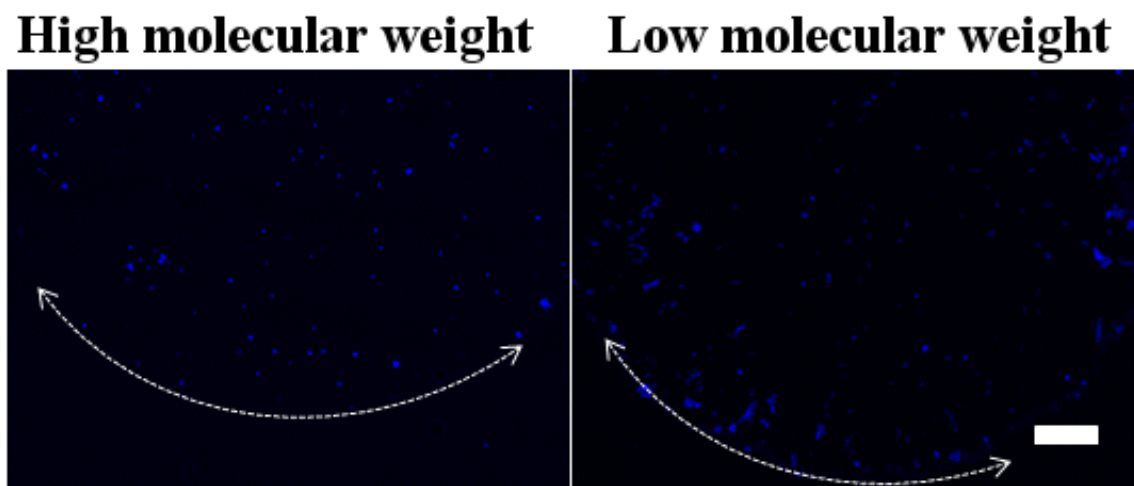


Figure 29: Endogenous RA did not induce EB formation from encapsulated ESCs. The results from ICC of cryosections of beads co-cultured with HGF11-derived MNs showed that there were very few aggregates within the beads, and that these aggregates were clustered near the edges of the beads. White dashed lines indicate the exterior edge of the alginate beads. Images were collected for $n=4$ independent experiments. Scale Bar: $200\mu\text{m}$

was not unexpected given that the standard concentration range of RA used for *in vitro* differentiation is 1nM to $1\mu\text{M}$.

EBs differentiated using RA were used as a positive control for the experiment to show the immunostaining was successful, and to demonstrate that the ESCs encapsulated in the alginate came from a cell population that was viable and capable of forming aggregates. The results from immunostaining showed that the cells encapsulated in the beads were negative for AFP, SMA, Nestin and β -III-tubulin, whereas the cells in EBs were positive for all four, indicating that the cells in the beads were not differentiating (see Figure 30). This was expected as there were very few aggregates present in the beads, and single cells are known to lose viability in alginate hydrogels.¹⁵⁰ Due to the expected cell death of single cells within alginate beads, and the limited numbers of aggregates observed encapsulated in the beads, the immunofluorescent images were only collected from areas of the beads that contained aggregates.

6.3.2 A localised retinoic acid gradient induced embryoid body differentiation

To investigate whether a more localised concentration gradient of RA, produced by the HGF11-derived MNs, could induce patterned differentiation, CGR8 ESCs and HGF11-derived LMC MNs were encapsulated together within alginate tubes. Preliminary tests of the gradi-

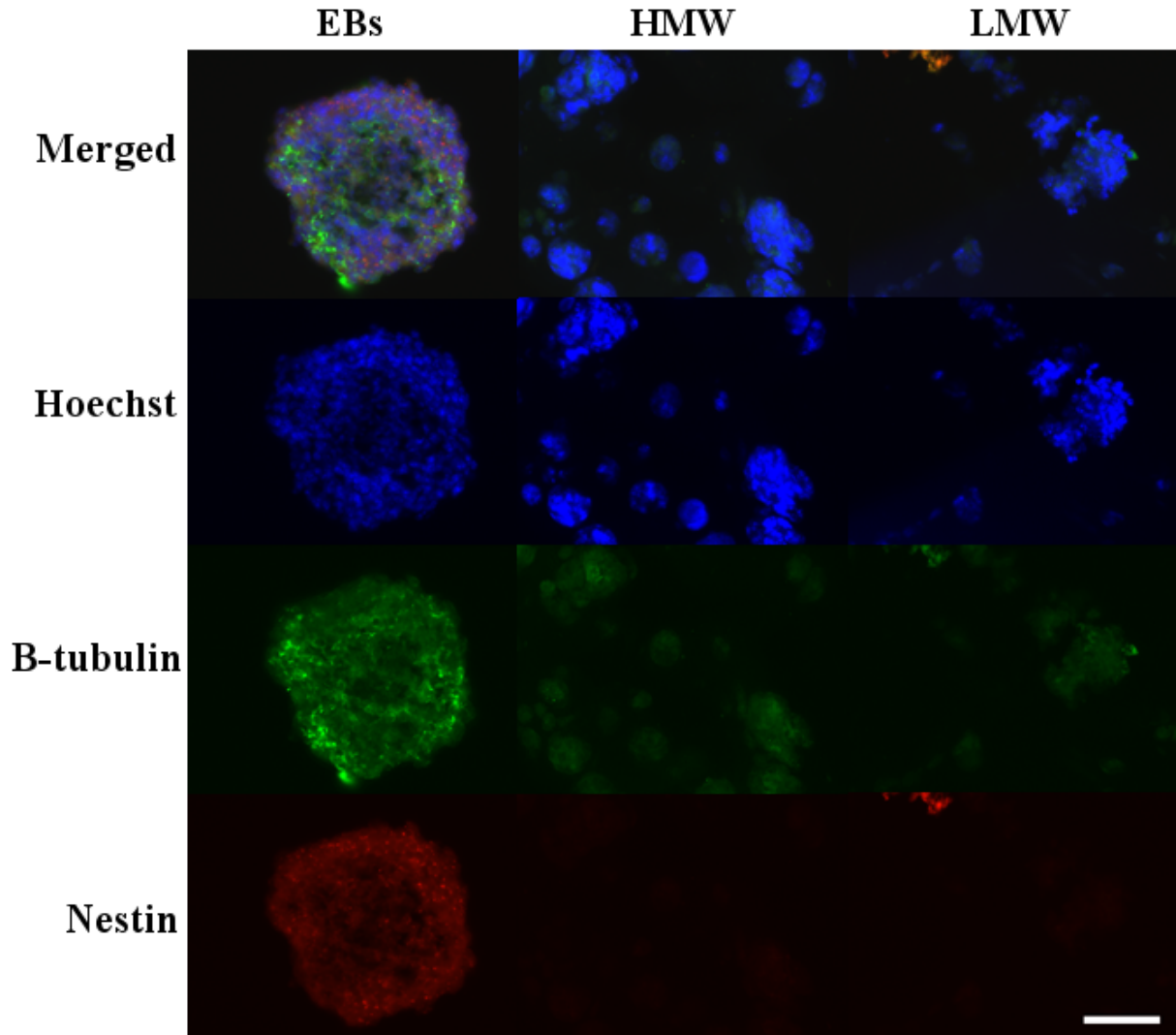


Figure 30: Encapsulated cells were not differentiated by the HGF11-MN source of RA. The results from immunostaining of cryosections of beads co-cultured with HGF11-derived MNs were negative for neural markers Nestin and β -III-tubulin, but EB positive controls had clear staining for both indicating neural differentiation. This demonstrated that the encapsulated cells were not differentiating toward a neural lineage. Images were collected for n=4 independent experiments. Scale Bar: 50 μ m

ent maker/tube formation using 1% w/v solutions of LMW and HMW alginate found that both solutions were too viscose to form alginate tubes using this protocol. During the tube formation, one chamber of the gradient maker was emptied rapidly, followed by the second chamber, thus the solutions were not mixed before being drawn through the tubing to form an alginate tube. To address this, the LMW alginate was diluted 1:2 in DMEM to form a 0.5% solution; the experiments prior to this point did not observe a significant difference in differentiation or viability between the LMW and HMW alginates, thus LMW alginate was chosen for its lower viscosity compared to HMW alginate.

Using the new 0.5% w/v alginate solution, the gradient maker functioned as expected, mixing the cell suspensions in chamber A and B, before drawing the alginate into the tubing. The resulting alginate tubes contained a constant cell density of CGR8 ESCs along the length of the tube, and a graded cell density of HGF11 LMC MNs, to provide a localised concentration gradient of RA within the tubes. The alginate tubes formed had a variable diameter along the length of the tube, and swelled over the course of the cell culture, but the majority of tube remained intact at day 6 (compare Figure 31a and 31b). Brightfield images of the leading and trailing edges, and the centre portion of the tubes, showed that the encapsulated cells had formed aggregates inside the tubes; there were also some free floating aggregates in the culture medium, as previously observed in experiments using alginate beads (see Figure 31c-e).

The presence of the aggregates inside the tubes indicated that unlike the encapsulated ESCs in the Boyden chamber co-culture experiments, the mouse ESCs encapsulated in alginate tubes alongside HGF11-derived LMC MNs, were exposed to sufficient levels of RA to induce aggregation. To determine whether the localised RA had induced ESC differentiation, and to investigate if the opposing concentrations of LMC MNs and the LMC-derived RA affected the level of differentiation, the trailing and leading ends of the alginate tube were cryosectioned and immunostained for markers of the three germ layers. The results observed the presence of cells from all three germ layers in both the trailing and the leading edge of the tubes. Figure 32 shows a comparison of AFP and SMA positive cells, and Figure 33 shows a comparison of the GFP and β -III-tubulin positive cells encapsulated in each end of the tube.

The outcomes from this experiment indicated that although the concentration of RA in the medium was lower than the physiological concentration, the localised RA concentration was sufficient to induce cell differentiation of the encapsulated aggregates. This was a novel

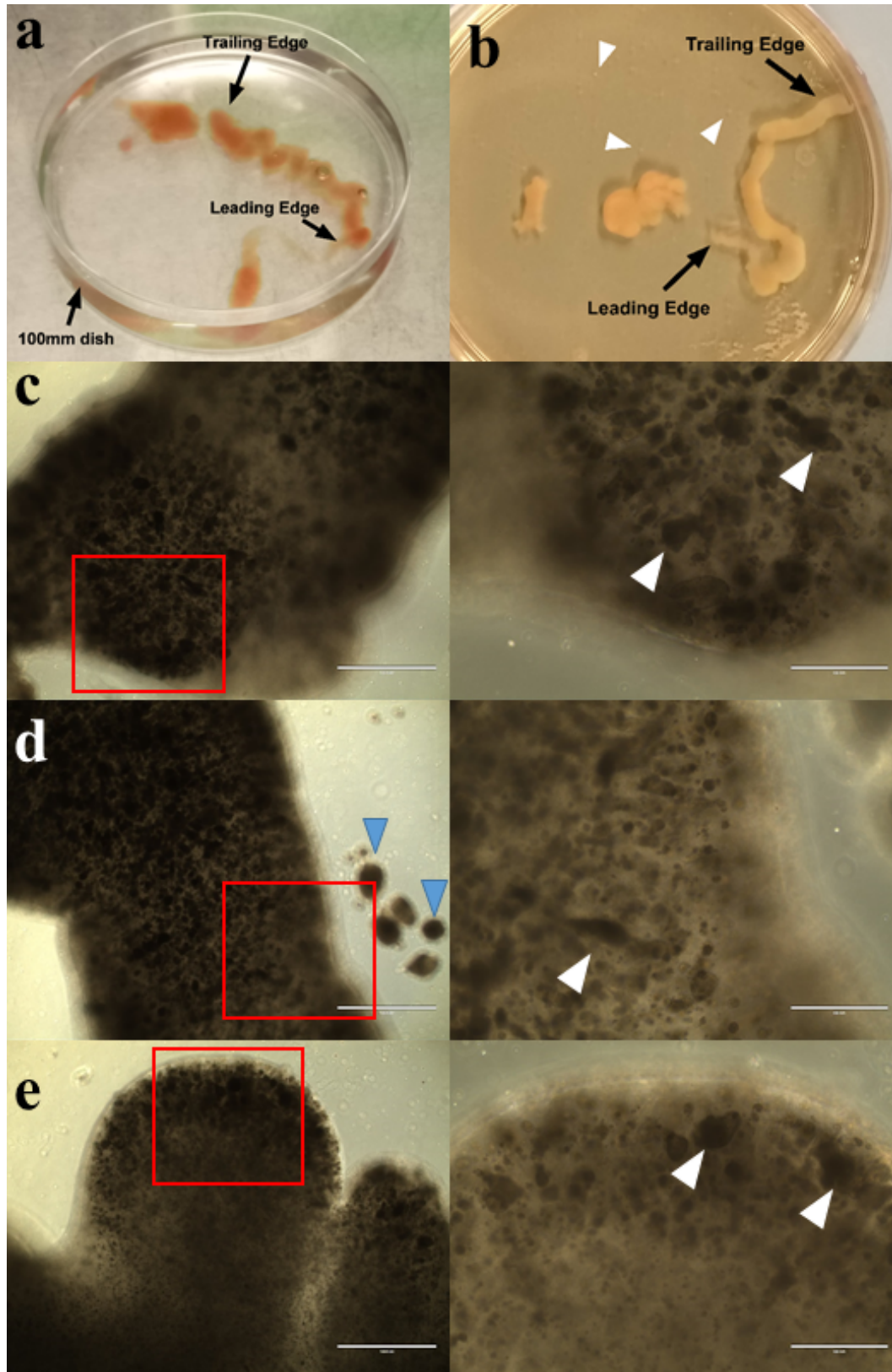


Figure 31: Brightfield images of alginate tubes formed using a gradient maker: (a) the diameter varied across the length of the tube, (b) at day 6, the tube was intact and aggregates were observed floating in the medium (white arrowheads). Low and high (red box) magnification images of the (c) leading, (d) central, and (e) trailing sections of a tube on day 6 showed encapsulated aggregates (white arrowheads), and escaped aggregates in the medium (blue arrowheads). Scale Bars: left panels 1mm, right panels 400 μ m

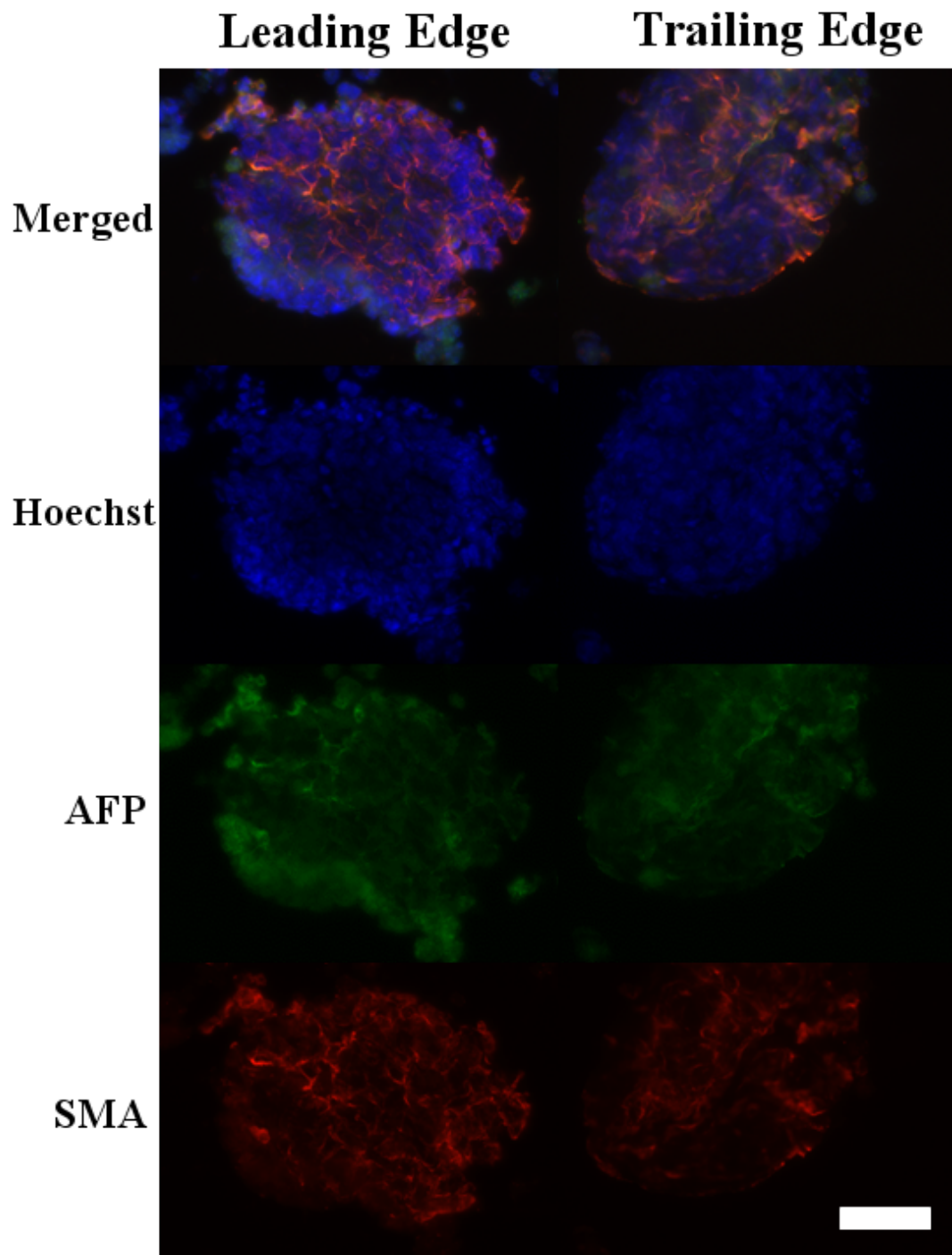


Figure 32: Alginate tubes contained markers for endoderm and mesoderm. The alginate tubes contained markers of endoderm and mesoderm germ layers at day 6 of differentiation. These were present at both the trailing and leading end of the tube. Scale Bar: 50 μ m

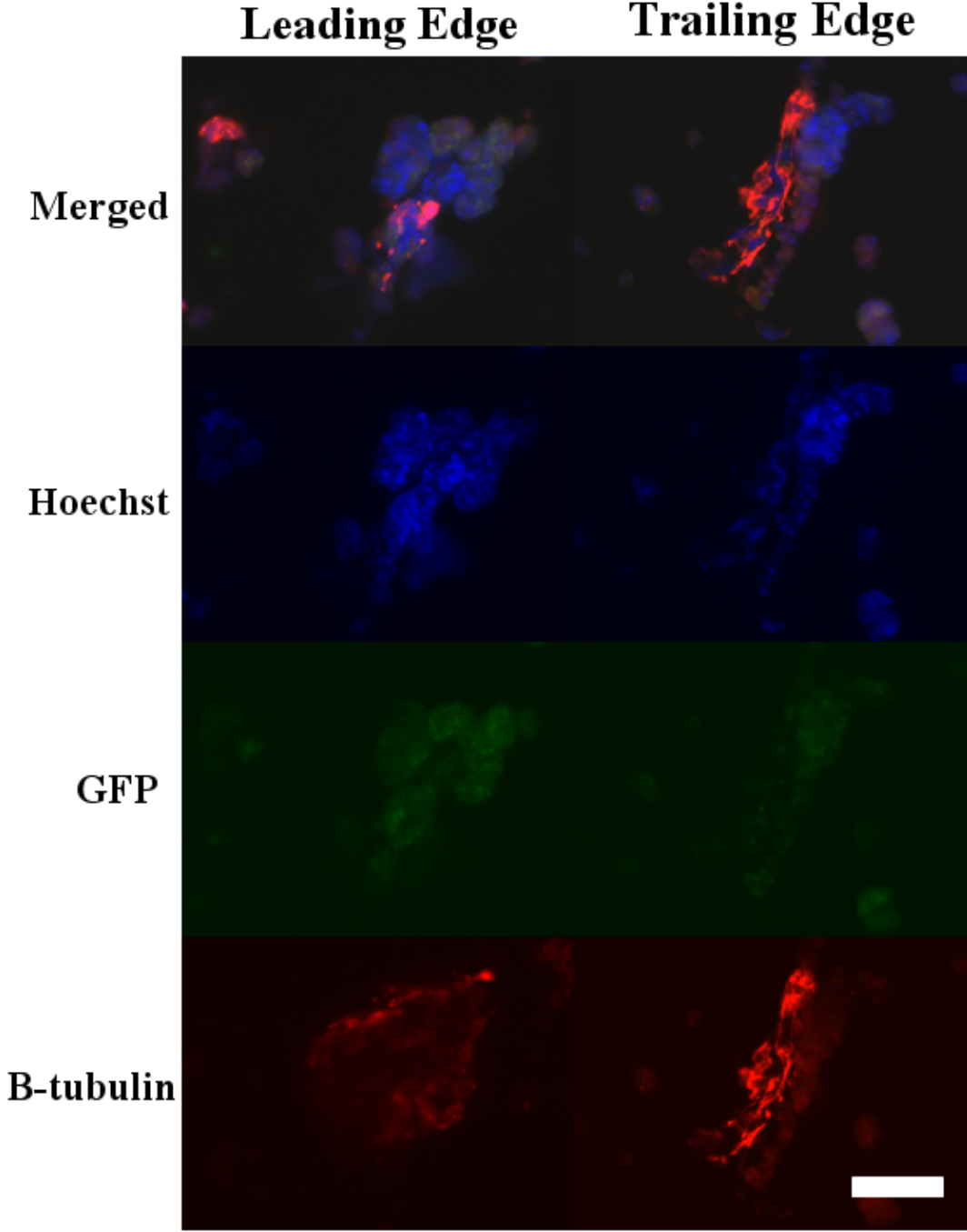


Figure 33: Alginate tubes contained ectoderm marker β -III-tubulin. The alginate tubes contained β -III-tubulin at both the trailing and leading end of the tube at day 6 of differentiation. The tube also contained GFP⁺ cells at both end of the tube. Scale Bar: 50 μ m

.....

result that indicated that this alginate platform holds potential for investigating the effects of a localised gradient of RA signalling on cell differentiation. The results also indicated that the encapsulated ESCs had differentiated toward cells from the three germ layers which was evidence that this hydrogel platform may be adapted and optimised for *in vitro* studies of embryogenesis. This experiment was a preliminary investigation to verify whether this novel co-culture platform was suitable for creating alginate tubes that remained intact in cell culture, could encapsulate gradients of cell densities within the tube and permitted the formation and differentiation of cell aggregates. Based on the results from Chapter 4 and Chapter 5, it was expected that the cells would only differentiate if they had a sufficient concentration of RA to initiate aggregate formation.

The results from Chapter 4 showed that the encapsulated ESCs exposed to 1 μ M of exogenous RA differentiate into cells from the three germ layers. Contrastingly, as observed in the Boyden chamber co-culture experiment, the encapsulated ESCs do not spontaneously differentiate with low concentrations of RA. These findings indicated that the ESCs within the scaffold can successfully form aggregates in the absence of exogenous RA and indicated that the concentration of 215-290pM RA was sufficient to differentiate ESCs. This supports the theory that the physiological concentrations reported for RA (1-100nM) may be considerably higher than the actual concentration(s) of RA available to the cells *in vivo* as the previously reported RA concentrations were quantified from whole tissues and do not account for the RA sequestered in the nuclei or by cellular RA binding proteins.^{76, 224, 225} The formation of aggregates observed in these experiments could be the result of ESC response to the localised production of RA by the HGF11-derived MNs co-encapsulated within the scaffold, or might be due to cell-cell interaction or perhaps paracrine signalling from the encapsulated MNs not via RA signalling. It was also possible that the combination of these three and other unknown variables contributed to the formation of aggregates.

The immunofluorescent images did not indicate whether there was variation in the level of differentiation at the trailing and leading edges of the tubes. A major limitation of this experiment was that the platform did not incorporate a method to track the previously differentiated HGF11-derived MNs or the CGR8, so the previously differentiated HGF11-derived MNs could not be isolated from cells that differentiated from the CGR8 ESCs. Future experiments could incorporate CellTracker or time-lapse imaging to record which cells were originating from each of the encapsulated cell populations. Although the results demonstrated

.....

that there were GFP⁺ cells in close proximity to GFP⁻/β-III-tubulin⁺ cells, which indicated that ESCs differentiated within the platform, there were no instances of GFP⁺/β-III-tubulin⁺ cells from the HGF11-derived MNs. It was possible that within the scaffold, the endogenous GFP was not visible in the images, and antibody staining for GFP may locate the HGF11-derived MNs. In addition, without incorporating a method to track which cells originated from which encapsulated population (CGR8 or HGF11-derived MNs), it was not possible to know whether cells that were positive for markers of the three germ layers differentiated from CGR8 or if they differentiated from carry-over ESCs in the dissociated MN population. As the EB differentiation protocol only generates 30% MNs, 70% of the population remained uncharacterised, thus the EB-generated MN populations may also have contained ESCs or cells from the three germ layers which were subsequently visualised in the alginate tubes.

6.4 Discussion

6.4.1 A cell-produced source of retinoic acid can be used for differentiation

Biomaterials have previously incorporated RA-loaded microcapsules or fibers into the biomaterial scaffolds to induce differentiation or patterned migration of the encapsulated cells.^{11,175} As discussed previously (see subsection 5.4.3), the largest limitation of these studies was the inability to control the release of RA from the scaffold. The previous chapter reported that the HGF11-derived MNs could produce endogenous RA, and the present chapter has demonstrated ESCs cultured in close proximity to these RA-producing cells was sufficient to support differentiation of the encapsulated ESCs towards cell fates from the three germ layers. This was a novel result and has provided evidence that HGF11-derived MNs are a tool for *in vitro* biomaterial differentiation protocols.

The results of these experiments were interpreted with caution as there were no control conditions for these tubes. The formation of aggregates and/or differentiation towards cell types from the germ layers might be due to a cell-cell interaction, a cell-matrix interaction or an RA-induced effect promoted by the HGF11-derived MNs. The results from the Boyden chamber experiment demonstrated that the presence of the HGF11-MNs in the medium was not sufficient to induce aggregate formation or differentiation of ESCs towards the three germ layers. These results indicated that the aggregate formation observed in the alginate tubes was linked to the presence of the HGF11-derived MNs in close range to the encapsulated ESCs, and this close proximity was responsible for the cell differentiation. Experiments to compare

ESC differentiation in the present platform, with a control group of ESCs co-cultured with a non-transgenic, non-RA producing MN population would distinguish between the influence of RA produced by the LMCs and the presence of the MN populations in the tubes.

Neural-antigen 2⁺ glia can produce RA in the spinal cord, and astrocytes can regulate RA signals in the brain.^{232,233} The present experiments did not investigate the presence of astrocytes in the alginate platform and thus an astrocyte-derived source of RA may have contributed to differentiating the encapsulated ESCs. In addition, the experiments did not test the concentrations of RA released locally within the tubes, thus there is no information on the extent of paracrine signalling from neighbouring sections of the tubes on ESC differentiation. A recommended approach to determine these effects is to utilise hybrid biomaterial scaffolds that allow layers of spatially distinct cell-laden biomaterials to be combined. This could easily be achieved by adapting the protocol characterised in these experiments, by swapping the alginate-cell suspension from one gradient maker chamber with a cell suspension in another biomaterial, thus separating the RA source (HGF11-derived MNs) and the pluripotent stem cells (CGR8) but continuing to allow diffusion of the RA through the scaffold. By introducing cell labelling to track the cells from each population (CGR8, LMCs) this layered platform would identify any cell migration in response to cell-cell or cell-matrix interaction. In addition, the layered scaffolds can be immunostained for astrocytes to determine whether an astrocyte-induced source of RA might be inducing cell differentiation. This approach would be possible with alginate-chitosan layered scaffolds,²³¹ fibrin layered scaffolds²³⁴ and alginate-collagen hybrid scaffolds.¹⁹⁰

Despite the limitations of the protocol, the results were promising for future research as using HGF11-derived MNs as a source of RA produced that was physiologically active within the scaffold. The results from chapter 5 showed that the concentration of RA was stable over time, which addresses the limitation of RA burst release into the culture medium as observed in the platforms reported by Binan et al., (2014) and Carpenedo et al., (2010).^{11,175} The cell-derived source of RA means that the RA concentration will be replenished by the encapsulated HGF11-derived MNs between medium changes, and addresses the limitation of light-degradation of RA. These cells are thus a novel tool for producing RA *in vitro* and can be exploited to investigate many aspects of cell development, and to examine the proposed varied signalling pathways activated by exogenous versus endogenous RA.^{71,73,212,235}

6.4.2 Alginate tubes are a novel platform for studying differentiation *in vitro*

Cell-laden alginate hybrid scaffolds are a current focus in biomaterials research due to their potential to support tissue regeneration. Seol et al., (2015)¹³⁴ used chondrocyte-laden alginate-ceramic hybrid hydrogels to regenerate cartilage tissue in rabbits, and Pfister et al., (2007)²³⁶ developed an alginate-chitosan hybrid nerve conduit that promoted cell infiltration into the conduit, and had low immune response to the conduit after it was implanted *in vivo*. Hybrid scaffolds have been used to alter the substrate stiffness throughout the cell culture period, and examine the subsequent changes in cell behaviour.^{166,202} Some protocols have exploited the properties of hydrogel scaffolds to regulate the dissolution of the scaffold *in vivo* and investigate the cell response.¹²² Alginate hydrogels can be adapted to regulate growth factor release from the scaffolds,^{143,168} to control the diffusion of growth factors toward the encapsulated cells¹⁵⁰ and can be loaded with signalling morphogens to induce localised changes in cell behaviour.^{143,180} The results from the current chapter have contributed a novel platform to the field of tissue engineering, that has the capacity to incorporate many of the above features in a single self-contained platform.

The platform presented here can be optimised for investigating cell behaviour and cell differentiation by capitalising on the inherent characteristics of alginate, including the ability to regulate alginate hydrogel substrate stiffness, cell adhesion molecules, diffusion through the hydrogel, and the dissolution rate of the hydrogel *in vivo*. The platform created here has the capacity to allow patterned differentiation of the encapsulated cells, using a novel endogenous source of RA. This platform is unlike the previously reported biomaterial scaffolds incorporating RA as it utilised a cell-produced endogenous source of RA that maintained a consistent concentration over several days. The findings were preliminary, and there are many factors that would need to be optimised to precisely investigate the extent of patterned differentiation capable using this platform but immunofluorescent images provided strong evidence that this platform can be adapted for studying embryogenesis *in vitro*.

6.4.3 Alginate tubes with graded cell densities are novel platforms for investigating gradients of signalling factors *in vitro*

There was high variability in the methods and protocols currently used for culturing cells in 3D biomaterials. These methods include: (i) encapsulating the cells,^{43,117,150,159} (ii) seeding

cells onto freshly formed biomaterials,^{180,204,237} (iii) adding cells to the biomaterial after pre-processing the scaffold to control porosity or topography,^{165,166} and (iv) changing the adhesive factors added to the scaffold^{238–240} to investigate cell behaviour. To record all of the potential effects of 3D culture or biomaterials culture on cell development or behaviour would be a highly labour-intensive process. Even within one 3D cell culture experiment, the studies cannot investigate all of the potential factors affected by the biomaterial-cell interaction, and typically select from a range of variables of interest such as cell viability, cell-cell interaction, cell-matrix interaction, matrix subtype interaction, variability between cell lines, cell fate specification and cell migration within the scaffold. Specifically in studies that used alginate, previous studies have examined the influence of substrate stiffness on cells seeded on a pre-polymerised scaffold,^{165,166} differentiation of ESCs within one type of alginate,^{43,159} or have examined the behaviour of differentiated cells on alginate scaffolds of varying molecular weight.¹⁸⁸

The platform presented here offers the potential to manipulate and control several microenvironment factors within an individual experimental platform. Future experiments to investigate the concentration of RA produced at the trailing/leading edge, across of range of cell seeding densities, and a range of alginate compositions, may shed light on the process of patterned ESC differentiation within alginate tubes. Additionally, the physical structure of the tube changed between the first and second experiment, with the second tube being shorter. This was the result of uneven extrusion of alginate from the tubing into the CaCl₂, which resulted in breakages of the initial portions of the tube. These are limitations that can be addressed by altering the viscosity of the alginate, the diameter of the tubing and the extrusion rate of the peristaltic pump, to create tubes of varying length, diameter, and cell density gradients. These varied tubes can then be characterised to identify the optimal conditions for a range of ESC differentiation experiments or to investigate aggregate formation and differentiation in a 3D platform. Alginate hydrogels are limited in their use for longer term culture, as they dissolve over time in culture medium, but layered alginate scaffolds with collagen or chitosan can be cultured for longer periods, and can be used to adopt this method for extended *in vitro* experiments. The method of tube fabrication is easy to manipulate by changing the soluble hydrogels loaded into each chamber of the gradient maker, for example to vary the porosity or substrate stiffness, or alternative the cell types encapsulated to alter the method of differentiation.

Previous studies have generated outputs that can be combined with the results presented here to build alternate scaffolds for investigating cell behaviour or differentiation. Chatterjee et al., (2011)²⁴¹ used an adapted gradient maker to produce a 3D PEG-dimethacrylate scaffold with an elastic modulus gradient from 10kPa to 300kPa, and encapsulated osteoblasts. They demonstrated selective osteogenic differentiation and mineral deposits at an elastic modulus of 225kPa and higher. Their platform demonstrated that an adapted gradient maker protocol can be used to modulate many of the variables involved in cell-matrix interaction, and highlights the potential for the gradient maker platform presented here to be expanded to include multiple microenvironment variables. Soundarajan et al., (2007)³⁴ generated a cell line that produces an endogenous form of Shh. This cell line can be incorporated into the gradient maker platform from this chapter to co-culture pluripotent stem cells with (i) the HGF11-produced source of RA characterised here, and (ii) the Shh producing cells. This hybrid platform could then form a model for neural tube patterning in a 3D biomaterial microenvironment. The gradient maker protocol outline by Chaterjee et al., (2011) produced a flat, rectangular scaffold that could be sliced into sections.²⁴¹ This protocol may be optimal for modelling the neural tube as cells could initially be cultured on top of the scaffold to examine the differentiation patterns, before incorporating the added variable of cells cultured in 3D (i.e. encapsulated in the scaffold). Developing such a neural tube model would require precise optimisation of the characteristics of the scaffold. A limitation of the alginate for that purpose was the lack of cell adhesion sites, thus manipulation of the attachment factors added to the alginate, or use of an alternative biomaterial allowing controlled cell adhesion would produce more tightly controlled results.¹⁴⁹

6.5 Conclusion

The experiments from this chapter have combined the tools developed in previous chapters to create a novel 3D platform for investigating patterned stem cell differentiation. The HGF11-derived MNs were shown to produce an endogenous source of physiologically active RA, capable of producing a localised source of RA inside alginate tubes. The alginate tubes were a prototype for a novel 3D platform to generate signalling morphogen gradients *in vitro*. The tunability of alginate as a biomaterial means that the 3D platform can be optimised to further investigate the influence of a localised RA gradient on ESC development in 3D. There is an increasing need for reproducible, *in vitro* models of embryogenesis, neurodevelopment, and

tissue regeneration, and the 3D platform presented in this chapter can contribute to each of these - by adapting the platform and incorporating different cells types, or different growth factor gradients, these 3D tubes can mimic the localised signalling gradients that occur *in vivo* and allow us to examine the response of encapsulated cells to a range of growth factors or cell-cell interactions in a 3D microenvironment.

.....

Summary discussion

8.1 Summary of results

The experiments presented in the current thesis have optimised and characterised alginate hydrogel beads as a scaffold for the 3D culture of mouse ESCs (Ch. 3), showed comparable levels of neural differentiation in LMW and HMW alginate beads versus EB suspension cultures, (Ch. 4), characterised a novel cell-produced source of endogenous RA from HGF11-derived LMC MNs (Ch. 5), and produced a novel 3D platform for investigating patterned ESC differentiation in response to morphogen gradients *in vitro* (Ch. 6).

8.2 Importance of the current results for 3D cell culture applications

8.2.1 Applications of embryoid body culture within alginate hydrogels

This thesis demonstrated for the first time that aggregates formed by ESCs encapsulated in alginate beads are canonical EBs containing cells from the three germ layers. In demonstrating the presence of the three germ layers, these experiments showed that alginate beads are suitable biomaterial for investigating EB differentiation in 3D. The implantation of EBs to a 3D gelatin scaffold was previously demonstrated to promote self-organisation of the embryonic germ layers.⁵⁵ As mentioned previously, one study allowed mouse ESCs to undergo extended differentiation in suspension culture, and showed that the resulting organoids contained tissues from the neural plate and spinal cord.³² More recently, a study combined mouse-EB cell cultures with extraembryonic trophoblast stem cells using a 3D Matrigel scaffold.²⁴² The study showed that the resulting embryos were a precise 3D model of embryogenesis that mimicked the self-organisation of embryogenesis *in vivo*, both temporally and spatially. The study also demonstrated that the *in vitro* scaffolds could be used to investigate the self-organisation of the embryos in response to Wnt, BMP and Nodal signalling.²⁴² The above studies demonstrated that a combination of 3D culture with EB differentiation holds potential to discover new information about the mechanisms of cell development. In verifying that alginate hydrogels support EB differentiation in 3D, the current thesis showed that alginate scaffolds are an alternative biomaterial for similar experiments. The tunability of alginate provides an additional benefit for choosing alginate hydrogels over alternative biomaterials for 3D culture applications. The properties of alginate hydrogels makes them highly tunable

for a given experimental paradigm, such that the characteristics of the hydrogel can be sequentially adapted to investigate the self-organisation of the EB germ layers in response to different microenvironments. In doing so, alginate:EB differentiation could be a new research tool for examining cell-matrix interaction effects on cell fate specification.

8.2.2 Co-culture experiments are important for 3D culture

HGF11-derived LMC MNs were established as a novel *in vitro* source of endogenous RA. The novel cell-produced source of RA is easy to generate, as it requires only basic cell culture equipment, a 6 day differentiation protocol and inexpensive reagents, thus can be easily adopted by other research groups as an *in vitro* tool. The MNs provided stable concentrations of RA, and furthermore, co-culturing the HGF11-MNs alongside ESCs within alginate tubes demonstrated that a localised source of RA influenced ESC aggregation and differentiation. The concentrations of RA produced by the MNs were low relative to the standard concentrations used *in vitro* (100nM to 1µM) and the reported concentrations *in vivo* (1-300nM) however the ability to introduce the RA in close proximity to the ESCs was a more important feature of this source of RA. As mentioned above, one study combined EB culture, trophoblast stem cell culture and biomaterial scaffolds to investigate the development of embryonic and extraembryonic tissues within the 3D platform. Their results are an example of the advantages of using co-culture methods to investigate cell behaviours.²⁴² In showing that co-encapsulation of LMC MNs and ESCs induced cell differentiation to fates from the three germ layers, this thesis provided further evidence that 3D co-culture experiments may provide new methods for examining the influence of cell-cell interaction, or paracrine signalling from neighbouring cells, on ESC differentiation.

In the Boyden chamber experiment (Ch.6, p.115) HGF11-MNs were cultured in the same medium as ESCs encapsulated in alginate beads. Over 6 days of cell culture, the encapsulated ESCs did not aggregate within the alginate beads, but when the two cell types were co-cultured, the ESCs aggregated and differentiated to cell types from the three germ layers. RA acts in a paracrine manner *in vivo* and the observed differentiation in the current experiments may have been an ESC response to the low levels of RA produced by the LMCs. Alternatively, the LMC MNs were encapsulated in close proximity to the ESCs in the platform so it is possible that the observed cell differentiation was the result of an uncontrolled variable occurring through cell-cell interactions, or signalling via another soluble factor re-

leased by the LMCs.⁶⁴ A previous study on ESC-derived germ layer cells reported that the cell-cell interactions and cell-matrix interactions were important for specifying cell fate,⁸¹ thus the same effect may occur within the platform described here. As the Boyden chamber experiment showed that ESCs did not aggregate when encapsulated alone (without LMCs), it was unlikely that a cell-matrix effect was responsible for the ESC aggregation and differentiation observed in the co-culture tube experiments. This instead points toward a cell-cell interaction through the actions of the LMCs. DEAB is an inhibitor of Raldh2 and could be used to interrupt the LMC MN-produced RA within the scaffolds, to observe any effects from non-RA induced effects by the co-culture paradigm.⁷⁷ Inhibiting Raldh2-synthesis of RA would determine if there are other non-RA induced, cell-cell interactions influencing ESC aggregation and differentiation.

8.2.3 The 3D platform for patterned differentiation addressed the limitations of previously reported 3D gradients of soluble factors

The novel alginate tubes created cross gradients of HGF11-derived MNs with stable cell densities of ESCs to investigate the influence of morphogen gradients on ESC differentiation. As mentioned previously, a major limitation of 2D cell culture is the inability to introduce soluble factor gradients to the cells.⁴ Gradients of signalling morphogens are challenging to produce in 3D, due to the burst release of soluble factors from biomaterials. One study reported a loss of 15% of the original concentration of NGF in a biomaterial scaffold after 1 day, and 35% after 1 week in culture medium.²⁴³ A second study used photopolymerisation of PEG-dimethacrylate hydrogels to incorporate IKVAV gradients within the scaffold, however the requirement for UV exposure (6min) makes these scaffolds unsuitable for cell encapsulation, but suitable for experiments where cells are seeded onto the scaffold after the gradients are introduced.¹³⁸

The LMC MN source of RA established in this thesis was stable over at least 5 days of cell culture thus addressed the limitation of burst release from biomaterials scaffolds as the source of RA originated within the scaffolds. In addition, the LMC-produced source of RA also reduced the variability introduced by light-induced degradation of exogenous RA, as the cells can replenish the RA concentration between medium changes after being replaced into the incubator. The concentration of RA released along the slope of the alginate tubes was not tested, but the 3D platform set a foundation for future experiments to optimise this

protocol. For example, Purcell et al., (2009) investigated the rates of growth factor release by encapsulated cells in G-rich and M-rich alginate hydrogel scaffolds.¹⁶⁹ They showed that the rates of growth factor release could be controlled using the alginate G:M ratio and whether the beads were coated or uncoated: (i) neural stem cells in G-rich alginates produced 3-fold more NGF relative to neural stem cells in M-rich alginates, (ii) PLL coated M-rich alginates produced 2-fold more NGF relative to uncoated M-rich alginates. Their results suggested that the 3D platform described here can be adapted to offer increased control over the concentrations of RA released, by changing the composition of the hydrogel tubes to promote RA synthesis by the encapsulated LMC MNs. This contributed to novel avenues for investigating the influence of 3D soluble factor gradients on ESC differentiation.

8.2.4 *In vivo* applications of the 3D platform for patterned differentiation

For *in vivo* applications, alginate hydrogels can be polymerised *in situ*¹²³ or can be surgically implanted to a lesion site.^{184,231} After spinal cord injury, the glial scar creates an increased elastic modulus in the area surrounding the lesion that inhibits cell differentiation.⁶⁴ Biomaterials can combat this effect, limiting glial scar formation and supporting tissue regeneration.¹³⁹ For example, Shin et al., (2018) surgically implanted a neural stem cell-laden poly-glycolic acid (PGA) scaffold at the site of spinal cord lesions in neonatal mice.²⁴⁴ Their results showed that the implanted scaffold reduced the formation of glial scarring at the site of injury, and that the encapsulated neural progenitor cells had migrated from the scaffolds, into the infarct, and differentiated into neurons and astrocytes. The authors also reported functional benefits to the cell:biomaterial implant: mice who received the combined cell:scaffold implant had improved motosensory recovery compared to mice receiving a cell-only or scaffold-only implant.²⁴⁴ Another study used a hybrid HA:astrocyte-derived ECM scaffold to promote V2a interneuron migration from the scaffolds and into the lesion site in mouse spinal cord.²⁴⁵ This study, and the studies discussed above highlight the need for 3D cell-laden scaffolds that are capable of delivering cells to the point of injury, and also permitting the implanted cells to penetrate the site of injury and promote regeneration or functional recovery of host tissue.

Within the peripheral nervous system, RA-induced activation of RARs after nerve injury promotes regeneration and previous *in vitro* studies demonstrated that RAR activation is sufficient to promote axonal regeneration of rat cortical neurons.⁶⁴ The 3D platform for

patterned differentiation can be used in a similar manner to the above studies, delivering a source of MNs to the site of spinal cord injury, and simultaneously a cell-produced source of RA. By implanting an LMC-laden alginate scaffold at the site of a spinal cord lesion (or polymerising the hydrogel *in situ*), the effects of endogenous RA on the regeneration of cells after injury in the CNS can be investigated. Optimised versions of the platform presented here, containing high purity LMCs and vitamin-A loaded microspheres, could monitor the effects of local peaks and troughs of RA on cell differentiation, regeneration and axonal guidance of limb-innervating MNs *in vivo*. The HGF11-derived MNs have previously been demonstrated to migrate towards the correct muscle targets after implantation.¹² This is evidence that delivering *in vitro* derived cell-analogues for *in vivo* cell types could be used to promote regeneration of the spinal cord after injury. In the paradigm outlined here, the LMCs would be capable of mimicking their *in vivo* counterparts and correctly projecting axonal trajectories to their target muscles. To build upon the platform presented here, further investigation of the concentration of RA produced along the slope of the cell density gradient could permit more fine-tuned investigations of cell development in the scaffold and be used to predict the *in vivo* response of the host tissues to the concentration gradient.

8.2.5 A novel platform for investigating 9-cis-RA activation of RAR/RXRs

RXRs are highly abundant at the limb-levels of the spinal cord, which indicates a relationship between the LMC MN-derived source of RA and activation of RXR/RAR complexes during limb innervation.^{100,221,246} As RARs form heterodimers with RXRs, there may be a role for 9-cis-RA in specifying LMC positional identities and muscular targets during limb-innervation.⁷⁴⁻⁷⁶ As mentioned previously, 9-cis-RA is only detected *in vivo* when embryos are exposed to supraphysiological concentrations of RA, thus 9-cis-RA may prevent teratogenic concentrations of RA from inducing off-target effects during LMC differentiation, such as abnormal cell fate specification or LMC innervation of the incorrect muscle.^{74,76}

The 3D platform for patterned differentiation described here is uniquely situated to investigate whether the effects of 9-cis-RA in response to supraphysiological concentrations of RA are a protective measure against RA-induced teratogenicity, or if there is another function for 9-cis-RA that has not been discovered. *In vitro* MN differentiation protocols use supraphysiological concentrations of exogenous RA, which are known to produce supraphysiological concentrations of 9-cis-RA, and are proposed to activate off-target signalling pathways.⁷⁵ By

.....

supplementing increasing concentrations of retinal to the medium of HGF11-derived LMCs, the LMCs may produce a supraphysiological concentration of RA.⁷⁶ The subsequent concentrations of endogenous 9-cis-RA in the medium, metabolised from supraphysiological concentrations of endogenous RA could then be quantified. Using the novel co-culture 3D platform presented here, the effects of supraphysiological levels of LMC-produced endogenous RA on 9-cis-RA concentration, RAR/RXR activation, and ESC differentiation can be examined. This would provide new information about the relationship between RA and 9-cis-RA concentrations *in vitro* that cannot be investigated using exogenous RA.

Alternatively, using the same methods as above to create supraphysiological concentrations of RA, and simultaneously antagonising RARs or RXRs in the encapsulated cells, the platform could be used to investigate whether RAR, RXR or combined RAR/RXR activation is necessary for inducing ESC differentiation *in vitro*. The rate of receptor activation in response to increasing concentrations of endogenous RA (due to supplementing retinol or retinal to the medium), and subsequently to the increasing concentrations of 9-cis-RA would provide new information about the relationship between teratogenic concentrations of RA and activation of RXRs. A previous study reported that 9-cis-RA and RA were capable of inducing differentiation in P19 embryonic carcinoma cells, but that 9-cis-RA was 50-100 times more potent compared to all-trans retinoic acid.²²⁴ Alternatively, another study showed that P19 cells expressed different RARs depending on the stage of development,²⁴⁷ which suggests there may be differential rates of RAR and RXR activation in differentiating ESCs, in response to either RA or 9-cis-RA, depending on the stage of differentiation. RAR α , RXR α and RXR β are widely expressed during development whereas RAR β , RAR γ and RXR γ have tissue-specific expression,⁶⁷ further suggesting that ligand binding of 9-cis-RA or RA to RAR/RXR receptor complexes has a stage-dependent effect on development. The influence of the RA in the medium on activation of LMC-specific RXRs and RARs, or the ESC-specific RXRs and RARs could further determine if there are differences in the rates of receptor activation depending on the cell type or cell stage of development. These experiments would answer some long standing questions about the role of 9-cis-RA in RA-induced differentiation *in vitro*, and can provide important information about the on-target and off-target effects of exogenous and endogenous RA during differentiation.

8.2.6 Concluding remarks

This experiments presented within this PhD thesis have contributed several novel results to the field of 3D cell culture. The 3D platform for patterned differentiation is a new tool for *in vitro* 3D cell culture that provides a foundation for a wide range experiments investigating patterned ESC differentiation. The platform can be optimised and adapted to investigate the impact of co-culture methods on ESC differentiation, to examine the RA specific and non-RA specific mechanisms involved in ESC differentiation and to examine the role of 9-cis-RA in *in vitro* neuronal differentiation protocols. The ability to introduce additional or alternative cell types, combined with growth factor gradients, makes the 3D platform a suitable tool to investigate the interdependence of cell-matrix, cell-cell and soluble factor effects during differentiation. The use of an adapted gradient maker protocol provides a technical benefit, as alternative biomaterials can be combined or interchanged with alginate; this would allow cell types that are not easily cultured in alginate to be combined with the 3D platform in an alternate biomaterial. The research opportunities provided by the 3D platform for patterned differentiation are substantial and the platform is thus an important tool that this thesis contributed to 3D cell culture applications.

The individual components of the platform also contributed novel tools and insights to *in vitro* cell culture. The cell-produced source of endogenous RA was used to provide a localised concentration gradient of RA to the encapsulated ESCs, and although the all or some of the observed patterned differentiation may be due to non-RA induced effects, the results have demonstrated that a co-culture paradigm is important for inducing ESC differentiation in 3D cultures. By validating that the LMC MNs are a stable source of RA, this thesis contributed a useful tool for providing localised, low level RA concentrations to ESCs. Although the protocol requires characterisation to determine the production rate and upper concentration of RA that can be achieved, the results as they stand have contributed towards new research avenues in 2D and 3D cultures, such as comparing the rates of ESC differentiation towards cell fates from each of the germ layers using cell-derived and exogenous RA, or creating RA gradients in alternative biomaterials to investigate if ESC differentiation can be induced in alternate scaffolds with differing properties.

A driving hypothesis behind the experiments comparing LMW and HMW alginate was that a direct comparison of alginate hydrogels of different G:M ratios would identify whether

high-G or high-M alginate hydrogels were optimal for ESC differentiation to cells from the germ layers. The results showed no significant difference between the two alginate compositions, which suggests that in contrast to the published studies, ESC differentiation in alginate may not be as sensitive to the 3D culture conditions as previously reported. The results showed, for the first time, that EBs in alginate beads are canonical EBs and contain cells from each of the three germ layers. The results definitively showed that cell fates from each of the three germ layers can be investigated in alginate, which demonstrated that alginate scaffolds are not only suitable for ESC encapsulation, but also that ESCs can be induced to form EBs in alginate hydrogels of different G- and M-residue content. Experiments building on this knowledge can investigate ESC differentiation towards derivatives of each germ layer in scaffolds of different G:M types, where the scaffold properties can be tuned to support the terminal cell fate. As the ESCs will differentiate in both high G- and high M-residue alginates, this allows for long term culture by creating hydrogels characteristics that will support the mature cells, and thus allows the influence of cell-matrix on later stages of development to be examined.

To conclude, this thesis answered questions about the utility of alginate hydrogels as 3D biomaterials, demonstrating that alginate can be used to support EB formation and differentiation from encapsulated ESCs. The thesis provided a novel solution that addresses the limitations of exogenous RA differentiation protocols, and can be applied in both 2D and 3D culture applications. This PhD created novel tools for *in vitro* culture that are easy to produce, affordable, adaptable and scalable, and in doing so contributed new knowledge to the field of 3D cell culture that will inform future experiments using alginate hydrogels.

Appendix 1

Item	Supplier	Code
Advanced DMEM-F12	Gibco	11540446
Alginate, high molecular weight	Acros Organics	17777
Alginate, low molecular weight	Sigma-Aldrich	71238
β -mercaptoethanol	Gibco	11528926
Calcium chloride, salt	Fisher Scientific	10161800
CF1 mouse embryonic fibroblasts	Merck	PMEF-CFL
CGR8 wildtype mouse ESCs	Sigma-Aldrich	08032901-1VL
DMEM , high glucose, no l-glutamine	Gibco	11500416
dPBS +MgCl ₂ , +CaCl ₂	Gibco	11580456
dPBS -MgCl ₂ , -CaCl ₂	Gibco	12559069
EDTA, disodium salt	Fisher Scientific	S311500
ESGRO mouse LIF, concentrated	Merck	ESG1107
ESGRO mouse LIF, non concentrated	Merck	ESG1106
FBS South American, EU Approved; Lot: FB-1001H	Gibco	11550356
Fluorescein diacetate	Sigma-Aldrich	F7378-5G
GDNF from mouse	Sigma-Aldrich	SRP3200
Gelatin 2% type B, porcine	Sigma-Aldrich	G1393-100ML
Gradient maker	Sigma-Aldrich	GESG100
Hepes	Fisher Scientific	10397023
ImmEdge hydrophobic pen	Vector Labs	H4000
Knockout serum replacement	Gibco	10828028
Laminin	Merck	CC095-5MG
L-glutamine	Gibco	11539876
Mitomycin C	Sigma-Aldrich	Y0000378
Mouse Ralhd2 ELISA Kit	MyBioSource	MBS7237205
Mouse RA ELISA Kit	MyBioSource	MBS706971
Neurobasal medium	Gibco	11570556

Appendix

.....

Item	Supplier	Code
Non-essential amino acids	Gibco	11140050
Normal goat serum	Gibco	16210072
Parafilm	Fisher Scientific	1535088
Paraformaldehyde 37%	Sigma-Aldrich	252549-500ML
PBS 1X tablets	Fisher Scientific	10388739
Penicillin/streptomycin	Gibco	11548876
Purmorphamine	Sigma-Aldrich	SML0868-5MG
Quantinova SYBR green kit	Qiagen	208054
Quantinova reverse transcription kit	Qiagen	205411
Retinoic acid	Sigma-Aldrich	R2625-50MG
RNeasy mini kit	Qiagen	74106
RNeasy min ELUTE	Qiagen	74204
Sodium chloride	Fisher Scientific	S271500
Sodium citrate	Fisher Scientific	S279500
Thiazole orange	Sigma-Aldrich	390062-250MG
Tissue-Tek OCT	VWR	62550-01
Triton X-100	Sigma-Aldrich	X100-100ML
Trypan blue	Gibco	15250061
Trypsin-EDTA	Gibco	11570626
Vectashield mounting medium	Vector Labs	H1000

References

- [1] S. Pauklin, R. A. Pedersen, and L. Vallier, “Mouse pluripotent stem cells at a glance,” *J. Cell Sci.*, vol. 124, no. 22, pp. 3727–3732, 2011.
- [2] M. Schindler, A. Nur-E-Kamal, I. Ahmed, J. Kamal, H.-Y. Liu, N. Amor, A. S. Ponery, D. P. Crockett, T. H. Grafe, H. Y. Chung, T. Weik, E. Jones, and S. Meiners, “Living in three dimensions: 3D nanostructured environments for cell culture and regenerative medicine,” *Cell Biochem. Biophys.*, vol. 45, no. 2, pp. 215–227, 2006.
- [3] J. A. Burdick and G. Vunjak-Novakovic, “Engineered Microenvironments for Controlled Stem Cell Differentiation,” *Tissue Eng. Part A*, vol. 15, pp. 205–219, feb 2009.
- [4] M. W. Tibbitt and K. S. Anseth, “Hydrogels as extracellular matrix mimics for 3D cell culture,” *Biotechnol. Bioeng.*, vol. 103, pp. 655–663, jul 2009.
- [5] K. I. Draget, G. Skjåk-Bræk, and B. T. Stokke, “Similarities and differences between alginate gels and ionically crosslinked alginate gels,” *Food Hydrocoll.*, vol. 20, no. 2-3 SPEC. ISS., pp. 170–175, 2006.
- [6] A. J. Engler, S. Sen, H. L. Sweeney, and D. E. Discher, “Matrix Elasticity Directs Stem Cell Lineage Specification,” *Cell*, vol. 126, pp. 677–689, aug 2006.
- [7] T. Maguire, E. Novik, R. Schloss, and M. Yarmush, “Alginate-PLL microencapsulation: Effect on the differentiation of embryonic stem cells into hepatocytes,” *Biotechnol. Bioeng.*, vol. 93, pp. 581–591, feb 2006.
- [8] D. A. Colón-Ramos, “Synapse Formation in Developing Neural Circuits,” in *Curr. Top. Dev. Biol.*, vol. 87, ch. 2, pp. 53–79, Burlington: Elsevier, 2009.
- [9] C. R. Kothapalli and R. D. Kamm, “3D matrix microenvironment for targeted differentiation of embryonic stem cells into neural and glial lineages,” *Biomaterials*, vol. 34, pp. 5995–6007, aug 2013.
- [10] T.-Y. Cheng, M.-H. Chen, W.-H. Chang, M.-Y. Huang, and T.-W. Wang, “Neural stem cells encapsulated in a functionalized self-assembling peptide hydrogel for brain tissue engineering,” *Biomaterials*, vol. 34, pp. 2005–2016, mar 2013.
- [11] L. Binan, C. Tendey, G. De Crescenzo, R. El Ayoubi, A. Ajji, and M. Jolicœur, “Differentiation of neuronal stem cells into motor neurons using electrospun poly-L-lactic acid/gelatin scaffold,” *Biomaterials*, vol. 35, no. 2, pp. 664–74, 2014.
- [12] K. L. Adams, D. L. Rousso, J. A. Umbach, and B. G. Novitch, “Foxp1-mediated programming of limb-innervating motor neurons from mouse and human embryonic stem cells,” *Nat. Commun.*, vol. 6, p. 6778, apr 2015.
- [13] L. Luo, “Actin Cytoskeleton Regulation in Neuronal Morphogenesis and Structural Plasticity,” *Annu. Rev. Cell Dev. Biol.*, vol. 18, pp. 601–635, nov 2002.
- [14] Z. Khosravizadeh, S. Razavi, H. Bahramian, and M. Kazemi, “The beneficial effect of encapsulated human adipose-derived stem cells in alginate hydrogel on neural differentiation,” *J. Biomed. Mater. Res. Part B Appl. Biomater.*, vol. 102, pp. 749–755, may 2014.
- [15] a. Fraichard, O. Chassande, G. Bilbaut, C. Dehay, P. Savatier, and J. Samarut, “In vitro differentiation of embryonic stem cells into glial cells and functional neurons,” *J. Cell Sci.*, vol. 108 (Pt 1, pp. 3181–3188, 1995.

- [16] J. A. Thomson, “Embryonic Stem Cell Lines Derived from Human Blastocysts,” *Science (80-.)*, vol. 282, pp. 1145–1147, nov 1998.
- [17] A. Montgomery, A. Wong, N. Gabers, and S. M. Willerth, “Engineering personalized neural tissue by combining induced pluripotent stem cells with fibrin scaffolds,” *Biomater. Sci.*, vol. 3, no. 2, pp. 401–413, 2015.
- [18] C. E. Pickford, R. J. Holley, G. Rushton, M. P. Stavridis, C. M. Ward, and C. L. Merry, “Specific Glycosaminoglycans Modulate Neural Specification of Mouse Embryonic Stem Cells,” *Stem Cells*, vol. 29, pp. 629–640, apr 2011.
- [19] B. J. Conley, J. C. Young, A. O. Trounson, and R. Mollard, “Derivation, propagation and differentiation of human embryonic stem cells,” *Int. J. Biochem. Cell Biol.*, vol. 36, pp. 555–567, apr 2004.
- [20] A. M. Wobus and K. R. Boheler, “Embryonic Stem Cells : Prospects for Developmental Biology and Cell Therapy,” *In Vitro*, vol. 85, no. 2, pp. 635–678, 2005.
- [21] B. V. Johnson, N. Shindo, P. D. Rathjen, J. Rathjen, and R. A. Keough, “Understanding pluripotency - How embryonic stem cells keep their options open,” *Mol. Hum. Reprod.*, vol. 14, no. 9, pp. 513–520, 2008.
- [22] H. Kurosawa, “Methods for inducing embryoid body formation: in vitro differentiation system of embryonic stem cells,” *J. Biosci. Bioeng.*, vol. 103, pp. 389–398, may 2007.
- [23] L. B. Hazeltine, J. A. Selekman, and S. P. Palecek, “Engineering the human pluripotent stem cell microenvironment to direct cell fate,” *Biotechnol. Adv.*, vol. 31, pp. 1002–1019, nov 2013.
- [24] H. Wichterle and M. Peljto, “Differentiation of Mouse Embryonic Stem Cells to Spinal Motor Neurons,” in *Curr. Protoc. Stem Cell Biol.*, pp. 1–9, Hoboken, NJ, USA: John Wiley & Sons, Inc., may 2008.
- [25] N. D. Evans, C. Minelli, E. Gentleman, V. LaPointe, S. N. Patankar, M. Kallivretaki, X. Chen, C. J. Roberts, and M. M. Stevens, “Substrate stiffness affects early differentiation events in embryonic stem cells,” *Eur. Cells Mater.*, vol. 18, pp. 1–13, 2009.
- [26] A. Ranga, M. Girgin, A. Meinhardt, D. Eberle, M. Caiazza, E. M. Tanaka, and M. P. Lutolf, “Neural tube morphogenesis in synthetic 3D microenvironments,” *Proc. Natl. Acad. Sci.*, vol. 113, pp. E6831–E6839, nov 2016.
- [27] I. Smith, V. Silveirinha, J. L. Stein, L. de la Torre-Ubieta, J. A. Farrimond, E. M. Williamson, and B. J. Whalley, “Human neural stem cell-derived cultures in three-dimensional substrates form spontaneously functional neuronal networks,” *J. Tissue Eng. Regen. Med.*, pp. n/a–n/a, feb 2015.
- [28] D. A. McCreedy, C. R. Rieger, D. I. Gottlieb, and S. E. Sakiyama-Elbert, “Transgenic enrichment of mouse embryonic stem cell-derived progenitor motor neurons,” *Stem Cell Res.*, vol. 8, pp. 368–378, may 2012.
- [29] D. E. Discher, D. J. Mooney, and P. W. Zandstra, “Growth Factors, Matrices, and Forces Combine and Control Stem Cells,” *Science (80-.)*, vol. 324, pp. 1673–1677, jun 2009.
- [30] J. Zhou, Y. Zhang, Q. Lin, Z. Liu, H. Wang, C. Duan, Y. Wang, T. Hao, K. Wu, and C. Wang, “Embryoid bodies formation and differentiation from mouse embryonic stem cells in collagen/Matrigel scaffolds,” *J. Genet. Genomics*, vol. 37, no. 7, pp. 451–460, 2010.

References

.....

- [31] Y. Okada, T. Shimazaki, G. Sobue, and H. Okano, “Retinoic-acid-concentration-dependent acquisition of neural cell identity during in vitro differentiation of mouse embryonic stem cells,” *Dev. Biol.*, vol. 275, pp. 124–142, nov 2004.
- [32] A. Meinhardt, D. Eberle, A. Tazaki, A. Ranga, M. Niesche, M. Wilsch-Bräuninger, A. Stec, G. Schackert, M. P. Lutolf, and E. M. Tanaka, “3D Reconstitution of the Patterned Neural Tube from Embryonic Stem Cells,” *Stem Cell Reports*, vol. 3, pp. 987–999, dec 2014.
- [33] D. Poli, V. P. Pastore, and P. Massobrio, “Functional connectivity in in vitro neuronal assemblies,” *Front. Neural Circuits*, vol. 9, no. October, pp. 1–14, 2015.
- [34] P. Soundararajan, B. W. Lindsey, C. Leopold, and V. F. Rafuse, “Easy and Rapid Differentiation of Embryonic Stem Cells into Functional Motoneurons Using Sonic Hedgehog-Producing Cells,” *Stem Cells*, vol. 25, no. 7, pp. 1697–1706, 2007.
- [35] Z.-B. Wang, X. Zhang, and X.-J. Li, “Recapitulation of spinal motor neuron-specific disease phenotypes in a human cell model of spinal muscular atrophy,” *Cell Res.*, vol. 23, pp. 378–393, mar 2013.
- [36] T. Richardson, P. N. Kumta, and I. Banerjee, “Alginate Encapsulation of Human Embryonic Stem Cells to Enhance Directed Differentiation to Pancreatic Islet-Like Cells,” *Tissue Eng. Part A*, vol. 20, no. 23-24, pp. 3198–3211, 2014.
- [37] B.-Y. Hu and S.-C. Zhang, “Differentiation of spinal motor neurons from pluripotent human stem cells,” *Nat. Protoc.*, vol. 4, pp. 1295–1304, aug 2009.
- [38] M. P. Stavridis and A. G. Smith, “Neural differentiation of mouse embryonic stem cells,” *Biochem. Soc. Trans.*, vol. 31, pp. 45–49, feb 2003.
- [39] G. Bain, D. Kitchens, M. Yao, J. E. Huettner, and D. I. Gottlieb, “Embryonic stem cells express neuronal properties in vitro.,” 1995.
- [40] M. Zhou, P. Li, L. Tan, S. Qu, Q. L. Ying, and H. Song, “Differentiation of mouse embryonic stem cells into hepatocytes induced by a combination of cytokines and sodium butyrate,” *J. Cell. Biochem.*, vol. 109, no. 3, pp. 606–614, 2010.
- [41] P. J. Johnson, A. Tatara, D. A. McCreedy, A. Shiu, and S. E. Sakiyama-Elbert, “Tissue-engineered fibrin scaffolds containing neural progenitors enhance functional recovery in a subacute model of SCI,” *Soft Matter*, vol. 6, no. 20, p. 5127, 2010.
- [42] M. A. Lancaster and J. A. Knoblich, “Generation of cerebral organoids from human pluripotent stem cells,” *Nat. Protoc.*, vol. 9, pp. 2329–2340, sep 2014.
- [43] C. Addae, X. Yi, R. Gernapudi, H. Cheng, A. Musto, and E. Martinez-Ceballos, “All-trans-retinoid acid induces the differentiation of encapsulated mouse embryonic stem cells into GABAergic neurons,” *Differentiation*, vol. 83, pp. 233–241, jun 2012.
- [44] A. M. Bratt-Leal, R. L. Carpenedo, and T. C. McDevitt, “Engineering the embryoid body microenvironment to direct embryonic stem cell differentiation,” *Biotechnol. Prog.*, vol. 25, pp. 43–51, jan 2009.
- [45] A. V. Ngangan, J. C. Waring, M. T. Cooke, C. J. Mandrycky, and T. C. McDevitt, “Soluble factors secreted by differentiating embryonic stem cells stimulate exogenous cell proliferation and migration,” *Stem Cell Res. Ther.*, vol. 5, no. 1, p. 26, 2014.

- [46] F. Neri, C. De Clemente, M. Orlandini, C. Lentucci, F. Anselmi, and F. Galvagni, “Murine Embryonic Stem Cells Synthesize Retinoic Acid to Promote their Own Differentiation,” *J. Stem Cell Res. Ther.*, vol. 05, no. 07, 2015.
- [47] H. Wichterle, I. Lieberam, J. A. Porter, and T. M. Jessell, “Directed Differentiation of Embryonic Stem Cells into Motor Neurons,” *Cell*, vol. 110, pp. 385–397, aug 2002.
- [48] T. Vazin, R. S. Ashton, A. Conway, N. A. Rode, S. M. Lee, V. Bravo, K. E. Healy, R. S. Kane, and D. V. Schaffer, “The effect of multivalent Sonic hedgehog on differentiation of human embryonic stem cells into dopaminergic and GABAergic neurons,” *Biomaterials*, vol. 35, pp. 941–948, jan 2014.
- [49] D. Choi, H.-J. Lee, S. Jee, S. Jin, S. K. Koo, S. S. Paik, S. C. Jung, S.-Y. Hwang, K. S. Lee, and B. Oh, “In Vitro Differentiation of Mouse Embryonic Stem Cells: Enrichment of Endodermal Cells in the Embryoid Body,” *Stem Cells*, vol. 23, no. 6, pp. 817–827, 2005.
- [50] D. A. McCreedy, T. S. Wilems, H. Xu, J. C. Butts, C. R. Brown, A. W. Smith, and S. E. Sakiyama-Elbert, “Survival, differentiation, and migration of high-purity mouse embryonic stem cell-derived progenitor motor neurons in fibrin scaffolds after sub-acute spinal cord injury,” *Biomater. Sci.*, vol. 2, pp. 1672–1682, jun 2014.
- [51] M. W. Amoroso, G. F. Croft, D. J. Williams, S. O’Keeffe, M. A. Carrasco, A. R. Davis, L. Roybon, D. H. Oakley, T. Maniatis, C. E. Henderson, and H. Wichterle, “Accelerated high-yield generation of limb-innervating motor neurons from human stem cells,” *J Neurosci*, vol. 33, no. 2, pp. 574–586, 2013.
- [52] C. Woodford and P. W. Zandstra, “Tissue engineering 2.0: guiding self-organization during pluripotent stem cell differentiation,” *Curr. Opin. Biotechnol.*, vol. 23, pp. 810–819, oct 2012.
- [53] A. G. Smith, “Embryo-derived stem cells: Of mice and men,” *Cell*, vol. 17, pp. 435–62, 2001.
- [54] H. Qi, Y. Du, L. Wang, H. Kaji, H. Bae, and A. Khademhosseini, “Patterned Differentiation of Individual Embryoid Bodies in Spatially Organized 3D Hybrid Microgels,” *Adv. Mater.*, vol. 22, pp. 5276–5281, dec 2010.
- [55] C. Fuchs, M. Scheinast, W. Pastener, S. Lagger, M. Hofner, A. Hoellrigl, M. Schultheis, and G. Weitzer, “Self-organization phenomena in embryonic stem cell-derived embryoid bodies: Axis formation and breaking of symmetry during cardiomyogenesis,” *Cells Tissues Organs*, vol. 195, no. 5, pp. 377–391, 2012.
- [56] K. Ishihara, A. Ranga, M. P. Lutolf, E. M. Tanaka, and A. Meinhardt, “Organ Regeneration,” *Cell*, vol. 146, no. 1, pp. 5–7, 2011.
- [57] P. B. Kuegler, B. Zimmer, T. Waldmann, B. Baudis, S. Ilmjärv, J. Hescheler, P. Gaughwin, P. Brundin, W. Mundy, A. K. Bal-Price, A. Schratzenholz, K.-H. Krause, C. van Thriel, M. S. Rao, S. Kadereit, and M. Leist, “Markers of murine embryonic and neural stem cells, neurons and astrocytes: reference points for developmental neurotoxicity testing,” *ALTEX*, vol. 27, no. 1, pp. 17–42, 2010.
- [58] I. Faravelli, M. Bucchia, P. Rinchetti, M. Nizzardo, C. Simone, E. Frattini, and S. Corti, “Motor neuron derivation from human embryonic and induced pluripotent stem cells: experimental approaches and clinical perspectives,” *Stem Cell Res. Ther.*, vol. 5, no. 4, p. 87, 2014.

References

.....

- [59] S. Muñoz-Descalzo, A.-K. Hadjantonakis, and A. M. Arias, “Wnt/ β -catenin signalling and the dynamics of fate decisions in early mouse embryos and embryonic stem (ES) cells,” *Semin. Cell Dev. Biol.*, aug 2015.
- [60] J. Briscoe and J. Ericson, “Specification of neuronal fates in the ventral neural tube,” *Curr. Opin. Neurobiol.*, vol. 11, pp. 43–49, feb 2001.
- [61] G. Sürmeli, T. Akay, G. C. Ippolito, P. W. Tucker, and T. M. Jessell, “Patterns of Spinal Sensory-Motor Connectivity Prescribed by a Dorsoventral Positional Template,” *Cell*, vol. 147, pp. 653–665, oct 2011.
- [62] S. Reijntjes, A. Blentic, E. Gale, and M. Maden, “The control of morphogen signalling: Regulation of the synthesis and catabolism of retinoic acid in the developing embryo,” *Dev. Biol.*, vol. 285, pp. 224–237, sep 2005.
- [63] I. Strate, T. H. Min, D. Iliev, and E. M. Pera, “Retinol dehydrogenase 10 is a feedback regulator of retinoic acid signalling during axis formation and patterning of the central nervous system,” *Development*, vol. 136, pp. 461–472, feb 2009.
- [64] M. Maden, “Retinoic acid in the development, regeneration and maintenance of the nervous system,” *Nat. Rev. Neurosci.*, vol. 8, pp. 755–765, oct 2007.
- [65] M. Paschaki, S.-C. Lin, R. L. Y. Wong, R. H. Finnell, P. Dollé, and K. Niederreither, “Retinoic Acid-Dependent Signaling Pathways and Lineage Events in the Developing Mouse Spinal Cord,” *PLoS One*, vol. 7, p. e32447, mar 2012.
- [66] S. Abu-Abed, P. Dollé, D. Metzger, B. Barbara, P. Chambon, and M. Petkovich, “The retinoic acid-metabolizing enzyme, CYP26A1, is essential for normal hindbrain patterning, vertebral identity, and development of posterior structures,” *Genes Dev.*, vol. 15, pp. 226–240, jan 2001.
- [67] M. Rhinn and P. Dollé, “Retinoic acid signalling during development,” *Development*, vol. 139, pp. 843–858, mar 2012.
- [68] J. Aoto, C. I. Nam, M. M. Poon, P. Ting, and L. Chen, “Synaptic Signaling by All-Trans Retinoic Acid in Homeostatic Synaptic Plasticity,” *Neuron*, vol. 60, pp. 308–320, oct 2008.
- [69] R. del Corral and A. Morales, “Retinoic Acid Signaling during Early Spinal Cord Development,” *J. Dev. Biol.*, vol. 2, pp. 174–197, jun 2014.
- [70] R. J. White, Q. Nie, A. D. Lander, and T. F. Schilling, “Complex Regulation of *cyp26a1* Creates a Robust Retinoic Acid Gradient in the Zebrafish Embryo,” *PLoS Biol.*, vol. 5, p. e304, nov 2007.
- [71] T. J. Cunningham and G. Duester, “Mechanisms of retinoic acid signalling and its roles in organ and limb development,” *Nat. Rev. Mol. Cell Biol.*, vol. 16, pp. 110–123, jan 2015.
- [72] S. R. Price and J. Briscoe, “The generation and diversification of spinal motor neurons: signals and responses,” *Mech. Dev.*, vol. 121, pp. 1103–1115, sep 2004.
- [73] R. A. Heyman, D. J. Mangelsdorf, J. A. Dyck, R. B. Stein, G. Eichele, R. M. Evans, and C. Thaller, “9-cis retinoic acid is a high affinity ligand for the retinoid X receptor,” *Cell*, vol. 68, pp. 397–406, jan 1992.

- [74] G. Allenby, M.-t. Bocquelt, M. Saunderst, S. Kazmer, J. Speck, M. Rosenbergerf, A. Lovey, P. Kastnert, J. F. Grippo, P. Chambont, and A. A. Levin, “Retinoic acid receptors and retinoid X receptors : Interactions with endogenous retinoic acids,” *Proc. Natl. Acad. Sci. U. S. A.*, vol. 90, no. January, pp. 30–34, 1993.
- [75] F. A. Mic, A. Molotkov, D. M. Benbrook, and G. Duester, “Retinoid activation of retinoic acid receptor but not retinoid X receptor is sufficient to rescue lethal defect in retinoic acid synthesis,” *Proc. Natl. Acad. Sci.*, vol. 100, no. 12, pp. 7135–7140, 2003.
- [76] S. M. Ulven, T. E. Gundersen, A. K. Sakhi, J. C. Glover, and R. Blomhoff, “Quantitative axial profiles of retinoic acid in the embryonic mouse spinal cord: 9-cis retinoic acid only detected after all-trans-retinoic acid levels are super-elevated experimentally,” *Dev. Dyn.*, vol. 222, no. 3, pp. 341–353, 2001.
- [77] S. Shimosono, T. Iimura, T. Kitaguchi, S.-i. Higashijima, and A. Miyawaki, “Visualization of an endogenous retinoic acid gradient across embryonic development,” *Nature*, vol. 496, pp. 363–366, apr 2013.
- [78] R. E. Hernandez, A. P. Putzke, J. P. Myers, L. Margaretha, and C. B. Moens, “Cyp26 enzymes generate the retinoic acid response pattern necessary for hindbrain development,” *Development*, vol. 134, pp. 177–187, jan 2007.
- [79] Y. Sakai, C. Meno, H. Fujii, J. Nishino, H. Shiratori, Y. Saijoh, J. Rossant, and H. Hamada, “The retinoic acid-inactivating enzyme CYP26 is essential for establishing an uneven distribution of retinoic acid along the antero-posterior axis within the mouse embryo,” *Genes Dev.*, vol. 15, no. 2, pp. 213–225, 2001.
- [80] S. S. Liour and R. K. Yu, “Differentiation of radial glia-like cells from embryonic stem cells,” *Glia*, vol. 42, pp. 109–117, apr 2003.
- [81] Y. C. Poh, J. Chen, Y. Hong, H. Yi, S. Zhang, J. Chen, D. C. Wu, L. Wang, Q. Jia, R. Singh, W. Yao, Y. Tan, A. Tajik, T. S. Tanaka, and N. Wang, “Generation of organized germ layers from a single mouse embryonic stem cell,” *Nat. Commun.*, vol. 5, no. May, pp. 1–12, 2014.
- [82] K. A. Sharow, B. Temkin, and M. A. Asson-Batres, “Retinoic acid stability in stem cell cultures,” *Int. J. Dev. Biol.*, vol. 56, no. 4, pp. 273–278, 2012.
- [83] V. B. Christie, D. J. Maltman, A. P. Henderson, A. Whiting, T. B. Marder, M. Lako, and S. A. Przyborski, “Retinoid supplementation of differentiating human neural progenitors and embryonic stem cells leads to enhanced neurogenesis in vitro,” *J. Neurosci. Methods*, vol. 193, no. 2, pp. 239–245, 2010.
- [84] T. J. Cunningham, A. Colas, and G. Duester, “Early molecular events during retinoic acid induced differentiation of neuromesodermal progenitors,” *Biol. Open*, p. bio.020891, 2016.
- [85] M. J. Ricard and L. J. Gudas, “Cytochrome P450 Cyp26a1 Alters Spinal Motor Neuron Subtype Identity in Differentiating Embryonic Stem Cells,” *J. Biol. Chem.*, vol. 288, pp. 28801–28813, oct 2013.
- [86] G. Duester, “Retinoid signaling in control of progenitor cell differentiation during mouse development,” *Semin. Cell Dev. Biol.*, vol. 24, pp. 694–700, dec 2013.
- [87] T. M. Jessell, “Neuronal specification in the spinal cord: inductive signals and transcriptional codes,” *Nat. Rev. Genet.*, vol. 1, pp. 20–29, oct 2000.

References

.....

- [88] M. Lek, J. M. Dias, U. Marklund, C. W. Uhde, S. Kurdija, Q. Lei, L. Sussel, J. L. Rubenstein, M. P. Matise, H.-H. Arnold, T. M. Jessell, and J. Ericson, “A homeodomain feedback circuit underlies step-function interpretation of a Shh morphogen gradient during ventral neural patterning,” *Development*, vol. 137, no. 23, pp. 4051–4060, 2010.
- [89] B. N. Davis-Dusenbery, L. A. Williams, J. R. Klim, and K. Eggan, “How to make spinal motor neurons,” *Development*, vol. 141, pp. 491–501, feb 2014.
- [90] J. S. Dasen and T. M. Jessell, “Hox Networks and the Origins of Motor Neuron Diversity,” in *Curr. Top. Dev. Biol.*, vol. 88, ch. 6, pp. 169–200, Elsevier Inc., 1 ed., 2009.
- [91] J. Jacob, A. Hacker, and S. Guthrie, “Mechanisms and molecules in motor neuron specification and axon pathfinding,” *BioEssays*, vol. 23, no. 7, pp. 582–595, 2001.
- [92] J. S. Dasen, B. C. Tice, S. Brenner-Morton, and T. M. Jessell, “A Hox Regulatory Network Establishes Motor Neuron Pool Identity and Target-Muscle Connectivity,” *Cell*, vol. 123, pp. 477–491, nov 2005.
- [93] S. a. D. T. di Sanguinetto, J. S. Dasen, and S. Arber, “Transcriptional mechanisms controlling motor neuron diversity and connectivity,” *Curr. Opin. Neurobiol.*, vol. 18, pp. 36–43, feb 2008.
- [94] D. D. McKinnon, A. M. Kloxin, and K. S. Anseth, “Synthetic hydrogel platform for three-dimensional culture of embryonic stem cell-derived motor neurons,” *Biomater. Sci.*, vol. 1, no. 5, p. 460, 2013.
- [95] K. Exelby, E. Herrera, V. Metzis, and J. Briscoe, “Boundary precision in the ventral neural tube,” *Mech. Dev.*, vol. 145, no. Suppl., p. S74, 2017.
- [96] X.-J. Li, B.-Y. Hu, S. A. Jones, Y.-S. Zhang, T. LaVaute, Z.-W. Du, and S.-C. Zhang, “Directed Differentiation of Ventral Spinal Progenitors and Motor Neurons from Human Embryonic Stem Cells by Small Molecules,” *Stem Cells*, vol. 26, pp. 886–893, apr 2008.
- [97] K. L. Adams, *Defining the Molecular and Functional Diversity of Stem Cell-Derived Motor Neurons*. Doctor of philosophy in molecular biology, University of California, Los Angeles, 2014.
- [98] J. A. Umbach, K. L. Adams, C. B. Gundersen, and B. G. Novitch, “Functional Neuromuscular Junctions Formed by Embryonic Stem Cell-Derived Motor Neurons,” *PLoS One*, vol. 7, p. e36049, may 2012.
- [99] B. Appel and J. S. Eisen, “Retinoids run rampant: Multiple roles during spinal cord and motor neuron development,” *Neuron*, vol. 40, no. 3, pp. 461–464, 2003.
- [100] J. Lacombe, O. Hanley, H. Jung, P. Philippidou, G. Surmeli, J. Grinstein, and J. S. Dasen, “Genetic and Functional Modularity of Hox Activities in the Specification of Limb-Innervating Motor Neurons,” *PLoS Genet.*, vol. 9, no. 1, 2013.
- [101] S. J. Ji, B. Zhuang, C. Falco, A. Schneider, K. Schuster-Gossler, A. Gossler, and S. Sockanathan, “Mesodermal and neuronal retinoids regulate the induction and maintenance of limb innervating spinal motor neurons,” *Dev. Biol.*, vol. 297, no. 1, pp. 249–261, 2006.
- [102] J. Vermot, B. Schuhbaur, H. Le Mouellic, P. J. McCaffery, J.-M. Garnier, D. Hentsch, P. Brûlet, K. Niederreither, P. Chambon, P. Dollé, and I. Le Roux, “Retinaldehyde

- dehydrogenase 2 and Hoxc8 are required in the murine brachial spinal cord for the specification of Lim1+ motoneurons and the correct distribution of Islet1+ motoneurons,” *Development*, vol. 132, no. 7, pp. 1611–1621, 2005.
- [103] M. P. Lutolf, P. M. Gilbert, and H. M. Blau, “Designing materials to direct stem-cell fate,” *Nature*, vol. 462, pp. 433–441, nov 2009.
- [104] M. Peljto, J. S. Dasen, E. O. Mazzoni, T. M. Jessell, and H. Wichterle, “Functional Diversity of ESC-Derived Motor Neuron Subtypes Revealed through Intraspinal Transplantation,” *Cell Stem Cell*, vol. 7, pp. 355–366, sep 2010.
- [105] M. Guvendiren and J. A. Burdick, “Engineering synthetic hydrogel microenvironments to instruct stem cells,” *Curr. Opin. Biotechnol.*, vol. 24, pp. 841–846, oct 2013.
- [106] D. Merryweather and P. Roach, “The need for advanced three-dimensional neural models and developing enabling technologies,” *MRS Commun.*, vol. 7, no. 3, pp. 309–319, 2017.
- [107] W. Ma, W. Fitzgerald, Q. Y. Liu, T. J. O’Shaughnessy, D. Maric, H. J. Lin, D. L. Alkon, and J. L. Barker, “CNS stem and progenitor cell differentiation into functional neuronal circuits in three-dimensional collagen gels,” *Exp. Neurol.*, vol. 190, no. 2, pp. 276–288, 2004.
- [108] A. M. Paşca, S. A. Sloan, L. E. Clarke, Y. Tian, C. D. Makinson, N. Huber, C. H. Kim, J.-Y. Park, N. A. O’Rourke, K. D. Nguyen, S. J. Smith, J. R. Huguenard, D. H. Geschwind, B. A. Barres, and S. P. Paşca, “Functional cortical neurons and astrocytes from human pluripotent stem cells in 3D culture,” *Nat. Methods*, vol. 12, pp. 671–678, may 2015.
- [109] M. Matyash, F. Despang, R. Mandal, D. Fiore, M. Gelinsky, and C. Ikonomidou, “Novel Soft Alginate Hydrogel Strongly Supports Neurite Growth and Protects Neurons Against Oxidative Stress,” *Tissue Eng. Part A*, vol. 18, pp. 55–66, jan 2012.
- [110] Y. L. Han, S. Wang, X. Zhang, Y. Li, G. Huang, H. Qi, B. Pingguan-Murphy, Y. Li, T. J. Lu, and F. Xu, “Engineering physical microenvironment for stem cell based regenerative medicine,” *Drug Discov. Today*, vol. 19, pp. 763–773, jun 2014.
- [111] L. E. Fitzpatrick and T. C. McDevitt, “Cell-derived matrices for tissue engineering and regenerative medicine applications,” *Biomater. Sci.*, vol. 3, no. 1, pp. 12–24, 2015.
- [112] C. A. Reinhart-King, “How Matrix Properties Control the Self-Assembly and Maintenance of Tissues,” *Ann. Biomed. Eng.*, vol. 39, pp. 1849–1856, jul 2011.
- [113] T. Lühmann and H. Hall, “Cell Guidance by 3D-Gradients in Hydrogel Matrices: Importance for Biomedical Applications,” *Materials (Basel)*, vol. 2, pp. 1058–1083, aug 2009.
- [114] D. Seliktar, “Designing Cell-Compatible Hydrogels for Biomedical Applications,” *Science (80-.)*, vol. 336, pp. 1124–1128, jun 2012.
- [115] Y. Li, M. Liu, Y. Yan, and S.-T. Yang, “Neural differentiation from pluripotent stem cells: The role of natural and synthetic extracellular matrix,” *World J. Stem Cells*, vol. 6, no. 1, p. 11, 2014.
- [116] R. Y. Tam, T. Fuehrmann, N. Mitrousis, and M. S. Shoichet, “Regenerative Therapies for Central Nervous System Diseases: a Biomaterials Approach,” *Neuropsychopharmacology*, vol. 39, pp. 169–188, jan 2014.

References

.....

- [117] A. Bozza, E. E. Coates, T. Incitti, K. M. Ferlin, A. Messina, E. Menna, Y. Bozzi, J. P. Fisher, and S. Casarosa, “Neural differentiation of pluripotent cells in 3D alginate-based cultures,” *Biomaterials*, vol. 35, pp. 4636–4645, may 2014.
- [118] A. Shridhar, E. Gillies, B. G. Amsden, and L. E. Flynn, “Composite Bioscaffolds Incorporating Decellularized ECM as a Cell-Instructive Component Within Hydrogels as In Vitro Models and Cell Delivery Systems,” in *Methods Mol. Biol.*, no. 1341, pp. 257–284, 2017.
- [119] M. P. Lutolf, P. M. Gilbert, and H. M. Blau, “Designing materials to direct stem-cell fate,” *Nature*, vol. 462, no. 7272, pp. 433–441, 2009.
- [120] J. L. Drury and D. J. Mooney, “Hydrogels for tissue engineering: scaffold design variables and applications,” *Biomaterials*, vol. 24, pp. 4337–4351, nov 2003.
- [121] B.-s. Kim and D. J. Mooney, “Development of biocompatible synthetic extracellular matrices for tissue engineering,” *Trends Biotechnol.*, vol. 16, pp. 224–230, dec 1998.
- [122] K. Y. Lee and D. J. Mooney, “Alginate : properties and biomedical applications,” *Prog. Polym. Sci.*, vol. 37, no. 1, pp. 106–126, 2012.
- [123] S.-K. Goh, P. Olsen, and I. Banerjee, “Extracellular Matrix Aggregates from Differentiating Embryoid Bodies as a Scaffold to Support ESC Proliferation and Differentiation,” *PLoS One*, vol. 8, p. e61856, apr 2013.
- [124] F. A. Muller, L. Muller, I. Hofmann, P. Greil, M. M. Wenzel, and R. Staudenmaier, “Cellulose-based scaffold materials for cartilage tissue engineering,” vol. 27, pp. 3955–3963, 2006.
- [125] M. T. Wolf, C. L. Dearth, S. B. Sonnenberg, E. G. Lobo, and S. F. Badylak, “Naturally derived and synthetic scaffolds for skeletal muscle reconstruction,” *Adv. Drug Deliv. Rev.*, vol. 84, pp. 208–221, apr 2015.
- [126] A. Sannino, C. Demitri, and M. Madaghiale, “Biodegradable Cellulose-based Hydrogels: Design and Applications,” pp. 353–373, 2009.
- [127] J. Stenberg, M. Elovsson, R. Strehl, E. Kilmare, J. Hyllner, and A. Lindahl, “Sustained embryoid body formation and culture in a non-laborious three dimensional culture system for human embryonic stem cells,” *Cytotechnology*, vol. 63, pp. 227–237, may 2011.
- [128] A. M. Kloxin, C. J. Kloxin, C. N. Bowman, and K. S. Anseth, “Mechanical properties of cellularly responsive hydrogels and their experimental determination,” *Adv. Mater.*, vol. 22, no. 31, pp. 3484–3494, 2010.
- [129] M. F. Griffin, “Control of stem cell fate by engineering their micro and nanoenvironment,” *World J. Stem Cells*, vol. 7, no. 1, p. 37, 2015.
- [130] M. D. Tang-Schomer, J. D. White, L. W. Tien, L. I. Schmitt, T. M. Valentin, D. J. Graziano, A. M. Hopkins, F. G. Omenetto, P. G. Haydon, and D. L. Kaplan, “Bioengineered functional brain-like cortical tissue,” *Proc. Natl. Acad. Sci.*, vol. 111, pp. 13811–13816, sep 2014.
- [131] C. Cunha, S. Panseri, O. Villa, D. Silva, and F. Gelain, “3D culture of adult mouse neural stem cells within functionalized self-assembling peptide scaffolds,” *Int. J. Nanomedicine*, vol. 6, no. April 2016, pp. 943–955, 2011.

-
- [132] D. Macaya and M. Spector, “Injectable hydrogel materials for spinal cord regeneration: a review,” *Biomed. Mater.*, vol. 7, p. 012001, feb 2012.
- [133] Q. Li, K. L. Chow, and Y. Chau, “Three-dimensional self-assembling peptide matrix enhances the formation of embryoid bodies and their neuronal differentiation,” *J. Biomed. Mater. Res. Part A*, vol. 102, pp. 1991–2000, jun 2014.
- [134] Y.-J. Seol, J. Y. Park, W. Jeong, T.-H. Kim, S.-Y. Kim, and D.-W. Cho, “Development of hybrid scaffolds using ceramic and hydrogel for articular cartilage tissue regeneration,” *J. Biomed. Mater. Res. Part A*, vol. 103, pp. 1404–1413, apr 2015.
- [135] B. Joddar, E. Garcia, A. Casas, and C. M. Stewart, “Development of functionalized multi-walled carbon-nanotube-based alginate hydrogels for enabling biomimetic technologies,” *Sci. Rep.*, vol. 6, no. May, pp. 1–12, 2016.
- [136] S. Camarero-Espinosa, B. Rothen-Rutishauser, C. Weder, and E. J. Foster, “Directed cell growth in multi-zonal scaffolds for cartilage tissue engineering,” *Biomaterials*, vol. 74, pp. 42–52, jan 2016.
- [137] B. R. Simona, L. Hirt, L. Demkó, T. Zambelli, J. Vörös, M. Ehrbar, and V. Milleret, “Density gradients at hydrogel interfaces for enhanced cell penetration,” *Biomater. Sci.*, vol. 3, no. 4, pp. 586–591, 2015.
- [138] Y.-H. Yang, Z. Khan, C. Ma, H. J. Lim, and L. A. Smith Callahan, “Optimization of adhesive conditions for neural differentiation of murine embryonic stem cells using hydrogels functionalized with continuous Ile-Lys-Val-Ala-Val concentration gradients,” *Acta Biomater.*, vol. 21, pp. 55–62, jul 2015.
- [139] S. Ali, I. B. Wall, C. Mason, A. E. Pelling, and F. S. Veraitch, “The effect of Young’s modulus on the neuronal differentiation of mouse embryonic stem cells,” *Acta Biomater.*, vol. 25, pp. 253–267, oct 2015.
- [140] O. Jeon, D. S. Alt, S. W. Linderman, and E. Alsberg, “Biochemical and Physical Signal Gradients in Hydrogels to Control Stem Cell Behavior,” *Adv. Mater.*, vol. 25, pp. 6366–6372, nov 2013.
- [141] K. Moore, M. Macsween, and M. S. Shoichet, “Immobilized Concentration Gradients of Neurotrophic Factors Guide Neurite Outgrowth of Primary Neurons in Macroporous Scaffolds,” *Tissue Eng.*, vol. 12, p. 060303124145002, mar 2006.
- [142] M. Chayosumrit, B. Tuch, and K. Sidhu, “Alginate microcapsule for propagation and directed differentiation of hESCs to definitive endoderm,” *Biomaterials*, vol. 31, pp. 505–514, jan 2010.
- [143] X. Wang, E. Wenk, X. Zhang, L. Meinel, G. Vunjak-Novakovic, and D. L. Kaplan, “Growth factor gradients via microsphere delivery in biopolymer scaffolds for osteochondral tissue engineering,” *J. Control. Release*, vol. 134, pp. 81–90, mar 2009.
- [144] Y. Wang and D. J. Irvine, “Engineering chemoattractant gradients using chemokine-releasing polysaccharide microspheres,” *Biomaterials*, vol. 32, pp. 4903–4913, jul 2011.
- [145] J. C. Gomez, J. M. Edgar, A. M. Agbay, E. Bibault, A. Montgomery, N. K. Mohitram, and S. M. Willerth, “Incorporation of Retinoic Acid Releasing Microspheres into Pluripotent Stem Cell Aggregates for Inducing Neuronal Differentiation,” *Cell. Mol. Bioeng.*, vol. 8, pp. 307–319, sep 2015.

References

.....

- [146] S. Sant, M. J. Hancock, J. P. Donnelly, D. Iyer, and A. Khademhosseini, "Biomimetic gradient hydrogels for tissue engineering," *Can. J. Chem. Eng.*, vol. 88, pp. 899–911, dec 2010.
- [147] S. A. Fisher, R. Y. Tam, and M. S. Shoichet, "Tissue Mimetics: Engineered Hydrogel Matrices Provide Biomimetic Environments for Cell Growth," *Tissue Eng. Part A*, vol. 20, pp. 895–898, mar 2014.
- [148] B. V. Slaughter, S. S. Khurshid, O. Z. Fisher, A. Khademhosseini, and N. A. Peppas, "Hydrogels in Regenerative Medicine," *Adv. Mater.*, vol. 21, pp. 3307–3329, sep 2009.
- [149] A. D. Augst, H. J. Kong, and D. J. Mooney, "Alginate hydrogels as biomaterials," *Macromol. Biosci.*, vol. 6, no. 8, pp. 623–633, 2006.
- [150] N. Wang, G. Adams, L. Buttery, F. H. Falcone, and S. Stolnik, "Alginate encapsulation technology supports embryonic stem cells differentiation into insulin-producing cells," *J. Biotechnol.*, vol. 144, pp. 304–312, dec 2009.
- [151] B. L. Strand, Y. A. Morch, and G. SKJAKBRK, "Alginate as immobilization matrix for cells," *Minerva Biotechnol.*, vol. 12, pp. 223–233, 2000.
- [152] H. Daemi and M. Barikani, "Synthesis and characterization of calcium alginate nanoparticles, sodium homopolymannuronate salt and its calcium nanoparticles," *Sci. Iran.*, vol. 19, no. 6, pp. 2023–2028, 2012.
- [153] R. L. Gardner, "Application of Alginate Gels to the Study of Mammalian Development," in *Germ Cell Protoc.* (H. Schatten, ed.), pp. 383–392, New Jersey: Humana Press, 2004.
- [154] C. K. Kuo and P. X. Ma, "Ionically crosslinked alginate hydrogels as scaffolds for tissue engineering: Part 1. Structure, gelation rate and mechanical properties," *Biomaterials*, vol. 22, pp. 511–521, mar 2001.
- [155] R. S. Ashton, A. Banerjee, S. Punyani, D. V. Schaffer, and R. S. Kane, "Scaffolds based on degradable alginate hydrogels and poly(lactide-co-glycolide) microspheres for stem cell culture," *Biomaterials*, vol. 28, no. 36, pp. 5518–5525, 2007.
- [156] O. Smidsrød, "Molecular basis for some physical properties of alginates in the gel state," *Faraday Discuss. Chem. Soc.*, vol. 57, no. 0, pp. 263–274, 1974.
- [157] U. Kandalam, A. I. Cabel, H. Omidian, and E. J. Stelnicki, "Viability of human umbilical cord-derived mesenchymal stem cells in G-rich and M-rich alginates," *J. Bioact. Compat. Polym.*, vol. 27, no. 2, pp. 174–182, 2012.
- [158] C. H. Goh, P. W. S. Heng, and L. W. Chan, "Alginates as a useful natural polymer for microencapsulation and therapeutic applications," *Carbohydr. Polym.*, vol. 88, no. 1, pp. 1–12, 2012.
- [159] L. Li, A. E. Davidovich, J. M. Schloss, U. Chippada, R. Schloss, N. a. Langrana, and M. L. Yarmush, "Neural lineage differentiation of embryonic stem cells within alginate microbeads," *Biomaterials*, vol. 32, pp. 4489–4497, jul 2011.
- [160] M. Verhulsel, M. Vignes, S. Descroix, L. Malaquin, D. M. Vignjevic, and J.-L. Viovy, "A review of microfabrication and hydrogel engineering for micro-organs on chips," *Biomaterials*, vol. 35, pp. 1816–1832, feb 2014.

-
- [161] C. M. Murphy, G. P. Duffy, A. Schindeler, and F. J. O'Brien, "Effect of collagen-glycosaminoglycan scaffold pore size on matrix mineralization and cellular behavior in different cell types," *J. Biomed. Mater. Res. Part A*, pp. n/a–n/a, oct 2015.
- [162] S. H. Oh, I. K. Park, J. M. Kim, and J. H. Lee, "In vitro and in vivo characteristics of PCL scaffolds with pore size gradient fabricated by a centrifugation method," *Biomaterials*, vol. 28, pp. 1664–1671, mar 2007.
- [163] I. Horiguchi, M. M. Chowdhury, Y. Sakai, and Y. Tabata, "Proliferation, morphology, and pluripotency of mouse induced pluripotent stem cells in three different types of alginate beads for mass production," *Biotechnol. Prog.*, vol. 30, pp. 896–904, jul 2014.
- [164] E. Delivopoulos, K. M. Shakesheff, and H. Peto, "Neuralization of mouse embryonic stem cells in alginate hydrogels under retinoic acid and SAG treatment," in *2015 37th Annu. Int. Conf. IEEE Eng. Med. Biol. Soc.*, pp. 3525–3528, IEEE, aug 2015.
- [165] S. Gerecht-Nir, S. Cohen, A. Ziskind, and J. Itskovitz-Eldor, "Three-dimensional porous alginate scaffolds provide a conducive environment for generation of well-vascularized embryoid bodies from human embryonic stem cells," *Biotechnol. Bioeng.*, vol. 88, no. 3, pp. 313–320, 2004.
- [166] J. Candiello, S. S. Singh, K. Task, P. N. Kumta, and I. Banerjee, "Early differentiation patterning of mouse embryonic stem cells in response to variations in alginate substrate stiffness," *J. Biol. Eng.*, vol. 7, no. 1, pp. 1–14, 2013.
- [167] S. Fang, Y.-d. Qiu, L. Mao, X.-l. Shi, D.-c. Yu, and Y.-t. Ding, "Differentiation of embryoid-body cells derived from embryonic stem cells into hepatocytes in alginate microbeads in vitro," *Acta Pharmacol. Sin.*, vol. 28, pp. 1924–1930, dec 2007.
- [168] Q. Qian, W. Bonani, D. Maniglio, J. Chen, and C. Migliaresi, "Modulating the release of drugs from alginate matrices with the addition of gelatin microbeads," *J. Bioact. Compat. Polym.*, vol. 29, pp. 193–207, may 2014.
- [169] E. K. Purcell, A. Singh, and D. R. Kipke, "Alginate Composition Effects on a Neural Stem Cell–Seeded Scaffold," *Tissue Eng. Part C Methods*, vol. 15, no. 4, pp. 541–550, 2009.
- [170] M. Hannig, H. R. Figulla, H. Sauer, and M. Wartenberg, "Control of leucocyte differentiation from embryonic stem cells upon vasculogenesis and confrontation with tumour tissue," *J. Cell. Mol. Med.*, vol. 14, no. 1-2, pp. 303–312, 2010.
- [171] H. J. Kong, M. K. Smith, and D. J. Mooney, "Designing alginate hydrogels to maintain viability of immobilized cells," *Biomaterials*, vol. 24, no. 22, pp. 4023–4029, 2003.
- [172] J. A. Rowley, G. Madlambayan, and D. J. Mooney, "Alginate hydrogels as synthetic extracellular matrix materials," *Biomaterials*, vol. 20, no. 1, pp. 45–53, 1999.
- [173] F. Ulloa-Montoya, C. M. Verfaillie, and W.-S. Hu, "Culture systems for pluripotent stem cells," *J. Biosci. Bioeng.*, vol. 100, pp. 12–27, jul 2005.
- [174] W. Zhang, S. Zhao, W. Rao, J. Snyder, J. K. Choi, J. Wang, I. a. Khan, N. B. Saleh, P. J. Mohler, J. Yu, T. J. Hund, C. Tang, and X. He, "A novel core–shell microcapsule for encapsulation and 3D culture of embryonic stem cells," *J. Mater. Chem. B*, vol. 1, no. 7, pp. 1002–1009, 2013.

References

.....

- [175] R. L. Carpenedo, S. A. Seaman, and T. C. McDevitt, "Microsphere size effects on embryoid body incorporation and embryonic stem cell differentiation," *J. Biomed. Mater. Res. Part A*, vol. 94, pp. 466–475, 2010.
- [176] M. Bibel, J. Richter, K. Schrenk, K. L. Tucker, V. Staiger, M. Korte, M. Goetz, and Y.-A. Barde, "Differentiation of mouse embryonic stem cells into a defined neuronal lineage," *Nat. Neurosci.*, vol. 7, pp. 1003–1009, sep 2004.
- [177] K. I. Draget, G. Skjak Braek, and O. Smidsrod, "Alginic acid gels: the effect of alginate chemical composition and molecular weight," *Carbohydr. Polym.*, vol. 25, no. 1, pp. 31–38, 1994.
- [178] S. C. Y. Lin, Y. Wang, D. F. Wertheim, and A. G. Coombes, "Production and in vitro evaluation of macroporous, cell-encapsulating alginate fibres for nerve repair," *Mater. Sci. Eng. C*, vol. 73, pp. 653–664, 2017.
- [179] J. L. Wilson, M. A. Najia, R. Saeed, and T. C. McDevitt, "Alginate encapsulation parameters influence the differentiation of microencapsulated embryonic stem cell aggregates," *Biotechnol. Bioeng.*, vol. 111, pp. 618–631, mar 2014.
- [180] Y. Zhang, J. Liu, L. Huang, Z. Wang, and L. Wang, "Design and performance of a sericin-alginate interpenetrating network hydrogel for cell and drug delivery.," *Sci. Rep.*, vol. 5, no. 4, p. 12374, 2015.
- [181] C. Capone, C. Filosa, G. Gigante, F. Ricci-Tersenghi, and P. D. Giudice, "Inferring synaptic structure in presence of neural interaction time scales," *PLoS One*, vol. 10, no. 3, pp. 1–21, 2015.
- [182] J. C. Breger, B. Fisher, R. Samy, S. Pollack, N. S. Wang, and I. Isayeva, "Synthesis of "click" alginate hydrogel capsules and comparison of their stability, water swelling, and diffusion properties with that of Ca⁺² crosslinked alginate capsules," *J. Biomed. Mater. Res. - Part B Appl. Biomater.*, vol. 103, no. 5, pp. 1120–1132, 2015.
- [183] M. S. Shoichet, R. H. Li, M. L. White, and S. R. Winn, "Stability of hydrogels used in cell encapsulation: An in vitro comparison of alginate and agarose," *Biotechnol. Bioeng.*, vol. 50, no. 4, pp. 374–381, 1996.
- [184] L. Wang, R. M. Shelton, P. R. Cooper, M. Lawson, J. T. Triffitt, and J. E. Barralet, "Evaluation of sodium alginate for bone marrow cell tissue engineering," *Biomaterials*, vol. 24, no. 20, pp. 3475–3481, 2003.
- [185] J. Kim, P. Sachdev, and K. Sidhu, "Alginate microcapsule as a 3D platform for the efficient differentiation of human embryonic stem cells to dopamine neurons," *Stem Cell Res.*, vol. 11, pp. 978–989, nov 2013.
- [186] D. Shahriari, J. Koffler, D. A. Lynam, M. H. Tuszynski, and J. S. Sakamoto, "Characterizing the degradation of alginate hydrogel for use in multilumen scaffolds for spinal cord repair," *J. Biomed. Mater. Res. - Part A*, vol. 104, no. 3, pp. 611–619, 2016.
- [187] S. Khetan, M. Guvendiren, W. R. Legant, D. M. Cohen, C. S. Chen, and J. A. Burdick, "Degradation-mediated cellular traction directs stem cell fate in covalently crosslinked three-dimensional hydrogels," *Nat. Mater.*, vol. 12, pp. 458–465, mar 2013.
- [188] F. R. Maia, K. B. Fonseca, G. Rodrigues, P. L. Granja, and C. C. Barrias, "Matrix-driven formation of mesenchymal stem cell–extracellular matrix microtissues on soft alginate hydrogels," *Acta Biomater.*, vol. 10, pp. 3197–3208, jul 2014.

-
- [189] H. Lee, G. A. Shamy, Y. Elkabetz, C. M. Schofield, N. L. Harrision, G. Panagiotakos, N. D. Socci, V. Tabar, and L. Studer, “Directed Differentiation and Transplantation of Human Embryonic Stem Cell-Derived Motoneurons,” *Stem Cells*, vol. 25, pp. 1931–1939, aug 2007.
- [190] O. Guillaume, S. M. Naqvi, K. Lennon, and C. T. Buckley, “Enhancing cell migration in shape-memory alginate-collagen composite scaffolds: In vitro and ex vivo assessment for intervertebral disc repair.,” *J. Biomater. Appl.*, vol. 29, no. 9, pp. 1230–46, 2015.
- [191] X. Li, T. Liu, K. Song, L. Yao, D. Ge, C. Bao, X. Ma, and Z. Cui, “Culture of Neural Stem Cells in Calcium Alginate Beads,” *Biotechnol. Prog.*, vol. 22, pp. 1683–1689, dec 2006.
- [192] M. Frega, M. Tedesco, P. Massobrio, M. Pesce, and S. Martinoia, “Network dynamics of 3D engineered neuronal cultures: a new experimental model for in-vitro electrophysiology,” *Sci. Rep.*, vol. 4, pp. 1–14, jun 2014.
- [193] X. Yuan, M. Zhou, J. Gough, A. Glidle, and H. Yin, “A novel culture system for modulating single cell geometry in 3D,” *Acta Biomater.*, vol. 24, pp. 228–240, sep 2015.
- [194] N. Siti-Ismail, A. E. Bishop, J. M. Polak, and A. Mantalaris, “The benefit of human embryonic stem cell encapsulation for prolonged feeder-free maintenance,” *Biomaterials*, vol. 29, no. 29, pp. 3946–3952, 2008.
- [195] F. C. Mansergh, C. S. Daly, A. L. Hurley, M. A. Wride, S. M. Hunter, and M. J. Evans, “Gene expression profiles during early differentiation of mouse embryonic stem cells,” *BMC Dev. Biol.*, vol. 9, no. 1, p. 5, 2009.
- [196] N. D. Leipzig and M. S. Shoichet, “The effect of substrate stiffness on adult neural stem cell behavior,” *Biomaterials*, vol. 30, no. 36, pp. 6867–6878, 2009.
- [197] K. Saha, A. J. Keung, E. F. Irwin, Y. Li, L. Little, D. V. Schaffer, and K. E. Healy, “Substrate Modulus Directs Neural Stem Cell Behavior,” *Biophys. J.*, vol. 95, pp. 4426–4438, nov 2008.
- [198] K. H. Nakayama, L. Hou, and N. F. Huang, “Role of Extracellular Matrix Signaling Cues in Modulating Cell Fate Commitment for Cardiovascular Tissue Engineering,” *Adv. Healthc. Mater.*, vol. 3, pp. 628–641, may 2014.
- [199] L. Wang, Y. Li, G. Huang, X. Zhang, B. Pingguan-Murphy, B. Gao, T. J. Lu, and F. Xu, “Hydrogel-based methods for engineering cellular microenvironment with spatiotemporal gradients,” *Crit. Rev. Biotechnol.*, vol. 00, pp. 1–13, jul 2015.
- [200] M. A. Kinney, T. A. Hookway, Y. Wang, and T. C. McDevitt, “Engineering Three-Dimensional Stem Cell Morphogenesis for the Development of Tissue Models and Scalable Regenerative Therapeutics,” *Ann. Biomed. Eng.*, vol. 42, pp. 352–367, feb 2014.
- [201] C. Chai and K. W. Leong, “Biomaterials approach to expand and direct differentiation of stem cells,” *Mol. Ther.*, vol. 15, no. 3, pp. 467–480, 2007.
- [202] J. E. Dixon, D. A. Shah, C. Rogers, S. Hall, N. Weston, C. D. J. Parmenter, D. McNally, C. Denning, and K. M. Shakesheff, “Combined hydrogels that switch human pluripotent stem cells from self-renewal to differentiation.,” *Proc. Natl. Acad. Sci. U. S. A.*, vol. 111, no. 15, pp. 5580–5, 2014.

References

.....

- [203] M. A. LeRoux, F. Guilak, and L. A. Setton, “Compressive and shear properties of alginate gel: Effects of sodium ions and alginate concentration,” *J. Biomed. Mater. Res.*, vol. 47, no. 1, pp. 46–53, 1999.
- [204] M. Guvendiren and J. a. Burdick, “Stiffening hydrogels to probe short- and long-term cellular responses to dynamic mechanics,” *Nat. Commun.*, vol. 3, p. 792, apr 2012.
- [205] J. Zhou, H. Y. Kim, and L. A. Davidson, “Actomyosin stiffens the vertebrate embryo during crucial stages of elongation and neural tube closure,” *Development*, vol. 136, no. 4, pp. 677–688, 2009.
- [206] A. Banerjee, M. Arha, S. Choudhary, R. S. Ashton, S. R. Bhatia, D. V. Schaffer, and R. S. Kane, “The influence of hydrogel modulus on the proliferation and differentiation of encapsulated neural stem cells,” *Biomaterials*, vol. 30, pp. 4695–4699, sep 2009.
- [207] Y. Murayama, J. Mizuno, H. Kamakura, Y. Fueta, H. Nakamura, K. Akaishi, K. Anzai, A. Watanabe, H. Inui, and S. Omata, “Mouse zona pellucida dynamically changes its elasticity during oocyte maturation, fertilization and early embryo development.,” *Hum. cell Off. J. Hum. Cell Res. Soc.*, vol. 19, no. 4, pp. 119–125, 2006.
- [208] S. H. Capone, M. Dufresne, M. Rechel, M. J. Fleury, A. V. Salsac, P. Paullier, M. Daujat-Chavanieu, and C. Legallais, “Impact of Alginate Composition: From Bead Mechanical Properties to Encapsulated HepG2/C3A Cell Activities for In Vivo Implantation,” *PLoS One*, vol. 8, no. 4, 2013.
- [209] M. Pekkanen-Mattila, M. Peltö-Huikko, V. Kujala, R. Suuronen, H. Skottman, K. Aalto-Setälä, and E. Kerkelä, “Spatial and temporal expression pattern of germ layer markers during human embryonic stem cell differentiation in embryoid bodies,” *Histochem. Cell Biol.*, vol. 133, no. 5, pp. 595–606, 2010.
- [210] K. S. Kolahi, A. Donjacour, X. Liu, W. Lin, R. K. Simbulan, E. Bloise, E. Maltepe, and P. Rinaudo, “Effect of substrate stiffness on early mouse embryo development,” *PLoS One*, vol. 7, no. 7, 2012.
- [211] H. L. Ang and G. Duyster, “Initiation of retinoid signaling in primitive streak mouse embryos: Spatiotemporal expression patterns of receptors and metabolic enzymes for ligand synthesis,” *Dev. Dyn.*, vol. 208, no. 4, pp. 536–543, 1997.
- [212] K. Niederreither, P. J. McCaffery, U. C. Dräger, P. Chambon, and P. Dollé, “Restricted expression and retinoic acid-induced downregulation of the retinaldehyde dehydrogenase type 2 (RALDH-2) gene during mouse development,” *Mech. Dev.*, vol. 62, no. 1, pp. 67–78, 1997.
- [213] N. Molotkova, A. Molotkov, I. O. Sirbu, and G. Duyster, “Requirement of mesodermal retinoic acid generated by Raldh2 for posterior neural transformation,” *Mech. Dev.*, vol. 122, no. 2, pp. 145–155, 2005.
- [214] F. A. Mic, R. J. Haselbeck, A. E. Cuenca, and G. Duyster, “Novel retinoic acid generating activities in the neural tube and heart identified by conditional rescue of Raldh2 null mutant mice,” *Development*, vol. 129, no. 9, pp. 2271–82, 2002.
- [215] I. O. Sirbu and G. Duyster, “Retinoic-acid signalling in node ectoderm and posterior neural plate directs left–right patterning of somitic mesoderm,” *Nat. Cell Biol.*, vol. 8, pp. 271–277, mar 2006.

-
- [216] R. D. Del Corral, I. Olivera-Martinez, A. Goriely, E. Gale, M. Maden, and K. Storey, “Opposing FGF and retinoid pathways control ventral neural pattern, neuronal differentiation, and segmentation during body axis extension,” *Neuron*, vol. 40, no. 1, pp. 65–79, 2003.
- [217] C. Horton and M. Maden, “Endogenous distribution of retinoids during normal development and teratogenesis in the mouse embryo,” *Dev. Dyn.*, vol. 202, no. 3, pp. 312–323, 1995.
- [218] M. L. Dubois-Dauphin, N. Toni, S. D. Julien, I. Charvet, L. E. Sundstrom, and L. Stopini, “The long-term survival of in vitro engineered nervous tissue derived from the specific neural differentiation of mouse embryonic stem cells,” *Biomaterials*, vol. 31, pp. 7032–7042, sep 2010.
- [219] S. M. Willerth, A. Rader, and S. E. Sakiyama-Elbert, “The effect of controlled growth factor delivery on embryonic stem cell differentiation inside fibrin scaffolds,” *Stem Cell Res.*, vol. 1, pp. 205–218, sep 2008.
- [220] L. Wilson and M. Maden, “The mechanisms of dorsoventral patterning in the vertebrate neural tube,” *Dev. Biol.*, vol. 282, no. 1, pp. 1–13, 2005.
- [221] S. Sockanathan and T. M. Jessell, “Motor Neuron-Derived Retinoid Signaling Specifies the Subtype Identity of Spinal Motor Neurons,” *Cell*, vol. 94, no. 4, pp. 503–514, 1998.
- [222] B. Dobbs-McAuliffe, Q. Zhao, and E. Linney, “Feedback mechanisms regulate retinoic acid production and degradation in the zebrafish embryo,” *Mech. Dev.*, vol. 121, pp. 339–350, apr 2004.
- [223] J. S. Dasen, A. De Camilli, B. Wang, P. W. Tucker, and T. M. Jessell, “Hox Repertoires for Motor Neuron Diversity and Connectivity Gated by a Single Accessory Factor, FoxP1,” *Cell*, vol. 134, no. 2, pp. 304–316, 2008.
- [224] D. Zhao, P. J. McCaffery, K. J. Ivins, R. L. Neve, P. Hogan, W. W. Chin, and U. C. Dräger, “Molecular identification of a major retinoic-acid-synthesizing enzyme, a retinaldehyde-specific dehydrogenase.,” *Eur. J. Biochem.*, vol. 240, no. 1, pp. 15–22, 1996.
- [225] P. J. McCaffery and U. C. Dräger, “Hot spots of retinoic acid synthesis in the developing spinal cord.,” *Proc. Natl. Acad. Sci. U. S. A.*, vol. 91, no. 15, pp. 7194–7, 1994.
- [226] Y.-T. L. Dingle, M. E. Boutin, A. M. Chirila, L. L. Livi, N. R. Labriola, L. M. Jakubek, J. R. Morgan, E. M. Darling, J. A. Kauer, and D. Hoffman-Kim, “Three-Dimensional Neural Spheroid Culture: An In Vitro Model for Cortical Studies,” *Tissue Eng. Part C Methods*, p. ten.tec.2015.0135, oct 2015.
- [227] O. a. Carballo-Molina and I. Velasco, “Hydrogels as scaffolds and delivery systems to enhance axonal regeneration after injuries,” *Front. Cell. Neurosci.*, vol. 9, p. 13, feb 2015.
- [228] P. Lu, Y. Wang, L. Graham, K. McHale, M. Gao, D. Wu, J. Brock, A. Blesch, E. S. Rosenzweig, L. A. Havton, B. Zheng, J. M. Conner, M. Marsala, and M. H. Tuszynski, “Long-Distance Growth and Connectivity of Neural Stem Cells after Severe Spinal Cord Injury,” *Cell*, vol. 150, pp. 1264–1273, sep 2012.
- [229] X.-f. Jiang, K. Yang, X.-q. Yang, Y.-f. Liu, Y.-c. Cheng, X.-y. Chen, and Y. Tu, “Elastic modulus affects the growth and differentiation of neural stem cells,” *Neural Regen. Res.*, vol. 10, no. 9, p. 1523, 2015.

References

.....

- [230] S. Joo, J. Yeon Kim, E. Lee, N. Hong, W. Sun, and Y. Nam, “Effects of ECM protein micropatterns on the migration and differentiation of adult neural stem cells,” *Sci. Rep.*, vol. 5, p. 13043, aug 2015.
- [231] Y.-C. Kuo and C.-C. Wang, “Guided differentiation of induced pluripotent stem cells into neuronal lineage in alginate–chitosan–gelatin hydrogels with surface neuron growth factor,” *Colloids Surfaces B Biointerfaces*, vol. 104, pp. 194–199, apr 2013.
- [232] J. Kern, K. Schrage, G. C. Koopmans, E. A. Joosten, P. J. McCaffery, and J. Mey, “Characterization of retinaldehyde dehydrogenase-2 induction in NG2-positive glia after spinal cord contusion injury,” *Int. J. Dev. Neurosci.*, vol. 25, no. 1, pp. 7–16, 2007.
- [233] K. D. Shearer, Y. D. Fragoso, M. Clagett-Dame, and P. J. McCaffery, “Astrocytes as a regulated source of retinoic acid for the brain,” *Glia*, vol. 60, no. 12, pp. 1964–1976, 2012.
- [234] J. Gerardo-Nava, D. Hodde, I. Katona, A. Bozkurt, T. Grehl, H. W. M. Steinbusch, J. Weis, and G. A. Brook, “Spinal cord organotypic slice cultures for the study of regenerating motor axon interactions with 3D scaffolds,” *Biomaterials*, vol. 35, pp. 4288–4296, may 2014.
- [235] D. J. Maltman, V. B. Christie, J. C. Collings, J. H. Barnard, S. Fenyk, T. B. Marder, A. Whiting, and S. A. Przyborski, “Proteomic profiling of the stem cell response to retinoic acid and synthetic retinoid analogues: identification of major retinoid-inducible proteins,” *Mol. Biosyst.*, vol. 5, no. 5, p. 458, 2009.
- [236] L. A. Pfister, M. Papaloïzos, H. P. Merkle, and B. Gander, “Hydrogel nerve conduits produced from alginate/chitosan complexes,” *J. Biomed. Mater. Res. Part A*, vol. 80A, pp. 932–937, mar 2007.
- [237] J. F. Harrison, M. L. Rinne, M. R. Kelley, N. M. Druzhyina, G. L. Wilson, and S. P. Ledoux, “Altering DNA base excision repair: use of nuclear and mitochondrial-targeted N-methylpurine DNA glycosylase to sensitize astroglia to chemotherapeutic agents,” *Glia*, vol. 55, no. 14, pp. 1416–1425, 2007.
- [238] H. Li, A. M. Koenig, P. Sloan, and N. D. Leipzig, “In vivo assessment of guided neural stem cell differentiation in growth factor immobilized chitosan-based hydrogel scaffolds,” *Biomaterials*, vol. 35, pp. 9049–9057, nov 2014.
- [239] C.-T. Kao, C.-C. Lin, Y.-W. Chen, C.-H. Yeh, H.-Y. Fang, and M.-Y. Shie, “Poly(dopamine) coating of 3D printed poly(lactic acid) scaffolds for bone tissue engineering,” *Mater. Sci. Eng. C*, vol. 56, pp. 165–173, nov 2015.
- [240] P. Friedl and E.-B. Bröcker, “T Cell Migration in Three-dimensional Extracellular Matrix: Guidance by Polarity and Sensations,” *Dev. Immunol.*, vol. 7, no. 2-4, pp. 249–266, 2000.
- [241] K. Chatterjee, M. F. Young, and C. G. Simon, “Fabricating Gradient Hydrogel Scaffolds for 3D Cell Culture,” *Comb. Chem. High Throughput Screen.*, vol. 14, pp. 227–236, may 2011.
- [242] S. E. Harrison, B. Sozen, N. Christodoulou, C. Kyprianou, and M. Zernicka-Goetz, “Assembly of embryonic and extraembryonic stem cells to mimic embryogenesis in vitro,” *Science (80-.)*, vol. 356, no. 6334, 2017.

-
- [243] T. A. Kapur and M. S. Shoichet, “Immobilized concentration gradients of nerve growth factor guide neurite outgrowth,” *J. Biomed. Mater. Res. Part A*, vol. 68A, pp. 235–243, feb 2004.
 - [244] J. E. Shin, K. Jung, M. Kim, K. Hwang, H. Lee, I.-S. Kim, B. H. Lee, I.-S. Lee, and K. I. Park, “Brain and spinal cord injury repair by implantation of human neural progenitor cells seeded onto polymer scaffolds,” *Exp. Mol. Med.*, vol. 50, no. 4, p. 39, 2018.
 - [245] R. E. Thompson, J. Pardieck, L. Smith, P. Kenny, L. Crawford, M. Shoichet, and S. Sakiyama-Elbert, “Effect of hyaluronic acid hydrogels containing astrocyte-derived extracellular matrix and/or V2a interneurons on histologic outcomes following spinal cord injury,” *Biomaterials*, vol. 162, pp. 208–223, 2018.
 - [246] J. S. Dasen, J.-P. Liu, and T. M. Jessell, “Motor neuron columnar fate imposed by sequential phases of Hox-c activity,” *Nature*, vol. 425, no. 6961, pp. 926–933, 2003.
 - [247] J. Rohwedel, K. Guan, and A. M. Wobus, “Induction of Cellular Differentiation by Retinoic Acid in vitro,” *Cells Tissues Organs*, vol. 165, no. 3-4, pp. 190–202, 1999.